

**Deformable Adult Human Phantoms for Radiation Protection Dosimetry:
Methods for Adjusting Body and Organ Sizes to Match
Population-Based Percentile Data**

by

Yong Hum Na

A Thesis Submitted to the Graduate

Faculty of Rensselaer Polytechnic Institute

in Partial Fulfillment of the

Requirements for the degree of

DOCTOR OF PHILOSOPHY

Major Subject: Biomedical Engineering

Approved by the
Examining Committee:

Dr. Xie George. Xu, Thesis Adviser

Dr. Peter F. Caracappa, Member

Dr. Xavier Intes, Member

Dr. Qiang Ji, Member

Dr. Robert L. Spilker, Member

Rensselaer Polytechnic Institute
Troy, New York

October, 2009
(For Graduation December 2009)

© Copyright 2009
by
Yong Hum Na
All Rights Reserved

CONTENTS

LIST OF TABLES.....	vi
LIST OF FIGURES	ix
ACKNOWLEDGMENT	xv
ABSTRACT	xvi
1. Introduction.....	1
1.1 Solid Geometry used for Human Computational Phantoms	2
1.1.1 Constructive Solid Geometry (CSG) Vs. Boundary REPresentation (BREP)	2
1.1.2 Boundary Representation	6
1.2 Anthropometric Consideration in Human Computational Phantoms	10
1.2.1 50 th -Percentile Population-Average Reference Phantoms	11
1.2.2 Percentile-Specific Phantoms.....	13
1.2.3 Breast Size-Adjustable Phantoms	14
1.2.4 Posture-Adjustable Phantoms	15
1.3 Radiation Dosimetry using Monte Carlo Methods and Computational Phantoms.....	17
1.4 Objectives and Tasks	19
1.5 Organization of the Ph.D. Dissertation	20
2. Methods to Develop Deformable Phantoms.....	22
2.1 50 th -Percentile Adult Phantoms	22
2.1.1 Primary Anatomical Organ Mesh Models	24
2.1.2 Anatomical References	27
2.1.3 Algorithms to Match with Reference Anatomical Parameters	28
2.2 Percentile-Specific Adult Phantoms	39
2.2.1 Deformation of the RPI-AM and RPI-AF Percentile Data	39
2.2.2 Definition of the Percentile-Specific Phantom Data.....	39
2.3 Breast Deformable Phantoms.....	51

2.3.1	Breast Size Determinant.....	51
2.3.2	Breast Deformation	52
2.4	Walking Posture Phantoms	54
2.4.1	Posture Phantoms	54
2.4.2	Walking Phantoms	54
2.5	Software Algorithms for Automatic Deformable Phantoms.....	56
3.	Results for the Deformable Phantoms	59
3.1	Validation of Deformable Phantoms.....	59
3.2	50 th -Percentile Reference Adult Phantoms	60
3.3	Percentile-Specific Adult Phantoms	71
3.4	Breast Deformable Female Phantoms	74
3.5	Walking Posture Adult Phantoms	75
4.	Demonstration and Discussion for Radiation Dose Calculations.....	77
4.1	Voxelization Procedures	77
4.2	Preparation of MCNPX Input Files with Specific Organ and Physical Properties	80
4.2.1	Organ Labeling and Physical Property Assignment	80
4.2.2	Organ Centroid.....	82
4.2.3	Implementation of Voxelized Phantoms in MCNPX	83
4.3	Monte Carlo Modeling for Organ Dose Comparisons	84
4.3.1	Organ Dosimetry using Deformable Phantoms and ICRP Adult Phantoms	85
4.3.2	Organ Dosimetry using Percentile-Specific Phantoms	87
4.3.3	Lung Counter Efficiency using Breast Deformable Female Phantoms	88
4.3.4	Environmental Dosimetry using Walking Posture Adult Phantoms....	91
4.4	Discussion on Results for Radiation Dose Calculations	92
4.4.1	RPI 50 th -Percentile Phantoms vs. ICRP Adult Phantoms	92

4.4.2	RPI Percentile-Specific Phantoms	96
4.4.3	RPI Breast Deformable Female Phantoms.....	98
4.4.4	RPI Walking Posture Phantoms	100
5.	Conclusions.....	103
5.1	Summary	103
5.1.1	RPI 50 th -Percentile Adult Phantoms	104
5.1.2	RPI Percentile-Specific Adult Phantoms	104
5.1.3	RPI Breast Deformable Adult Female Phantoms.....	105
5.1.4	RPI Walking Posture Adult Phantoms	105
5.2	Future Research.....	105
5.3	List of Peer-reviewed Journal Articles and Conference Proceedings.....	106
6.	Bibliography	109
Appendix A.	Organ/Tissue Data for 50 th -Percentile Adult phantoms	119
Appendix B.	Organ/Tissue Data for Percentile-Specific Phantoms	127

LIST OF TABLES

Table 1.1: Summary of the 50 th -Percentile Caucasian reference adult phantoms classified according to different types of modeling.....	12
Table 2.1: List of organs for the mesh-based phantoms and their corresponding organ IDs.....	25
Table 2.2: Percentile values of the RPI-Adult whole-body sizes.	41
Table 2.3: The RPI-AM weight percentiles based on the NHANES BMI.	44
Table 2.4: The RPI-AF weight percentile based on the NHANES BMI.	45
Table 2.5: Lung mass values of the reference adult male and female (mean \pm SD).	47
Table 2.6: Mass and volume percentile values for the left and right lungs in adults.	48
Table 2.7: Mean and Standard Deviation (Mean \pm SD) in major internal organ volume and mass values for the RPI adult phantoms.	50
Table 2.8: Cup size ranges letter code according to (EN 13402-3:2004).....	52
Table 3.1: List of organs for the RPI 50 th -percentile adult male and female.	68
Table 3.2: Male and female phantoms designed to represent the 5 th , 50 th , 95 th specific height and weight-percentile.	73
Table 3.3: The measured anthropometric data of the deformable breast phantoms sorted by the cup size (CS), busts girth (BG), and under bust girth (UBG).	74
Table 4.1: Organ-specific mass fractions for various tissue composition materials.	81
Table 4.2: Nuclides and their photon energies used for the virtual calibration of the lung counter (Only photons with emission probabilities greater than 0.01 were considered) (Hegenbart et al. 2008).....	90
Table 4.3: The E breast cup size phantom's lung counting efficiency in comparison with 7% glandularity and with the ICRP recommended glandularity of 40% (Hegenbart et al. 2008).	99
Table 4.4: Organ dose rates (nGy hour ⁻¹) of the RPI standing and walking phantoms on radioactive contamination ground with concentration of 30kBq m ⁻² (adopted from Han et al. 2009).....	100
Table A. 1: Organ/tissue masses, densities, and volumes for the 50 th -percentile RPI-AM phantom.	119

Table A. 2: Organ/tissue masses, densities, and volumes for the 50 th -Percentile RPI-AF phantom	123
Table B. 1: Percentile values for the mass and volume of left and right adrenal glands in adults	129
Table B. 2: Percentile values for mass and volume of the trachea in adults	131
Table B. 3: Percentile values for mass and volume of the bronchi in adults.....	133
Table B. 4: Percentile values for mass of male skeletons.....	135
Table B. 5: Percentile values for volume of male skeletons.....	137
Table B. 6: Percentile values for mass of female skeletons.	139
Table B. 7: Percentile values for volume of female skeletons.	141
Table B. 8: Percentile values for mass and volume of the brain in adults.....	144
Table B. 9: Percentile values for mass and volume of the left and right breasts in adult female.....	146
Table B. 10: Percentile values for mass and volume of the gallbladder in adults.....	148
Table B. 11: Percentile values for mass and volume of the stomach in adults.....	150
Table B. 12: Percentile values for mass and volume of the small intestines in adults..	152
Table B. 13: Percentile values for mass and volume of the large intestines wall in adult male.....	154
Table B. 14: Percentile values for mass and volume of the large intestines content in adult male.....	155
Table B. 15: Percentile values for mass and volume of the large intestines wall in adult female.....	156
Table B. 16: Percentile values for mass and volume of the large intestines content in adult female.....	157
Table B. 17: Percentile values for mass and volume of the heart in adults.....	159
Table B. 18: Percentile values for mass and volume of the left and right kidneys in adult male.....	161
Table B. 19: Percentile values for mass and volume of the left and right kidneys in adult female.....	162
Table B. 20: Percentile values for mass and volume of the liver in adults.....	164

Table B. 21: Percentile values for mass and volume of the left and right lungs in adults.....	166
Table B. 22: Percentile values for mass and volume of the skeleton muscles in adult male.....	168
Table B. 23: Percentile values for mass and volume of the skeleton muscles in adult female.....	169
Table B. 24: Percentile values for mass and volume of the oesophagus in adults.	171
Table B. 25: Percentile values for mass and volume of the left and right ovaries in adult female.....	173
Table B. 26: Percentile values for mass and volume of the brain in adults.....	175
Table B. 27: Percentile values for mass and volume of the prostate in adult male.	177
Table B. 28: Percentile values for mass and volume of the salivary glands in adults... ..	179
Table B. 29: Percentile values for mass and volume of the spleen in adults.....	181
Table B. 30: Percentile values for mass and volume of the thymus in adults.	183
Table B. 31: Percentile values for mass and volume of the thyroid gland in adults.	185
Table B. 32: Percentile values for mass and volume of the tongue in adults.	187
Table B. 33: Percentile values for mass and volume of the urinary bladder in adults. .	189
Table B. 34: Percentile values for mass and volume of the uterus in adult female.....	191

LIST OF FIGURES

Figure 1.1: A cube in Boundary REPresentation (BREP): (a) geometry; (b) topology ...	3
Figure 1.2: Flowchart showing typical steps in the Monte Carlo simulation of particle transport.	18
Figure 2.1: Flowchart of the process used to develop the deformable RPI-AM and RPI-AF phantoms.	24
Figure 2.2: Topology involving vertex numbering and triangular surface normals.....	29
Figure 2.3: Comparison of mesh quality with and without mesh preprocessing of the mandible and teeth: (a) Before the pre-processing the meshes have a lot of surface cracks; (b) The corrected meshes are closed and result in smooth surfaces.	30
Figure 2.4: Example of a simple polyhedron geometry (V_0 is $\{0, 0, 0\}$).	31
Figure 2.5: Comparisons of scale adjustment and vertex normal adjustment using an example of the 7 th rib spongiosa (inner mesh) that is created by the 7 th cortical rib (outer mesh): (a) When the 7 th cortical bone (outer mesh) was deformed by the uniform scale factor, the result of the spongiosa mesh is not located inside the cortical rib mesh; (b) Using the unique scalar factor to each of vertex normals, the deformed mesh (spongiosa) fits the inside of cortical bone.....	33
Figure 2.6: Primary mesh model's kidney deformation to person-specific kidney using specific mesh-based deformation method: (a) vectorizations of direction vectors from the center of mesh to the end of each vertex; (b) union of the direction vectors; (c) extension of the direction to reach the person-specific mesh surface with detecting of all intersectional points using ray casting algorithm; (d) rearrangement the new vertices and faces based on the intersected points and original faces information.	34
Figure 2.7: Illustration of the collision detection algorithm for Mesh surfaces A and B representing two organ surfaces. A collision event between two surfaces occurs when the distance between a vertex (labeled as \otimes) and the other surface along the normal (\uparrow or \downarrow) direction is less than a pre-determined value. The	

detection continues until all the vertices on both surfaces have been examined this way.....	35
Figure 2.8: The right lung and liver both increase in volumes: (a) mesh deformation with vertex normal vectors; (b) with collision detection and correction methods; (c) with collision detection and correction methods; the bottom surface of the right lung, which has a lower density, is deformed and pushed upward by the adjacent liver after collision detection and deformation.....	36
Figure 2.9: Polygonal mesh deformation with collision detection and correction.....	37
Figure 2.10: Special mesh deformation operations for certain organs and tissues: (a) Arm bone structures; (b) Arm muscles.....	38
Figure 2.11: Height and weight percentiles for the RPI-AM and RPI-AF using data adapted from CDC (McDowell et al. 2005): (a) Height percentiles; (b) Weight percentiles	41
Figure 2.12: Weight percentiles upon different heights for the RPI-AM and RPI-AF using data adapted from CDC(McDowell et al. 2005): (a) RPI-AM; (b) RPI-AF.	43
Figure 2.13: Statistical analysis for the lungs of reference adult male: (a) Probability Density Function (PDF); (b) Cumulative Density Function (CDF).	48
Figure 2.14: Method of measurement both BG and UBG: (a) axial breast cutting plan on the portion of breast for BG measurement; (b) extracted breast skin contour of the BG portion; (c) axial breast cutting plan on the portion of breast for UBG measurement; (d) extracted breast skin contour of the UBG portion; (e) real measurement of BG using ruler; (f) implemented measurement of BG using rolling boll method (Armato et al. 1999); (e) real measurement of UBG using ruler; (f) implemented measurement of UBG using rolling boll method.....	53
Figure 2.15: Normal gait cycle of adults.	55
Figure 2.16: Software GUI for deformable phantom operations showing various tools [Na et al. 2009b (images are courtesy of Mr. Aiping Ding)]: (a) different percentile phantoms; (2) the female phantom whose breast size is specified by a user.....	58

Figure 3.1: Deformability validation of deformable RPI-AM in deforming the body and organs' shapes and locations from (a) RPI-AM to (b) ICRP-REX; (c) deformed RPI-AM to REX; (d) two phantoms (b, c) with the same origin coordinate system.	60
Figure 3.2: Skeletal structures for the RPI adult phantoms with the organ ID numbers circled: (a) Cortical bones; (b) Spongiosa (contained red bone marrow) and medullary cavity (contained yellow bone marrow).....	61
Figure 3.3: Anatomical structures of detailed internal organs with organ ID circled for the RPI Adults in anterior (left), posterior (middle), and lateral (right), respectively: (a) Adult male; (b) Adult female.....	62
Figure 3.4: Anatomical structures of detailed blood vessels with organ ID circled for the RPI Adults in anterior (left), posterior (middle), and lateral (right), respectively: (a) Adult male; (b) Adult female.....	63
Figure 3.5: Anatomical structures of detailed lymphatic nodes with organ ID circled for the RPI Adults in anterior (left), posterior (middle), and lateral (right), respectively: (a) Adult male; (b) Adult female.....	64
Figure 3.6: Anatomical structures of detailed muscles with organ ID circled for the RPI Adults in anterior (left), posterior (middle), and lateral (right), respectively: (a) Adult male; (b) Adult female.....	65
Figure 3.7: 3D view of the RPI-AM phantom: (a) anterior; (b) posterior.....	66
Figure 3.8: 3D view of the RPI-AF phantom: (a) anterior; (b) posterior	67
Figure 3.9: 3D front views of phantoms of the same height (males at 176cm and females at 163 cm) but with different weight percentiles (5 th , 25 th , 50 th , 75 th , 95 th) representing variation in the body, respectively: (a) The males (58.5 kg 66.3 kg 73.1 kg 86.4 kg 103.8 kg); (b) the females (46.5 kg 55.8 kg 64.0 kg 78.9 kg 95.9 kg).	72
Figure 3.10: 3D anterior and posterior view views of 5 th , 50 th , 95 th percentile-specific adult male and female models, respectively: (a) The males (165 cm, 176 cm, and 188 cm in height, respectively, and 56 kg, 73 kg, and 110 kg in weight, respectively); (b) the females (152 cm, 163 cm, and 173 cm in height, respectively, and 41 kg, 60 kg, and 91 kg in weight, respectively).....	73

Figure 3.11: Different breast sizes of the female phantom according to the brassiere cup size definition (AA to G) by European clothes sizes standard (EN 13402)	75
Figure 3.12: 3D views for various postures of male and female phantoms, respectively: (a) Standing; (b) walking.....	76
Figure 4.1: Visual inspection of the skeleton certifies the accuracy of the voxelization process transforming from mesh to voxel geometry: (a) mesh-based skull;(b) voxelized skull; (c) mesh-based skeleton; (d)voxelized skeleton..	79
Figure 4.2: Software GUI for voxelization tools (Image is courtesy of Mr. Aiping Ding).	84
Figure 4.3: Six-standard external source geometries for external photon dose calculations: (a) anterior-posterior (AP); (b) posterior-anterior (PA); (c) right lateral (RLAT); (d) left lateral (LLAT); (e) rotational (ROT); (f) isotropic (ISO).	86
Figure 4.4: Phantoms representing workers of 5 th -, 50 th -, 95 th - weight and height percentile (weight: 56-, 73-, 110-kg and height: 165-, 176-, 188-cm, respectively) exposure to 0.5 MeV and 1 MeV phantom beams in AP irradiation geometry (Na et al. 2009b).....	87
Figure 4.5: The position of the lung counter in the virtual calibration (Hegenbart et al. 2008): (a) the central axis indicating the center-of-mass of the two lungs defined in the MCNPX; (b)Phoswich detector placed on the surface of the chest for lung counting measurement.....	89
Figure 4.6: Walking postures of the RPI-AM and RPI-AF on the contaminated ground: 70cm and 45cm of step lengths for male and female phantoms, respectively. (Han et al. 2009).....	92
Figure 4.7: RPI-AM's organ doses in comparison with REX (Zhang et al. 2009): (a) the lungs absorbed dose ratio of the RPI-AM to REX with different photon energies; (b) cross-sectional images showing the position of lungs marked grid (#) for the RPI-AM; (c) cross-sectional images showing the position of lungs marked grid (#) for REX	94
Figure 4.8: RPI-AF's organ doses in comparison with REGINA (Zhang et al. 2009): (a) the breasts absorbed dose ratio of the RPI-AF to REGINA in different	

photon energies; (b) cross-sectional images showing the position of breast tissues marked grid (#) for the RPI-AF; (c) cross-sectional images showing the position of breast tissues marked grid (#) for REGINA.	95
Figure 4.9: Organ dose differences of 5 th -, 50 th -, 95 th -weight and height percentile (weight: 56-, 73-, 110-kg and height: 165-, 176-, 188-cm, respectively) phantoms of AP irradiation geometry (Na et al. 2009b): (a) 0.5 MeV; (b) 1.0 MeV.	97
Figure 4.10: Relative counting efficiencies (counts per particle history) of the three nuclides, Am-241 (squares, dotted line), Cs-137 (diamonds, solid line), Co-60 (triangles, dashed line), normalized by the AA-model as a function of the total breast mass. The effects of chest attenuation on the counting efficiency and potential improvement to the use of one-size physical phantom are demonstrated in this “virtual calibration.” (Hegenbart et al. 2008).	99
Figure 4.11: Organ absorbed doses ratios of the walking to standing phantoms on Cs-137 and Co-60 contaminated ground with concentration of 30 kBq/m ² ; (a) the RPI-AM; (b) the RPI-AF. (Han et al. 2009).	102
Figure B. 1: RPI deformable phantoms: adrenal glands percentiles.	193
Figure B. 2: RPI deformable phantoms: trachea percentiles.	193
Figure B. 3: RPI deformable phantoms: bronchia percentiles.	194
Figure B. 4: RPI deformable phantoms: brain percentiles.	194
Figure B. 5: RPI deformable female phantom: breast tissue percentiles.	195
Figure B. 6: RPI deformable phantoms: gall bladder percentiles.	195
Figure B. 7: RPI deformable phantoms: stomach percentiles.	196
Figure B. 8: RPI deformable phantoms: small intestine percentiles.	196
Figure B. 9: RPI deformable male phantom: large intestine percentiles.	197
Figure B. 10: RPI deformable female phantom: large intestine percentiles.	197
Figure B. 11: RPI deformable phantoms: heart percentiles.	198
Figure B. 12: RPI deformable phantoms: kidney percentiles.	198
Figure B. 13: RPI deformable phantoms: liver percentiles.	199
Figure B. 14: RPI deformable phantoms: lung percentiles.	199
Figure B. 15: RPI deformable phantoms: muscle percentiles.	200

Figure B. 16: RPI deformable phantoms: oesophagus percentiles.....	200
Figure B. 17: RPI deformable phantoms: pancreas percentiles.....	201
Figure B. 18: RPI deformable phantoms: salivary gland percentiles.....	201
Figure B. 19: RPI deformable phantoms: spleen percentiles.....	202
Figure B. 20: RPI deformable phantoms: thymus percentiles.....	202
Figure B. 21: RPI deformable phantoms: thyroid percentiles.....	203
Figure B. 22: RPI deformable phantoms: tongue percentiles.....	203
Figure B. 23: RPI deformable phantoms: urinary bladder percentiles.....	204
Figure B. 24: RPI deformable male phantom: prostate & RPI deformable female phantom: ovary and uterus percentiles.....	204

ACKNOWLEDGMENT

I would like to express my sincerest gratitude to my advisor and committee chair Dr. X. George Xu for his generous guidance, invaluable mentoring and encouragement over the course of the doctoral program. It has been my great honor and privilege to work under his supervision. He has given me a lot of knowledge, worthwhile suggestions, thoughtful advices and ideas, which deeply inspired me in profound academic thinking during my study and research.

I would also like to thank my committee members, Dr. Peter F. Caracappa, Dr. Xavier Intes, Dr. Qiang Ji, and Dr. Robert L. Spilker, who enhanced my doctoral research skills as well as the completion of this dissertation. I am also grateful to the following former members, Dr. Juying Zhang, Dr. Binquan, and Dr. Lars Hegenbart, and current colleagues, Mr. Aiping Ding and Mr. Bin Han, for their various forms of support during this research project.

My family deserves more thanks than I could ever give them. I am greatly indebted to my father, Kie Jun Na, my mother, Jae Sun Choi, my sister, Eun Joo Na, and my brother in law, Sun Bum Kim, for their constant prayers, unconditional love and support. I would also like to extend my appreciation to my church family and friends.

Above all, I give thanks and praise to God giving me the wisdom and strength to finish my doctoral study.

“I can do everything through him who gives me strength.” Philippians 4:13 (NIV)

ABSTRACT

To determine radiation doses in the human body from exposures to various radiation sources, computational phantoms representing workers and patients are used with sophisticated Monte Carlo simulations. Nearly all existing phantoms, however, were purposely designed to match internal and external anatomical features of the Reference Man approximating the 50th-percentile of the adult male and female population as defined by the International Commission on Radiological Protection (ICRP). To reduce uncertainty in dose calculations caused by anatomical variations, a new generation of deformable phantoms of varying organ and body sizes has been recently proposed by the research community. This dissertation demonstrates methods to develop such deformable phantoms representing a range of adult individuals from the 5th percentile to 95th-percentile in terms of the body height, body weight, and internal organ volume/mass. Used to directly design such deformable phantoms, anatomical data in tables and graphs cover two different sets of information: (1) the whole-body height and weight percentile data from the National Health and Nutrition Examination Survey (NHANES); (2) individual internal organ size and volume/mass percentile data derived from those recommended in the ICRP Publications 23 and 89. As a starting point, a pair of 50th-percentile phantoms of the adult male and female, RPI-Adult Male and RPI-Adult Female, were first developed using entirely polygonal mesh surfaces. Embedded software tools were then developed to extend these two basic phantoms, on demand, to percentile-specific and posture-specific phantoms by altering organ boundaries according to the tabulated anthropometric data. Algorithms were developed to automatically match the organ volumes and masses with desired values. Finally, these mesh-based deformable phantoms were converted into voxel-based phantoms for Monte Carlo radiation transport simulations. The dissertation then demonstrates the usage of these percentile-specific phantoms for organ dose calculations for exposure to 0.5-MeV and 1-MeV external photon beams. Finally, this dissertation discusses future research directions that can further improve radiation dose assessment using this new type of deformable and size-adjustable computational phantoms.

1. Introduction

To understand the amount of radiation and associated risk to nuclear workers and patients who are exposed to ionizing radiation sources, the radiation dose to critical organs of the body must be accurately determined. There are two different approaches to the determination of organ doses: experimental and computational. The experimental approach involves physical measurements using a simple-geometry physical human phantom that allows tiny radiation dosimeters to be inserted into various organ locations to register the amount of radiation dose. Although such physical experiments are important in verifying dosimetry data, the procedures are time-consuming, labor-intensive expensive and potentially unsafe. On the other hand, the computational simulation methods are increasingly used for organ dose calculations with the availability of detailed computerized human models and rapidly advancing computer technologies. Today, computational phantoms of the human body are essential tools in the fields of health physics (radiation protection) and medical physics (imaging and radiotherapy).

This dissertation is about the development of a new type of computational phantoms that are deformable in body shape and size, thus them can more accurately represent different populations than the existing phantoms. The idea is that, using special geometrical data, these phantoms can be deformed to match with the anatomical characteristics defined for average man and female. Furthermore, for individuals who have larger or smaller body sizes than the averaged values, the phantoms can be automatically adjusted to parameters reported in the population surveys using automated deformable algorithms. This overall research effort is challenging in that it requires an interdisciplinary approach involving expertise in medical image processing, geometry computation, radiation dosimetry, and software development. Clearly, it is critical in this research for us to fully understand the following issues: the geometrical data used to design the deformable phantoms, anthropometric data for various body and organ sizes, computational algorithms to carry out the deformation process, and the procedure to implement the new phantoms for radiation dose simulations. In the sub-sections below, background information for each of these issues are introduced.

1.1 Solid Geometry used for Human Computational Phantoms

The fertile advancements of medical imaging devices and computer technologies have enabled the development of whole-body human computational phantoms used for various radiological studies. In the past 40 years, a large number of phantoms, spanning three generations, have been developed and applied for both ionizing and non-ionizing radiation studies (Eckerman et al. 2009, Xu 2009). Although more than 100 computational phantoms have been reported, they can be categorized two different generations; (1) Constructive Solid Geometry (CSG) phantoms; (2) Boundary REPresentation (BREP) phantoms.

1.1.1 Constructive Solid Geometry (CSG) Vs. Boundary REPresentation (BREP)

CSG modeling typically uses simple object shapes (e.g., cuboids, cylinders, prisms, pyramids, spheres, cones, and ellipsoid) described by quadric equations and it allows Boolean operators to assemble these primitives into complex geometries. On the other hand, the BREP modeling can be particularized by the geometrical and topological information. The BREP geometrical information contains the location of points (vertices with x, y, and z coordinator values), curves (edges; a set of connected vertices), and surfaces (faces; a set of connected edges). Topological information describes the orientation and relationship of vertices, edges, and faces in terms of a piecewise simple surface (Stroud 2006). As an illustration, Figure 1.1 shows a BREP model of a very simple cube with the information of geometry in (a) and topology in (b).

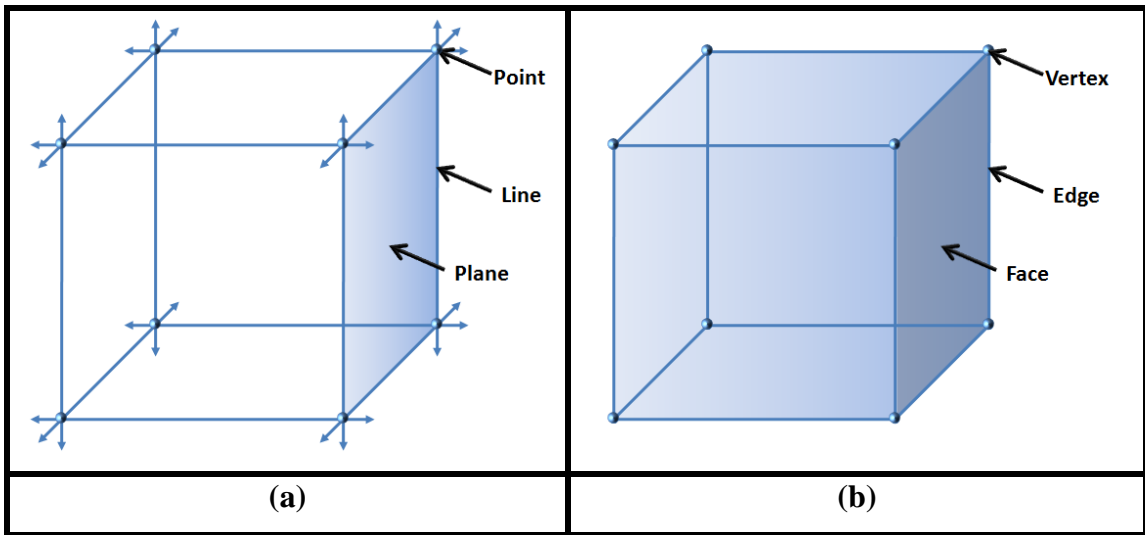


Figure 1.1: A cube in Boundary REPresentation (BREP): (a) geometry; (b) topology.

1.1.1.1 Stylized Phantoms

The first computational phantom was designed by Fisher and Snyder at Oak Ridge National Laboratory (ORNL) in 1960s (Fisher and Snyder 1968, Fisher and Snyder 1976.). This anthropomorphic phantom tried to mimic certain stylized anatomical shapes, consisting of simple quadric equations using the CSG. As aforementioned, the CSG method defines solid objects with Boolean operators to combine simple geometric elements such as cuboids, cylinders, prisms, pyramids, spheres, cones, and ellipsoid. In 1969, through follow-up activities on computational phantom development, Snyder's research group reported the first heterogeneous phantom which contained more than 20 organs with detailed anatomical features. A skeleton, lungs, the remainder (soft tissue) were characterized by density differences. Three different anatomical parts were described by elliptical cylinders and cones, such as an elliptical cylinder standing for the arm, torso, and hips; truncated elliptical cones appearing for the legs and feet; and an elliptic cylinder representing the head and neck. The organ masses were followed by the data recommended for the so-called Reference Man in the ICRP Publication 23 (ICRP 1975). This phantom, widely referred as the "MIRD-5 Phantom," was adopted officially by the Medical Internal Radiation Dosimetry (MIRD) Committee of the Society of

Nuclear Medicine Phantom (Snyder et al. 1969, Snyder et al. 1978, Cristy and Eckerman 1987). The formulation of the geometries was on the result of reference data and limited computational capabilities available at that time. This original phantom was revised later to produce a family of phantoms of both genders and different ages (Cristy and Eckerman 1987).

Since the primary development of the first set of stylized anthropomorphic phantoms, the updates have been reported in the past 40 years (Xu 2009). These anatomically simplified phantoms have been used as one of “standard” representations of ICRP “Reference Man” paradigm based on “population-average” 50th-percentile anatomical parameters (ICRP 1975, ICRP 2002). Many applications of these stylized phantoms in radiation protection, radiotherapy and medical imaging have been reported (ICRU 1992). The stylized phantoms have provided very useful organ dose data to support international and national guidelines and regulations associated with industrial and medical activates of ionizing radiation.

Although the stylized phantoms made it possible to compute the radiation doses using Monte Carlo simulations with a comparatively lower-level of computer requirements, the anatomical features in these phantoms had to be compromised during the development. For this reason, by the late 1980s, several groups of researchers began to search for new ways to improve anatomically realistic phantoms.

1.1.1.2 Voxel-Based Phantoms

To remedy the lack of anatomical realism and detail in the stylized phantoms, an entirely new method in phantom development began to emerge in late 1980s. With great strides of computer technologies, Computed Tomography (CT) and Magnetic Resonance Imaging (MRI), it became possible to visualize internal organ structures of a human body in three dimensions (3D). Through these advantages, a new generation of anatomically realistic voxel or tomographic phantoms began to be developed from the 1980s to 2000s as summarized in several recent review articles (Caon 2004, Zaidi and Xu 2007, Xu 2009).

Although both stylized phantoms and voxel (tomographic) phantom belong to the same class of CGS geometries, the development approach of a voxel phantom is

essentially distinct from the stylized ones. A voxel phantom is constructed by assembling of massive voxel chunks represented various anatomical structures unlike stylized phantoms based on quadric surface equations. The volume of each voxel is derived from multiplying the single pixel size in two-dimensional (2D) image by the slice thickness of the image. A tomographic image data set is composed of many slices keeping the detailed information of realistic patient internal anatomical structures. To create a voxel phantom, four main procedures are considered: (1) archival of a tomographic image data set from CT, MRI, or anatomical color photography covering whole-body; (2) segmentation of internal organs or tissues of interests assigning every pixel with identification number; (3) assignment of densities and chemical compositions for internal organs and tissues; (4) construction of 3D volume for entire anatomical structures in order to reach a 3D representation of the body frame as well as internal organs by stacking up the segmented 2D image slices.

In the 1980s, the first tomographic image-based phantoms were developed by Gibbs from Vanderbilt University (Gibbs and Pujol 1982, Gibbs et al. 1984, Gibbs et al. 1987). During the similar time period, a family of 12 voxel phantoms was developed independently by Zankl and her colleagues at GSF-National Research Center for Environment and Health in Germany using tomographic images based on healthy volunteers (Williams et al. 1986, Zankl et al. 1988, Petoussi-Henss et al. 2002, Zankl et al. 2002, Fill et al. 2004, Zankl et al. 2005, Becker et al. 2008). Other voxel phantoms were also reported (Caon 2004, Zaidi and Xu 2007, Xu 2009).

Notably, in 2000, Xu's group at Rensselaer Polytechnic Institute (RPI) reported the development of an adult male patient phantom, named VIP-Man (VIisible Photographic Man) (Xu et al. 2000). As the first cross-sectional color photographic image based computational phantom, the VIP-Man phantom was created using a cadaver (39-year-old male with 103kg weight and 186cm height) from the famous Visible Human Project(NLM 1990, Ackerman 1995). The digitized photos have 0.33 mm x 0.33 mm pixel resolution with successive 1-mm slice thickness (more than 3.7 billion voxels). Although only approximately 80 were adopted for radiation dosimetry, the VIP-Man has more than 1400 segmented internal organs and tissues. The finalized VIP-Man phantom was served as an interesting variation from the ICRP reference values, and used for

various studies in health and medical physics with all inner and outer anatomical details such as small and radiosensitive tissues; stomach mucosa, skin, eye lenses, and red bone marrow.

Up to now, a total of 74 voxel phantoms have been developed for both male and female and various ages (Xu 2009). These voxel phantoms, mainly used for radiation protection dosimetry, were developed using the ICRP "Reference Man" paradigm (ICRP 1975, ICRU 1992, ICRP 2002). To be compatible to the Reference Man, voxel-based reference phantoms must satisfy three main factors: (1) the whole-body individual tomographic image data are acquired to have as closely as possible data of the reference male and female in terms of height and weight; (2) individual anatomical details are able to adjust to match with the recommended reference values such as organ mass/volume values including skeleton masses and volumes; (3) all these requirements can be processed in voxel representation.

Voxel phantoms can provide an anatomically true representation of the subject who often differs from the average individual. Therefore, it became clear that some degree of adjustment in organ and body masses had to be made. Unfortunately, the format of the voxels is not easy for geometric modifications and deformation.

1.1.2 Boundary Representation

Realizing the need for additional phantoms in more convenient geometry adjustments, Xu and others proposed in early 2000s that the voxel phantoms could be replaced by the BREP phantoms (Xu 2009). There are several remarkable attractive advances in the BREP methods on behalf of phantom developers: (1) previously developed stylized or voxel phantoms are reused or updated because it is easy to extract the surfaces from the CSG; (2) the anatomical realism in external whole-body profiles and internal organ shapes are preserved from the voxel phantoms, and, at the same time, organ motions and other modeling can be carried out through convenient ways of anatomical deformation.

The BREP phantoms are in the form of either the Non-Uniform Rational B-Splines (NURBS), or polygonal meshes. BREP phantoms are found to be better suited than voxels for geometrical deformation and shape adjustment owing to a richer set of

computational operations. NURBS, for example, has shown to be capable of real-time cardiac and respiratory motion simulations (Segars et al. 2001, Segars and Tsui 2002, Zhang et al. 2008) although the method tends to trade computational performance and accuracy with anatomical realism.

1.1.2.1 NURBS-Based Phantoms

A set of control points is used to form NURBS equations that formulate a NURBS surface. NURBS surface shape and volume are able to be automatically changed through the changing of the positions of control points. This feature is very useful in time-dependent, 4D human body modeling. Coming with the advantages of NURBS modeling and anatomical details of the Visible Human CT data set from the National Library of Medicine, the spline-based MCAT Phantoms phantom was reported by Segars et al. (2001). This phantom was the basis of four dimensional (4D) NCAT representing cardiac and respiratory motions with more realistic anatomy modeling for cardiac system of a common patient (Segars and Tsui 2002). The 4D NCAT has used for the investigation of nuclear medicine imaging to evaluate and improve myocardial Single Photon Emission Computed Tomography (SPECT) imaging. The next version of the 4D NCAT, 4D Extended Cardiac-torsos (XCAT), was recently developed. The XCAT phantom involves more realistic anatomy and physiology based on whole-body male and female anatomies from the high-resolution Visible Male and Female anatomical data.

Through several research groups, the NURBS modeling is being widely applied to and integrated with the previous methods used for voxel (tomographic) phantom developments, under the name of hybrid-NURB modeling. In 2005 Xu's group from Rensselaer created the 4D VIP-Man Chest phantom used to study external beam treatment planning for a lung cancer patient (Xu and Shi 2005, Zhang et al. 2008). This phantom used the gated respiratory motion from the NCAT phantom in order to simulate respiratory motions of the 3D VIP-Man phantom. In 2007, his group used the BREP techniques to more challengeable studies to develop a series of computational phantoms such as pregnant phantoms, called the RPI Pregnant Females (RPI-P series), representing a pregnant woman and her fetus in different gestational stages; end of 3-, 6-, and 9-month gestations (Xu et al. 2007). Each of the RPI-P series has a total of 35 organs and

tissues which were explicitly defined. In order to design the individual parts of the body including fetus, these phantoms were composed of two separate surface structures: (1) NURBS surfaces extracted from a 30-week pregnant woman CT images (bladder, spleen, uterus, ovaries, and placenta) (Shi and Xu 2004) and VIP-Man model (esophagus, thyroid, thymus, trachea, and adrenals); (2) polygonal mesh surfaces from mesh organ models(rest of the organs including the fetus, skeleton of the mother, and the skin of the mother).

In 2007 and 2008, Bolch's group from the University of Florida (UF) group led by Bolch developed Hybrid BREP phantom series, called UFH-NURBS phantoms, from the segmented patient-specific CT image data for male and female both newborn and 15-year old adolescent (Lee et al. 2007, Lee et al. 2008). In 2008, Stabin's group from Vanderbilt University also reported a family of adult and pediatric phantoms which from the adjustment of NURBS-based NCAT adult male and female phantoms. The basic procedures for the development of the UFH-NURBS phantoms are as follows: (1) generate polygonal organ mesh surfaces from segmented patient-specific CT images; (2) extract several contours from the polygonal organ mesh surface to create a new NURBS surface of the same organ. This step was done by a commercial software tool, called "lofting"; (3) adjust the NURBS organ surface to match the volume to the ICRP recommended value (ICRP 2002).

Along the NURBS-based phantom developments and studies, Xu and his students realized that the NURBS surface modeling has more advantage for the real-time motion simulations (e.g., respiratory motion) using simple shapes of organs. NUBRS modeling was not always able to preserve the complicated organs, especially, the cases of thin organ object shapes, because NURBS geometry has a tendency to severely approximate complicated organ shapes to be simple ones due to the limitation of control points.

Consequently, Xu's group from Rensselaer adopted the polygonal mesh structure because they believed that the mesh-based geometrical tructures had the advantage in both anatomical realism and computational efficiency.

1.1.2.2 Polygonal Mesh-Based Phantoms

A polygon mesh or unstructured grid is composed of a set of vertices, edges, and faces that identify the shape of a polyhedral object in three-dimension (3D). The mesh surface is defined by a series of connected faces, which are shaped like polygons, most commonly triangles. Each face is made up a certain number of linear edges which are in turn defined by two vertices.

There are a number of remarkable advantages of polygonal mesh modeling for the development of whole-body phantoms: (1) mesh surfaces depicting human anatomy are able to be derived from real patient images as well as commercial human anatomy mesh models (www.anatomium.com). These mesh models were recreated by expert modelers with the help of anatomists, and they are very useful to overcome the insufficient whole-body images of a worker or patient; (2) the BREP (NURBS, polygon mesh, or a combination of both) modeling, especially in a polygonal mesh representation, has much more flexibility in geometry and topology adjustments because a richer set of computerized operations is available (e.g., extrusion, chamfering, blending, drafting, shelling and tweaking). For these reasons, the polygonal modeling technique is ideally suited for surface deformation and adjustment required for the sizes of individual whole-body and each of organs. The topological structure of the modeling allows more complicated solid objects characterizing human anatomy and body with less computational memory than CSG representation. These features make it possible for mesh-based phantoms to describe very complex anatomical features; (3) most of commercial computer aided design (CAD) software tools (e.g., Rhinoceros®, AutoCAD®, Visualization Toolkit, etc) provide various useful functions, such as an alternative converting tool between NURBS and mesh, 3D surface editing tools.

All of these advantages were successfully demonstrated in the work to develop phantoms representing three pregnant patients (Xu et al. 2007) as discussed earlier. A total of 35 organs and tissues were created by a hybrid BREP representation; 10 organs using NURBS and the rest of others using polygonal meshes. This experience led Xu's group from Rensselaer to conceive that the polygonal meshes were a better choice for developing “deformable phantoms.”

1.2 Anthropometric Consideration in Human Computational Phantoms

Throughout the history of phantom development for radiation protection, the general approach has been influenced by the need to represent the average population defined by the “Reference Man” paradigm. As such, a computational phantom needs to be designed to match the anthropometric 50th-percentile values in terms of age and gender-specific body height and weight. In addition, up to now, the majority of existing phantoms have a rigid, upright standing posture with arms typically on the sides of the body. Clearly, if these phantoms are used for individuals who are larger or smaller, having a different posture such as walking, then the overall uncertainties in the calculated organ doses may not be acceptable.

Consequently, it was proposed by a group of researchers (Xu et al. 2009c) that there was a need in research to develop methods that allow the reference 50th-percentile phantoms to be extended to various shapes of the phantoms in terms of ranges of whole-body sizes and postures. The ranges are defined from population survey data that typically cover from 5th to 95th percentiles of the population in terms of body and organs. To some degree, different body portions can also be adjusted to extend the upright standing to others such as sitting, raised up arms and walking, as well as special phantoms such as phantoms representing female works having different chest thickness.

From the technical point of view, such a future phantom is no longer an assembly of just one set of voxelized geometric data representing a rigid anatomy. Instead, the phantom is designed to be deformable, capable of being morphed into a new phantom of desirable anatomy according to the demand (Xu et al. 2008). It is apparent to us that the term “deformable phantom” implies a software component that can reliably carry out complex data operational processes starting with a basic pair of phantoms with pre-determined anatomical percentiles. The term “deformable phantom” is interchangeable with “size- and/or optional body- adjustable phantom” throughout this dissertation.

1.2.1 50th-Percentile Population-Average Reference Phantoms

Under the current radiation protection dosimetry paradigm established on the “Reference Man” concept, computational phantoms must contain anatomical parameters defined by the ICRP for average populations (ICRP 1975, ICRP 2002).

As reference computational phantoms, the REX and REGINA are being released from the ICRP (Schlattl et al. 2007, Zankl et al. 2007). The REX and REGINA were developed by the radiation protection research group at GSF-National Research Center for Environment and Health in German. These phantoms were based on the patient specific CT image data with a number of voxel adjustments for their organ volume and mass values in agreement with the recommended values reported by the ICRP Publications70 and 89 (ICRP 1995, 2002) (Becker et al. 2007). However, the voxel adjustment limited the anatomical accuracy of the REX and REGINA due to the voxel sizes, $2.137 \times 2.137 \times 8.0 \text{ mm}^3$ and $1.775 \times 1.775 \times 4.84 \text{ mm}^3$, respectively. Table 1.1 summarizes the current existing 50th-percentile Caucasian reference adult phantoms classified according to different types of modeling.

Table 1.1: Summary of the 50th-Percentile Caucasian reference adult phantoms classified according to different types of modeling.

Model Type	Phantom structure	Name	Reference
CSG	Stylized	MIRD-5	(Snyder et al. 1969, Snyder et al. 1978, Cristy and Eckerman 1987)
	Voxel	MAX06 and FAX06	(Kramer et al. 2006)
	Voxel	REX and REGINA	(Schlattl et al. 2007, Zankl et al. 2007)
	Voxel	NORMAN-05 and NAOMI	(Ferrari and Gualdrini 2005) (Dimbylow 2005a , Dimbylow 2005b)
	Voxel/Stylized	Pregnant Series (3,6,9 months of gestation)	(Chen, 2004)
BREP	NURBS	ICRP89-based adult male and female	(Stabin et al. 2008)
	NURBS/Polygonal Mesh	RPI-Pregnant Females (3,6,9 months of gestation)	(Xu et al. 2007)
	Polygonal Mesh	RPI-AM and RPI-AF	(Xu et al. 2008, Hegenbart et al. 2008, Na et al. 2009a, Zhang et al. 2009)

When the research community was realizing that phantoms should be standardized with the “Reference Man” concept in a radiation protection field, phantom developers were trying to correct the original body size and organ shapes of previously developed phantoms. Stylized phantoms are more flexible than voxel-based (tomographic) phantoms to reconstruct whole-body size and individual organs volumes but are not sufficient to provide anatomical details. Whereas, voxel-based phantoms can provide realistic anatomy descriptions but have a lot more difficulty to remodel their rigid structure and even the anatomic realism can be distorted by the corrections.

Owing to the recent recommendations by a group of researchers (Xu et al. 2009c), radiation protection dosimetry community is beginning to actively consider methods of developing phantoms that represent not only the 50th-percentile populations, but also percentile-specific individuals for applications such as medical imaging, radiotherapy, and high-dose rate occupational exposures that need to use whole-body phantoms to assess organ doses. The population percentile phantom concepts can be categorized by two main factors: (1) weight dependent percentile phantoms which have a same height but different weight; (2) weight and height dependent percentile phantoms which have different height and weight.

1.2.2 Percentile-Specific Phantoms

In 2008, research group from the University of Florida presented six different 15-year male and female adolescent phantoms for investigation of delivered organ dose variations under multi-slice CT imaging. These phantoms were created by hybrid format using combination of NURBS surface and polygonal mesh modeling. The phantoms included body weight information in terms of 10th, 50th, and 90th -percentiles with the same height for each of males and females (Lee et al. 2008). The anthropometric data of different body sizes and weights were derived from the Centers for Diseases Control and Prevention (CDC) growth curves (Kuczmarski et al. 2002). The developers assumed that the weight changes were related to the different body fat types, such as subcutaneous fat (SF) and intra-abdominal fat (IAF), and skeletal muscles not by the internal organ masses. Although these adolescent phantoms are providing a couple of weight percentile series, these are still not enough to support nearly all of the adolescent population.

The term, “weight and height dependent percentile phantoms,” refers to a fact that both the weight and height can vary according to population survey data. Thus, it is mandatory that these phantoms must have unique organ volumes and masses. The existing 50th-percentile reference computational phantoms follow the data for body size (i.e., weight and height) and organ volume and mass provided well defined by the ICRP “Reference Man” paradigm (Schlattl et al. 2007, Zankl et al. 2007). However, there is little research on how to define the internal organs to match other 5th- to 95th percentiles. It should be noted it is impractical to measure the volume and mass of individual organs from specific patients, thus the percentile-specific phantoms need to be based on “average” percentile data from the literature.

This dissertation covers that the weight dependent percentile phantoms which were deformed with automatic deformation methods in the ranges of 5th, 25th, 50th, 75th, and 95th percentiles based on the deformable 50th-percentile reference RPI-AM and RPI-AF phantoms. The weight and height dependent percentile phantoms are described from 5th to 95th percentiles. The RPI-AM and RPI-AF reference phantoms are deformed to match with two principal percentile data sets: (1) the whole-body size percentile data defined by the anthropometric parameters such as height and weight from the National Health and Nutrition Examination Survey (NHANES); (2) individual internal organ percentile data derived by the statistical analysis using the ICRP Publications 23 and 89 (ICRP 1975, ICRP 2002), as well as various other organ measurement reports (McDowell 2005).

In the past 40 years, research on ionizing and non-ionizing radiation protection has lead to more than 121 computational phantoms (Xu 2009). However, these phantoms have only fixed upright standing postures. Only a few phantoms contain a very limited ability to represent movable arms or legs.

1.2.3 Breast Size-Adjustable Phantoms

The importance of a deformable phantom can be demonstrated by the application to consider various chest thicknesses in bioassay measurement involving female workers who have radionuclide contamination in their lungs. In this application, the chest thickness related the breast size can affect the radiation counting results. The breast

anthropometric data (dimension, tissue composition, total volume and mass) has been discussed in several reports (ICRP 1975, Kramer and Drexler 1981, Cristy 1982). To estimate the representative data on the breast, statistical information on women brasserie (bra) sizes was analyzed by Kramer and Drexler (1981). In 1985, Berger and Lane reported the biometric estimation of chest wall thickness (CWT) of female radiation workers. Simple measurements of chest circumferences in the vertical and supine positions of 77 women were involved in deriving an empirical formula for female CWT. With increasing female body size over last two decades, updated formula has been proposed (Odgen et al. 2006, Lee et al. 2007).

The recommended values of mass and fraction of glandular tissue standing for average adult female breast were reported in the ICRP Publication 89 (ICRP 2002) but without the breast dimensions. To obtain precise breast size and shape in realistic measurements, recently, various 3D body scanners have been used. However, it is not easy to cover all hidden areas of nude breasts (Lee et al. 2004). Another challenge is that the female breast size and shape can be affected by various factors such as race, culture, age, diet and social status. Therefore, reliable anthropometric data on female breast is difficult to find.

For this PhD research, brasserie manufacturing standards and mesh deformation techniques are employed to create a breast size-adjustable female phantom. The basic procedures for the development of the phantoms are as follows: (1) the breast portions of the adult female phantom, RPI-AF, are segmented from the whole body frame; (2) the segmented breast portions are measured by the difference between Bust Girth (BG) and Under Bust Girth (UBG); (3) according to the European clothes sizes standard (EN 13402-1 2001, EN 13402-2 2002, EN 13402-3 2004), the brassiere cup sizes (i.e., AA, A, B, C, D, E, F, G) are characterized; (4) downward gravity forces on the breasts are considered to manufacture realistic results, which demonstrate the geometric flexibility of mesh-based phantoms.

1.2.4 Posture-Adjustable Phantoms

In 1999 and 2002, Dawson et al. from the University of Victoria in Canada introduced voxel-based sitting and outstretched arms phantoms (Dawson et al. 1999,

Dawson et al. 2002). These phantoms were used for numerical evaluation of the effects of postures for non-uniform magnetic field exposures. In order to create the phantoms, the limbs of the upright phantom had been rotated by manual editing. From 2003 to 2006, several research groups developed voxel-based posture phantoms using manual editing (e.g., cutting, rotating, and re-attaching) methods to transform the upright standing body to various postures (Allen et al. 2003, Allen et al. 2005, Findlay and Dimbylow 2005, Findlay and Dimbylow 2006a, Findlay and Dimbylow 2006b).

In 2008, Nagaoka and Watanabe at the National Institute of Information and Communications Technology in Japan developed six different posture phantoms for electromagnetic dosimetry (Nagaoka and Watanabe 2008). These phantoms were based on the Japanese adult male and female voxel-based phantoms in upright postures (Nagaoka et al. 2004). To deform a 3D solid geometry, free-form deformation (FFD) transformation method (Sederberg and Parry 1986) was used. The basic procedures are as follows: (1) segment the whole-body into several body portions based on the articulations; (2) define the control lattice points for the FFD methods; (3) set around the whole body to move and/or rotate the body portions; (4) obtain an arbitrary posture through the relocating of the control points of each body portion. During the deforming process, several additional steps are taken to avoid any empty spaces in or between relocated voxels; (i) all solid geometry surfaces of the body portions have to be extracted as polygonal mesh surfaces; (ii) extracted polygonal meshes will be deformed according to the relocation of control points; (iii) the deformed polygonal meshes need to be re-voxelized to have smooth voxel representation; (iv) deformed internal organ data such as volumes and masses have to be checked whether the values are close enough to the original ones. Although the FFD is a useful tool for a 3D solid geometry model, some difficulties still exist for maintaining the anatomical details, especially for the rigid organ structures and skeleton (Nagaoka et al. 2004).

In 2007, Akkurt and Eckerman (Akkurt and Eckerman 2007) from Oak Ridge National Laboratory (ORNL) reported PIMAL (Phantom wIth Moving Arms and Legs) phantoms for the assessment of organ doses. These phantoms were based on the revised MIRD-5 stylized phantom called ORNL-UF (Han et al. 2006). To change the postures, the arms and legs were disconnected from the torso, and each of parts was segmented by

upper and lower arms and legs. The torso was kept from the ORNL-UF due to the difficulty to reposition all internal organs. Although work demonstrated the need and the feasibility to design phantoms of moving arms and legs through software processing, their work is based the stylized geometry thus suffers from the lack of anatomical details.

1.3 Radiation Dosimetry using Monte Carlo Methods and Computational Phantoms

The most intensive applications of the Monte Carlo simulation methods were associated with the development of the atomic bombs at the Los Alamos National Laboratory in the 1940s (Hammersley and Handscomb 1964). The methods were later widely applied to nuclear engineering, health physics and medical physics. Monte Carlo simulation is widely regarded as a reliable computational experiment to stand-in for various cases of physical experiments that are either expensive or dangerous, or both.

In radiation dosimetry, we are interested in the radiation absorbed dose which is determined as the quotient of energy deposited in the target and the mass. In order to determine the energy and pattern of radiation integration, radiation transport inside various materials is closely tracked by Monte Carlo software package. The flowchart in Figure 1.2 illustrates the procedure of simulating radiation transport using the Monte Carlo methods. Computer generated random numbers are used to determine the distance and fate of a nuclear particle by considering the probabilities of all interactions for each geometric region of interest. This process requires typically following the basic steps: (1) define the initial state in terms of energy, weight, position, and direction for a certain source of particle to be simulated. This initial state is described by a state vector contains the characters of the particle. With this initial state, the history of the particle is tended to be either updated or terminated according to the inspection of significance in next steps; (2) during the traveling of this particle, its significance (e.g., energy cutoff, weight cutoff, etc) is tested; if there is no significance to continue the traveling, the history of this particle will be terminated. Else, the particle will be supposed to have further interaction between either the boundaries or any spot of the ROI; (3) if the distance to next interaction is smaller than the distance to the boundary of the ROI, the particle will deposit energy and other offspring interactions will be considered inside of the ROI. On

the other hand the particle will escape from the ROI; (4) these whole processes above will be iterated until the particle in a history deposits whole energy or escapes from the ROI. Single history is appointed by the entire process of the particle. The result can come out with acceptable statistical uncertainty for the average of a large number of histories.

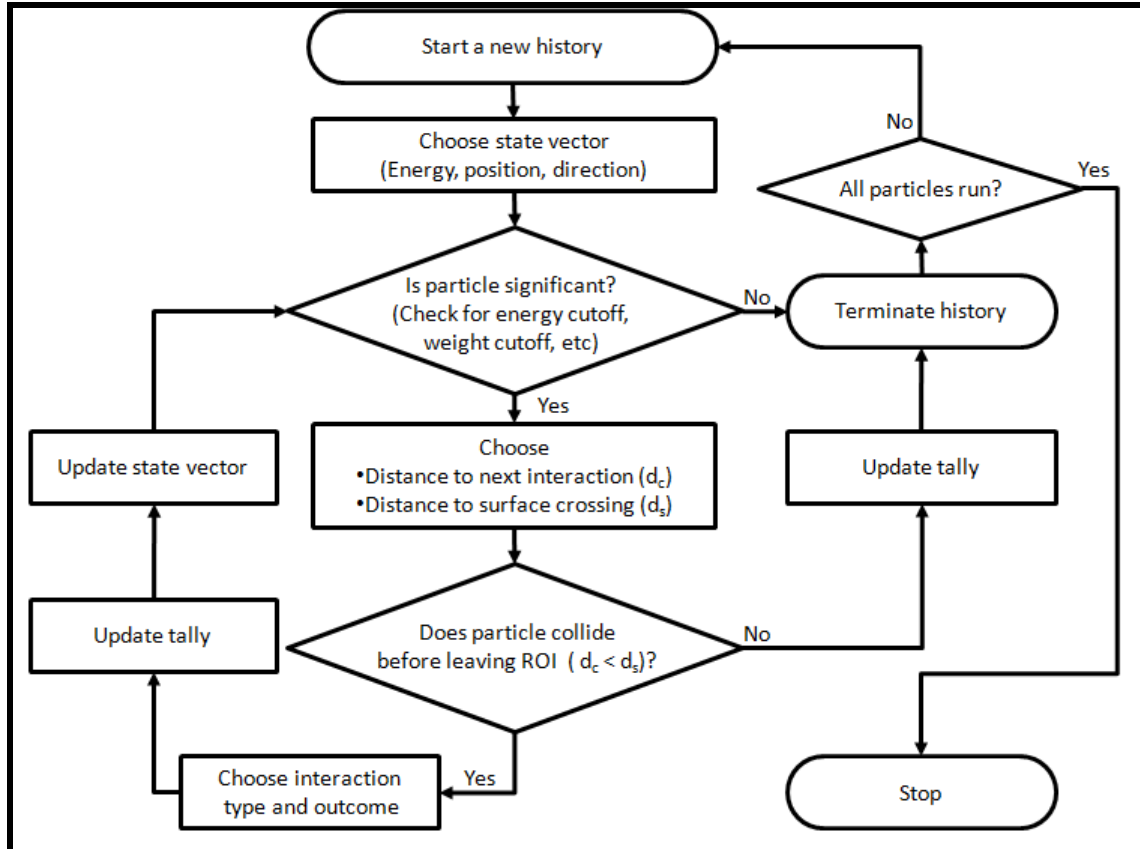


Figure 1.2: Flowchart showing typical steps in the Monte Carlo simulation of particle transport.

Several widely used Monte Carlo codes are available today. Among these, *Monte Carlo N-Particle eXtended (MCNPX)* is a code that is the most popular among nuclear engineers and the work at Rensselaer on organ dose calculations has involved this code for more than decade. The MCNPX code was made available in 1994 as a merger of MCNP 4B (Briesmeister 1997) and LaHET 2.8 (Prael RE and Madland DG 1995). It has a capability to support Monte Carlo simulations for multiple particles with the extended

range from eV to TeV. The 2.5.0 version of MCNPX added more standard features to describe voxel geometry for radiation transport simulation (Pelowitz 2005). MCNPX code is capable to handle any 3D geometry constructed by CSG modeling. The MCNPX code has been successfully used for various applications in nuclear engineering (designing and shielding nuclear energy systems for nuclear reactors and particle accelerators) and health physics and medical physics radiotherapies, dosimetry, medical imaging). Especially, in our work on computational phantoms, the output tally and geometry definitions in the MCNPX are effectively used for the simulations of the stylized and voxel-based geometries.

1.4 Objectives and Tasks

Computational phantoms of the human body are important tools used to assess organ doses in diverse radiation protection applications. The research development has shown a strong trend towards phantoms of size- and posture-adjustable, heterogeneous tissue structures that are sharply different from the stylized, rigid phantoms. The long term objective of this PhD research project was to take advantage of the experience we have accumulated since early 1990s and to demonstrate for the first time the feasibility of developing full automated deformable phantoms. The research was designed to address several technological issues:

- To investigate the methodologies behind the polygonal mesh modeling such as mesh preprocessing, volume calculation, deformation algorithm, collision detection and correction algorithm.
- To develop a pair of polygonal mesh-based deformable adult male and female phantoms those are representative of 50th-percentile populations.
- To derive and evaluate a comprehensive listing of anthropometric parameters for the whole-body covering the 5th to the 95th percentiles of the population using statistical data on the height and weight from the National Health and Nutrition Examination Survey (NHANES).

- To derive and evaluate internal organ percentile data covering the 5th to the 95th percentiles using data from the ICRP Publication 23 and 89, as well as various organ measurement reports.
- To demonstrate the feasibility of developing deformable phantoms by transforming the 50th-percentile phantoms into new phantoms of various sizes and postures.
- To apply these newly created deformable phantoms to Monte Carlo-based radiation dose simulations using the MCNPX code.

1.5 Organization of the Ph.D. Dissertation

Chapter 1 introduces basic concepts and provides a historical review of computational phantoms used for radiation protection dosimetry.

Chapter 2 focuses on the methods and algorithms used to develop the deformable RPI-AM and RPIAF phantoms representing reference 50th-percentile populations of adults. This chapter also describes methods to create percentile-specific and posture-specific phantoms that are based on the 50th-percentile phantoms and software-based deformation algorithms.

Chapter 3 summarizes the detailed anatomical structures of the deformable RPI adult phantoms.

Chapter 4 demonstrates the use of Monte Carlo code to calculate organ doses in these deformable phantoms including the preparation and implementation of the phantom data in the MCNPX code.

Chapter 5 summarizes the research project and presents conclusions with discussions about future research.

Appendix A tabulates a large number of organ/tissue data for the 50th-percentile RPI adult phantoms in Tables A.1 and A.2.

Appendix B describes the organ-specific percentile data for major internal organs according to the organ ID numbers. The organ volume and mass values and the mesh-based anatomical structures are listed to easily compare with information in Tables B. 1-34 and Figure B. 1-24.

2. Methods to Develop Deformable Phantoms

Size- and posture-adjustable phantoms are computational models of the human body that have the ability to automatically or semi-automatically deform in order to define various organ shapes and volumes, as well as body postures. This type of deformable phantoms has been recently found to be easier to develop with BREP geometry definition methods in the form of either NURBS, polygon mesh, or a combination of both (Xu et al. 2007). Compared to voxel models, BREP models are better suited for geometry deformation and adjustment because a richer set of computerized operations can be utilized. These operations include extrusion, chamfering, blending, drafting, shelling and tweaking. One of the most attractive applications of adjustable phantoms is their ability to “morph” into an existing reference phantom or into a new anatomy of a worker or patient for whom there does not exist sufficient whole-body image data.

This chapter describes the primary methodologies to develop a pair of adult male and female deformable phantoms and the associated automatic geometry deformation algorithms.

2.1 50th-Percentile Adult Phantoms

Strategically, a so-called “deformable phantom” should include two components in the dataset: (1) a reference phantom with anatomical parameters that match reference values for “average” individuals having the 50th-percentile population body sizes defined by the ICRP; (2) a software program that automatically morphs the reference phantom into a different phantom having other percentiles defined by a set of new anatomical parameters. Although in principle any solid-geometry structure is a likely candidate, polygon meshes were employed in this project because they offer high anatomical fidelity and computational efficiency. Polygonal meshes are composed of a set of vertices, edges, and faces that identify the shape of a polyhedral object in 3D. A mesh surface is defined by a series of connected polygon-shaped faces, most commonly triangles. Each face is made up a certain number of linear edges which are in turn defined by two vertices, as illustrated previously in Figure 1.1. This data structure allows

very complex geometries such as human organs and the body surfaces to be described in sufficient anatomical detail without overwhelming a computer.

In sections below, the development of a pair of ICRP 50th-percentile adult male and female phantoms is discussed. The organ deformation methods include a collision detection algorithm as part of the automatic mesh deformation computational process. This is followed by a description of the voxelization process which prepares the deformed mesh phantoms for Monte Carlo calculations.

Figure 2.1 illustrates the general steps in designing and applying deformable mesh-based phantoms. The process starts with initial anatomical mesh-files that were chosen as primary 3D organ surface models. A key step of this process is to match the surfaces of these primary organ meshes with the ICRP references (or other anatomies in other applications) for the 50th-percentile populations. To avoid introducing surface overlaps between adjacent organs, an automatic collision detection and correction algorithm was included as a very important part of the development of a deformable phantom. This pair of phantoms is expected to satisfy the current radiation protection dosimetry paradigm established on the “Reference Man” concept and the deformable mesh-based computational phantoms contain 50th-percentile anatomical parameters defined by the ICRP for average populations (ICRP 1975, ICRP 2002).

As ICRP-compatible reference phantoms, the mesh-based deformable adult male and female phantoms, RPI-AM and RPI-AF, were developed. These phantoms are in agreement with the ICRP-89 50th-percentile adult males and adult females. Moreover, the whole body frame can be deformed to represent various whole-body percentiles and portion-body anatomical features such as postures and breast sizes using local mesh deformation procedures.

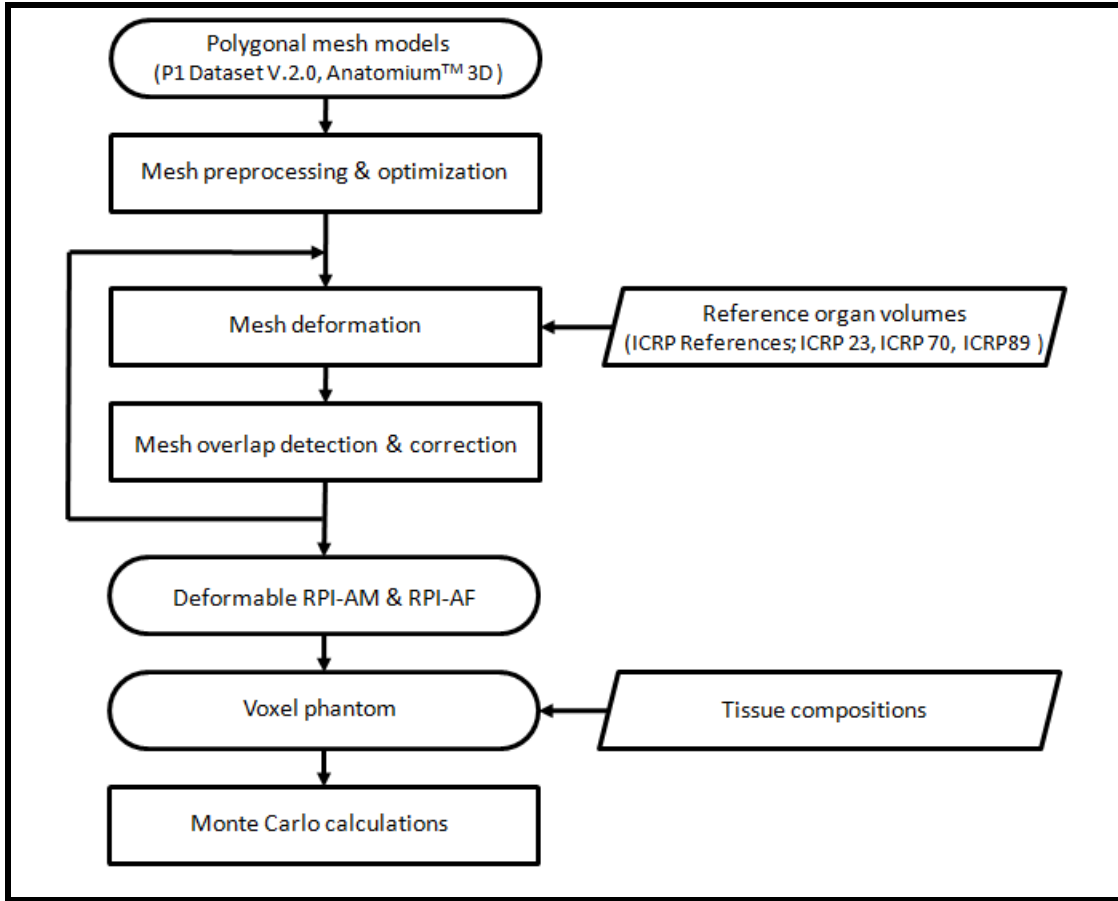


Figure 2.1: Flowchart of the process used to develop the deformable RPI-AM and RPI-AF phantoms.

Since most of the Monte Carlo codes do not currently handle the BREP-type of geometries directly, a mesh-based phantom needs to be converted to voxels for Monte Carlo dose calculations. The final step of this workflow is to link the voxel phantom with correct tissue density and elemental composition information so that radiation transport through the human-body phantom is modeled correctly in a Monte Carlo code.

2.1.1 Primary Anatomical Organ Mesh Models

In the past, mesh-based organ models have been created from the VIP-Man and other anatomical images developed at Rensselaer. The creation of such mesh models requires extremely time-consuming anatomical modeling and verification at the organ level. The commercially available Anatomium™ 3D (www.anatomium.com) male and

female mesh models were adopted as the base anatomical models in this project. This set of mesh data consists of 140 internal organs and skeletal structures (out of a possible 500 in the dataset) that were reportedly derived from CT image data. The mesh models were refined by computer graphics modelers with the help of clinical anatomists to ensure anatomical accuracy. The most significant benefits of employing such dataset are following: (1) this data represents up-right standing posture in which the gravitational effects on organs and skins are similar to those of a real worker; (2) The dataset covers the whole-body while most medical images only cover partial body.

In this dataset, the topological information of each organ was stored in a common triangular mesh-file format known as the Wavefront Object (OBJ). Individual organ mesh-files were collected and stored to establish two anatomical organ libraries: one for a male and one for a female with a main difference in gender-specific sex organs. A unique ID number was given to each organ in the male and female organ libraries. Table 2.1 summarizes the organs described in the male and female phantoms along with their corresponding ID numbers.

Table 2.1: List of organs for the mesh-based phantoms and their corresponding organ IDs.

ID	Organ / Tissue	ID	Organ / Tissue
1	Adrenal, left	69	Eye bulb, right
2	Adrenal, right	70	Gall bladder wall
3	Extrathoracic (ET)	71	Gall bladder contents
5	Oral mucosa, tongue	72	Stomach wall
7	Trachea	73	Stomach contents
8	Bronchi	75	Small intestine
9	Blood vessels, head	76	Ascending colon wall
10	Blood vessels, trunk	77	Ascending colon contents
11	Blood vessels, arms	78	Transverse colon wall, right
12	Blood vessels, legs	79	Transverse colon contents, right
13	Humeri, upper half, cortical	80	Transverse colon wall, left
14	Humeri, upper half, spongiosa	81	Transverse colon contents, left

15	Humeri, upper half, medullary cavity	82	Descending colon wall
16	Humeri, lower half, cortical	83	Descending colon contents
17	Humeri, lower half, spongiosa	84	Sigmoid colon wall
18	Humeri, lower half, medullary cavity	85	Sigmoid colon contents
19	Ulnae and radii:Ulnae and radii, cortical	86	Rectum wall
20	Ulnae and radii, spongiosa	87	Heart wall
21	Ulnae and radii, medullary cavity	88	Heart contents(blood)
22	Wrists and hand bones, cortical	89	Kidney, left, cortex
23	Wrists and hand bones, spongiosa	90	Kidney, left, medulla
24	Clavicles, cortical	91	Kidney, left, pelvis
25	Clavicles, spongiosa	92	Kidney, right, cortex
26	Cranium, cortical	93	Kidney, right, medulla
27	Cranium, spongiosa	94	Kidney, right, pelvis
28	Femora, upper half, cortical	95	Liver
29	Femora, upper half, spongiosa	97	Lung, left, tissue
30	Femora, upper half, medullary cavity	99	Lung, right, tissue
31	Femora, lower half, cortical	100	Lymphatic nodes, extrathoracic airways
32	Femora, lower half, spongiosa	101	Lymphatic nodes, thoracic airways
33	Femora, lower half, medullary cavity	102	Lymphatic nodes, head
34	Tibiae, fibulae and patellae, cortical	103	Lymphatic nodes, trunk
35	Tibiae, fibulae and patellae, spongiosa	104	Lymphatic nodes, arms
36	Tibiae, fibulae and patellae, medullary cavity	105	Lymphatic nodes, legs
37	Ankles and foot bones, cortical	106	Muscle, head
38	Ankles and foot bones, spongiosa	107	Muscle, trunk
39	Mandible, cortical	108	Muscle, arms
40	Mandible, spongiosa	109	Muscle, legs
41	Pelvis, cortical	110	Oesophagus
42	Pelvis, spongiosa	111	Ovary, left(female only)
43	Ribs, cortical	112	Ovary, right(female only)
44	Ribs, spongiosa	113	Pancreas
45	Scapulae, cortical	114	Pituitary gland
46	Scapulae, spongiosa	115	Prostate(male only)
47	Cervical spine, cortical	119	Residual tissue
48	Cervical spine, spongiosa	120	Salivary glands, left
49	Thoracic spine, cortical	121	Salivary glands, right

50	Thoracic spine, spongiosa	125	Skin
51	Lumbar spine, cortical	126	Spinal cord
52	Lumbar spine, spongiosa	127	Spleen
53	Sacrum, cortical	128	Teeth
54	Sacrum, spongiosa	129	Testis, left(male only)
55	Sternum, cortical	130	Testis, right(male only)
56	Sternum, spongiosa	131	Thymus
58	Catilage	132	Thyroid
61	Brain	133	Tongue (inner part)
62	Breast, left, adipose tissue	134	Tonsils
63	Breast, left, glandular tissue	135	Ureter, left
64	Breast, right, adipose tissue	136	Ureter, right
65	Breast, right, glandular tissue	137	Urinary bladder wall
66	Eye lense, left	138	Urinary bladder contents
67	Eye bulb, left	139	Uterus(female only)
68	Eye lense, right	140	Air inside body

2.1.2 Anatomical References

To create phantoms that represent the characteristics of the ICRP Reference Man for the 50th-percentile population, a list of anatomical reference data was carefully compiled and later used to adjust the mesh-based organ models. The key information considered was the height and weight, as well as the mass, density, and elemental contents of individual organs—much of which was available from the ICRP Publication 89 (ICRP 2002). The recommend ICRP reference volume and mass values can be calculated from the mass and density data. Additional anatomical data from the VIP-Man phantom (Xu et al. 2000), the RPI-P series pregnant female phantoms(Xu et al. 2007), and the REX/REGINA (Schlattl et al. 2007, Zankl et al. 2007) were also considered in this project for the purposes of testing the ability for these mesh-based phantoms to flexibly deform into a different anatomy.

The following sections highlight the most important contributions to the subjects of the needs and the methods to process the primary anatomical mesh models according to the given anatomical references.

2.1.3 Algorithms to Match with Reference Anatomical Parameters

The polygonal mesh processing and the deformation algorithms were implemented by in-house MATLAB® 7.4 codes (<http://www.mathworks.com/>) with original Anatomium™ 3D models whose organ geometries were morphed to agree with the ICRP reference male and female organ mass/volume data within 0.5%, relative error. These mesh morphing algorithms were used to automatically preprocessing the Anatomium™ 3D P1 dataset to have unique mesh information in each of organ meshes and deform the whole meshes based on the ICRP reference without unwanted surface overlapping through the special mesh overlap avoiding process. After all of mesh deformation, the size-adjustable whole-body mesh-based phantoms were identified as RPI Adult Male and RPI Adult Female.

2.1.3.1 Mesh Preprocessing

Computer graphics literature suggests that 3D objects can be defined with specific types of meshes, such as manifold or non-manifold, connected or disconnected, and open or closed. Computational anatomical models, such as the Anatomium™ 3D dataset, have well-defined human anatomical shapes and structures, but the mesh geometries are not always conducive for morphing operations. In order to facilitate necessary procedures in this project, the organ geometries in the Anatomium™ 3D dataset were carefully preprocessed to ensure that they were all defined by connected and closed meshes. This was achieved through mesh triangulation and preprocessing methods described below.

The first step in mesh triangulation is to index each of the three vertices of every triangular face in the organ mesh in a counterclockwise fashion (i.e., loop₁: $V_3 \rightarrow V_1 \rightarrow V_2$, loop₂: $V_4 \rightarrow V_3 \rightarrow V_2$, loop₃: $V_4 \rightarrow V_2 \rightarrow V_5$). The directions of triangular surface normals can then be determined by the right-hand rule as demonstrated in Figure 2.2. This ensures that the surface normals, $\vec{N}_{3,1,2}$, $\vec{N}_{4,3,2}$, and $\vec{N}_{4,2,5}$ of triangles $\triangle V_3V_1V_2$, $\triangle V_4V_3V_2$, and $\triangle V_4V_2V_5$, are oriented in a consistent outward-pointing direction (when looking at the mesh geometry from the outside) (Beall and Shephard 1997). Another requirement of a mesh is that common edges, such as V_3V_2 and V_2V_4 , should be

associated with loops which traverse them in opposite directions (i.e., In loop₁ and loop₂, the edge $\overline{V_2V_3}$ is traversed in opposite directions; $V_2 \rightarrow V_3$ versus $V_3 \rightarrow V_2$. Likewise, in loop₂ and loop₃, the edge $\overline{V_2V_4}$ is traversed in opposite directions; $V_2 \rightarrow V_4$ versus $V_4 \rightarrow V_2$). If these requirements do not hold, the mesh is called “open” because this signifies the presence of a “hole” or a “bad connection.” The opposite of an “open” mesh is a “closed” mesh. The distinction between an open and closed mesh is important because the volume of organ mesh geometries is only well-defined if they are described by closed surfaces (Ohbuchi et al. 2003, Jain and Zhang 2007). The aforementioned preprocessing methods ensure that all of the organ meshes in the two phantom libraries were ready for the later steps described below.

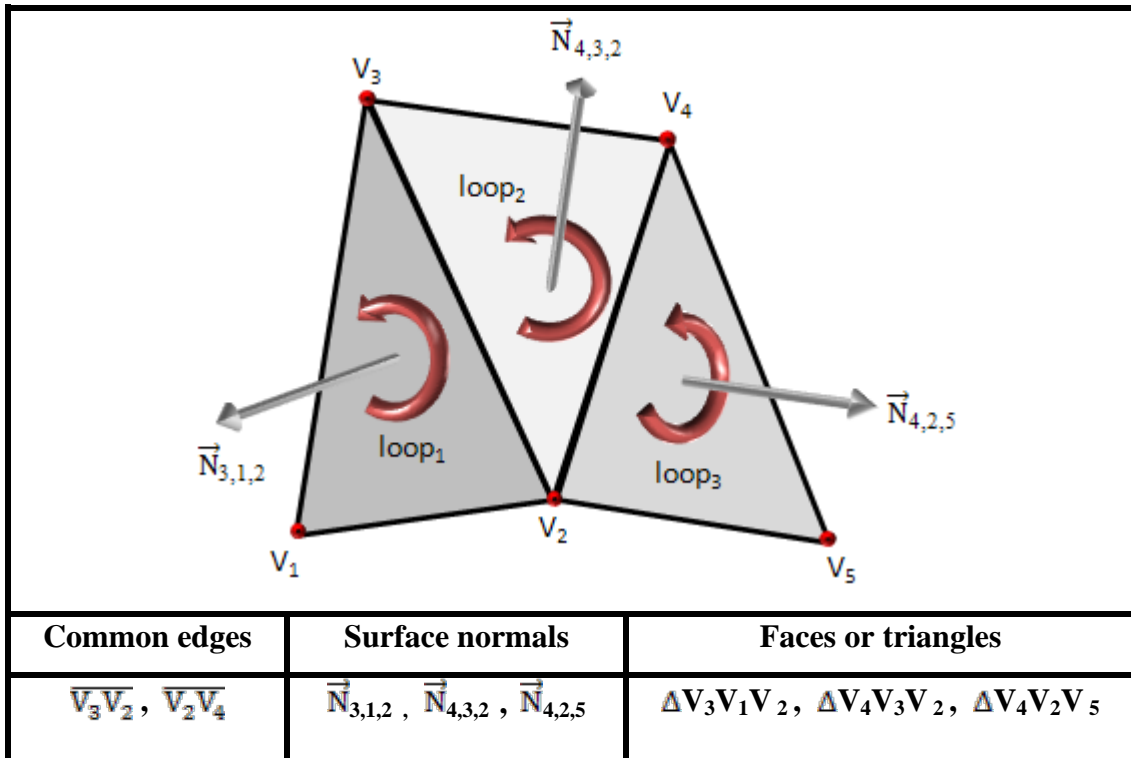


Figure 2.2: Topology involving vertex numbering and triangular surface normals.

Figure 2.3 compares the mesh quality of the mandible and teeth before and after the mesh preprocessing. In this example, the original mesh file for the “mandible and teeth” has a total of 32,622 vertices among which 8.85% are found to be duplicated and a total

of 61,640 faces among which 2.82% are found to be duplicated, leading to many holes and cracks as illustrated in Figure 2.3a. Through the mesh preprocessing, the problematic open-meshes were carefully corrected. Figure 2.3b shows the corrected meshes that yield smooth surfaces.

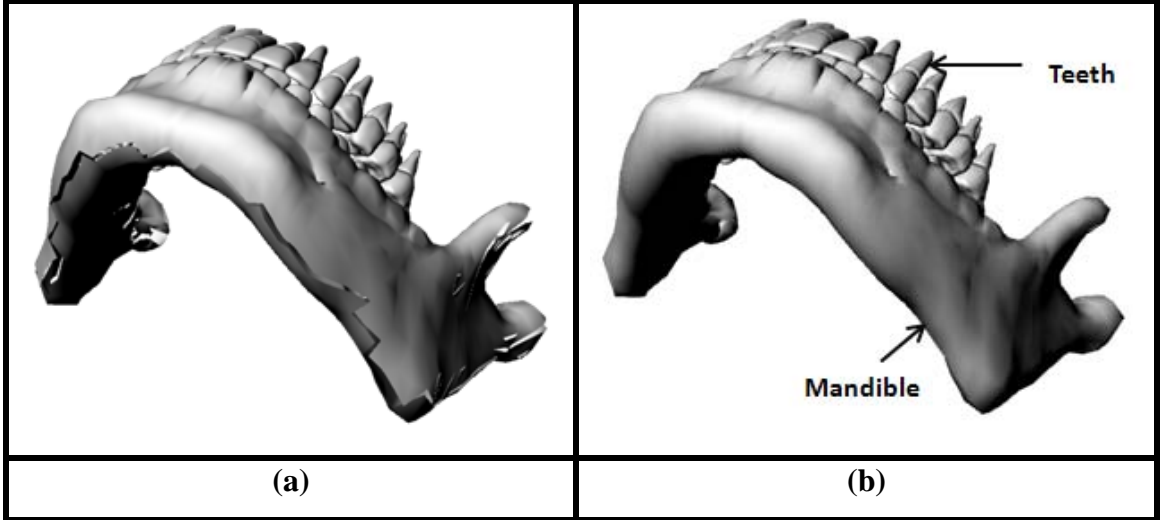


Figure 2.3: Comparison of mesh quality with and without mesh preprocessing of the mandible and teeth: (a) Before the pre-processing the meshes have a lot of surface cracks; (b) The corrected meshes are closed and result in smooth surfaces.

2.1.3.2 Mesh Volume Calculation

For a solid volume of 3D organ meshes, the surface normals of each face must all be oriented in the outward pointing direction as described in the section above. The key to calculating the volume defined by a triangular mesh is to decompose it into several elementary tetrahedrons (Ohanian 2005). Figure 2.4 depicts an example of a mesh volume calculation involving a simplest polyhedron, a tetrahedron, with vertices. Note how the geometry is decomposed into four different tetrahedrons with the same origin V_0 which is {0, 0, 0}: $\{V_0, V_1, V_3, V_2\}$, $\{V_0, V_1, V_2, V_4\}$, $\{V_0, V_3, V_2, V_4\}$, and $\{V_0, V_3, V_1, V_4\}$.

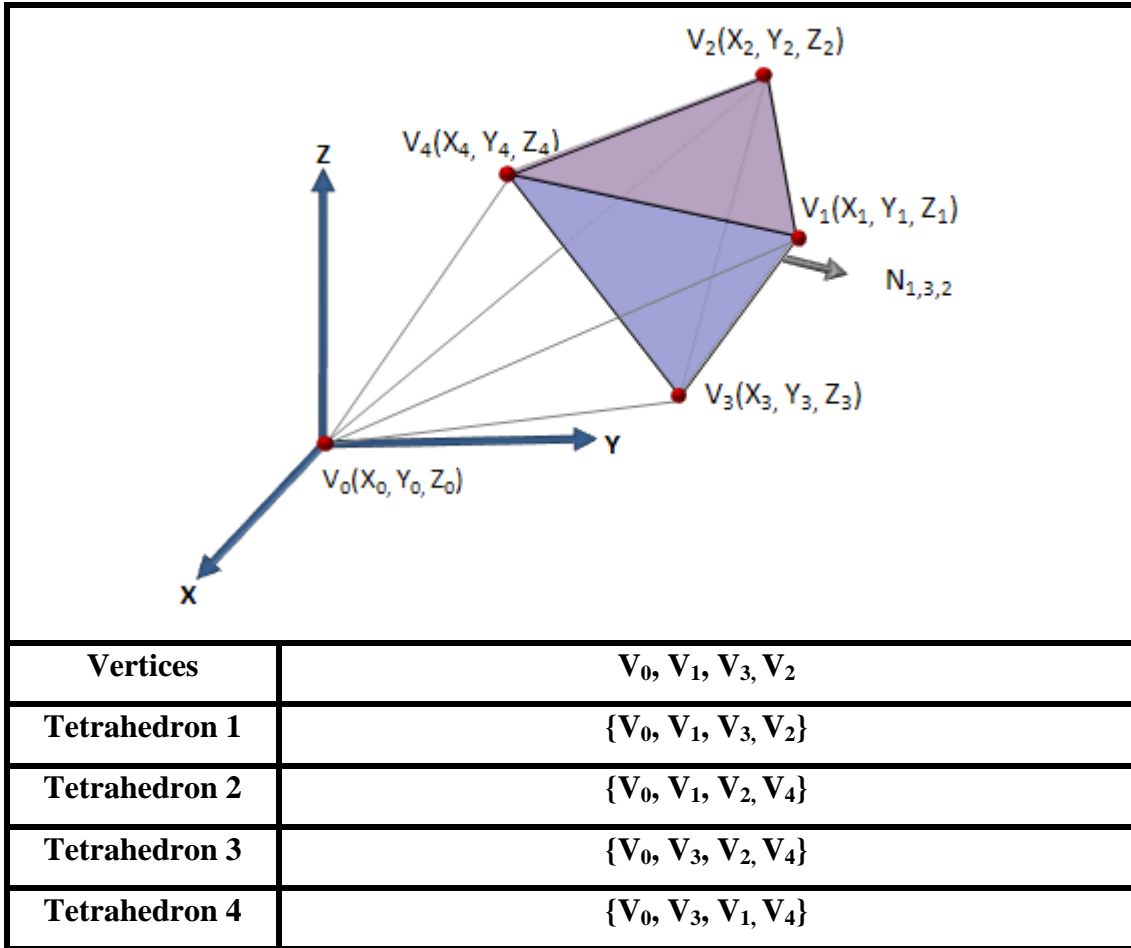


Figure 2.4: Example of a simple polyhedron geometry (V_0 is $\{0, 0, 0\}$).

The volume of a single tetrahedron, $\{V_0, V_1, V_3, V_2\}$, can then be calculated with the following equation:

$$|Volume_{V_{0,1,3,2}}| = \left| \frac{1}{6} (-X_3 Y_2 Z_1) + X_2 Y_3 Z_1 + X_3 Y_1 Z_2 - X_1 Y_3 Z_2 - X_2 Y_1 Z_3 + X_1 Y_2 Z_3 \right|$$

(2.1)

In general, to calculate the volume of a closed triangular mesh of arbitrary shape, it can be decomposed into many tetrahedral sub-volumes. Then by using Equation 2.1, the sums over the volumes of each of these tetrahedrons to obtain the volume of the original triangular mesh. The total volume of the triangular mesh is given by the following equations:

$$Volume_{Vi'} = \frac{1}{6} (-X_{i3}Y_{i2}Z_{i1} + X_{i2}Y_{i3}Z_{i1} + X_{i3}Y_{i1}Z_{i2} - X_{i1}Y_{i3}Z_{i2} - X_{i2}Y_{i1}Z_{i3} + X_{i1}Y_{i2}Z_{i3})$$

$$Volume_{Vt'} = \sum_i Volume_{Vi'}$$

(2.2)

where, i is the index of elementary tetrahedrons or triangles. Triangle i has the coordinates of vertices, $\{V_{i1}, V_{i2}, V_{i3}\}$, $\{V_{i2}, V_{i3}, V_{i1}\}$, and $\{V_{i3}, V_{i1}, V_{i2}\}$ which are ordered in such a way that the triangle surface normals are consistent with each other (Zhang and Chen 2001).

2.1.3.3 Mesh Deformation Algorithm

After the mesh volume calculations have been performed, each mesh is ready for deformation according to a user-defined algorithm. In order to match internal organ volume to the ICRP recommended values (ICRP 1975, ICRP 2002), three different adjustment approaches to the mesh deformation are considered as follows: (1) uniform scale factor adjustment: displacement of each vertex point by a uniform scale factor in relation to the organ centroid, which keeps the overall mesh shape, but scales the volume; (2) unique scalar factor adjustment: translation of each vertex point along the direction of vertex normals by a unique scalar factor. In this approach, every vertex point was aligned as an origin of a single ray. Then, the distance between the origin and the reflecting point of the ray on an adjacent organ surface was calculated to determine whether the vertex could be relocated in the same direction of the ray. The unique scalar factor of each vertex was applied to relocate deforming vertex; (3) specific mesh-based deformation: tracking of mesh surface geometry by a union of direction vectors at the center of each vertex of the polygonal mesh using ray casting algorithm (Arthur 1968). This approach is used for deforming the primary organ meshes to person-specific organs collected from scanned image data using general radiological modalities (i.e., CT, MRI, Ultrasonography).

In our applications, the 2nd approach was primarily used first for the deformation of the skeletal structures to obtain proper position and reference volume information, and then deforming the other organs in a priority order while checking for collisions with the

skeleton and each other as described below. The priority list is headed by the internal organs of the chest and abdomen and followed by the minor organs and distributed tissues such as muscle and fat. In each of deformation operations, the magnitudes of the deformation are chosen until an “acceptance criteria” meets 0.5% relative error between the deformed organ mesh volume and the ICRP recommended values for all organs except the eye lens (about 3%). To achieve this small a volume error, both the uniform scale factor and the unique scalar were evaluated using the Newton’s method, a well-known numerical analysis iterative technique (Deuflhard 2004). A solution, which satisfies the acceptance criteria, could take a minimal computational cost. Once the desired mesh volume and deformation factors had been chosen for a user-defined “acceptable error,” all the organ mesh were automatically deformed accordingly to account for this change in volume. The center of mass of each organ does not change during this deformation process. Figure 2.5 demonstrates the visual difference between the uniform scale factor adjustment and unique scalar factor adjustment.

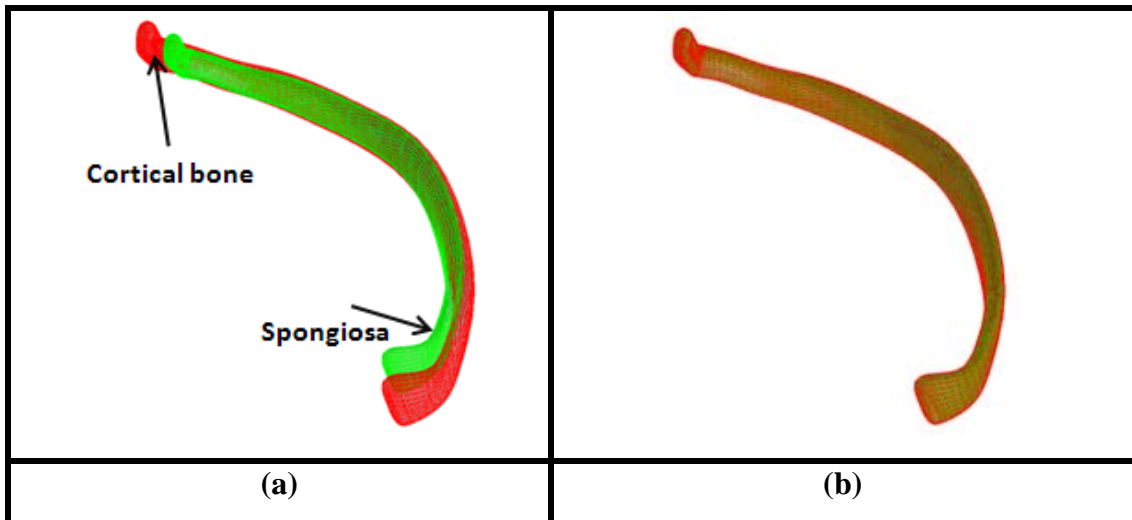


Figure 2.5: Comparisons of scale adjustment and vertex normal adjustment using an example of the 7th rib spongiosa (inner mesh) that is created by the 7th cortical rib (outer mesh): (a) When the 7th cortical bone (outer mesh) was deformed by the uniform scale factor, the result of the spongiosa mesh is not located inside the cortical rib mesh; (b) Using the unique scalar factor to each of vertex normals, the deformed mesh (spongiosa) fits the inside of cortical bone.

The specific mesh-based deformation method is described in Figure 2.6 with an example of the primary mesh model's right kidney and the person-specific right kidney. The final deformed kidney shape is indistinguishable from the person-specific kidney, but the primary mesh geometry is still preserved.

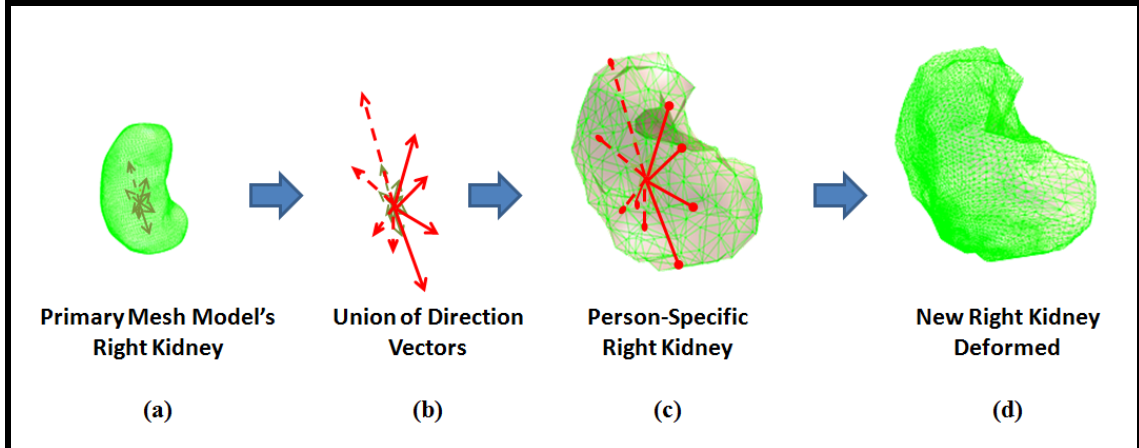


Figure 2.6: Primary mesh model's kidney deformation to person-specific kidney using specific mesh-based deformation method: (a) vectorizations of direction vectors from the center of mesh to the end of each vertex; (b) union of the direction vectors; (c) extension of the direction to reach the person-specific mesh surface with detecting of all intersectional points using ray casting algorithm; (d) rearrangement the new vertices and faces based on the intersected points and original faces information.

2.1.3.4 Collision Detection to Avoid Organ Overlaps

During the deformation process, the proximity of mesh surfaces must be considered to avoid unwanted mesh overlaps since each mesh-based phantom contains more than 70 organs (i.e., tissues, contents) and 45 bone structures (cortical bone, spongiosa, medullary cavity). The ray-casting method (Amanatides and Choi 1997) was used to avoid surface collisions by examining the distance between adjacent vertices in two different organ meshes. In this approach, every vertex point was designated as an origin of a single ray with the normal pointing at the other organ surface, as shown in Figure

2.7. Then, the distance between the origin and the reflecting point of the ray on an adjacent organ surface was calculated. Two surfaces are considered to be in a collision if the distance between two vertices on each of the mesh-surfaces is less than a pre-determined value, such as 3 mm used for this project, as shown in Figure 2.7. After a surface collision has been detected, the colliding vertex (denoted as a \otimes mark in Figure 2.7) stops in that position and does not undergo further deformation. This process continues until the entire surface of each organ has been examined and the volume of the organ has matched with the given volume information.

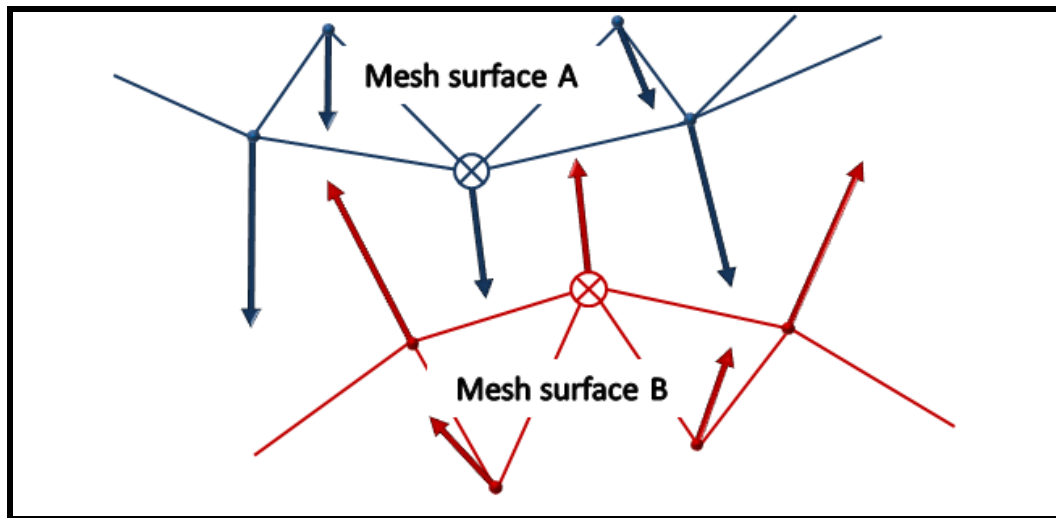


Figure 2.7: Illustration of the collision detection algorithm for Mesh surfaces A and B representing two organ surfaces. A collision event between two surfaces occurs when the distance between a vertex (labeled as \otimes) and the other surface along the normal (\uparrow or \downarrow) direction is less than a pre-determined value. The detection continues until all the vertices on both surfaces have been examined this way.

It must be noted that this procedure assumes that one of the two adjacent organs has a higher priority in a collision. The “priority organ” can expand its volume while the other organ gives away the space without changing its volume. Ideally, the organ deformation method should take into account of point-wise, physics-based tissue elasticity. In this project, however, the recommended ICRP organ density information

was used to decide the priority of deformation between two organ surfaces (i.e., a softer organ gives away the space in a collision). Figure 2.8 shows how the density is used to prioritize the deformation process involving the liver and the right lung. In this example, the bottom of the right lung which is less dense is pushed upward by the liver using the mesh deformation and collision detection methods.

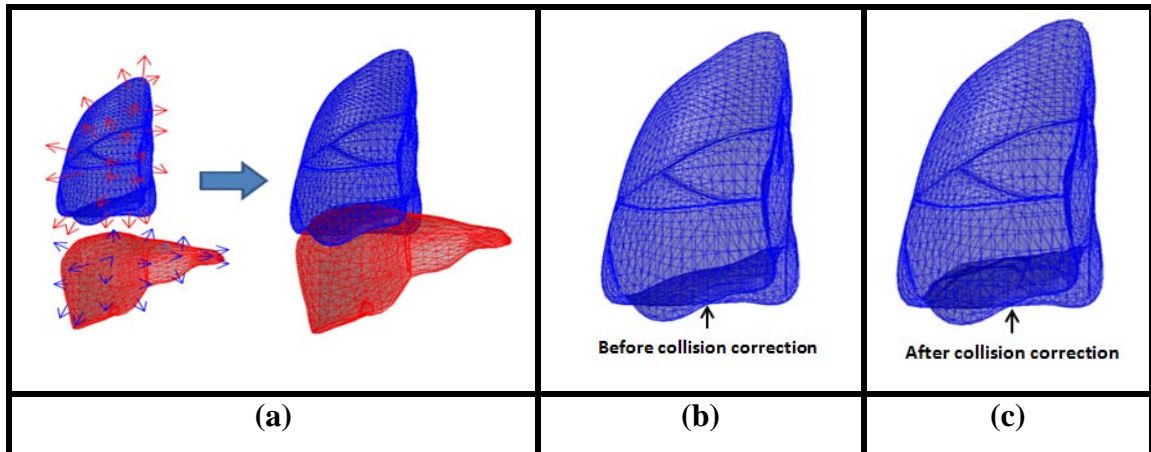


Figure 2.8: The right lung and liver both increase in volumes: (a) mesh deformation with vertex normal vectors; (b) with collision detection and correction methods; (c) with collision detection and correction methods; the bottom surface of the right lung, which has a lower density, is deformed and pushed upward by the adjacent liver after collision detection and deformation.

The algorithms were first developed and fine-tuned using the MATLABTM 7.4. Figure 2.9 shows detailed polygonal mesh deformation algorithm with collision detection and correction.

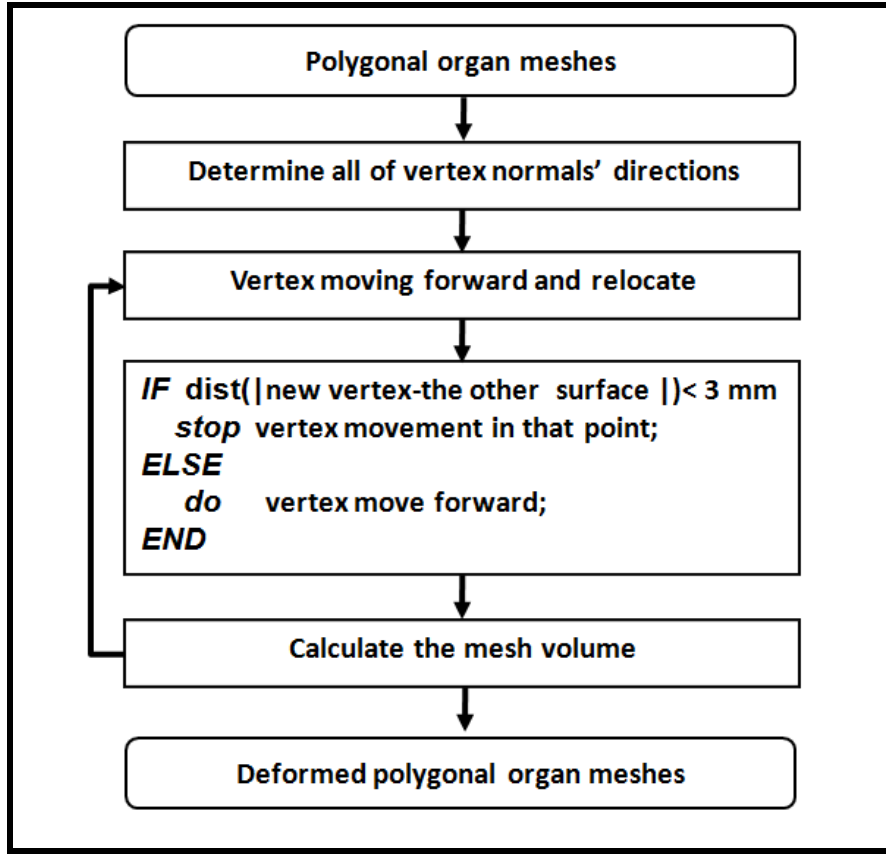


Figure 2.9: Polygonal mesh deformation with collision detection and correction.

2.1.3.5 Special Mesh Deformation Operations

Because several organs have very complex geometric shapes, a few specialized deformation maneuvers were required. Specialized procedures were applied for the skeleton, stomach, urinary bladder, intestines that consist of multiple outer-inner layers, or wall-contents structures. While a typical primary organ mesh consists of only one closed surface, these special anatomical structures must be described by a double-layer mesh surface. In addition, special procedures were used to adjust the breast size of the adult female mesh-model for virtual lung counting applications.

In order to describe these hollow organ geometries using both outer and inner layer structures in the mesh domain (see Figure 2.10a), the original meshes were first used to create the outer layer surface meshes according to the desired volume. Next, outer meshes are deformed to create the inner layer surface meshes through the deformation

and collision detection algorithms described above. For bone components, each part of the outer layer surface mesh (e.g., cortical bones) of the bone should be decomposed to two different types of inner bone meshes (spongiosa and cavities) before the deformation takes place. Eventually, each of the two finalized mesh-based adult male/female phantoms was defined by a total of 70 internal organs, 45 bone components and 4 muscle structures (458 mesh structures). Figure 2.10 shows an example of the detailed cortical bone, spongiosa contained red bone marrow, and medullary cavity cortical bone, as well as anatomically realistic muscles.

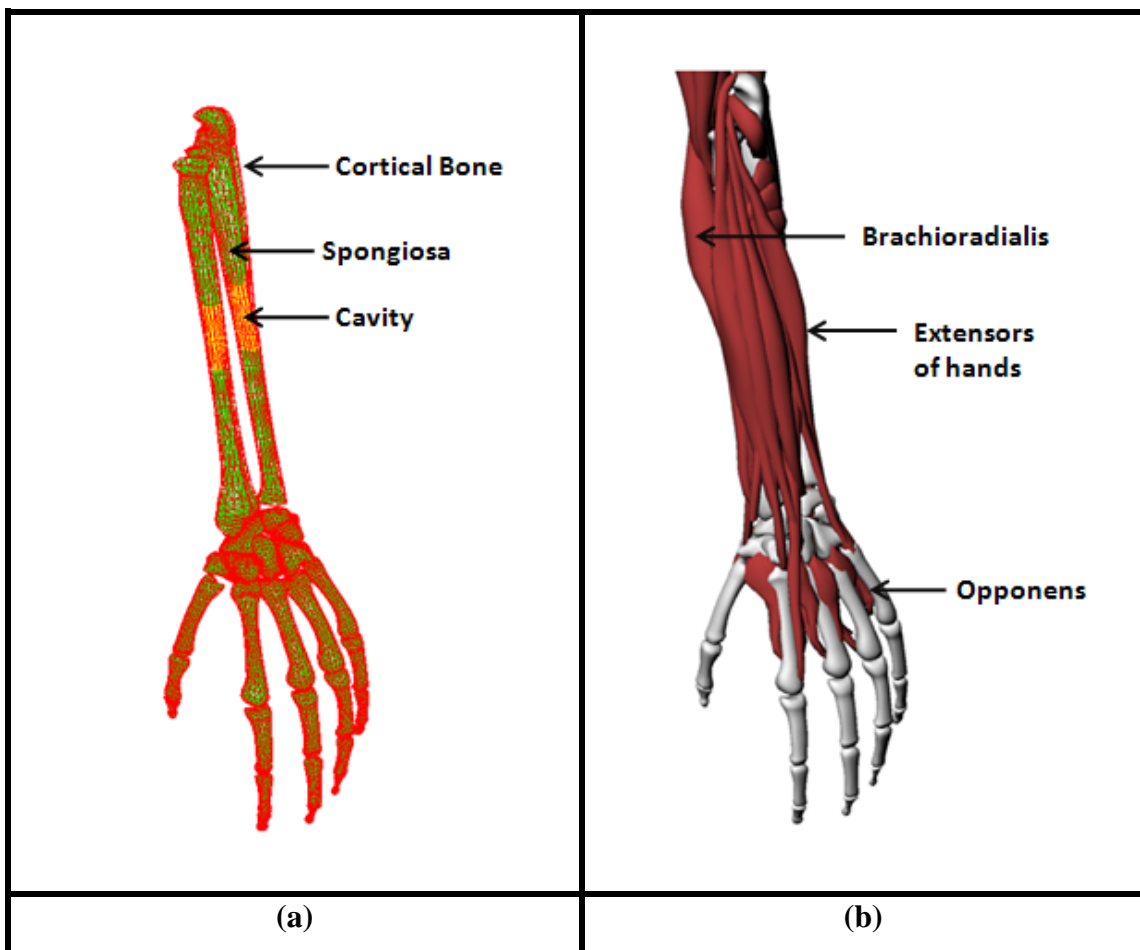


Figure 2.10: Special mesh deformation operations for certain organs and tissues:
(a) Arm bone structures; (b) Arm muscles.

2.2 Percentile-Specific Adult Phantoms

In this section, percentile-specific phantoms are described with a comprehensive listing of anthropometric parameters and internal organ volume/mass values that cover from the 5th to the 95th percentiles.

2.2.1 Deformation of the RPI-AM and RPI-AF Percentile Data

The deformable phantom dataset contains algorithms that were implemented in MATLAB® 7.4. The 50th-percentile phantom, RPI-AM and RPI-AF were used as the starting point for the development of percentile-specific adult male and female phantoms on demand. The mesh-based reference RPI-AM and RPI-AF phantoms were mainly deformed according to two different percentile data: (1) the whole-body size percentile data which were defined by the anthropometric parameters such as height and weight from the NHANES (McDowell et al. 2005); (2) individual internal organ percentile data which were derived by the cumulative pattern analysis based on the ICRP Publication 23 and 89 (ICRP 1975, ICRP 2002). These values are used to deform individual internal organs of the RPI-AM and RPI-AF phantoms into new ones to be assembled inside of new whole-body frames reshaped by the anthropometric data.

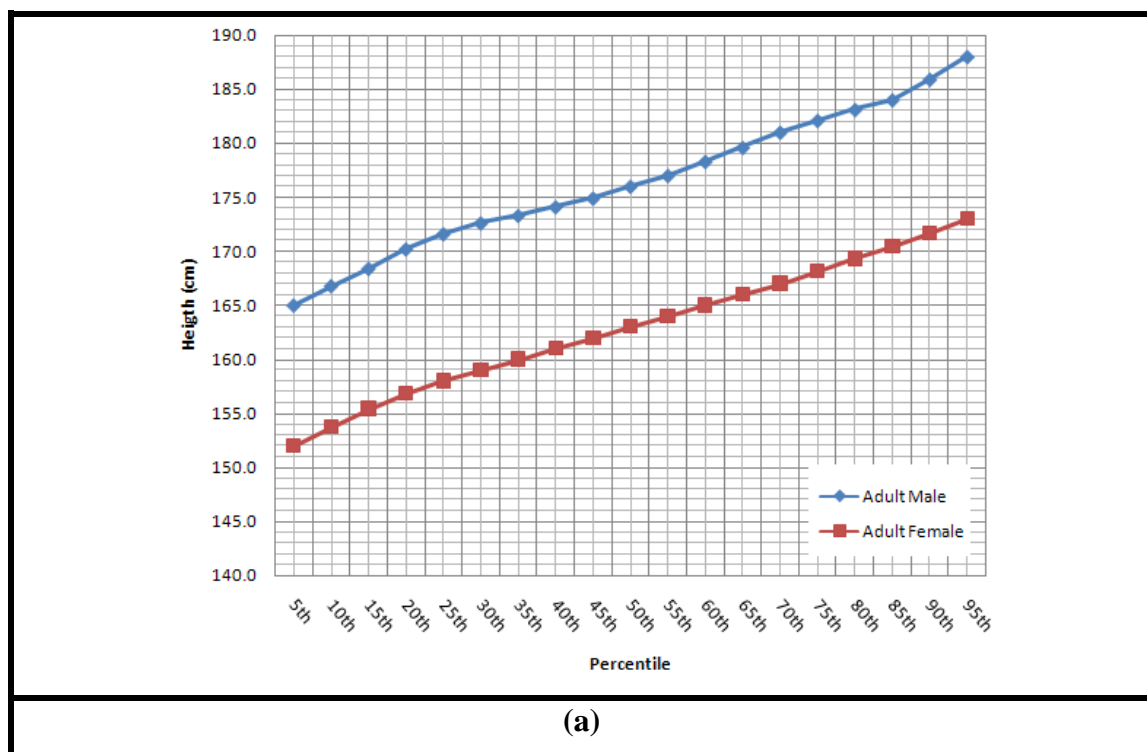
With employing the mesh deformation methods with collision detection and correction algorithms used for the development of the RPI-AM and RPI-AF mesh-based phantoms, the deformability of the mesh-based RPI reference phantoms were represented by transforming the phantoms into new percentile-specific series phantoms between 5th and 95th percentiles. Finally, these newly created phantoms were prepared for radiation transport simulations using the MCNPX code (Pelowitz 2005).

2.2.2 Definition of the Percentile-Specific Phantom Data

2.2.2.1 Percentiles of Whole-Body Sizes

The CDC has been performing periodical surveys of the U.S. population and the anthropometric reference data is available as the NHANES (1999-2002) (McDowell et al. 2005). The latest report released in 2005 provides the heights and weights percentiles for 5th, 10th, 15th, 25th, 50th, 75th, 85th, 90th, and 95th. The height and weight survey data from

the NHANES was adopted by this study as a primary reference for deforming the RPI-AM and RPI-AF phantoms beyond the 50th-percentile (McDowell et al. 2005). It was assumed that male and female computational phantoms may be needed to represent individual with heights and weights at every 5th-percentile increment between the 5th and 95th percentiles. Therefore, percentile data missing from the NHANES report was estimated using linear interpolation. The height and weight percentile data for deforming the RPI-AM and RPI-AF phantoms are shown in Figures 2.11a and 2.11b, respectively. According to this data, the whole-body sizes of the RPI-AM and RPI-AF mesh-based phantoms were adjusted by scale factor-based deformation method which was applied to the body frame of each reference phantom as well to the skeleton (including cortex, sponge, cavity bone divisions) and internal organs. During this scaling process, the skeleton and organs stayed with the body frame. Table 2.2 shows percentile values of whole-body sizes.



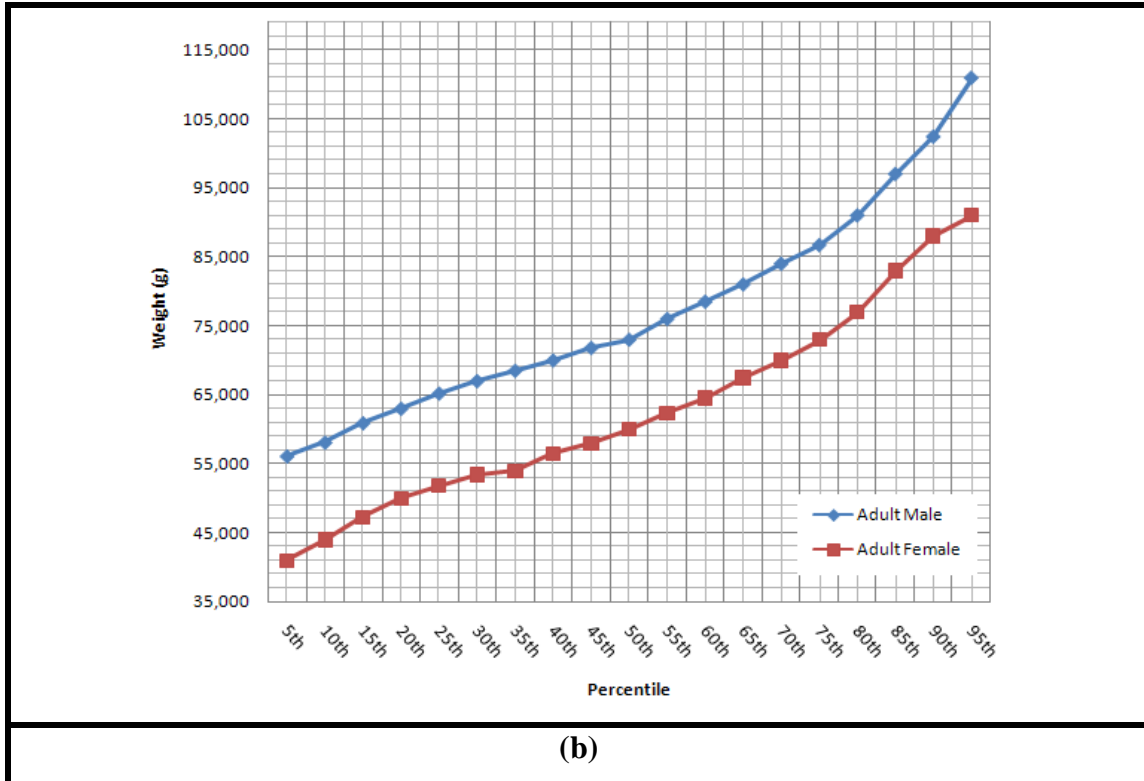


Figure 2.11: Height and weight percentiles for the RPI-AM and RPI-AF using data adapted from CDC (McDowell et al. 2005): (a) Height percentiles; (b) Weight percentiles.

Table 2.2: Percentile values of the RPI-Adult whole-body sizes.

Percentile	Adult Male			Adult Female		
	Height (cm)	Weight(g)	Volume (cm ³)	Height (cm)	Weight(g)	Volume (cm ³)
5th	165.0	56100	52430	152.0	41000	39423
10th	166.8	58100	54299	153.7	44000	42308
15th	168.4	60900	56916	155.4	47200	45385
20th	170.2	63000	58879	156.8	50000	48077
25th	171.6	65200	60935	158.0	51800	49808
30th	172.6	67000	62617	159.0	53400	51346
35th	173.3	68500	64019	160.0	54000	51923
40th	174.1	70000	65421	161.0	56500	54327
45th	174.9	71800	67103	162.0	58000	55769
50th	176.0	73000	68224	163.0	60000	57692

55th	177.0	76000	71028	164.0	62400	60000
60th	178.3	78500	73365	165.0	64500	62019
65th	179.6	81000	75701	166.0	67500	64904
70th	181.0	84000	78505	167.0	70000	67308
75th	182.1	86700	81028	168.2	73000	70192
80th	183.1	91000	85047	169.3	77000	74039
85th	184.0	97000	90654	170.5	83000	79808
90th	185.9	102400	95701	171.7	88000	84615
95th	188.0	110900	103645	173.0	91000	87500

2.2.2.2 Percentiles of Height-Dependent Weight

Figure 2.11 above does not include data for an individual whose height and weight differ both from the 50th percentiles. To take into account individuals having other height and weight, the Body Mass Index (BMI), defined by the CDC, is a convenient parameter:

$$\text{Body Mass Index (BMI)} = \text{Weight (kg)} / \text{Height (m}^2\text{)}$$

In this study, the body weight as a function of the height was estimated from the BMI values reported in the NHANES (1999-2002) (McDowell et al. 2005). Figure 2.12 represents the RPI-AM and RPI-AF phantom after the weight percentiles have been adjusted according to different heights. The percentile values of height-dependent weights are shown in Table 2.3 and 2.4 for the RPI-AM and RPI-AF, respectively. Due to the lack of data on the fat ratio of adult populations, the whole-body sizes were deformed first to match with the BMI values. The whole-body weight then was estimated using the hollow type of deformable skin surface meshes in accordance with the reference skin densities. After the total weight of all deformed internal organs have been finalized, the remainder was treated as the total body fat according to the following:

$$\text{Total Fat (kg)} = \text{Weight estimated from the hollow body skin surface} - \text{Total internal organ weight}$$

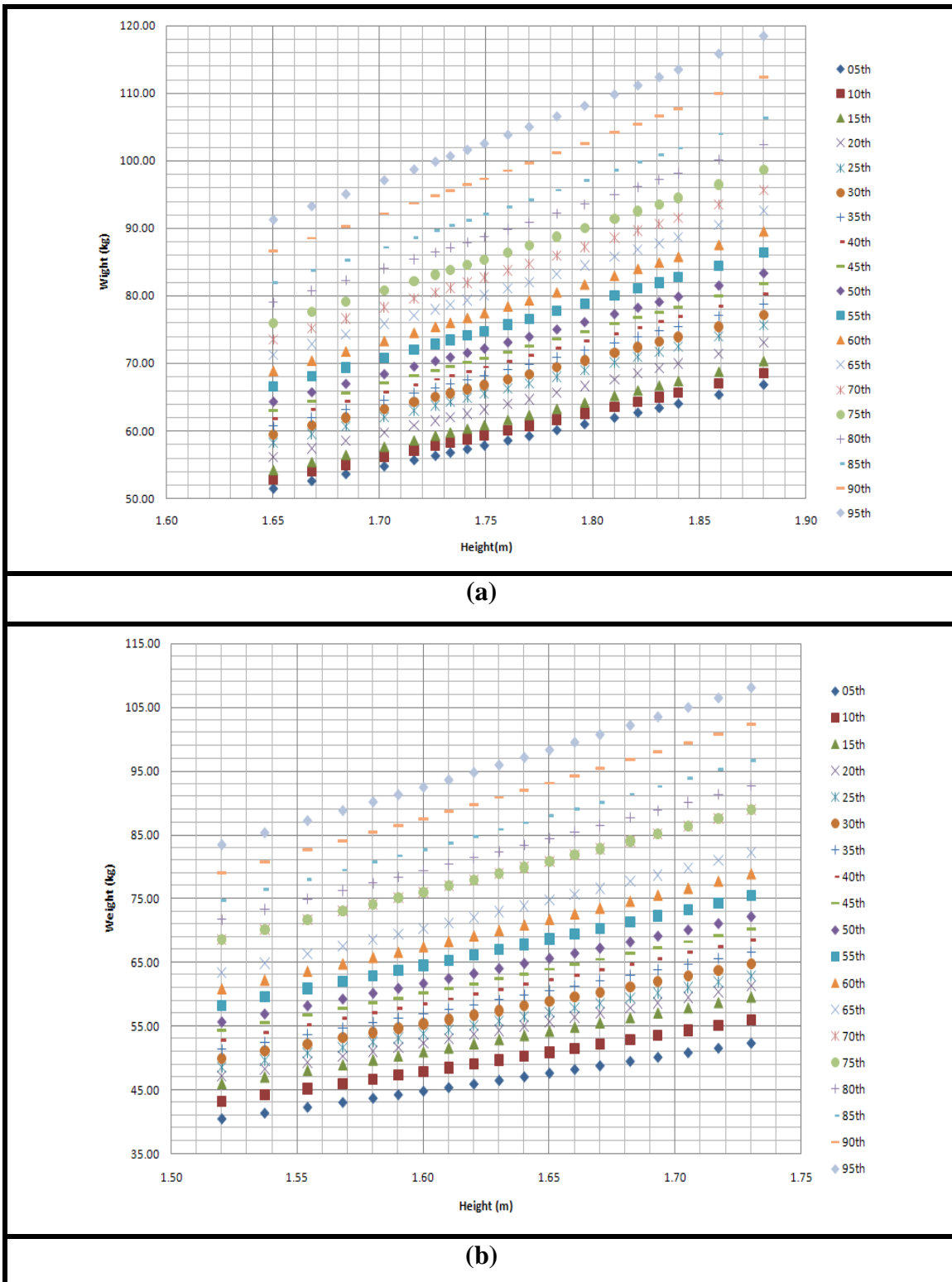


Figure 2.12: Weight percentiles upon different heights for the RPI-AM and RPI-AF using data adapted from CDC(McDowell et al. 2005): (a) RPI-AM; (b) RPI-AF.

Table 2.3: The RPI-AM weight percentiles based on the NHANES BMI.

Percentile		5th	10th	15th	20th	25th	30th	35th	40th	45th	50th	55th	60th	65th	70th	75th	80th	85th	90th	95th
	Height(m)	1.65	1.67	1.68	1.7	1.72	1.73	1.73	1.74	1.75	1.76	1.77	1.78	1.8	1.81	1.82	1.83	1.84	1.86	1.88
	BMI(kg/m ²)	Weight(kg)																		
5th	18.90	51.46	52.58	53.60	54.75	55.65	56.30	56.76	57.29	57.82	58.54	59.21	60.08	60.96	61.92	62.67	63.36	63.99	65.32	66.80
10th	19.40	52.82	53.98	55.02	56.20	57.13	57.79	58.26	58.80	59.34	60.09	60.78	61.67	62.58	63.56	64.33	65.04	65.68	67.04	68.57
15th	19.90	54.18	55.37	56.43	57.65	58.60	59.28	59.77	60.32	60.87	61.64	62.34	63.26	64.19	65.19	65.99	66.72	67.37	68.77	70.33
20th	20.65	56.22	57.45	58.56	59.82	60.81	61.52	62.02	62.59	63.17	63.97	64.69	65.65	66.61	67.65	68.48	69.23	69.91	71.36	72.99
25th	21.40	58.26	59.54	60.69	61.99	63.02	63.75	64.27	64.87	65.46	66.29	67.04	68.03	69.03	70.11	70.96	71.74	72.45	73.96	75.64
30th	21.84	59.46	60.76	61.94	63.27	64.31	65.06	65.59	66.20	66.81	67.65	68.42	69.43	70.45	71.55	72.42	73.22	73.94	75.48	77.19
35th	22.28	60.66	61.99	63.18	64.54	65.61	66.37	66.91	67.53	68.15	69.01	69.80	70.83	71.87	72.99	73.88	74.70	75.43	77.00	78.75
40th	22.72	61.86	63.21	64.43	65.82	66.90	67.68	68.23	68.87	69.50	70.38	71.18	72.23	73.29	74.43	75.34	76.17	76.92	78.52	80.30
45th	23.16	63.05	64.44	65.68	67.09	68.20	69.00	69.56	70.20	70.85	71.74	72.56	73.63	74.71	75.87	76.80	77.65	78.41	80.04	81.86
50th	23.60	64.25	65.66	66.93	68.36	69.49	70.31	70.88	71.53	72.19	73.10	73.94	75.03	76.12	77.32	78.26	79.12	79.90	81.56	83.41
55th	24.46	66.59	68.05	69.37	70.86	72.03	72.87	73.46	74.14	74.82	75.77	76.63	77.76	78.90	80.13	81.11	82.00	82.81	84.53	86.45
60th	25.32	68.93	70.45	71.80	73.35	74.56	75.43	76.04	76.75	77.45	78.43	79.33	80.49	81.67	82.95	83.96	84.89	85.72	87.50	89.49
65th	26.18	71.28	72.84	74.24	75.84	77.09	77.99	78.63	79.35	80.08	81.10	82.02	83.23	84.45	85.77	86.81	87.77	88.64	90.47	92.53
70th	27.04	73.62	75.23	76.68	78.33	79.62	80.55	81.21	81.96	82.72	83.76	84.71	85.96	87.22	88.59	89.67	90.65	91.55	93.45	95.57
75th	27.90	75.96	77.62	79.12	80.82	82.16	83.12	83.79	84.57	85.35	86.42	87.41	88.70	89.99	91.40	92.52	93.54	94.46	96.42	98.61
80th	29.00	78.95	80.68	82.24	84.01	85.40	86.39	87.10	87.90	88.71	89.83	90.85	92.19	93.54	95.01	96.17	97.22	98.18	100.22	102.50
85th	30.10	81.95	83.74	85.36	87.19	88.63	89.67	90.40	91.24	92.08	93.24	94.30	95.69	97.09	98.61	99.81	100.91	101.91	104.02	106.39
90th	31.80	86.58	88.47	90.18	92.12	93.64	94.73	95.50	96.39	97.28	98.50	99.63	101.10	102.57	104.18	105.45	106.61	107.66	109.90	112.39
95th	33.50	91.20	93.20	95.00	97.04	98.65	99.80	100.61	101.54	102.48	103.77	104.95	106.50	108.06	109.75	111.09	112.31	113.42	115.77	118.40

Table 2.4: The RPI-AF weight percentile based on the NHANES BMI.

Percentile		5th	10th	15th	20th	25th	30th	35th	40th	45th	50th	55th	60th	65th	70th	75th	80th	85th	90th	95th
	Height(m)	1.52	1.54	1.55	1.57	1.58	1.59	1.60	1.61	1.62	1.63	1.64	1.65	1.66	1.67	1.68	1.69	1.71	1.72	1.73
	BMI(kg/m ²)	Weight(kg)																		
5th	17.50	40.43	41.34	42.26	43.03	43.69	44.24	44.80	45.36	45.93	46.50	47.07	47.64	48.22	48.81	49.51	50.16	50.87	51.59	52.38
10th	18.70	43.20	44.18	45.16	45.98	46.68	47.28	47.87	48.47	49.08	49.68	50.30	50.91	51.53	52.15	52.90	53.60	54.36	55.13	55.97
15th	19.90	45.98	47.01	48.06	48.93	49.68	50.31	50.94	51.58	52.23	52.87	53.52	54.18	54.84	55.50	56.30	57.04	57.85	58.67	59.56
20th	20.45	47.25	48.31	49.39	50.28	51.05	51.70	52.35	53.01	53.67	54.33	55.00	55.68	56.35	57.03	57.86	58.61	59.45	60.29	61.20
25th	21.00	48.52	49.61	50.71	51.63	52.42	53.09	53.76	54.43	55.11	55.79	56.48	57.17	57.87	58.57	59.41	60.19	61.05	61.91	62.85
30th	21.62	49.95	51.07	52.21	53.16	53.97	54.66	55.35	56.04	56.74	57.44	58.15	58.86	59.58	60.30	61.17	61.97	62.85	63.74	64.71
35th	22.24	51.38	52.54	53.71	54.68	55.52	56.22	56.93	57.65	58.37	59.09	59.82	60.55	61.28	62.03	62.92	63.75	64.65	65.57	66.56
40th	22.86	52.82	54.00	55.20	56.20	57.07	57.79	58.52	59.26	59.99	60.74	61.48	62.24	62.99	63.75	64.67	65.52	66.45	67.39	68.42
45th	23.48	54.25	55.47	56.70	57.73	58.62	59.36	60.11	60.86	61.62	62.38	63.15	63.92	64.70	65.48	66.43	67.30	68.26	69.22	70.27
50th	24.10	55.68	56.93	58.20	59.25	60.16	60.93	61.70	62.47	63.25	64.03	64.82	65.61	66.41	67.21	68.18	69.08	70.06	71.05	72.13
55th	25.22	58.27	59.58	60.90	62.01	62.96	63.76	64.56	65.37	66.19	67.01	67.83	68.66	69.50	70.34	71.35	72.29	73.32	74.35	75.48
60th	26.34	60.86	62.22	63.61	64.76	65.76	66.59	67.43	68.28	69.13	69.98	70.84	71.71	72.58	73.46	74.52	75.50	76.57	77.65	78.83
65th	27.46	63.44	64.87	66.31	67.51	68.55	69.42	70.30	71.18	72.07	72.96	73.86	74.76	75.67	76.58	77.69	78.71	79.83	80.95	82.19
70th	28.58	66.03	67.52	69.02	70.27	71.35	72.25	73.16	74.08	75.01	75.93	76.87	77.81	78.76	79.71	80.86	81.92	83.08	84.26	85.54
75th	29.70	68.62	70.16	71.72	73.02	74.14	75.08	76.03	76.99	77.94	78.91	79.88	80.86	81.84	82.83	84.02	85.13	86.34	87.56	88.89
80th	31.00	71.62	73.23	74.86	76.22	77.39	78.37	79.36	80.36	81.36	82.36	83.38	84.40	85.42	86.46	87.70	88.85	90.12	91.39	92.78
85th	32.30	74.63	76.30	78.00	79.41	80.63	81.66	82.69	83.72	84.77	85.82	86.87	87.94	89.01	90.08	91.38	92.58	93.90	95.22	96.67
90th	34.20	79.02	80.79	82.59	84.08	85.38	86.46	87.55	88.65	89.75	90.87	91.98	93.11	94.24	95.38	96.76	98.03	99.42	100.82	102.36
95th	36.10	83.41	85.28	87.18	88.76	90.12	91.26	92.42	93.57	94.74	95.91	97.09	98.28	99.48	100.68	102.13	103.47	104.94	106.43	108.04

2.2.2.3 Percentiles of Internal Organs

After the whole-body size adjustments, most major organs were deformed by the given percentile organ data which were documented with reliable assumption. Each distribution of major internal organ volume and mass was assumed to follows the Gaussian normal distribution. The percentile data of each major internal organ was then derived from the cumulative pattern analysis in a normal distribution (Zelen and Seviro 1972). The Probability Density Function (PDF) of individual organ masses was derived from the given mean and standard deviation according to Equation 2.3. The Cumulative Distribution Function (CDF) in Equation 2.4 gives the probability that the random variable of the certain size of organs is less than or equal to the given percentile according to the PDF with Gaussian error function, as defined by Equation 2.5. The PDF was derived from the mean and standard deviation of volume and mass with the variation of each specific organ.

$$pdf = \frac{1}{\sigma\sqrt{2\pi}} e^{-\frac{(x-\mu)^2}{2\sigma^2}} \quad (2.3)$$

$$\Phi_{\mu,\sigma^2}(x) = \frac{1}{2} [1 + G(\frac{x-\mu}{\sigma})] \quad (2.4)$$

where, μ is the mean value, σ is the standard deviation (SD).

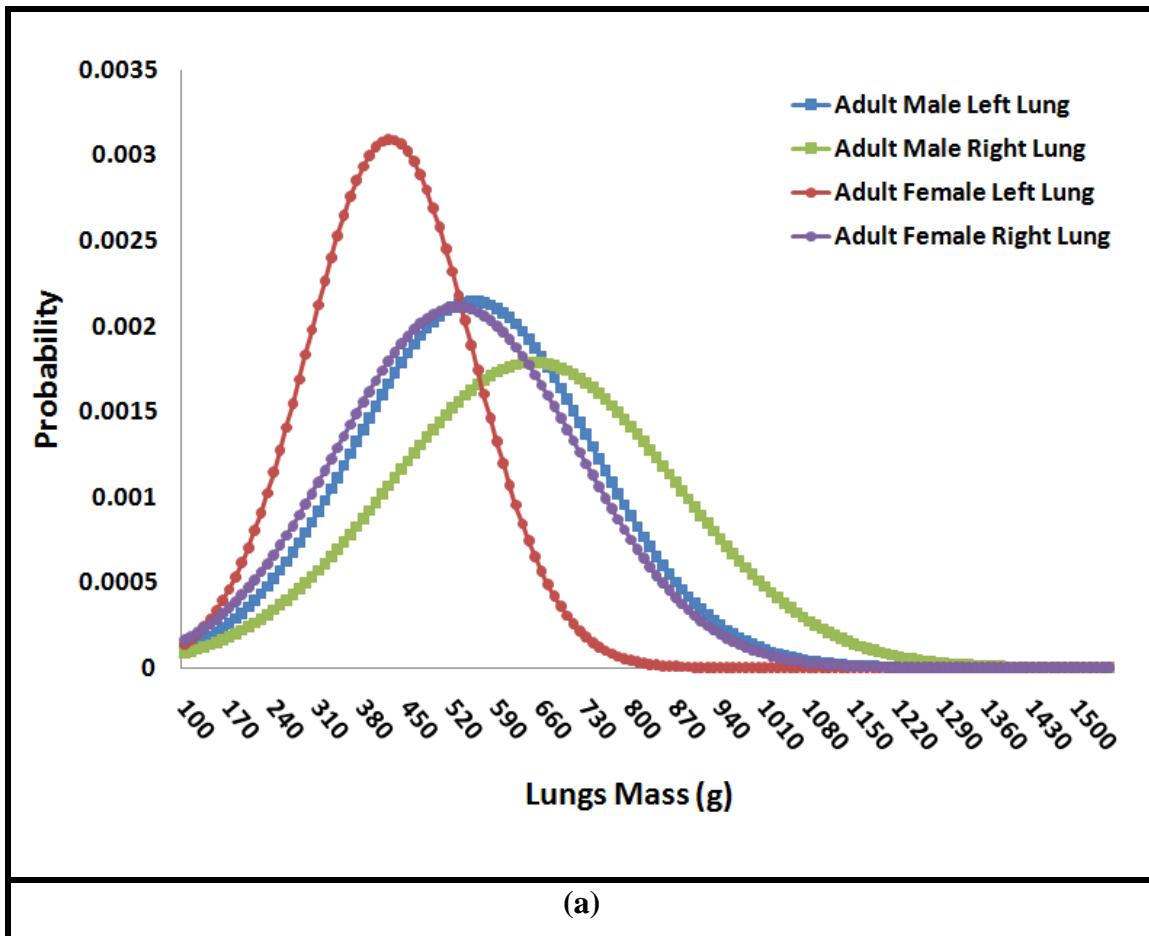
The Gaussian error $G(x)$ is defined as:

$$G(x) = \frac{2}{\sqrt{\pi}} \int_0^x e^{-t^2} dt \quad (2.5)$$

As an example, Table 2.5 shows the lung mass values of the adult male and female's lung masses, and the PDF and CDF are plotted in Figure 2.13a and Figure 2.13b, respectively.

Table 2.5: Lung mass values of the reference adult male and female (mean \pm SD).

Gender	Left Lung (g)	Right Lung (g)
Male	553 ± 186	647 ± 223
Female	422 ± 129	528 ± 189



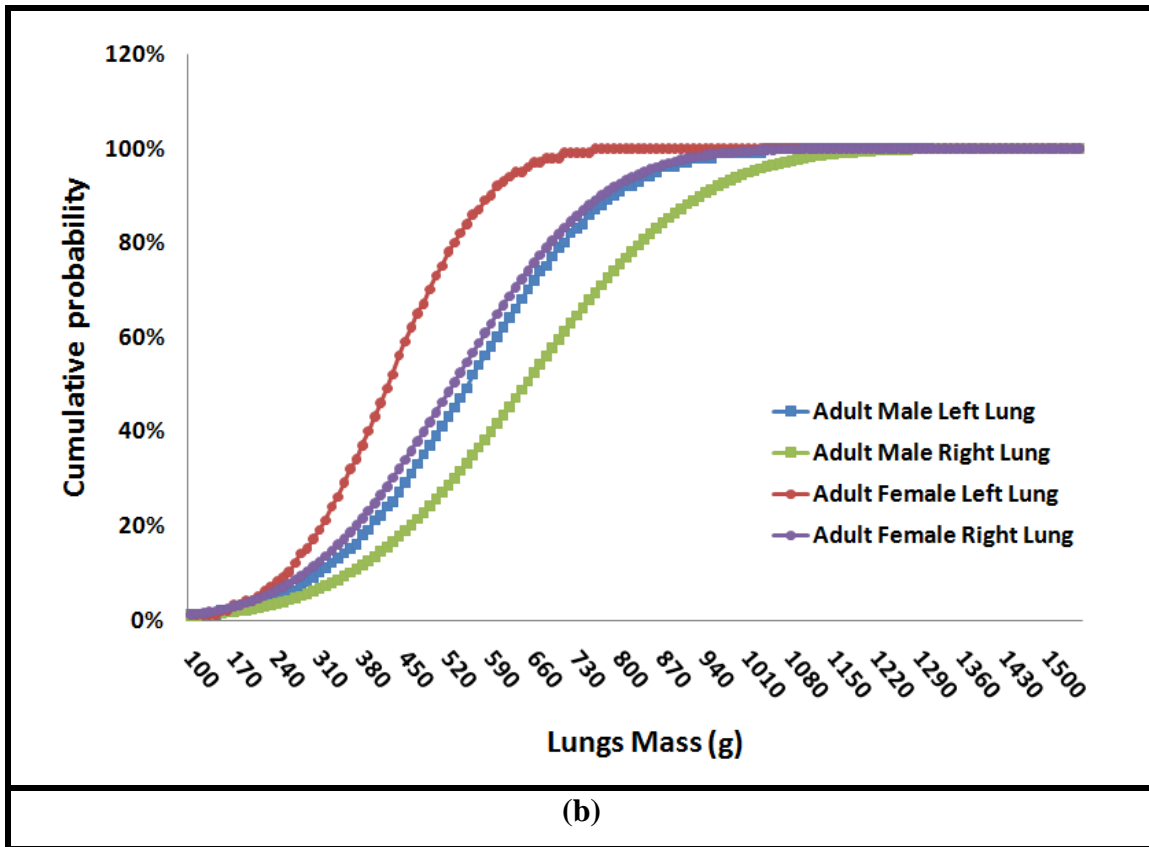


Figure 2.13: Statistical analysis for the lungs of reference adult male: (a) Probability Density Function (PDF); (b) Cumulative Density Function (CDF).

Table 2.6 lists the right and left lung masses of adult male from 5th percentile to 95th percentile. For the density of lung of 0.25 g/cm³, the lung volume could also be calculated.

Table 2.6: Mass and volume percentile values for the left and right lungs in adults.

Percentile	Adult Male				Adult Female			
	Mass (g)		Volume (cm ³)		Mass (g)		Volume (cm ³)	
	Left	Right	Left	Right	Left	Right	Left	Right
5th	247.06	280.20	988.24	1120.80	209.81	217.12	839.24	868.48
10th	314.63	361.21	1258.52	1444.84	256.68	285.79	1026.72	1143.16
15th	360.22	415.88	1440.88	1663.52	288.3	332.11	1153.20	1328.44
20th	396.46	459.32	1585.84	1837.28	313.43	368.93	1253.72	1475.72
25th	427.54	496.59	1710.16	1986.36	334.99	400.52	1339.96	1602.08

30th	455.46	530.06	1821.84	2120.24	354.35	428.89	1417.40	1715.56
35th	481.33	561.07	1925.32	2244.28	372.29	455.17	1489.16	1820.68
40th	505.88	590.50	2023.52	2362.00	389.32	480.12	1557.28	1920.48
45th	529.63	618.98	2118.52	2475.92	405.79	504.25	1623.16	2017.00
50th	553.00	647.00	2212.00	2588.00	422.00	528.00	1688.00	2112.00
55th	576.37	675.02	2305.48	2700.08	438.21	551.75	1752.84	2207.00
60th	600.12	703.50	2400.48	2814.00	454.68	575.88	1818.72	2303.52
65th	624.67	732.93	2498.68	2931.72	471.71	600.83	1886.84	2403.32
70th	650.54	763.94	2602.16	3055.76	489.65	627.11	1958.60	2508.44
75th	678.46	797.41	2713.84	3189.64	509.01	655.48	2036.04	2621.92
80th	709.54	834.68	2838.16	3338.72	530.57	687.07	2122.28	2748.28
85th	745.78	878.12	2983.12	3512.48	555.7	723.89	2222.80	2895.56
90th	791.37	932.79	3165.48	3731.16	587.32	770.21	2349.28	3080.84
95th	858.94	1013.80	3435.76	4055.20	634.19	838.88	2536.76	3355.52

The major organs of percentile volume and mass data for both the adult male and female in this study were derived using the normal CDF of 99.7% of the observations within almost three standard deviations of the mean. Table 2.7 shows the mean and standard deviation (Mean \pm SD) in major internal organ volume and mass values for the RPI-AM and RPI-AF phantoms. The standard deviation values allow other percentiles from 5th to 95th values to be specified.

Table 2.7: Mean and Standard Deviation (Mean \pm SD) in major internal organ volume and mass values for the RPI adult phantoms.

ID	Organ Name	RPI-AM (Mean \pm SD)		RPI-AF (Mean \pm SD)		Reference*
		Mass (g)	Volume (cm ³)	Mass (g)	Volume (cm ³)	
1	Adrenal, left	7 \pm 2.0	6.86 \pm 1.96	6.5 \pm 2.0	6.37 \pm 1.96	(Tanaka et al. 1979)
2	Adrenal, right	7 \pm 2.0	6.86 \pm 1.96	6.5 \pm 2.0	6.37 \pm 1.96	
61	Brain	1450.00 \pm 115.00	1394.23 \pm 110.58	1300.00 \pm 125.00	1250.00 \pm 120.19	(Tanaka et al. 1979)
72	Stomach wall	150.00 \pm 20.00	144.23 \pm 19.23	140.00 \pm 18.00	134.62 \pm 17.31	(Tipton and Cook 1969), (Dekaban and Sadowsky 1978), (IAEA 1998)
75	Small intestine	650.00 \pm 78.00	625.00 \pm 75.00	600.00 \pm 76.00	576.00 \pm 73.08	(Tipton and Cook 1969)
76	Ascending colon wall	90.00 \pm 14.00	86.54 \pm 13.46	90.00 \pm 15.00	86.54 \pm 14.42	
78	Transverse colon wall, right	60.00 \pm 12.00	57.69 \pm 11.54	55.00 \pm 7.00	52.88 \pm 6.73	
80	Transverse colon wall, left	60.00 \pm 12.00	57.69 \pm 11.54	55.00 \pm 7.00	52.88 \pm 6.73	(Tipton and Cook 1969)
82	Descending colon wall	90.00 \pm 23.00	86.54 \pm 22.12	90.00 \pm 15.00	86.54 \pm 14.42	
84 & 86	Sigmoid colon & Rectum wall	70.00 \pm 12.00	67.31 \pm 11.54	70.00 \pm 12.00	67.31 \pm 11.54	
111	Ovary, left(female only)	N/A	N/A	5.5 \pm 1.78	5.29 \pm 1.71	(Munn et al. 1986), (Pavlik et al. 2000),
112	Ovary, right(female only)	N/A	N/A	5.5 \pm 1.78	5.29 \pm 2.06	(Hongning et al. 2001)
113	Pancreas	140.00 \pm 35.00	133.33 \pm 33.33	120.00 \pm 33.00	114.29 \pm 31.43	(IAEA 1998), (de la Grandmaison et al. 2001)
115	Prostate(male only)	17.00 \pm 8.80	16.19 \pm 8.38	N/A	N/A	(IAEA 1998)
127	Spleen	150.00 \pm 29.00	141.51 \pm 27.36	130.00 \pm 20.00	122.64 \pm 18.87	(Boyd 1933, 1941, 1952), (IAEA 1998)
132	Thyroid	20.00 \pm 6.0	19.05 \pm 5.71	17.00 \pm 6.0	16.19 \pm 5.71	(de la Grandmaison et al. 2001)
139	Uterus(female only)	N/A	N/A	80.00 \pm 8.00	76.19 \pm 7.62	(Platt et al. 1990)

* ICRP (1975, 2002) summarized several papers that provided information of organ-specific standard deviation (SD). The papers are listed below.

Some of percentile data were linearly scaled by the volume and mass values of the ICRP reference adults. In each summary of key organs, the organ volume and mass values and the mesh-based anatomical structures are listed to easily compare with detailed information in Appendix B.

With advantages of the deformable RPI-AM and RPI-AF phantoms that allow a mesh-based phantom to “morph” into a different phantom or to create specific features to support diversities of radiation exposure environments.

2.3 Breast Deformable Phantoms

As a good example of these phantoms presented by Hegenbart et al. (2008), accurate in-vivo lung counting measurements for female workers must account for the chest thickness. A “virtual calibration” of a lung counter for female workers can be performed using a female computational phantom with adjustable breast sizes. For this project, a mesh-based breast-size adjustable adult female phantom from the RPI-AF phantom was demonstrated using data on female brassiere cup sizes. First, a female breast model was isolated from the female whole-body phantom. Then, the breast model was deformed automatically.

2.3.1 Breast Size Determinant

The first attempt of establishing female brassiere sizing in 1926 (Morris et al.), female breast size has been determined by two primary measurements: (1) the bust girth (BG); the maximum horizontal girth; (2) the underbust girth (UBG); the horizontal girth just below the breast.

The European Committee for Standardization (EN 13402-1 2001) defined these two measurements in the norm of size designation of clothes. Using these two measured data, EN 13402-2 and -3 (EN 13402-2 2002, EN 13402-3 2004) characterized a secondary dimension, called cup size (CS) by the difference between BG and UBG:

$$\text{Cup Size (CS)} = \text{Bust Girth (BG)} - \text{Under Bust Girth (UBG)}$$

The CS determines a size of female breast in terms of brassiere labels using 8 different letter codes. Table 2.8 shows the brassiere labels according to the European Committee for Standardization.

Table 2.8: Cup size ranges letter code according to (EN 13402-3:2004).

Code	AA	A	B	C	D	E	F	G
CS range (cm)	10-12	12-14	14 -16	16-18	18-20	20-22	22-24	24-26

2.3.2 Breast Deformation

The deformable RPI-AF mesh-based phantom was used as a basis for a breast size-adjustable phantom which has the ability to change its breast shape and size to different cup sizes from AA to G. The basic procedures for the development of the breast deformable phantoms are as follows: (1) relocation of the vertices and faces, which are representing the breast portion of whole-body, through the vertex normal vector direction; (2) assigning the effect of gravity to the breast deforming procedures to simulate a realistic result of a brassiere wearing female. A 60-degree downward angle was used for this project; (3) Laplacian smoothing to provide a smooth surface during the vertices transitions on the breast surface portion; (4) aligning the unchanged glandular tissues to close the new position of nipples; (5) determination of the CS by measuring of the BG and UBG.

Figure 2.14 shows how to measure both BG and UBG. The BG and UBG, outmost breast skin contours, are extracted using the axial breast cutting plans which have maximum horizontal contours in each mesh-based phantom to agree with the description of BG and UBG (EN 13402-1 2001), as shown in Figure 2.14a and 2.14c. The contours in Figure 2.14b and 2.14d are representing the skin contours of BG and UBG respectively. Because the perimeters of the breast portion of skin are different from the measuring ruler, the contours of rulers, shown in Figure 2.14e and 2.14g, are implemented by the rolling ball method (Armato et al. 1999). The contours of rulers are illustrated in Figure 2.14f and 2.14h. The rolling ball method allows skipping the

cleavage in-between the mammarys to have a similarity to real BG measurements. Total 8 mesh-based phantoms with 8 different cup sizes of AA, A, B, C, D, E, F, and G were preferred from a variety of deformed mesh-based phantoms.

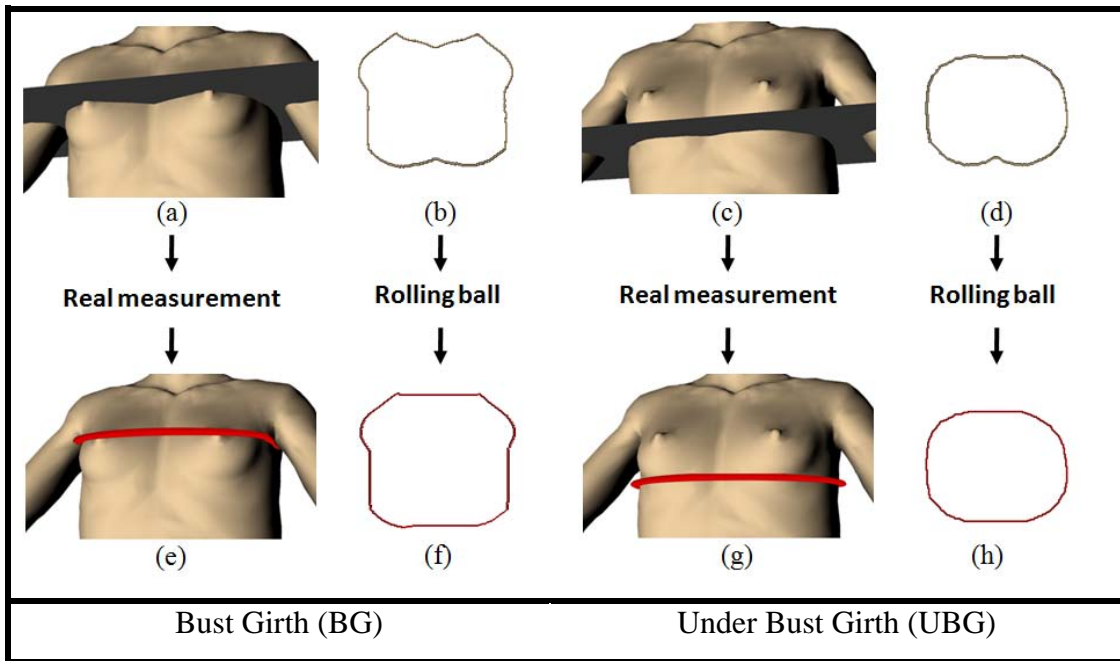


Figure 2.14: Method of measurement both BG and UBG: (a) axial breast cutting plan on the portion of breast for BG measurement; (b) extracted breast skin contour of the BG portion; (c) axial breast cutting plan on the portion of breast for UBG measurement; (d) extracted breast skin contour of the UBG portion; (e) real measurement of BG using ruler; (f) implemented measurement of BG using rolling ball method (Armato et al. 1999); (g) real measurement of UBG using ruler; (f) implemented measurement of UBG using rolling ball method.

After all of mesh deformation from the RPI-AF mesh-based phantoms, the breast size-adjustable whole-body individual phantoms were transformed to the solid geometries in the voxel domain. During the voxelization procedure, the adipose tissues are allocated between glandular tissues and breast skin. The RPI-AF's organs were kept the same positions with their center of mass except the glandular and adipose tissues which were repositioned by the breast deformation.

2.4 Walking Posture Phantoms

2.4.1 Posture Phantoms

In order to reduce the uncertainty in organ dose assessment, the irradiation condition for a worker must be considered as realistically as possible. A worker can walk on radiation-contaminated ground or can hold a container of high-level radioactive materials. These radiation environments can cause damage to radiosensitive organs. As an example presented by Han et al. (2009), the radiosensitive gonads in a walking posture with legs apart from each other can be exposed to a greater amount of radiation from the ground than that from a standing phantom with legs closed together. Therefore, it is necessary to investigate the use of deformable phantom for radiation exposure situations where more precise dosimetry is desired. This section presents the modeling of posture adjustable phantoms using a pair of stationary RPI-AM and RPI-AF mesh-based phantoms.

Dynamic postures of the RPI-AM and RPI-AF phantoms with articulated arms and legs require several issues to be addressed: (1) the skeleton is defined with a large number of bones and joints; (2) the musculature consists of contractile muscles and immovable tendons; (3) the skin surfaces at the articulated body portions need to be smooth; (4) the potential overlap of adjacent organs and tissues to be carefully avoided. In this section, the detailed modeling of posture phantom is discussed focusing especially on the walking phantoms.

2.4.2 Walking Phantoms

The act of walking is composed of two main phases (i.e., stance phase and swing phases) in normal gait cycle (Inman et al. 1981). The foot is on the ground during the stance phase, while the same foot is no longer in touch with the ground and the leg is swinging through in preparation for the next strike in swing phase. Figure 2.15 shows three subdivided phases of the stance phase: (1) first double support when both feet touch the ground; (2) single lime stance when the left foot is swinging through and the right foot contacts the ground; (3) second double support when both feet retouch the ground.

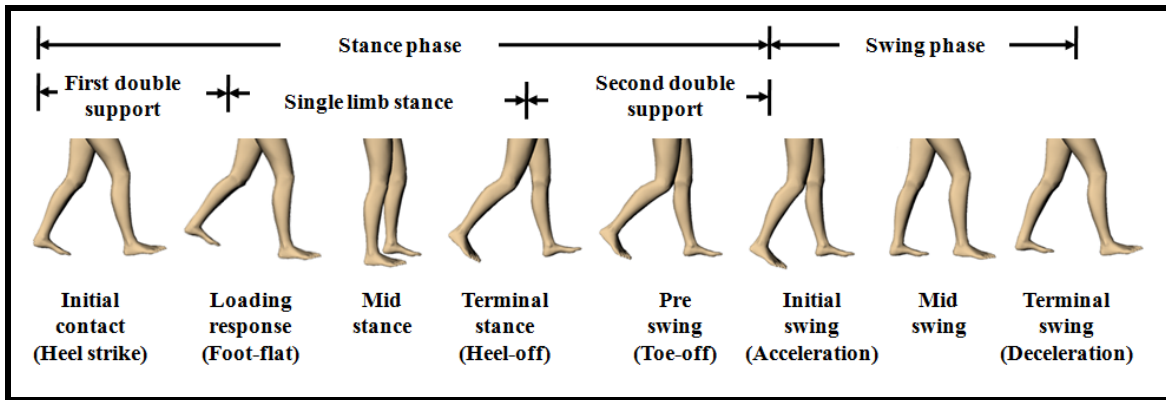


Figure 2.15: Normal gait cycle of adults.

For organ dose calculations, the normal gait cycle is simplified as four different positions: (1) initial-contact with taking left leg backward and right leg forward; (2) mid-stance with both legs in a closed position; (3) mid-swing with taking left leg backward and right leg forward; (4) between mid-swing and terminal-swing with both legs in a closed position. The distances between two feet for the initial-contact and mid-swing are approximated by 70 cm for adult male and 45 cm for adult female.

With the advantages afforded by the mesh geometry, the RPI-AM and RPI-AF deformable phantoms can be changed in their body postures to represent initial-contact and mid-swing stages. During the deformation procedures, all internal organ volumes and masses s in both adult male and female are matched with the recommended ICRP values (ICRP 1975, ICRP 2002) through the collision detection and correction algorithms. The stationary RPI-AM and RPI-AF phantoms coincide with the mid-stance stage and the stage of mid-swing and terminal-swing of the walking phantoms. These new mesh-based adult posture phantoms are finally voxelized to be used for average organ dose calculations by Monte Carlo method.

2.5 Software Algorithms for Automatic Deformable Phantoms

All of the above mesh deformation and voxelization algorithms involved in creating deformable phantoms were implemented in a software program. The software was developed using the programming language Microsoft® Visual C#. Adopted in both the Windows and Web applications, C# is a more powerful and simpler platform than C++. Furthermore, C# has the additional advantage of being compatible with the .NET framework. The mesh deformation and collision detection algorithms can be implemented as the Component Object Model (COM) which is an interface standard component in Microsoft®. It allows building applications through C#, Visual Basic (VB), Visual C++ (VC++), or any other languages that are able to support the COM. This component-packaging approach makes this software design very robust and convenient in both mesh deformation and visualization. The mesh-based phantoms can be inspected in the main window of the software using the Visualization Toolkit tool (VTK) (<http://www.vtk.org/>). Even though the organ volume and overlap were automatically checked during the entire procedures, visual inspections were still useful. Figure 2.16 shows the software GUI and the tools in a pull-down menu used for the deformable adult phantoms and breast size adjustable female phantoms. The software GUI was developed in Microsoft® Visual C# for breast deformation.

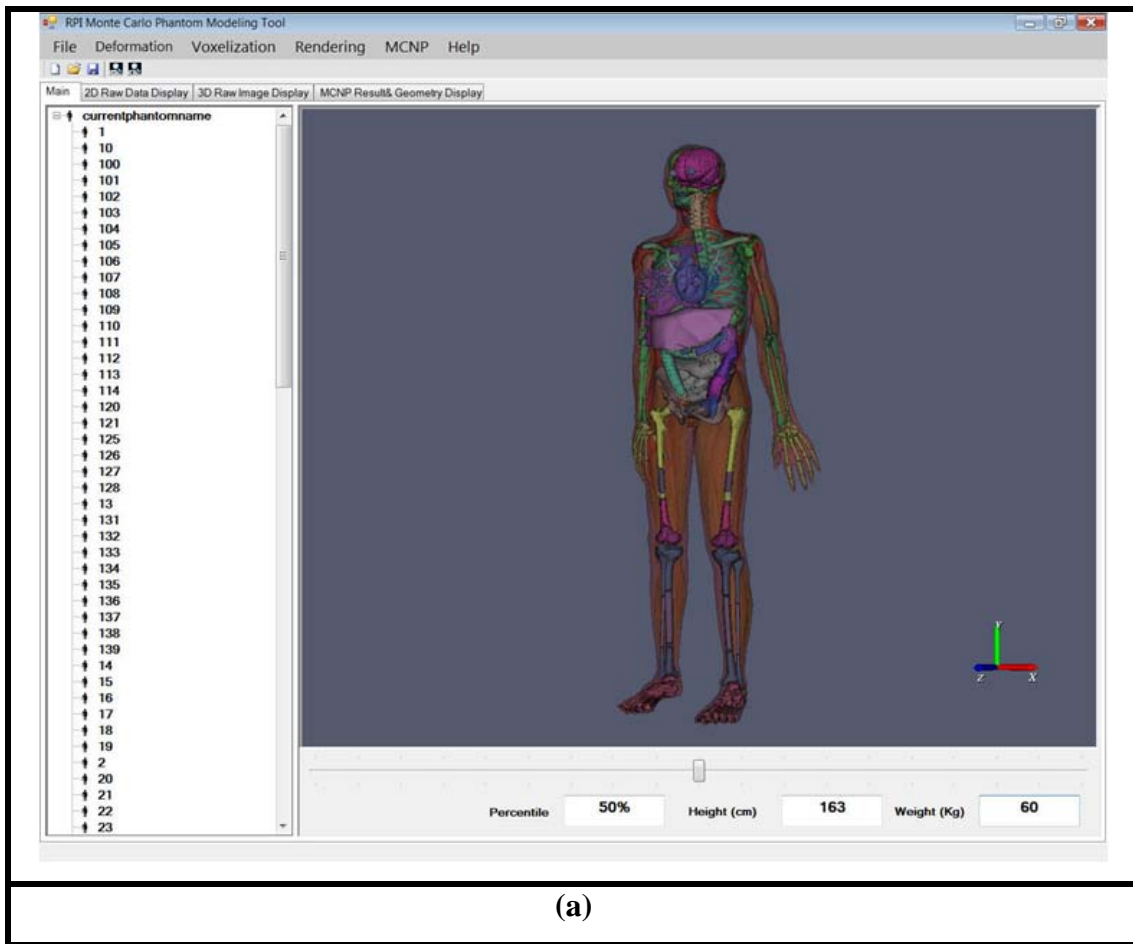
The primary features of the software package are summarized below:

3D Visualization of the mesh files. In the 3D display function, a mesh file can be easily handled, either in the wireframe data format or the surface rendering format. By using mouse clicking and wheel scrolling operations, a user can rotate and zooming in and out of 3D rendered mesh model.

Interactive organ deformation. Based on a user's initial definition of deformation factors such as organ volume, the mesh deformation can be carried out automatically in about 3 minutes on a PC operated in Intel® Pentium(R) with a 2.66-GHz CPU and a 3-GB RAM.

Other automatic operations. The software menu comes with several automatic operations that are critical to the deformable phantom software program. Using an in-house voxelization algorithm, the mesh-based phantom is converted to a voxel-based phantom for the purposes of Monte Carlo radiation transport simulations. During the

voxelization processing, the data of physical properties for the organs are translated and updated using the Microsoft® Access technology. The voxelized data are then automatically exported to a geometry format acceptable to the MCNPX code (Pelowitz 2005). Organ properties are defined by a materials library that can be easily updated through an interactive editing function of the software.



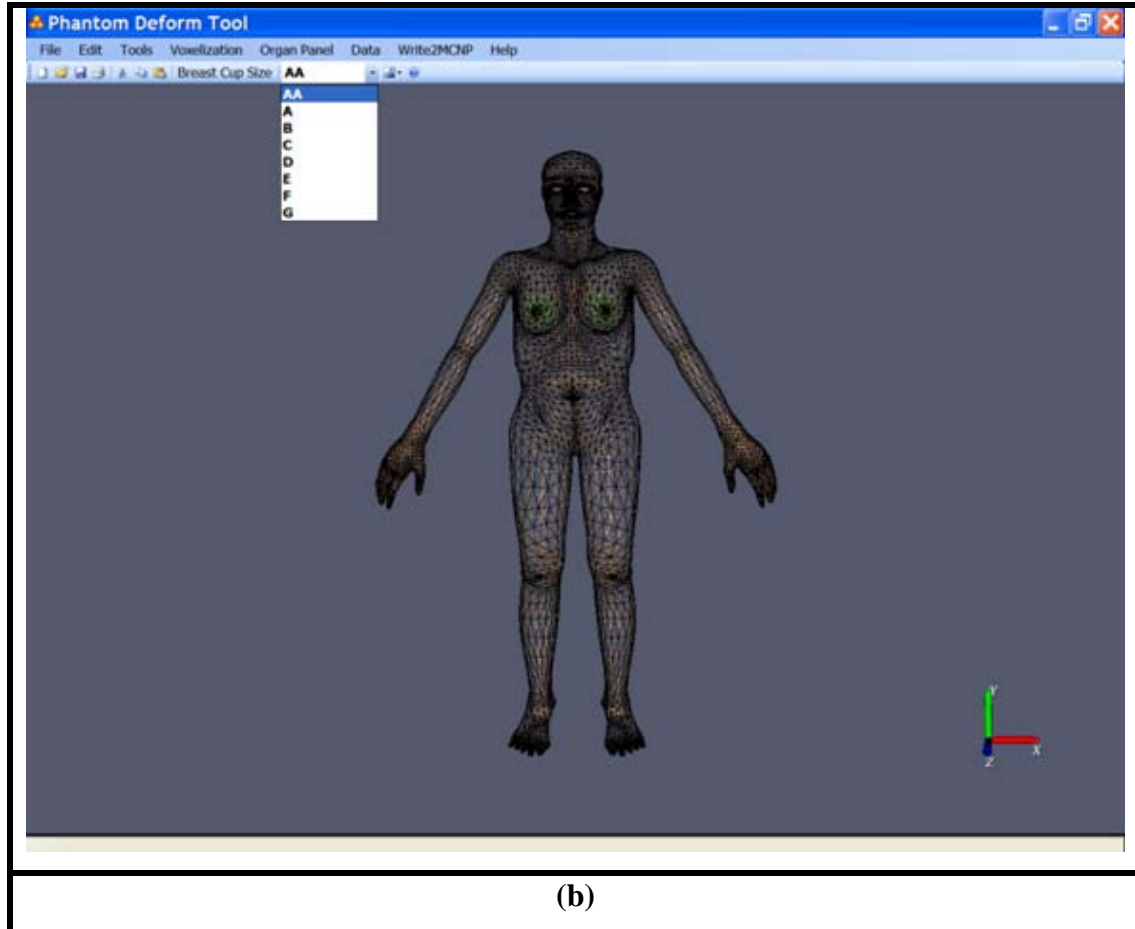


Figure 2.16: Software GUI for deformable phantom operations showing various tools [Na et al. 2009b (images are courtesy of Mr. Aiping Ding)]: (a) different percentile phantoms; (2) the female phantom whose breast size is specified by a user.

3. Results for the Deformable Phantoms

This section describes the results of development computational phantoms in mesh and voxel domains. In addition, the applications of these phantoms in radiation protection dosimetry are also discussed.

3.1 Validation of Deformable Phantoms

The organ volumes and masses of the RPI phantoms and other phantoms developed by other groups are matching the ICRP recommended reference parameters to represent the 50th-percentile of the adult population. However, the organ shapes and locations can be reasonably varied within a different body frame. Therefore, the validation of deformable phantoms was performed in two different considerations: (1) comparison of relative errors of organ volume and mass values of the mesh- and voxel-based RPI-AM and RPI-AF with the ICRP reference adult male (REX) and female (REGINA) developed by the GSF research group using voxel by voxel adjustment to match the same ICRP reference values (Becker et al. 2007, ICRP 2009); (2) deformability of the body frame and each organ's shapes and locations from the RPI phantoms to the ICRP phantoms.

The final organ volume and mass values of the deformable RPI phantoms in mesh representation have an acceptable relative error, less than 0.5%, according to the acceptance criteria in mesh deformation algorithms. To accomplish acceptable results, several iterations were required for some of the internal organs. The eye lens of both the RPI-AM and RPI-AF has about 3% relative error (reference volume of 0.18 cm^3 , 0.19 cm^3 for male and female, respectively) in voxel representation due to the voxelization process because these organs are very thin surface layers. A detailed comparison of the RPI-AM and RPI-AF with ICRP reference adult male and female is summarized in Appendix A, respectively. The deformed organ shapes and locations of the deformable RPI to the ICRP phantoms are shown in Figure 3.1 as an example of the RPI-AM and the REX.

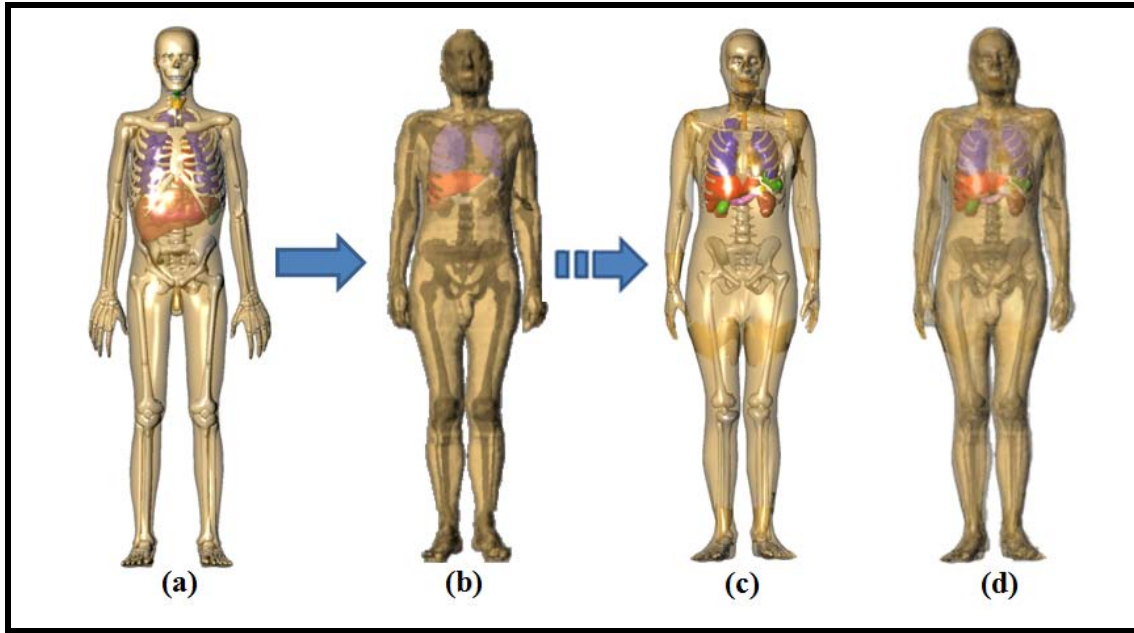


Figure 3.1: Deformability validation of deformable RPI-AM in deforming the body and organs' shapes and locations from (a) RPI-AM to (b) ICRP-REX; (c) deformed RPI-AM to REX; (d) two phantoms (b, c) with the same origin coordinate system.

3.2 50th-Percentile Reference Adult Phantoms

The deformable RPI-AM and RPI-AF were composed of a total of 70 internal organs, 45 bone components and 4 muscle structures. Figure 3.2a shows the established cortical bone structures for the RPI adult phantoms with the organ ID numbers circled. The spongiosa contained red bone marrow and medullary cavity contained yellow bone marrow are depicted in Figure 3.2b. The anatomical structures of detailed major internal organs for the RPI-AM and RPI-AF are shown in Figures 3.3a and 3.3b, respectively. Figure 3.4 shows the blood vessel structures (i.e., head, trunk, arms, and legs) of the RPI-AM in Figure 3.4a and RPI-AF in Figure 3.4b. The lymphatic nodes (i.e., extra thoracic airways, thoracic airways, head, trunk, arms, and legs) of the RPI-AM and RPI-AF are illustrated in Figures 3.5a and 3.5b. In Figure 3.6a and Figure 3.6b, the muscles structures (i.e., head, trunk, arms, and legs) are shown for the RPI-AM and RPI-AF. All anatomical structures gathered inside body skins of the RPI-AM and RPI-AF are shown in Figure 3.7 and Figure 3.8, respectively.

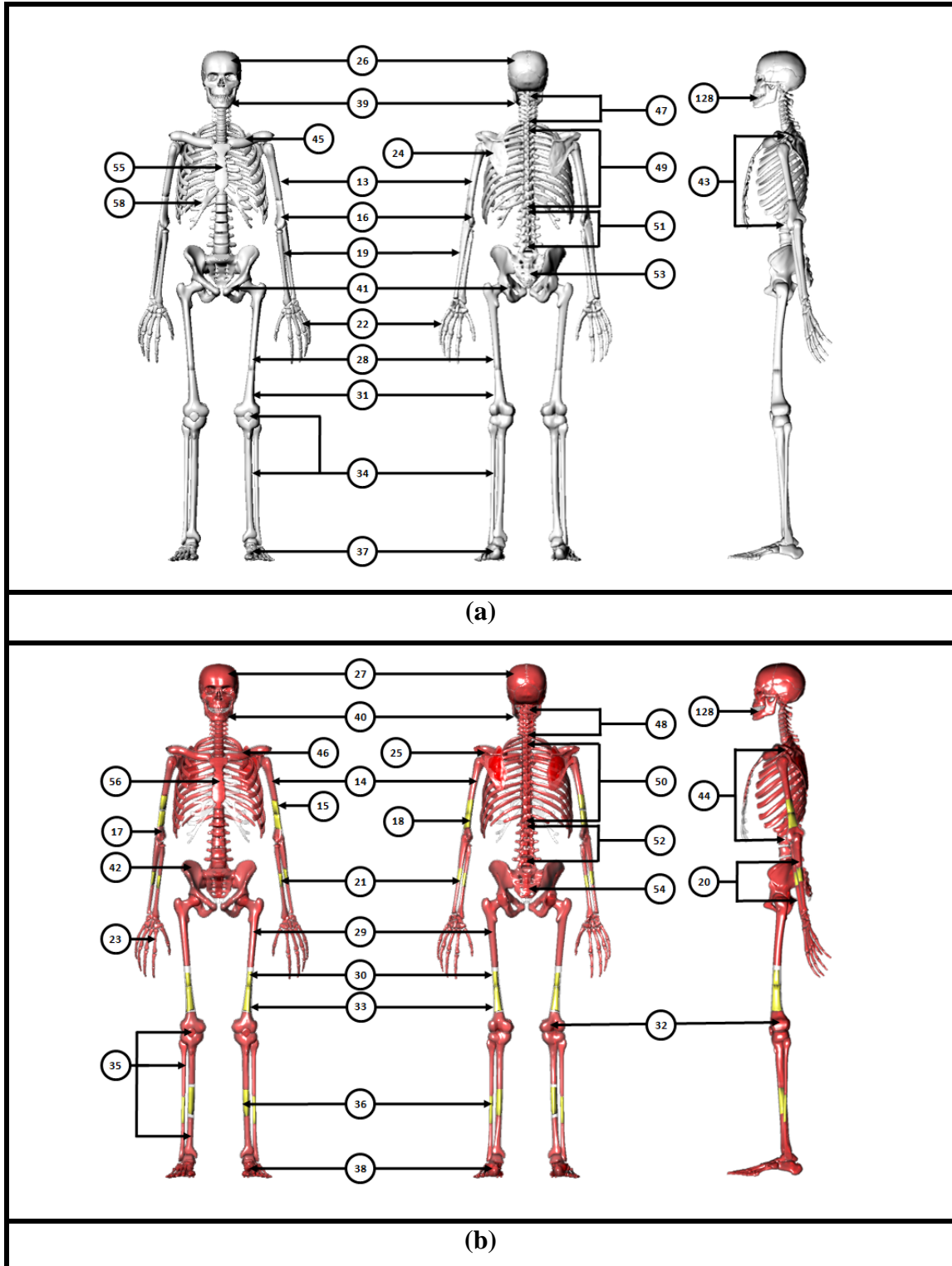


Figure 3.2: Skeletal structures for the RPI adult phantoms with the organ ID numbers circled: (a) Cortical bones; (b) Spongiosa (contained red bone marrow) and medullary cavity (contained yellow bone marrow).

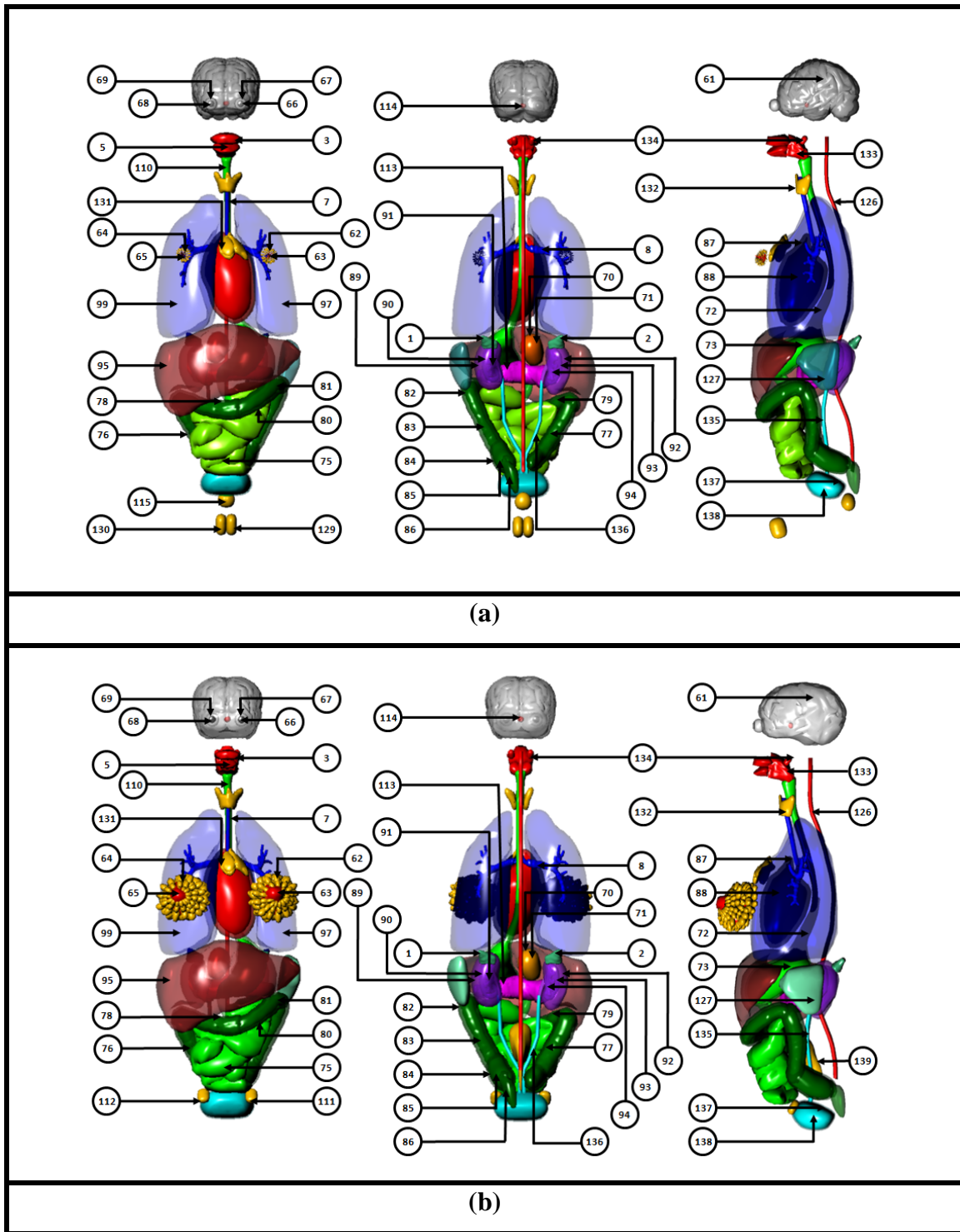


Figure 3.3: Anatomical structures of detailed internal organs with organ ID circled for the RPI Adults in anterior (left), posterior (middle), and lateral (right), respectively: (a) Adult male; (b) Adult female.

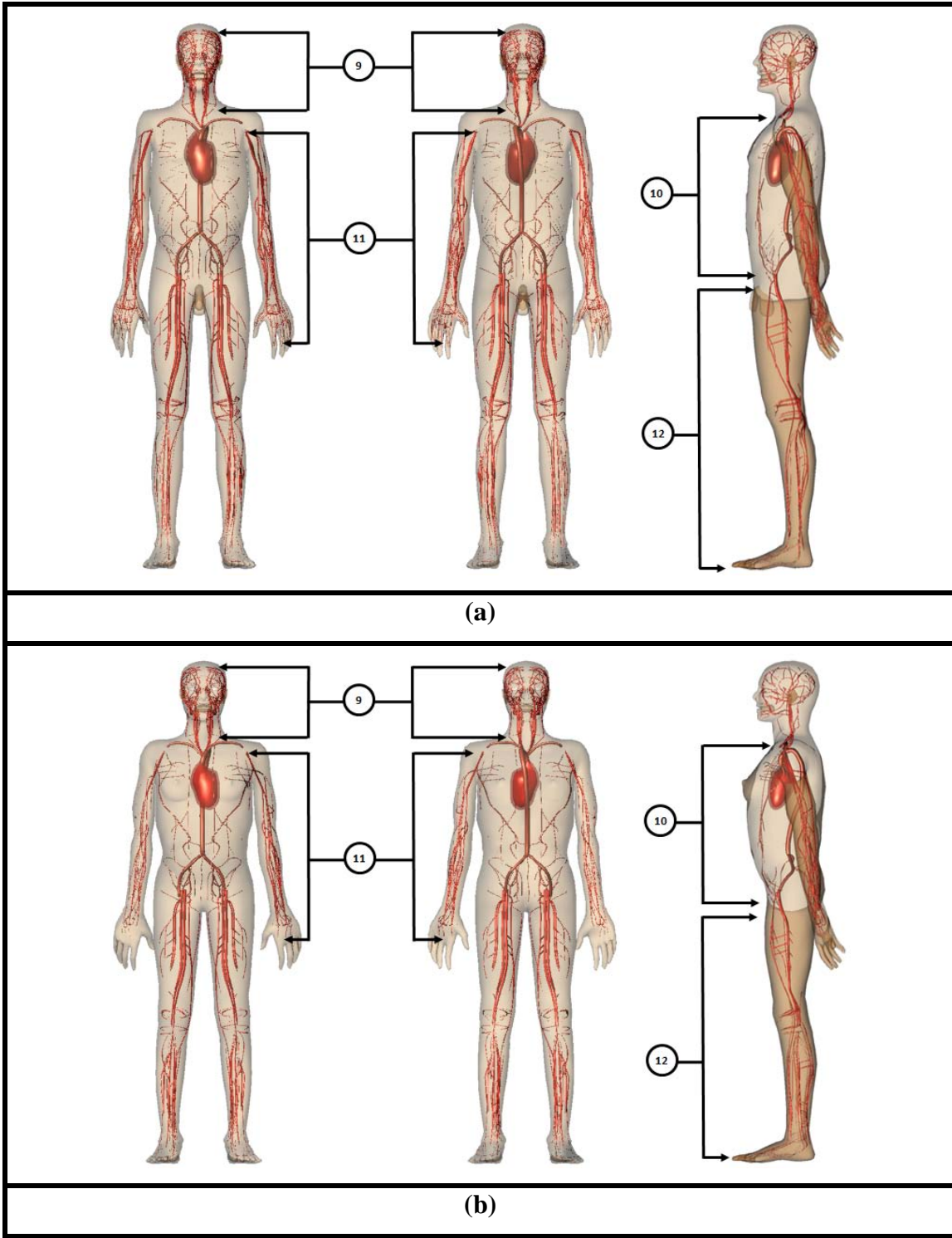


Figure 3.4: Anatomical structures of detailed blood vessels with organ ID circled for the RPI Adults in anterior (left), posterior (middle), and lateral (right), respectively: (a) Adult male; (b) Adult female.

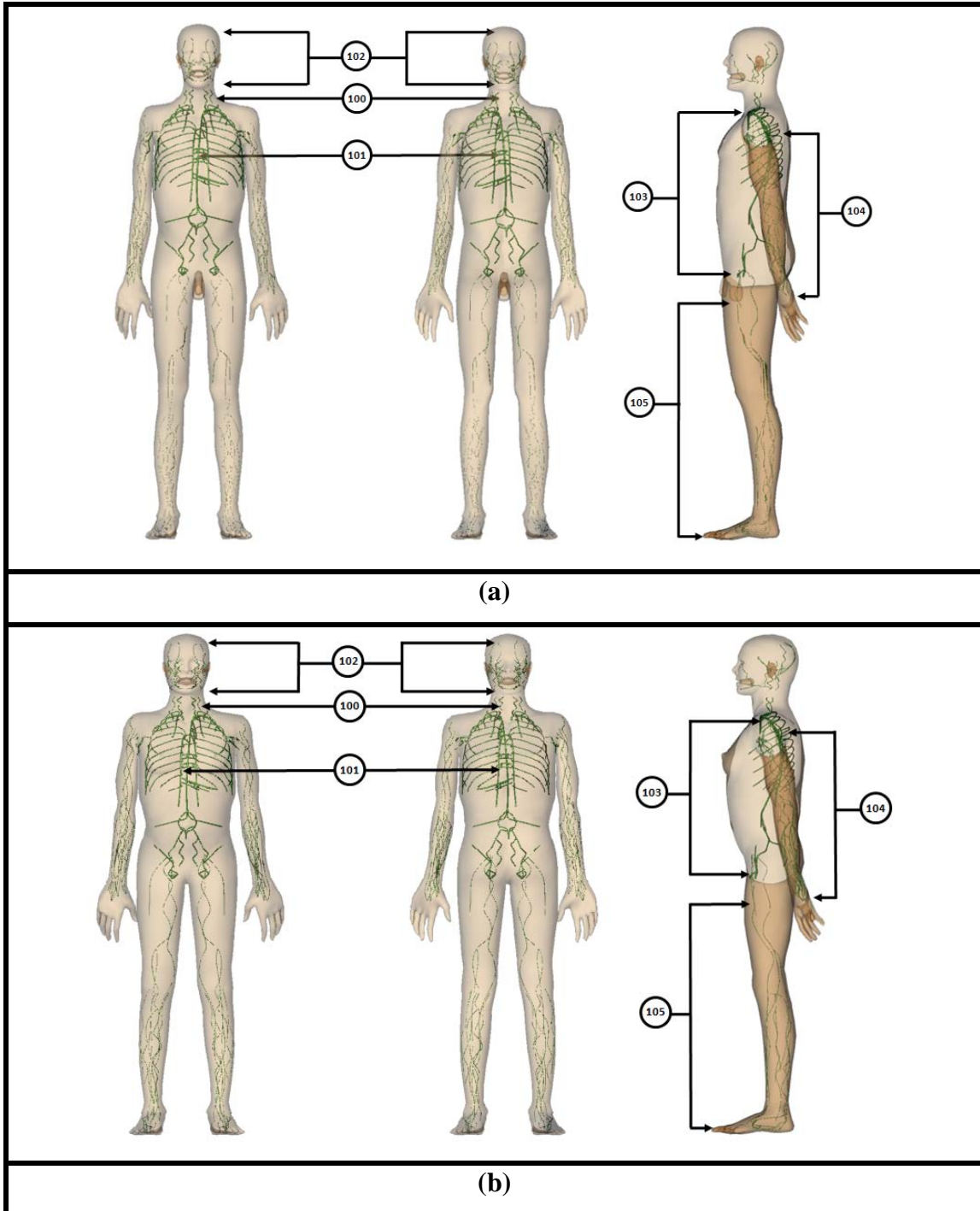


Figure 3.5: Anatomical structures of detailed lymphatic nodes with organ ID circled for the RPI Adults in anterior (left), posterior (middle), and lateral (right), respectively: (a) Adult male; (b) Adult female.

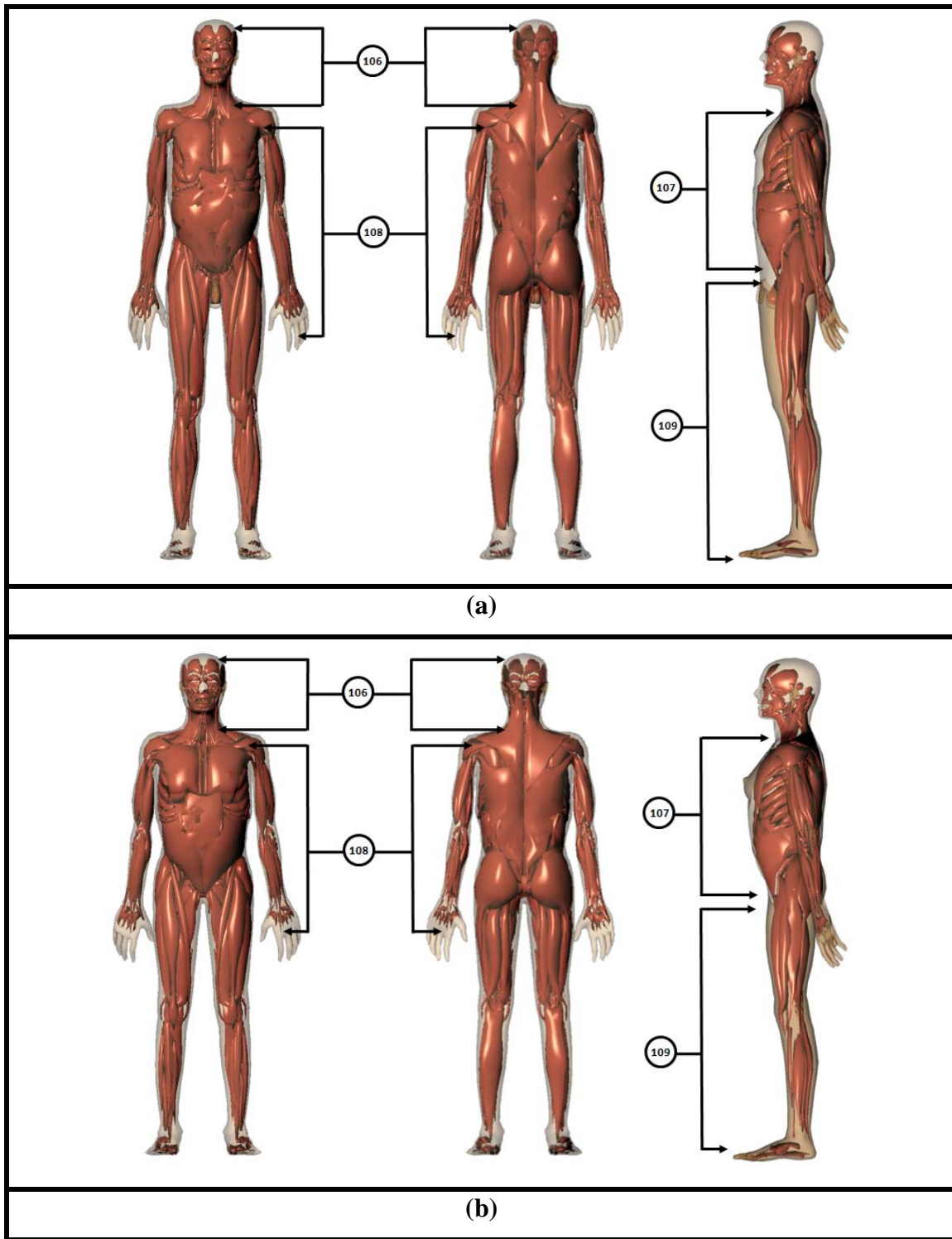


Figure 3.6: Anatomical structures of detailed muscles with organ ID circled for the RPI Adults in anterior (left), posterior (middle), and lateral (right), respectively: (a) Adult male; (b) Adult female.

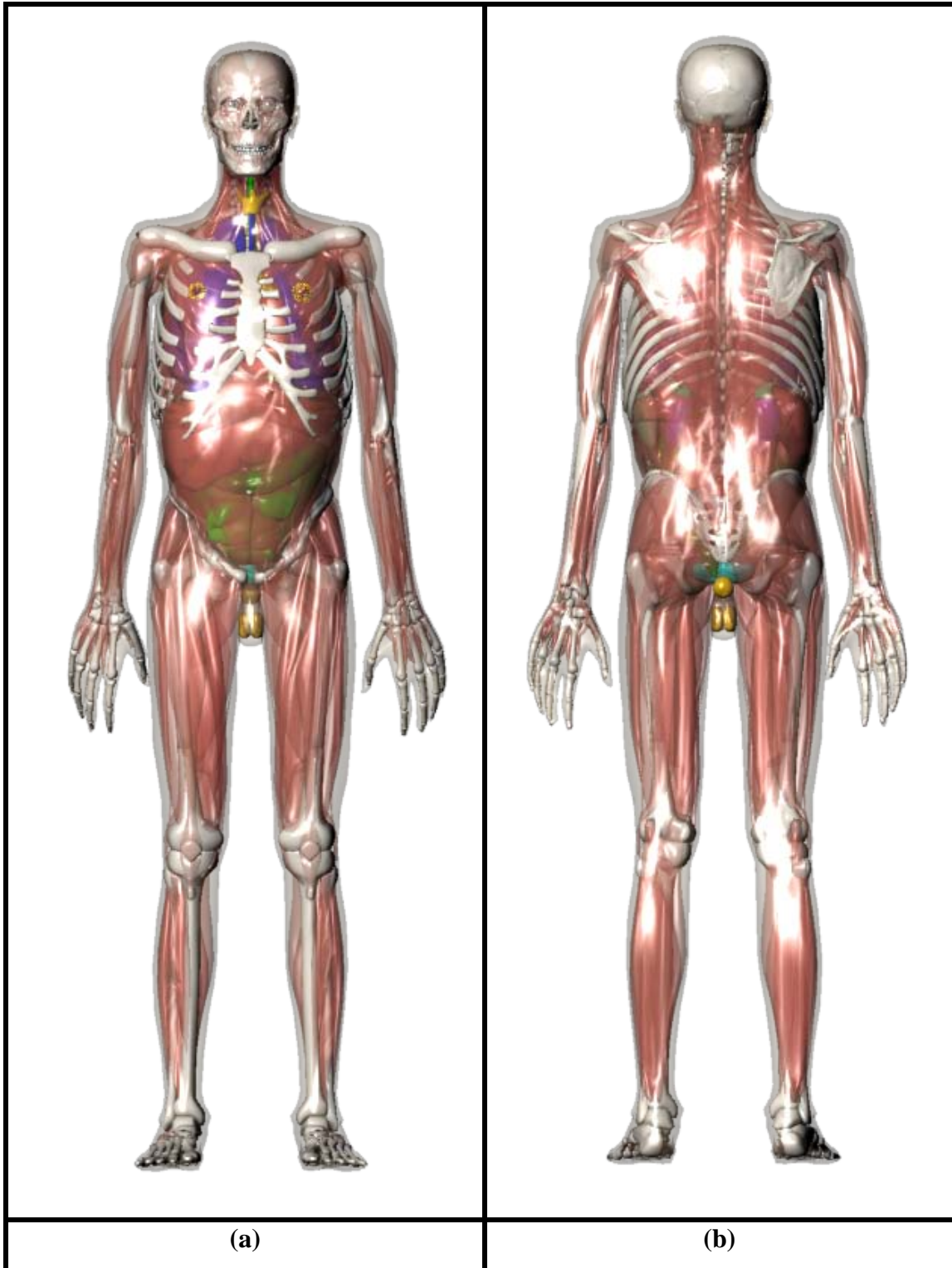


Figure 3.7: 3D view of the RPI-AM phantom: (a) anterior; (b) posterior.

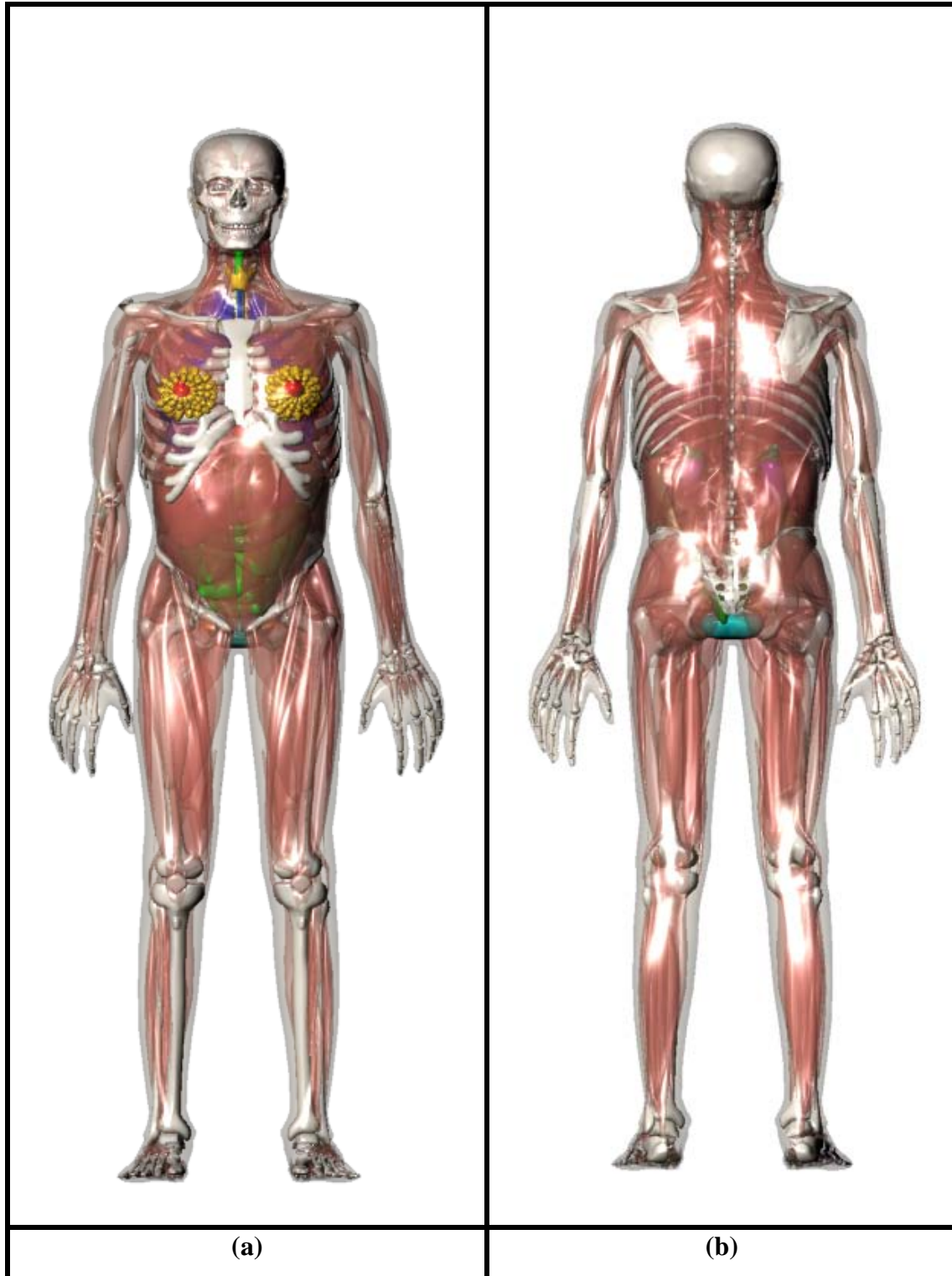


Figure 3.8: 3D view of the RPI-AF phantom: (a) anterior; (b) posterior.

Table 3.1 tabulates the organ/tissue masses, densities, and volumes for the RPI-AM and RPI-AF phantoms.

Table 3.1: List of organs for the RPI 50th-percentile adult male and female.

ID	Organ Name	RPI-AM			RPI-AF		
		Mass (g)	Volume (cm ³)	Density (gcm ⁻³)	Mass (g)	Volume (cm ³)	Density (gcm ⁻³)
1	Adrenal, left	7.00	6.86	1.02	6.50	6.37	1.02
2	Adrenal, right	7.00	6.86	1.02	6.50	6.37	1.02
3	Extrathoracic (ET)	39.44	38.29	1.03	18.61	18.07	1.03
5	Oral mucosa, tongue	31.00	29.52	1.05	9.00	8.57	1.05
7	Trachea	10.00	9.71	1.03	8.00	7.77	1.03
8	Bronchi	30.00	29.13	1.03	25.00	24.27	1.03
9	Blood vessels, head	0.85	0.80	1.06	6.06	5.72	1.06
10	Blood vessels, trunk	271.93	256.54	1.06	242.38	228.66	1.06
11	Blood vessels, arms	15.72	14.83	1.06	43.24	40.79	1.06
12	Blood vessels, legs	83.04	78.34	1.06	92.64	87.40	1.06
13	Humeri, upper half, cortical	135.26	70.45	1.92	112.60	58.65	1.92
14	Humeri, upper half, spongiosa	184.86	154.05	1.20	111.90	94.83	1.18
15	Humeri, upper half, medullary cavity	33.48	34.16	0.98	19.89	20.30	0.98
16	Humeri, lower half, cortical	128.03	66.68	1.92	102.21	53.23	1.92
17	Humeri, lower half, spongiosa	59.73	53.81	1.11	52.78	47.13	1.12
18	Humeri, lower half, medullary cavity	37.13	37.89	0.98	20.55	20.97	0.98
19	Ulnae and radii:Ulnae and radii, cortical	270.80	141.04	1.92	155.14	80.80	1.92
20	Ulnae and radii, spongiosa	181.91	163.88	1.11	91.24	81.46	1.12
21	Ulnae and radii, medullary cavity	22.67	23.13	0.98	33.59	34.28	0.98
22	Wrists and hand bones, cortical	179.74	93.61	1.92	104.08	54.21	1.92
23	Wrists and hand bones, spongiosa	139.59	125.76	1.11	72.84	65.04	1.12
24	Clavicles, cortical	47.78	24.89	1.92	32.50	16.93	1.92
25	Clavicles, spongiosa	53.06	46.14	1.15	40.45	33.99	1.19
26	Cranium, cortical	562.85	293.15	1.92	403.60	210.21	1.92
27	Cranium, spongiosa	451.06	388.84	1.16	417.09	334.93	1.25
28	Femora, upper half, cortical	261.68	136.29	1.92	247.75	129.04	1.92
29	Femora, upper half, spongiosa	472.05	421.47	1.12	225.05	214.33	1.05
30	Femora, upper half, medullary cavity	25.78	26.31	0.98	39.51	40.32	0.98
31	Femora, lower half, cortical	294.09	153.17	1.92	232.47	121.08	1.92
32	Femora, lower half, spongiosa	438.57	395.11	1.11	174.67	155.96	1.12

33	Femora, lower half, medullary cavity	80.89	82.54	0.98	55.43	56.56	0.98
34	Tibiae, fibulae and patellae, cortical	531.35	276.74	1.92	618.85	322.32	1.92
35	Tibiae, fibulae and patellae, spongiosa	729.38	657.10	1.11	586.52	523.68	1.12
36	Tibiae, fibulae and patellae, medullary cavity	78.67	80.28	0.98	87.65	89.44	0.98
37	Ankles and foot bones, cortical	232.56	121.13	1.92	171.75	89.45	1.92
38	Ankles and foot bones, spongiosa	507.78	457.46	1.11	270.35	241.38	1.12
39	Mandible, cortical	76.12	39.65	1.92	44.94	23.41	1.92
40	Mandible, spongiosa	73.90	60.08	1.23	34.67	29.13	1.19
41	Pelvis, cortical	398.62	207.61	1.92	259.84	135.33	1.92
42	Pelvis, spongiosa	681.18	608.20	1.12	445.07	400.96	1.11
43	Ribs, cortical	365.16	190.19	1.92	162.87	84.83	1.92
44	Ribs, spongiosa	520.06	444.50	1.17	258.96	237.58	1.09
45	Scapulae, cortical	221.13	115.17	1.92	120.45	62.73	1.92
46	Scapulae, spongiosa	192.21	162.89	1.18	96.87	85.73	1.13
47	Cervical spine, cortical	102.92	53.60	1.92	70.88	36.92	1.92
48	Cervical spine, spongiosa	73.55	70.05	1.05	72.81	63.87	1.14
49	Thoracic spine, cortical	286.58	149.26	1.92	203.78	106.14	1.92
50	Thoracic spine, spongiosa	335.34	313.40	1.07	252.56	233.85	1.08
51	Lumbar spine, cortical	186.19	96.97	1.92	154.62	80.53	1.92
52	Lumbar spine, spongiosa	302.07	272.14	1.11	261.28	223.32	1.17
53	Sacrum, cortical	109.23	56.89	1.92	N/A	N/A	N/A
54	Sacrum, spongiosa	173.51	168.46	1.03	140.44	133.75	1.05
55	Sternum, cortical	9.89	5.15	1.92	1.67	0.87	1.92
56	Sternum, spongiosa	56.31	54.14	1.04	47.41	43.90	1.08
58	Catilage	88.67	80.61	1.10	313.61	285.10	1.10
61	Brain	1450.00	1394.23	1.04	1300.00	1250.00	1.04
62	Breast, left, adipose tissue	7.50	7.89	0.95	150.00	157.89	0.95
63	Breast, left, glandular tissue	4.99	4.89	1.02	100.00	98.04	1.02
64	Breast, right, adipose tissue	7.50	7.89	0.95	150.00	157.89	0.95
65	Breast, right, glandular tissue	4.99	4.89	1.02	100.00	98.04	1.02
66	Eye lense, left	0.20	0.18	1.10	0.20	0.18	1.10
67	Eye bulb, left	7.30	7.09	1.03	7.30	7.09	1.03
68	Eye lense, right	0.20	0.18	1.10	0.20	0.18	1.10
69	Eye bulb, right	7.30	7.09	1.03	7.30	7.09	1.03
70	Gall bladder wall	10.00	9.71	1.03	8.00	7.77	1.03
71	Gall bladder contents	58.00	56.31	1.03	48.00	46.60	1.03
72	Stomach wall	150.00	144.23	1.04	140.00	134.62	1.04
73	Stomach contents	250.00	240.38	1.04	230.00	221.15	1.04
75	Small intestine	1000.00	961.54	1.04	880.00	846.15	1.04

76	Ascending colon wall	89.99	86.53	1.04	90.00	86.54	1.04
77	Ascending colon contents	55.02	52.90	1.04	100.00	96.15	1.04
78	Transverse colon wall, right	60.00	57.69	1.04	55.00	52.88	1.04
79	Transverse colon contents, right	95.00	91.35	1.04	59.99	57.68	1.04
80	Transverse colon wall, left	60.00	57.69	1.04	55.00	52.88	1.04
81	Transverse colon contents, left	40.01	38.47	1.04	30.01	28.86	1.04
82	Descending colon wall	89.99	86.53	1.04	90.00	86.54	1.04
83	Descending colon contents	35.00	33.65	1.04	50.00	48.08	1.04
84	Sigmoid colon wall	40.01	38.47	1.04	45.01	43.28	1.04
85	Sigmoid colon contents	74.97	72.09	1.04	79.99	76.91	1.04
86	Rectum wall	29.98	28.83	1.04	24.99	24.03	1.04
87	Heart wall	330.00	314.29	1.05	250.00	238.10	1.05
88	Heart contents(blood)	510.00	481.13	1.06	370.00	349.06	1.06
89	Kidney, left, cortex	107.12	102.02	1.05	104.63	99.65	1.05
90	Kidney, left, medulla	38.25	36.43	1.05	37.37	35.59	1.05
91	Kidney, left, pelvis	7.63	7.27	1.05	7.48	7.12	1.05
92	Kidney, right, cortex	109.92	104.69	1.05	87.87	83.69	1.05
93	Kidney, right, medulla	39.25	37.38	1.05	31.38	29.89	1.05
94	Kidney, right, pelvis	7.87	7.50	1.05	6.28	5.98	1.05
95	Liver	1800.00	1714.29	1.05	1400.00	1333.33	1.05
97	Lung, left, tissue	553.00	2212.00	0.25	422.00	1688.00	0.25
99	Lung, right, tissue	647.00	2588.00	0.25	528.00	2112.00	0.25
100	Lymphatic nodes, extrathoracic airways	2.26	2.19	1.03	1.34	1.30	1.03
101	Lymphatic nodes, thoracic airways	6.40	6.21	1.03	3.86	3.75	1.03
102	Lymphatic nodes, head	5.98	5.81	1.03	2.58	2.50	1.03
103	Lymphatic nodes, trunk	104.40	101.36	1.03	57.66	55.98	1.03
104	Lymphatic nodes, arms	7.83	7.60	1.03	3.90	3.79	1.03
105	Lymphatic nodes, legs	11.10	10.78	1.03	9.80	9.51	1.03
106	Muscle, head	1217.81	1159.82	1.05	401.97	382.83	1.05
107	Muscle, trunk	15006.82	14292.21	1.05	8518.23	8112.60	1.05
108	Muscle, arms	2750.53	2619.55	1.05	1524.87	1452.26	1.05
109	Muscle, legs	10024.97	9547.59	1.05	7054.94	6718.99	1.05
110	Oesophagus	40.00	38.83	1.03	35.00	33.98	1.03
111	Ovary, left(female only)	N/A	N/A	N/A	5.50	5.29	1.04
112	Ovary, right(female only)	N/A	N/A	N/A	5.50	5.29	1.04
113	Pancreas	140.00	133.33	1.05	120.00	114.29	1.05
114	Pituitary gland	0.60	0.58	1.03	0.60	0.58	1.03
115	Prostate(male only)	17.00	16.19	1.05	N/A	N/A	N/A
119	Residual tissue	N/A	N/A	N/A	N/A	N/A	N/A

120	Salivary glands, left		42.50	40.48	1.05	35.00	33.33	1.05
121	Salivary glands, right		42.50	40.48	1.05	35.00	33.33	1.05
125	Skin	3300.00	7333.33	0.45	2300.00	N/A	N/A	
126	Spinal cord	30.00	28.85	1.04	28.00	26.92	1.04	
127	Spleen	150.00	141.51	1.06	130.00	122.64	1.06	
128	Teeth	50.00	18.18	2.75	40.00	14.55	2.75	
129	Testis, left(male only)	17.50	16.83	1.04	N/A	N/A	N/A	
130	Testis, right(male only)	17.50	16.83	1.04	N/A	N/A	N/A	
131	Thymus	25.00	24.27	1.03	20.00	19.42	1.03	
132	Thyroid	20.00	19.05	1.05	17.00	16.19	1.05	
133	Tongue (inner part)	42.00	40.00	1.05	50.00	47.62	1.05	
134	Tonsils	3.00	2.91	1.03	3.00	2.91	1.03	
135	Ureter, left	8.50	8.25	1.03	7.50	7.28	1.03	
136	Ureter, right	7.50	7.28	1.03	7.50	7.28	1.03	
137	Urinary bladder wall	50.00	48.08	1.04	40.00	38.46	1.04	
138	Urinary bladder contents	200.00	192.31	1.04	200.00	192.31	1.04	
139	Uterus(female only)	N/A	N/A	N/A	80.00	76.19	1.05	

3.3 Percentile-Specific Adult Phantoms

Each individual organ's volume and mass values within the 5th-to-95th percentile range were defined. Using the same height of 176 cm (males) and 163 cm (females), Figure 3.9 shows the 5th, 25th, 50th, 75th, 95th weight-percentile male and female phantoms representing individuals with variation in body weight (while the heights are kept the same). In order to realistically depict individuals of underweight or overweight, the skin meshes from an open source software, MakeHuman™ version 0.9.1 RC1I (<http://www.makehuman.org/>), were adopted. These skins were preprocessed to yield manifold meshes before being deformed to match the volume and mass of the given skin. Most organ volumes were kept the same as the 50th-percentile RPI-AM and RPI-AF phantoms; the entire body weight was adjusted by reducing or adding fat under the skin.

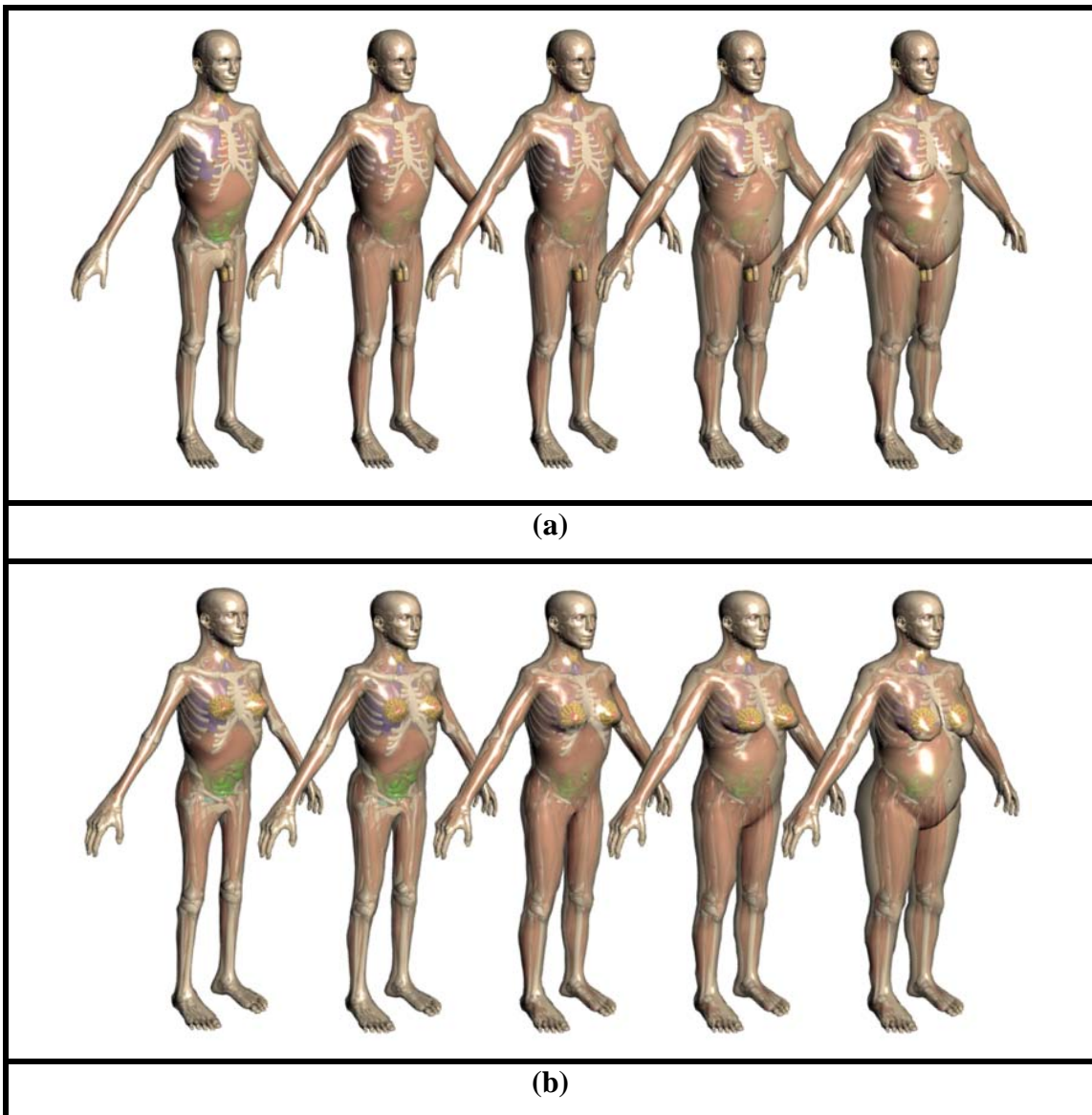


Figure 3.9: 3D front views of phantoms of the same height (males at 176cm and females at 163 cm) but with different weight percentiles (5th, 25th, 50th, 75th, 95th) representing variation in the body, respectively: (a) The males (58.5 kg 66.3 kg 73.1 kg 86.4 kg 103.8 kg); (b) the females (46.5 kg 55.8 kg 64.0 kg 78.9 kg 95.9 kg).

When both the height and weight change, there are many possible combination, making the management of these data and corresponding phantoms difficult. Table 3.2 and Figure 3.10 present adult male and female phantoms that are designed to represent

the 5th, 50th, 95th specific height and weight percentiles for given height and weight references. The percentile data are individually classified according to the height, weight, and each internal organ volume and mass.

Table 3.2: Male and female phantoms designed to represent the 5th, 50th, 95th specific height and weight-percentile.

Gender	Percentile	5 th	50 th	95 th
Male	Height(cm)	165	176	188
	Weight(kg)	56.1	73	110.9
Female	Height(cm)	152	163	173
	Weight(kg)	41	60	91

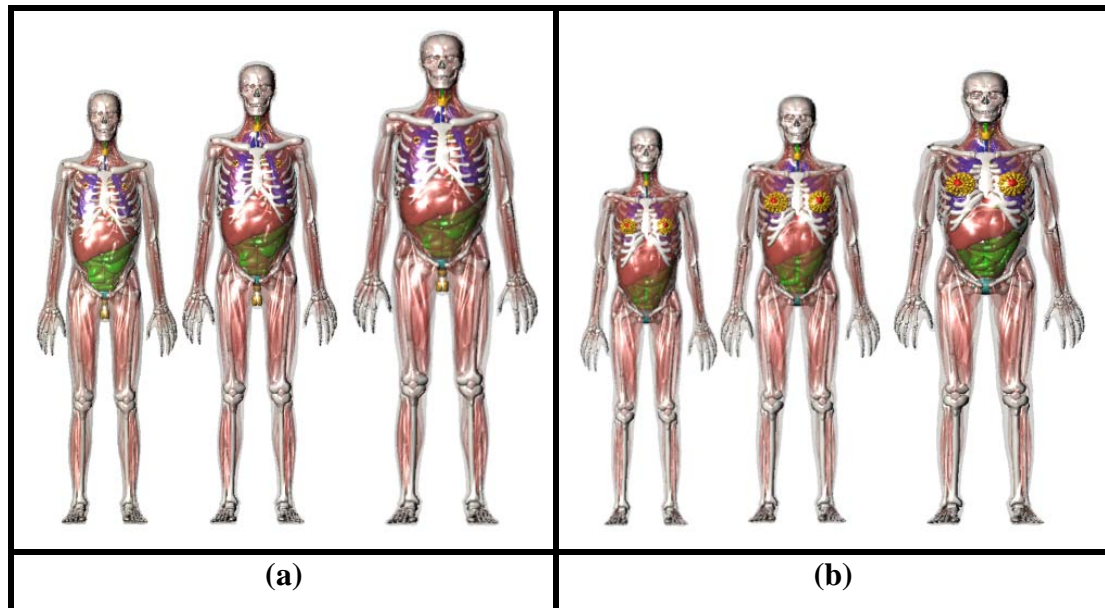


Figure 3.10: 3D anterior and posterior view views of 5th, 50th, 95th percentile-specific adult male and female models, respectively: (a) The males (165 cm, 176 cm, and 188 cm in height, respectively, and 56 kg, 73 kg, and 110 kg in weight, respectively); (b) the females (152 cm, 163 cm, and 173 cm in height, respectively, and 41 kg, 60 kg, and 91 kg in weight, respectively).

The entire organ deforming process was completed automatically within about 5 minutes on a PC operated in Intel® Centrino® Duo CPU of 2GHz with 1GB of RAM. The percentile-specific phantoms have the same number of organs and muscles, as well as the bone structures (total of 70 internal organs, 45 bone components and 4 muscle structures) as the RPI-AM and RPI-AF phantoms for 50th percentiles.

3.4 Breast Deformable Female Phantoms

Specific parameters of the Bust Girth (BG) and the Under Bust Girth (UBG) recommended by the European cloth size standard were considered (EN 13402-1 2001, EN 13402-2 2002, EN 13402-3 2004). According to EN 13402-2 and -3, the brassiere cup sizes (i.e., AA, A, B, C, D, E, F, G) were characterized by the difference between BG and UBG which were measured by the perimeter of the outermost breast skin contour. Table 3.3 summarizes the measured anthropometric data, and provides the glandularity, and total mass of the breasts of the phantoms used in this study.

Table 3.3: The measured anthropometric data of the deformable breast phantoms sorted by the cup size (CS), busts girth (BG), and under bust girth (UBG).

CS code letter	BG	UBG	CS	Glandularity	Mass
Model	(cm)	(cm)	(cm)	(%)	(g)
AA	99.6	89.2	10.4	40	500
A	102.6	89.2	13.4	15	1317
B	104.6	89.2	15.4	12	1700
C	105.8	89.2	16.6	11	1897
D	107.6	89.2	18.4	9	2331
E	110	89.2	20.8	7	2791
E40	112	89.2	22.8	40	2854
F	112	89.2	22.8	6	3304
G	114	89.2	24.8	5	3855

In addition, the female breast model was deformed by a 60-degree downward angle along each vertex normal direction to simulate the effect of gravity for a bra-wearing woman. Figure 3.11 summarizes the adjustable breast phantoms. The application of such a breast-adjustable female phantom will be described later in this chapter.

Code	AA	A	B	C	D	E	F	G
Cup size	10~12	12~14	14~16	16~18	19~20	20~22	22~24	24~26
Range (cm)								
								

Figure 3.11: Different breast sizes of the female phantom according to the brassiere cup size definition (AA to G) by European clothes sizes standard (EN 13402).

3.5 Walking Posture Adult Phantoms

The whole-body frames of the RPI-AM and RPI-AF are deformed their default upright standing posture to various body postures such as sitting, walking, raised-arm up, with keeping detailed anatomical features shown in Figure 3.12. The phantoms are having ability to change their size to match with aforementioned percentile-specific phantoms. The posture-specific phantoms have the same number of organs and muscles, as well as bone structures; total of 70 internal organs, 45 bone components and 4 muscle structures based on the RPI reference adults.

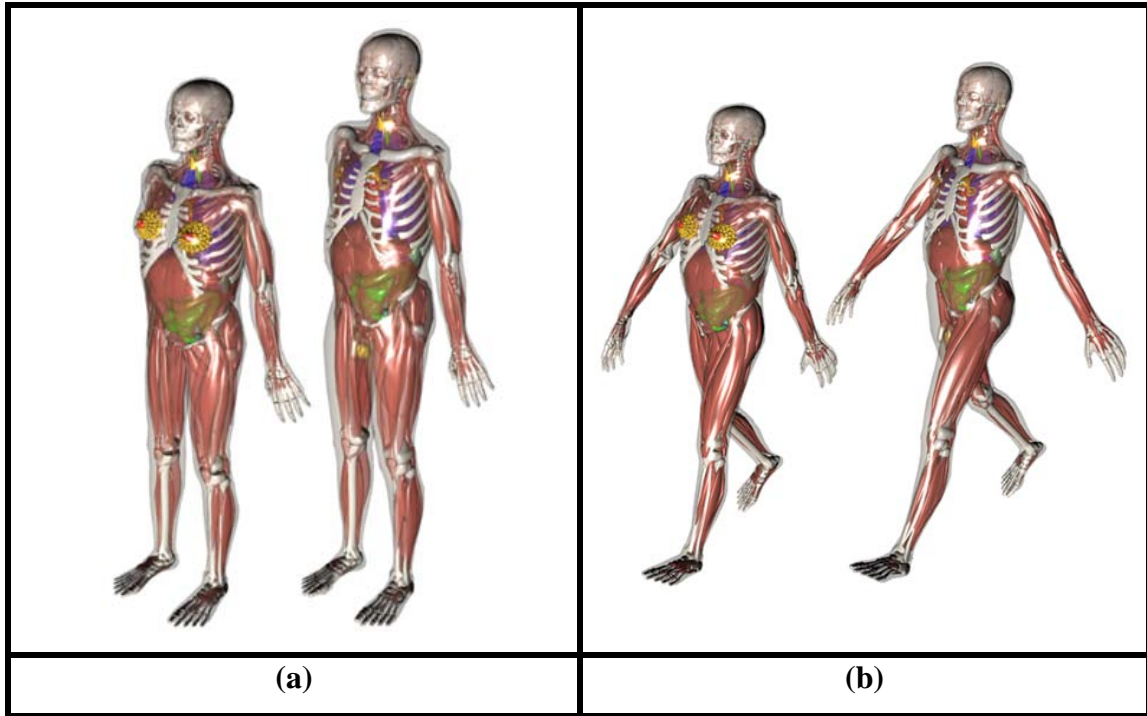


Figure 3.12: 3D views for various postures of male and female phantoms, respectively: (a) Standing; (b) walking.

4. Demonstration and Discussion for Radiation Dose Calculations

A phantom voxelization software tool was developed using the programming language Microsoft® Visual C# and VTK. The deformable mesh-based RPI-AM and RPI-AF phantoms were converted into the desired voxel-based phantoms with desired voxel resolution. Those voxel geometries can be adopted into Monte Carlo radiation transport calculations. Each voxel was labeled with one unique organ ID to describe its own physical properties.

4.1 Voxelization Procedures

First, each organ of the deformable mesh-based RPI-AM and RPI-AF phantoms was saved as a single 3D surface file in the organ library. Second, a bounding box (phantom box) enclosing the entire mesh-based phantom is specified. Next, the user defines the voxel resolution for the phantoms, with the default size of 1 mm. The in-house voxelization software, called “*mesh2voxel*” is based on the parity-counting and ray-stabbing methods (Nooruddin et al. 2003) for closed-mesh polygonal surfaces. The ray-stabbing method is suitable for perfect closed-mashes, but the parity-counting method was also used in this process for certain geometrically complicated tissues, such as the vessels and muscles, that may still contain open-meshes. Considering different organ mesh shapes and structures, the specific voxelization procedures are required as follows:

The bones and organs with outer/inner layers. Each organ in this group was converted to the voxel format by first voxelizing the inner layer structures (i.e., the contents of a walled organ or the spongiosa of a bone). The outer layer structures (i.e., the surface of an organ) are then voxelized as the remaining space between the outer and inner layer surfaces by taking into account of their respective reference tissue information.

The vessels and muscles. After the mesh preprocessing, the complicated vessel structures (i.e., for blood vessels and lymphatic vessels) and muscle structures (i.e., for head, body, arms, and legs) needed to be checked as they tend to produce overlaps with other organs. To this end, the volumes of these organs were re-evaluated in the voxel domain at the last step after other internal organs have been finalized.

The skin. The skin is difficult to model in either voxel or mesh format because it is a very thin layer on the surface of the body with a thickness less than 1 mm. A representation by a double-layer mesh for the skin is not acceptable in the voxel domain. For this reason, as is done in most voxel phantoms in existence, the skin was defined during the voxelization process by adding a single layer of voxels around the body excluding the eye lenses and eye balls. This caused the skin's volume to differ from the reference value, depending on the chosen voxel resolution. To maintain the total reference skin masses—3.3 kg for the reference male and 2.3 kg for the reference female—the skin's density was defined as the reference mass divided by the skin's volume in the voxel domain (Xu et al. 2007).

The breast size deformable female phantoms. The voxelization for the female breast phantoms was based on the density and elemental composition information obtained from the ICRP references (ICRP 1975, ICRP 2002). The density of the breast skin in the AA-size phantom, however, was modified from the nominal value to agree with the recommended mass by the ICRP. In addition, the E-size phantom which has 7% glandularity was revised to have 40% glandular tissue based on the recommended ICRP (2002) for the reference adult female, and was named as the E40 to be distinguished from the original E-size phantom.

The visual inspection of voxelized phantoms. Visual inspections required to assure the fidelity of the conversion process. As examples of mesh format and its voxelized format, the visual inspections are respectively shown in Figure 4.1 for skull (Figure 4.1a and Figure 4.1b) and skeleton (Figure 4.1c and Figure 4.1d).

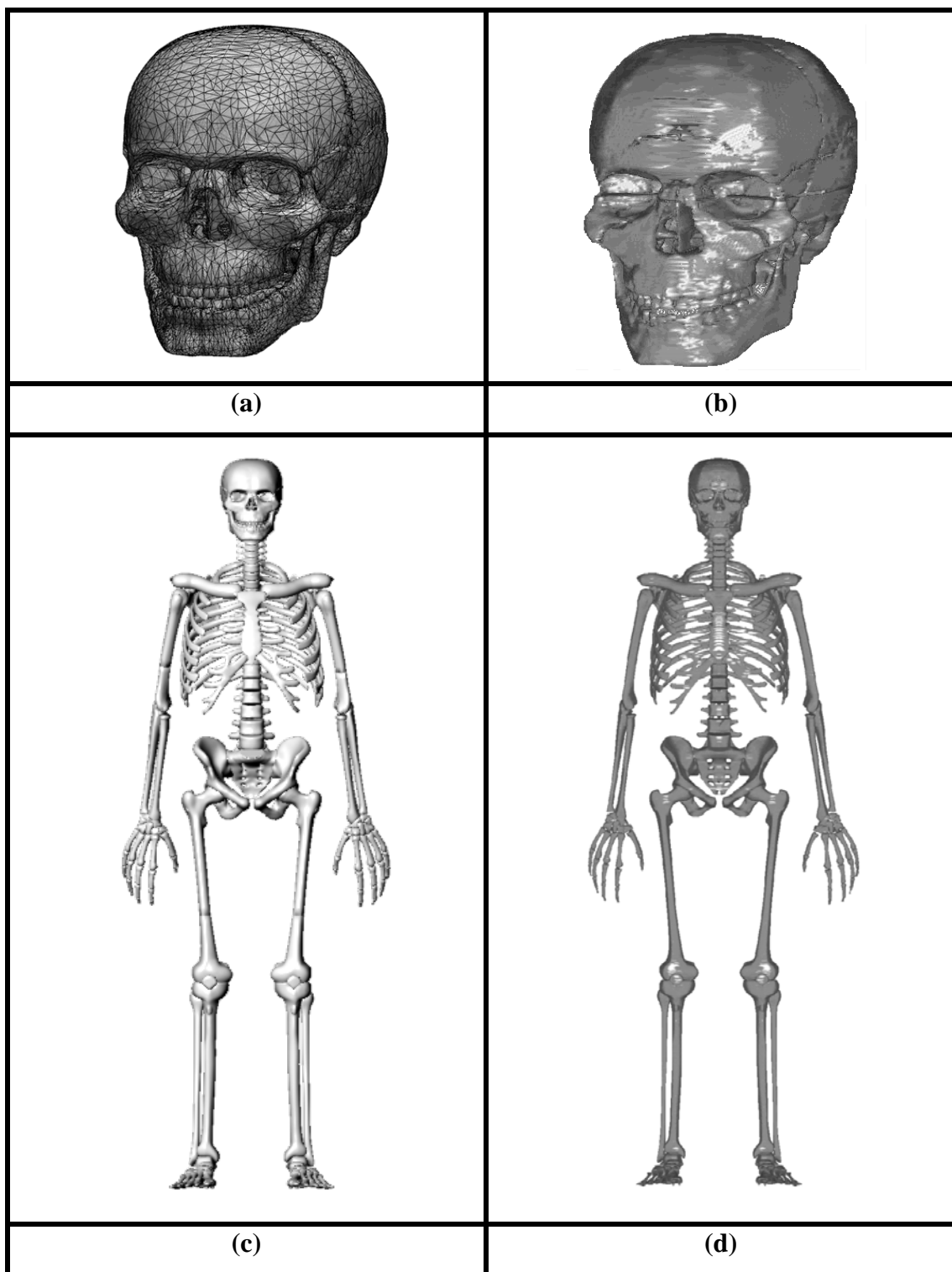


Figure 4.1: Visual inspection of the skeleton certifies the accuracy of the voxelization process transforming from mesh to voxel geometry: (a) mesh-based skull; (b) voxelized skull; (c) mesh-based skeleton; (d) voxelized skeleton.

4.2 Preparation of MCNPX Input Files with Specific Organ and Physical Properties

During MCNPX simulations, a large number of particles and the tracking of each particles in the voxel-based phantoms can be processed iteratively until all of the particle energy is absorbed with controlling the inherent statistical uncertainty less than 1%. This uncertainty even more precise than an physical experiment results through a physical phantoms having a dosimeter which is able to quantitatively measure the abosbed doses.

The procedure of computational simulation is as follows: (1) defining acceptable geometries for Monte Carlo code with involving anatomical whole-body phantoms; (2) particularizing the density and chemical compositions of tissues and internal organs; (3) determining the radiation source terms matching to specific source-to-human-body irradiation condition. The most common irradiation geometries of external radiation used external parallel beams impinging on the entire whole-body phantoms which are vertically standing in a vacuum. Six external particle irradiation directions are defined as standard geometries: anterior-posterior (AP), posterior-anterior (PA), left lateral (LLAT), right lateral (RLAT), rotational (ROT) and isotropic (ISO); (4) estimating the organ doses using normalization through the particle fluence or air-kerma measured by radiation detector.

4.2.1 Organ Labeling and Physical Property Assignment

In this study, a voxel-phantom is constructed using a lattice of organ IDs so that the MCNPX code is able to correctly calculate energy deposition in each organ during the radiation transport simulations. During the constructing of a voxel phantom, each organ ID is assigned according to the organ library, so that each voxel has its particular ID to which it belongs.

In the recent versions of MCNPX (Pelowitz2005), the maximum number of voxels allowed is 25 million, so that the voxel resolutions of the adult male and adult female were set to 3.0 mm and 2.5 mm, respectively. The total number of voxels in each phantom is about 24 milion. Table 4.1 summarizes the organ elemental compositions data which were used. These values are based on the reference values provided by the ICRP Publications 89, 108, and ICRU 46 (ICRP 2002, ICRP 2009, ICRU 1992).

According to the ICRP Publication 23 (ICRP 1975), the average densities of the reference adult male and female were $1.07 \text{ g}\cdot\text{cm}^{-3}$ and $1.04 \text{ g}\cdot\text{cm}^{-3}$, respectively. The average volume of the whole body could be derived from dividing the whole body's reference mass by the density. For the purpose of defining the connecting tissues that do not belong to any specific organ, a “remainders” tissue was defined to make up the mass difference between the total body and all explicitly accounted organs.

Table 4.1: Organ-specific mass fractions for various tissue composition materials.

ID	Tissue material											
	H	C	N	O	Na	P	S	Cl	K	Ca	Mg	others
1,2,7,8,70,71,110,												
114,115,120,121,	0.105	0.256	0.027	0.602	0.001	0.002	0.003	0.002	0.002	-	-	-
126,131,134~136												
61	0.107	0.145	0.022	0.712	0.002	0.004	0.002	0.003	0.003	-	-	-
72~86	0.106	0.115	0.022	0.751	0.001	0.001	0.001	0.002	0.001	-	-	-
87	0.104	0.139	0.029	0.718	0.001	0.002	0.002	0.002	0.003	-	-	-
89~94	0.103	0.132	0.03	0.724	0.002	0.002	0.002	0.002	0.002	0.001	-	-
95	0.103	0.186	0.028	0.671	0.002	0.002	0.003	0.002	0.003	-	-	-
97,99	0.103	0.105	0.031	0.749	0.002	0.002	0.003	0.003	0.002	-	-	-
111,112	0.105	0.093	0.024	0.768	0.002	0.002	0.002	0.002	0.002	-	-	-
113	0.106	0.169	0.022	0.694	0.002	0.002	0.001	0.002	0.002	-	-	-
62,64,119	0.106	0.315	0.024	0.547	0.001	0.002	0.002	0.001	0.002	-	-	-
13,16,19,22,24,26,												
28,31,34,37,39,41,	0.035	0.16	0.042	0.445	0.003	0.095	0.003	-	-	0.215	0.002	-
43,45,47,49,51,53,55												
125	0.1	0.204	0.042	0.645	0.002	0.001	0.002	0.003	0.001	-	-	-
127	0.103	0.113	0.032	0.741	0.001	0.003	0.002	0.002	0.003	-	-	-
132	0.104	0.119	0.024	0.745	0.002	0.001	0.001	0.002	0.001	-	-	I:0.001
137,138	0.105	0.096	0.026	0.761	0.002	0.002	0.002	0.003	0.003	-	-	-
139	0.106	0.315	0.024	0.547	0.001	0.002	0.002	0.001	0.002	-	-	-
66~69	0.096	0.195	0.057	0.646	0.001	0.001	0.003	0.001	-	-	-	-
140	-	0	0.755	0.232	-	-	-	-	-	-	-	Ar:0.0128
5,106~109,133	0.102	0.143	0.034	0.71	0.001	0.002	0.003	0.001	0.004	-	-	-
3	0.096	0.099	0.022	0.744	0.005	0.022	0.009	0.003	-	-	-	-
9~12,88	0.102	0.11	0.033	0.745	0.001	0.001	0.002	0.003	0.002	-	-	Fe:0.001

128	0.022	0.095	0.029	0.421	-	0.137	-	-	-	0.289	0.007	-
129,130	0.106	0.099	0.02	0.766	0.002	0.001	0.002	0.002	0.002	-	-	-
100~105	0.108	0.041	0.011	0.832	0.003	-	0.001	0.004	-	-	-	-
63,65	0.114	0.598	0.007	0.278	0.001	-	0.001	0.001	-	-	-	-
14	0.084	0.3	0.027	0.481	0.003	0.035	0.004	0.001	-	0.065	0.001	-
17,20,23,32,35,38	0.096	0.443	0.017	0.373	0.002	0.023	0.003	0.001	-	0.042	-	-
25	0.09	0.361	0.024	0.439	0.002	0.028	0.003	0.001	-	0.051	0.001	-
27	0.089	0.35	0.025	0.448	0.002	0.028	0.003	0.001	-	0.052	0.001	-
29	0.093	0.398	0.022	0.413	0.002	0.024	0.003	0.001	-	0.043	0.001	-
40	0.081	0.276	0.027	0.497	0.003	0.038	0.004	0.001	-	0.071	0.001	-
42	0.093	0.38	0.025	0.431	0.002	0.023	0.003	0.001	-	0.041	0.001	-
44	0.088	0.315	0.029	0.48	0.002	0.028	0.004	0.001	-	0.051	0.001	-
46	0.086	0.322	0.026	0.467	0.003	0.032	0.004	0.001	-	0.059	0.001	-
48	0.103	0.438	0.027	0.405	0.001	0.009	0.002	-	-	0.013	0.001	Fe:0.001
50	0.099	0.41	0.027	0.422	0.002	0.013	0.003	-	-	0.022	0.001	Fe:0.001
52	0.094	0.369	0.028	0.447	0.002	0.02	0.003	-	-	0.035	0.001	-
54	0.105	0.46	0.027	0.391	0.001	0.005	0.002	-	-	0.006	0.001	Fe:0.001
56	0.104	0.449	0.027	0.398	0.001	0.007	0.002	-	-	0.01	0.001	Fe:0.001
15,18,21,30,33,36	0.115	0.644	0.007	0.231	0.001	0.001	0.001	-	-	-	-	-

4.2.2 Organ Centroid

In order to estimate the distance in-between organs, the organ centroid are used by defining a 3D coordinate system. The ranges of the system are described as box with the width, length, and height of a rectangular prism, called phantom box. The voxelized computational phantom is exactly placed inside the prism (phantom box). The positive direction of the x-axis (width), y-axis (length), and z-axis (height) are heading toward left side to right side of the phantom, front to back, and head to feet, respectively. The coordinate value of the organ centroid can be described by the following equations:

$$(\bar{x}, \bar{y}, \bar{z}) = \frac{1}{n} \left(\sum_{i=1}^n x_i, \sum_{i=1}^n y_i, \sum_{i=1}^n z_i \right) \quad (3.1)$$

where $(\bar{x}, \bar{y}, \bar{z})$ is the (x, y, z) coordinate of organ centroid, (x_i, y_i, z_i) is the (x, y, z) coordinate of each organ, n is the number of organ voxels.

4.2.3 Implementation of Voxelized Phantoms in MCNPX

The voxel-based computational phantoms converted from the mesh-based phantoms are used to Monte Carlo dose calculations because current Monte Carlo codes do not allow using the mesh-based geometries directly. The voxel-based phantoms are composed of the data array of their organ IDs assigned by a unique organ ID number in each organ and tissue through the voxelizatoin processing. For this reason, the relative positions of organ-voxels in array determine each position of organs.

The MCNPX code used for the Monte Carlo dose calculation is based on the iterative structure to carry out the voxel geometry. The cells and surfaces in the MCNPX code only require one time description although they appear more than that time in the array (Bozkurt et al. 2000).

A software package, called “*voxel2mcnp*”, was developed in-house to create MCNPX input files. The input file size is able to be reduced by more than 60% using the MCNPX repeating function when the voxels have identical organ IDs in the sequential array positions. The relative errors of the final organ masses are less than 0.5% except for the small eye lens (about 3% error) of reference volume of 0.18182 cm^3 . Figure 4.2 shows in-house developed voxelization software tools.

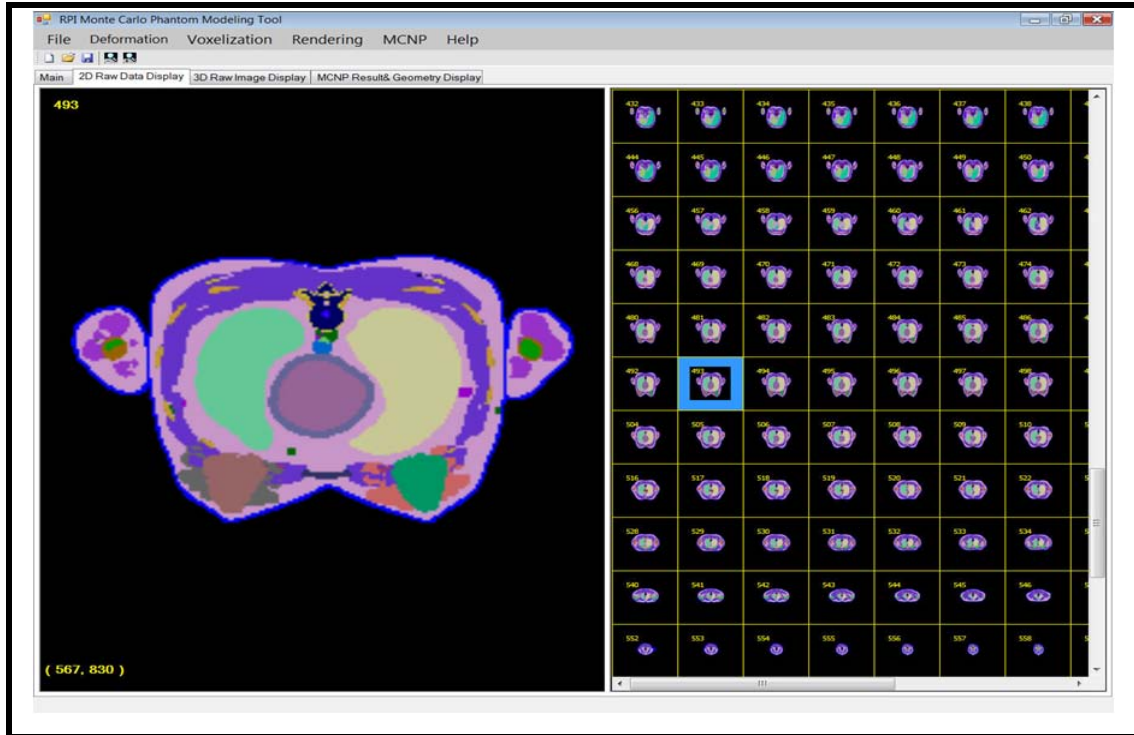


Figure 4.2: Software GUI for voxelization tools (Image is courtesy of Mr. Aiping Ding).

4.3 Monte Carlo Modeling for Organ Dose Comparisons

This study focused on the geometrical phantom development. However, to show how these newly developed phantoms can be used for a variety of radiation dose calculations, the sections below present several examples in which the Monte Carlo dose calculations were performed by fellow students at Rensselaer. These examples cover: (1)¹ organ dosimetry using RPI adult phantoms and ICRP Adult Phantoms; (2)^a organ dosimetry using RPI percentile-specific adult phantoms; (3)² lung counter efficiency using breast deformable female phantoms; (4)³ environmental dosimetry using walking posture adult phantoms

¹ Work performed jointly with Mr. Zhang Juying (Zhang et al. 2009)

² Work performed jointly with Mr. Hegenbart Lars (Hegenbart et al. 2008)

³ Work performed jointly with Mr. Han Bin (Han et al. 2009)

4.3.1 Organ Dosimetry using Deformable Phantoms and ICRP Adult Phantoms

Organ doses for the RPI-AM phantom and RPI-AF phantom both respectively having cubic voxel sizes of 3.0 mm and 2.5 mm were estimated for external photon sources implemented into MCNPX code. The elemental compositions of individual organs were based of the ICRP Publication 89 (ICRP 2002).

The external source exposures were used described by six-standard source geometry: (1) project anterior-posterior (AP); (2) posterior-anterior (PA); (3) right lateral (RLAT); (4) left lateral (LLAT); (5) rotational (ROT); (6) isotropic (ISO). Figure 4.3 shows the external source geometries.

With the photon energy ranges between 10 keV and 10 MeV, the MCPLIB04 photon cross-sectional library based on EPDL 97 evaluation was used for the anatomic interactions. The organ doses for the ICRP adult male and female (REX and REGINA) phantoms (Schlattl et al. 2007, Zankl et al. 2007) and the RPI-AM and RPI-AF were compared and were analyzed by the anatomical details (Zhang et al. 2009).

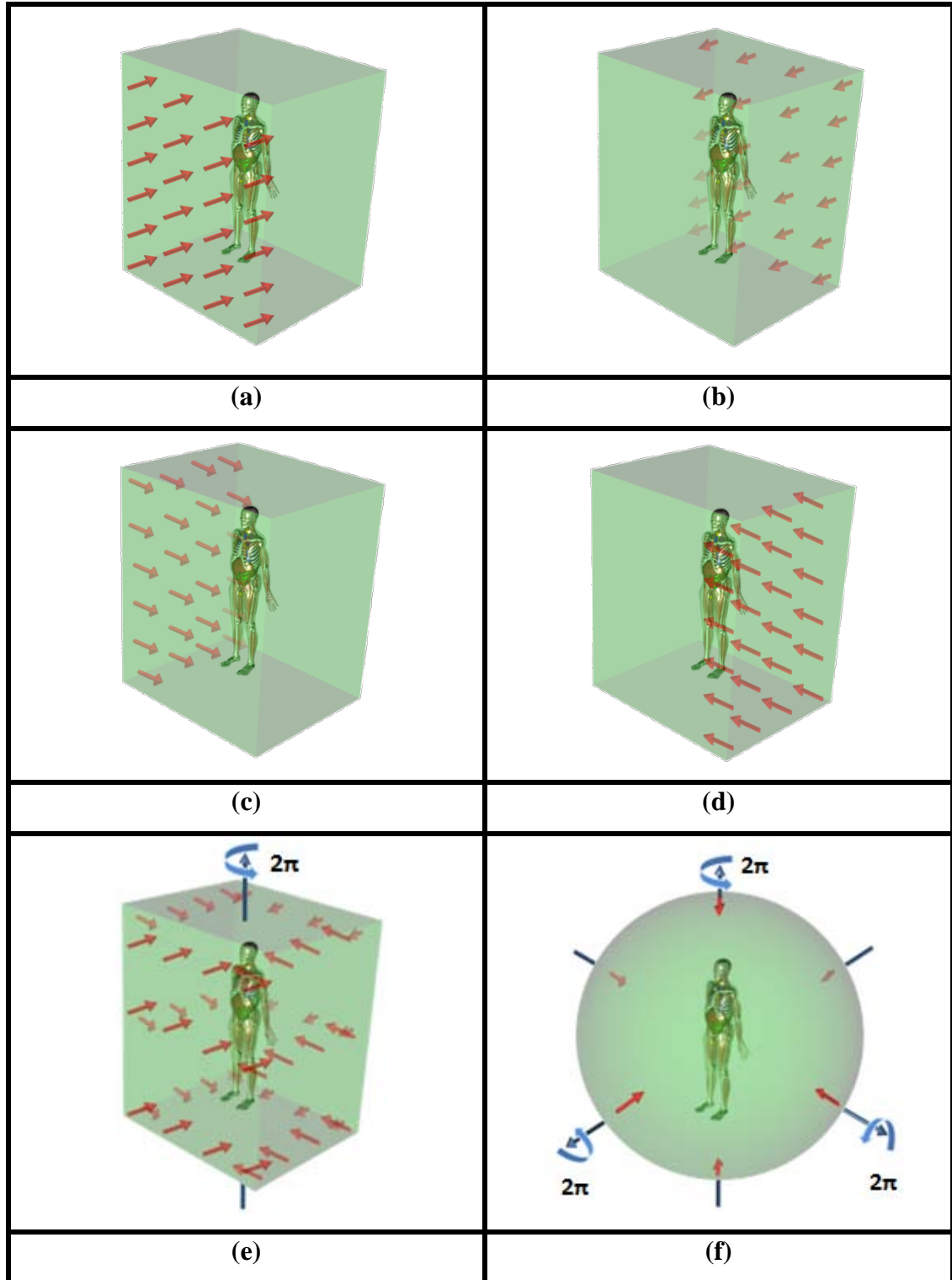


Figure 4.3: Six-standard external source geometries for external photon dose calculations: (a) anterior-posterior (AP); (b) posterior-anterior (PA); (c) right lateral (RLAT); (d) left lateral (LLAT); (e) rotational (ROT); (f) isotropic (ISO).

4.3.2 Organ Dosimetry using Percentile-Specific Phantoms

According to the information of tissue density and elemental composition (ICRU 1992), the assessment of organ doses for the voxelized percentile-specific phantoms were obtained using Monte Carlo simulation of radiation transport. In this study, the MCNPX code was used for organ dose calculations (Pelowitz 2005). The absorbed organ doses for the external photon exposures in anterior-posterior (AP) direction with different percentile phantoms were calculated and compared as shown in Figure 4.4. Each specific organ elemental composition was based on the reference values in the ICRP Publication 89. Two photon energies are presented: 0.5 MeV and 1 MeV. The MCPLIB04 cross-sectional library for the anatomic interactions based on EPDL 97 evaluation was used. For electron transport, the standard library EL03 was used (Na et al. 2009b).

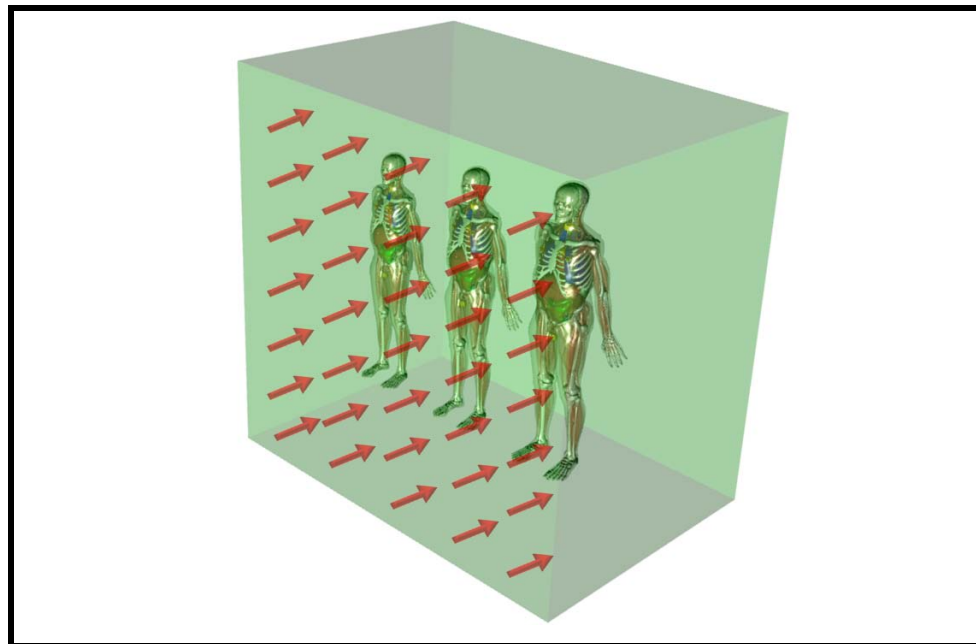


Figure 4.4: Phantoms representing workers of 5th-, 50th-, 95th- weight and height percentile (weight: 56-, 73-, 110-kg and height: 165-, 176-, 188-cm, respectively) exposure to 0.5 MeV and 1 MeV phantom beams in AP irradiation geometry (Na et al. 2009b).

4.3.3 Lung Counter Efficiency using Breast Deformable Female Phantoms

A bioassay procedure for a worker who has been exposed to airborne radioactive materials requires the estimation of radioactivity burden inside the lung. A lung counter is an in-vivo measuring device which consists of radiation detectors sensitive to photons emitted from the radionuclides in the lungs. Placed on or near the surface of the body as shown in Figure 4.5, a lung counter can be used to quantify internally accumulated radionuclides. However, a calibration must be performed before the detector response can be directly correlated with the retained radioactivity inside the lungs. In most cases, the calibration can be performed using a physical lung phantom with known radioactivity and type of radionuclides, such the Lawrence Livermore National Laboratory Torso-Phantom that has removable chest plates (Griffith 1978). In the case of female workers, however, a “virtual calibration” method using computer phantoms is more effective because the deformable mesh-based RPI-AF phantom can be used to account for a variety of breast sizes and shapes. To demonstrate the usefulness of the deformable phantoms described earlier, a set of 8 female phantoms have been developed with a range of different breast sizes.

The voxelization for the female breast phantoms was based on the density and elemental composition information obtained from ICRP references (ICRP 1975, ICRP 2002). The density of the breast skin in the AA-size phantom, however, was modified from the nominal value to agree with the recommended mass by the ICRP. In addition, the E-size phantom which has 7% glandularity was revised to have 40% glandular tissue based on the recommended ICRP⁸ for the reference adult female, and was named as the E40 to be distinguished from the original E-size phantom (Hegenbart et al. 2008).

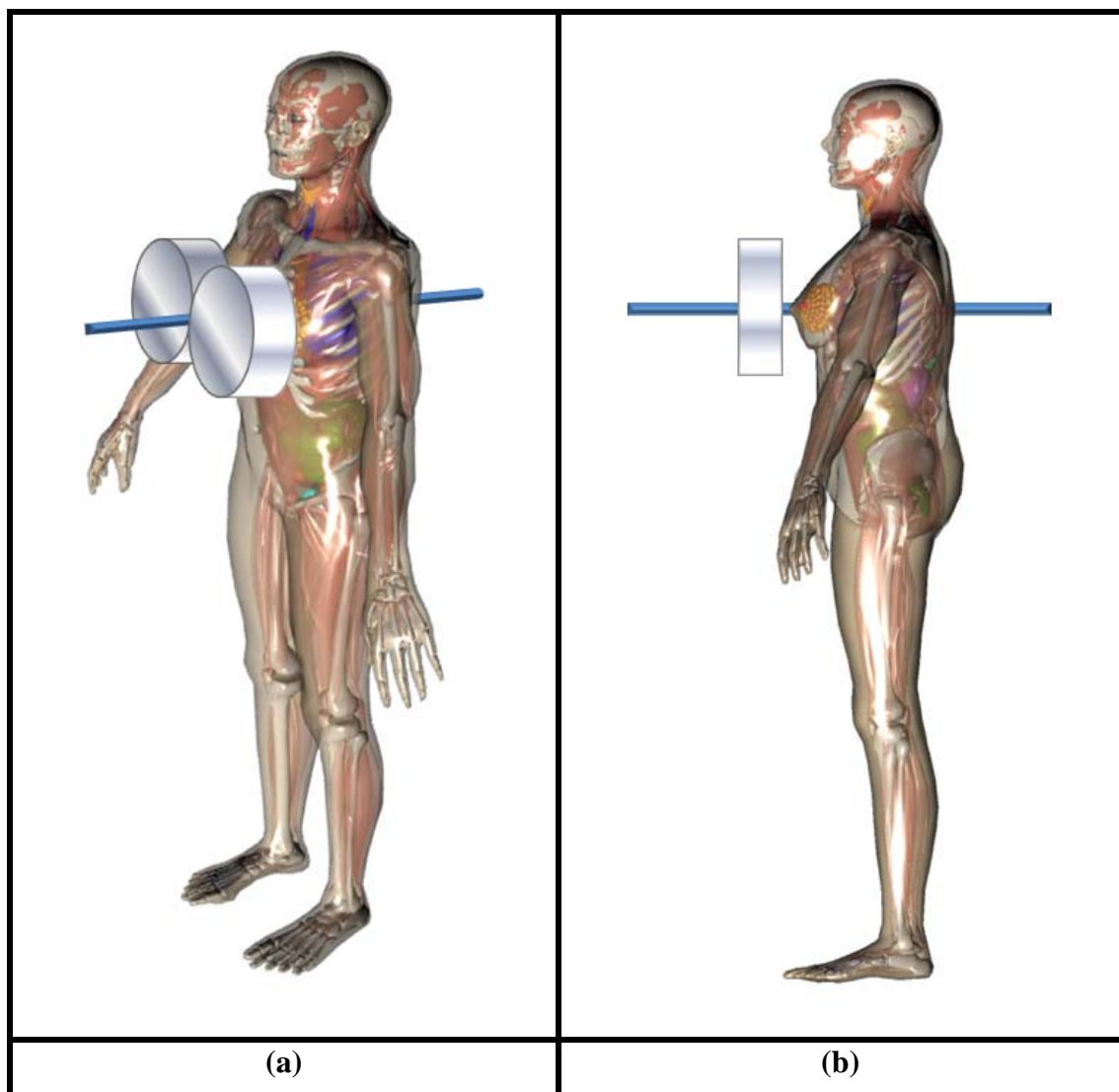


Figure 4.5: The position of the lung counter in the virtual calibration (Hegenbart et al. 2008): (a) the central axis indicating the center-of-mass of the two lungs defined in the MCNPX; (b) Phoswich detector placed on the surface of the chest for lung counting measurement.

Three radionuclides, Am-241(low energy), Cs-137(medium energy) and Co-60(high energy) listed in Table 4.2, were chosen to investigate the energy dependence of the counting efficiency. The radionuclides were uniformly distributed throughout the entire lung volumes.

Table 4.2: Nuclides and their photon energies used for the virtual calibration of the lung counter (Only photons with emission probabilities greater than 0.01 were considered) (Hegenbart et al. 2008).

Nuclide	Photon energy (MeV)	Emission probability
Am-241	0.01376	0.0108
	0.0139	0.1193
	0.01754	0.1861
	0.02101	0.0482
	0.02634	0.024
	0.05954	0.359
Cs-137	0.03182	0.0195
	0.03219	0.0359
	0.0364	0.01055
	0.6616	0.85
Co-60	1.17323	0.9985
	1.33249	0.99983

There are several types of lung counters, one of which is the so-called Phoswich scintillation detector (Hegenbart et al. 2008). The thickness of the NaI(Tl)-crystal is 1.0 mm and the diameter is 203.2 mm for low-energy photons. For high-energy photons, the CsI(Tl)-crystal, which had a 50.8 mm thickness and 203.2 mm diameter, is coupled to the NaI(Tl)-crystal. Another non-doped NaI-crystal was located beyond the detector crystals. All crystals were embedded in the Al₂O₃ power, which was sealed airtight in the steel housing with a Beryllium front window. To simplify the detector model, other parts of detector (e.g., photomultiplier) were not considered. The Gaussian Energy Broadening (GEB) in the MCNPX code was used to improve the realism of the simulated gamma spectra Empirical data for Full Width at Half Maximum (FWHM) for photopeak was adopted as the GEB parameters. The energy range for Am-241 was 20 keV to 80 keV. For Cs-137, the energy range was set to ± 1.25 FWMH around its peak

energy of 661.6 keV. For Co-60, the energy range was also set to ± 1.25 FWMH around its peak energies of 1.17323 MeV and 1.33249 MeV. For each Monte Carlo simulation, a total of 5-million particle histories were run to yield relative statistic uncertainties (one standard deviation) less than 0.4 %.

4.3.4 Environmental Dosimetry using Walking Posture Adult Phantoms

The mesh-based walking postures phantoms of the RPI-AM and RPI-AF were voxelized. The voxel geometries then were implemented into the MCNPX code for organ dose calculations (Pelowitz 2005). The cubic voxel sizes of 4.25 mm and 3.2 mm for walking male and female phantoms were respectively employed because of the voxel limitation in the MCNPX code. The voxelized phantoms were validated by the ICRP recommended reference values (ICRP 2002). The 0.29 g cm^{-3} and 0.30 g cm^{-3} skin densities for male and female walking phantoms were respectively assigned. The reference values for the tissue elemental composition were based on the ICRP (2002) and ICRU (1992) to simulate the radiation transport using Monte Carlo methods.

The contaminated ground was implemented by the planar sources of Cs-137 and Co-60 with 30 kBq/m^2 contamination concentration to assume equal deposition on the soil of radioactive dust or the result of a nuclear accident (Shutov et al. 2002).

The organ dose calculations results were compared to the upright standing RPI-AM and RPI-AF. Figure 4.6 illustrates the walking postures of RPI-AM and RPI-AF on the contaminated ground (Han et al. 2009).

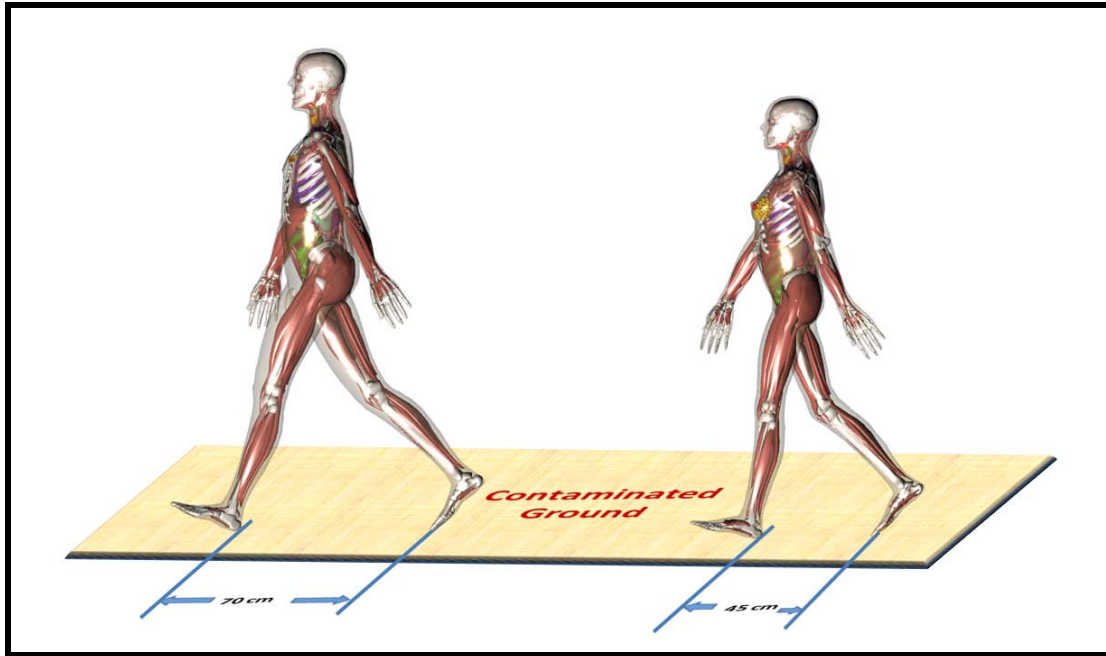


Figure 4.6: Walking postures of the RPI-AM and RPI-AF on the contaminated ground: 70cm and 45cm of step lengths for male and female phantoms, respectively. (Han et al. 2009).

4.4 Discussion on Results for Radiation Dose Calculations

As noted in earlier sections, the applications of the deformable RPI-AM and RPI-AF phantoms in radiation protection dosimetry are plentiful with different types and sources of ionizing and non-ionizing radiations, as well as various radiation environments. In this section, the results of Monte Carlo dose calculations are summarized and discussed.

4.4.1 RPI 50th-Percentile Phantoms vs. ICRP Adult Phantoms

In a joint effort with a former student, Juying Zhang, the results of the organ dose assessment associated with the RPI-AM and RPI-AF were compared with the ICRP reference adult male and female phantoms, REX and REGINA, respectively (Zhang et al. 2009). The statistical uncertainty (Briestmeister 1997) in most organ absorbed doses for the RPI-AM and RPI-AF is less than 2%, except the eye lens for which were less than 10% of the statistical uncertainty. The dose estimation can be extensively rated as a

reliable consequence if the statistical uncertainty is less than 10%. The RPI adult phantoms and the ICRP reference phantoms were implemented in a same manner as the MCNPX codes with setting up six-standard source geometry. For this reason, the results comparing organ doses calculated with these phantoms are relatively similar in higher photon energies as shown in Figure 4.7 and Figure 4.8. On the other hand, the differences of organ doses observed in lower photon energies were attributed to the combination of anatomical structures variances and the voxel sizes: REX and REGINA ($2.137 \times 2.137 \times 8 \text{ mm}^3$, $1.775 \times 1.775 \times 4.84 \text{ mm}^3$), the RPI-AM and RPI-AF ($3.0 \times 3.0 \times 3.0 \text{ mm}^3$, $2.5 \times 2.5 \times 2.5 \text{ mm}^3$), respectively.

Figure 4.7a shows the results of the RPI-AM lung absorbed doses in comparison with REX. The pronounced differences are observed in lateral irradiation geometries (i.e., LLAT and RLAT source directions) with the photon energies below 1 MeV. The RPI-AM receives higher absorbed dose to lungs than REX because the arm positions of REX can cause less photon attenuation as depicted in Figure 4.7b and Figure 4.7c.

The comparison of the breast absorbed doses is shown in Figure 4.8a. At photon energies below 100 MeV, the dose to breast in REGINA is higher than those in the RPI-AF because REGINA has a comparatively thicker glandular tissue surrounded by thinner layer of adipose tissue than those in the RPI-AF. Whereas photon energies above 8 MeV, the thinner layer of adipose tissue in REGINA causes a loss of charged particle equilibrium, especially, for the AP irradiation geometry, so that it can also lead to lower dose to breast in REGINA than the RPI-AF. Figure 4.8b and Figure 4.8c illustrate the differences of breast tissue structures between the RPI-AF and REGINA.

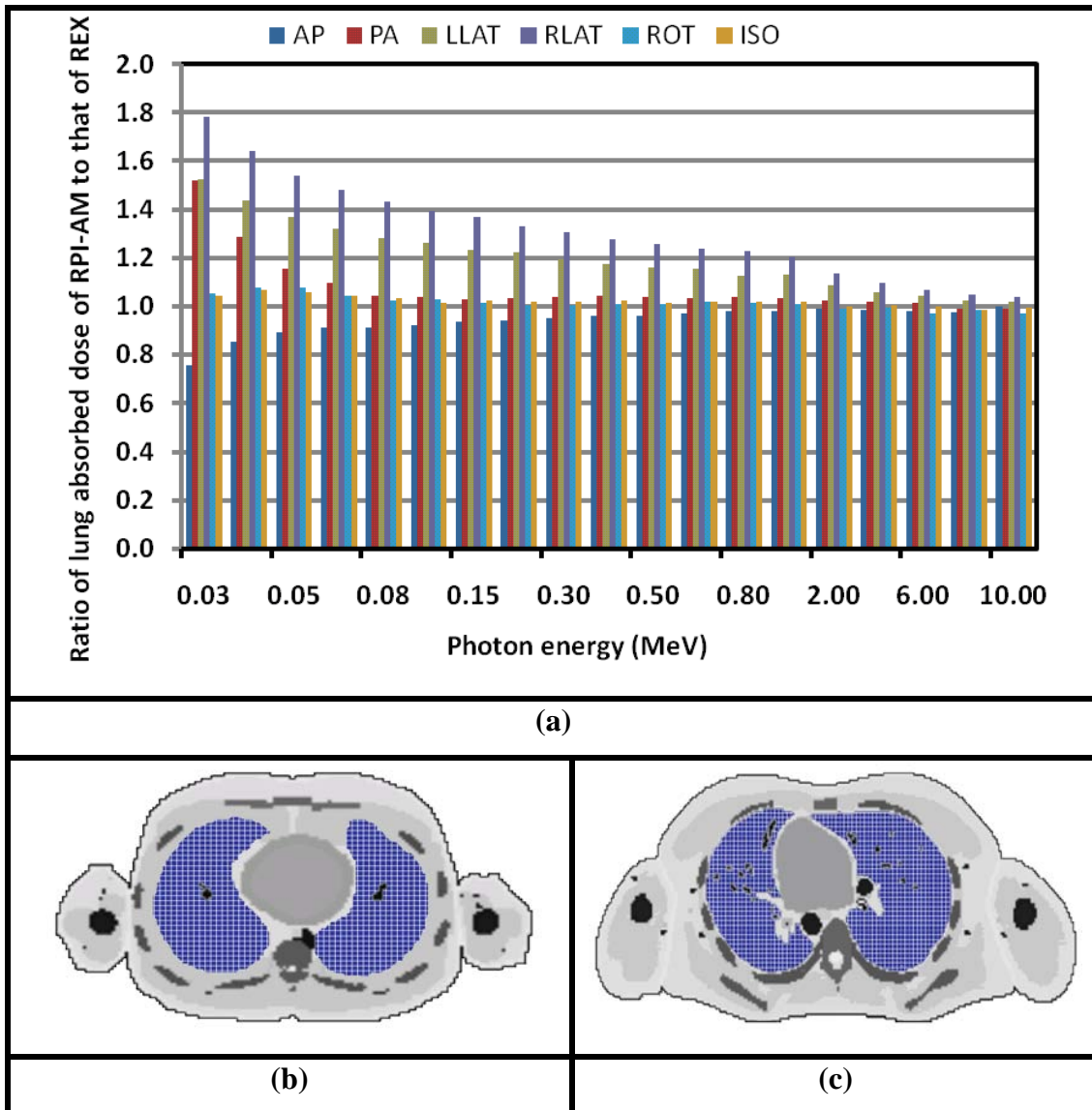


Figure 4.7: RPI-AM's organ doses in comparison with REX (Zhang et al. 2009): (a) the lungs absorbed dose ratio of the RPI-AM to REX with different photon energies; (b) cross-sectional images showing the position of lungs marked grid (#) for the RPI-AM; (c) cross-sectional images showing the position of lungs marked grid (#) for REX.

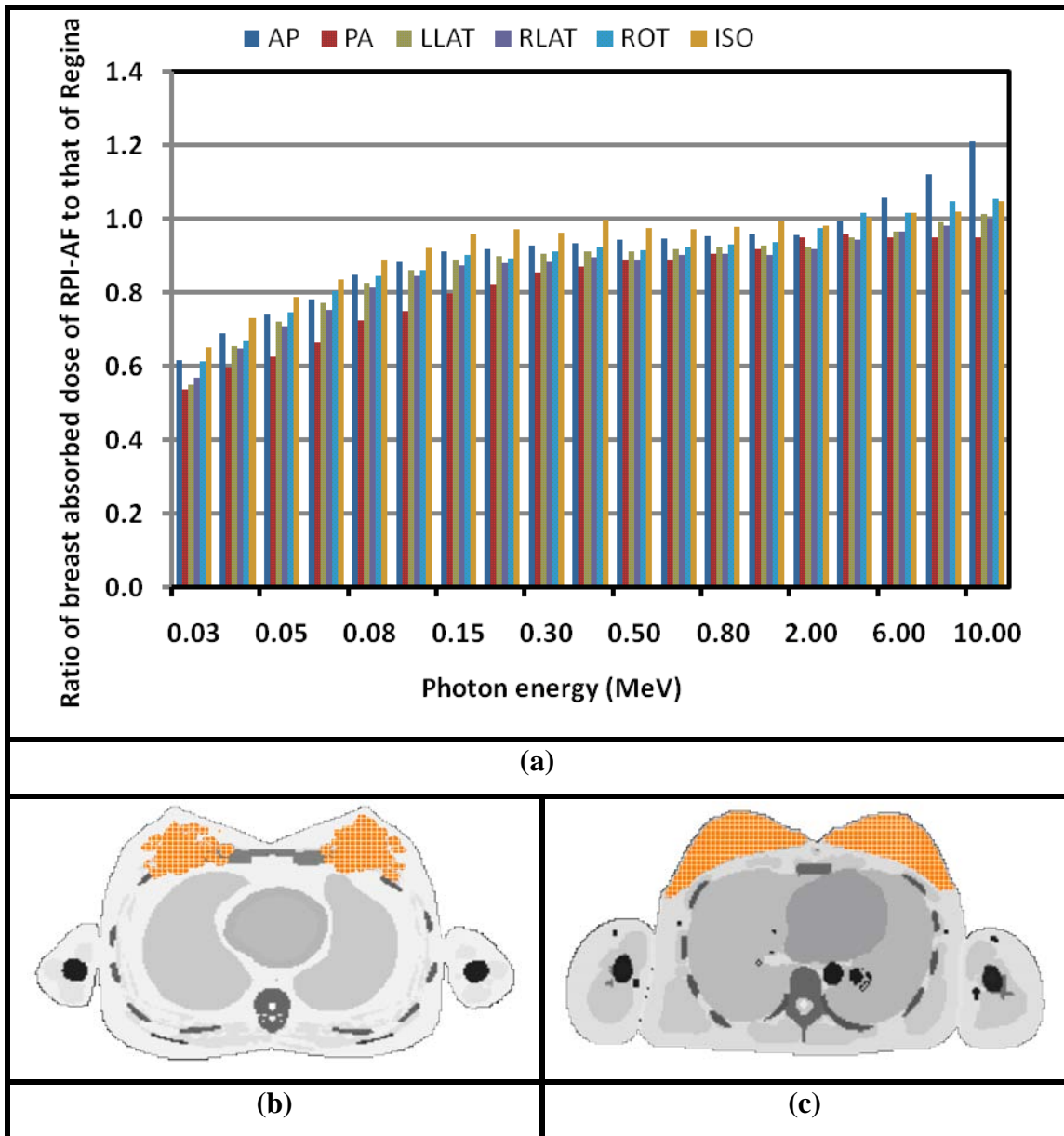


Figure 4.8: RPI-AF's organ doses in comparison with REGINA (Zhang et al. 2009):
(a) the breasts absorbed dose ratio of the RPI-AF to REGINA in different photon energies; **(b)** cross-sectional images showing the position of breast tissues marked grid (#) for the RPI-AF; **(c)** cross-sectional images showing the position of breast tissues marked grid (#) for REGINA.

4.4.2 RPI Percentile-Specific Phantoms

The organ dose calculations involved three adult male phantoms representing the 5th, 50th, and 95th percentiles (165 cm, 176 cm, and 188 cm in height and 56 kg, 73 kg, and 110 kg in weight), respectively. In the MCNPX simulations, each of these phantoms was irradiated by the 0.5 MeV and 1 MeV broad external photon beams. Organ doses from the 50th-percentile phantom—one that resembles the Reference Man—were used to normalize organ doses from the other two phantoms and the conversion coefficients of internal organs are compared in Figure 4.9a and Figure 4.9b, respectively, with 0.5 MeV and 1 MeV phantom beams in AP irradiation geometry.

It can be observed that the 5th-percentile phantom receives higher organ doses than the 50th-percentile phantom because of less photon attenuation from smaller amount of body fat in a skinner and shorter individual male. In particular, the doses to the prostate and adrenal in the 5th-percentile phantom are about 10% more than those in the 50th-percentile phantom. By comparison, the 95th-percentile phantoms resulted on a reduction in most organ doses and the doses to the prostate and adrenal are approximately 20% greater than those in the 50th-percentile phantom. It is clear from the data that the variation in the body fat which is concentrated near the abdominal regions is responsible for the dose differences. The results for the 0.5 MeV and 1 MeV photon beams have a very similar pattern as shown in Figure 4.9. The results suggest a general finding that phantoms representing a skinner and shorter individual male received higher organ doses because of less photon attenuation due to smaller amount of body fat. Although beyond the scope of this study, more radiation types and energies should be investigated in the future to fully understand the dosimetric differences in phantoms of difference sizes (Na et al. 2009b).

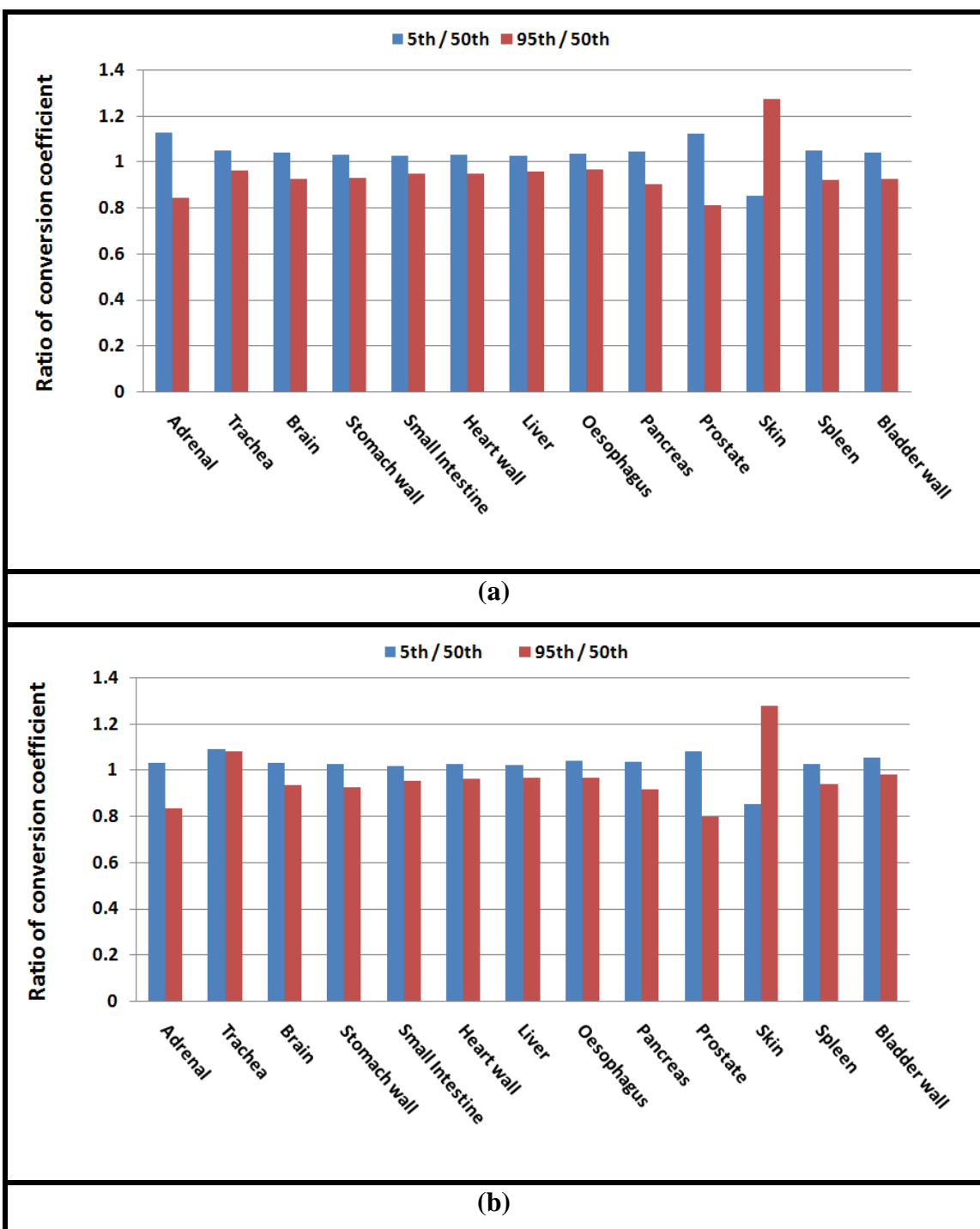


Figure 4.9: Organ dose differences of 5th-, 50th-, 95th-weight and height percentile (weight: 56-, 73-, 110-kg and height: 165-, 176-, 188-cm, respectively) phantoms of AP irradiation geometry (Na et al. 2009b): (a) 0.5 MeV; (b) 1.0 MeV.

4.4.3 RPI Breast Deformable Female Phantoms

To compare the results of virtual calibration for an in-vivo lung counting system using female phantoms in different brassiere cup sizes, the counting efficiencies of both detectors were summed and normalized to the efficiency of the AA-model with a joint effort with a former student (Hegenbart et al. 2008). The statistical uncertainties in all Monte Carlo calculations are less than 0.5%. For larger breast cup sizes, the attenuation of the photons is greater and the counting efficiency is smaller. Am-241, which emits low-energy photons, shows the greatest difference in counting efficiencies for the G-sized phantom. The detector counting efficiency was decreased about 50% as compared to the AA-size phantom. This value was about 58% for the high-energy photon emitters, Co-60, and about 55% for Cs-137. Figure 4.10 summarizes the normalized counting efficiencies and the cup sizes. The values from the left to right are the breast mass in grams corresponding to the cup size of AA, A, B, C, D, E, E40, F and G. The relationship for each radionuclide can be approximated with the 2nd order polynomial fit with R²-values of at least 99.2%.

With increasing the glandularity to the ICRP recommended value of 40% from the one of 7% for the phantom having E brassiere cup size, the lung counting efficiency for Am-241 decreased by 2% as shown in Table 4.3. This application clearly shows that the virtual calibration with the unique female breast phantoms will allow the uncertainty caused by unknown chest attenuation in calibrations performed with a one-size physical phantom to be accurately quantified and corrected.

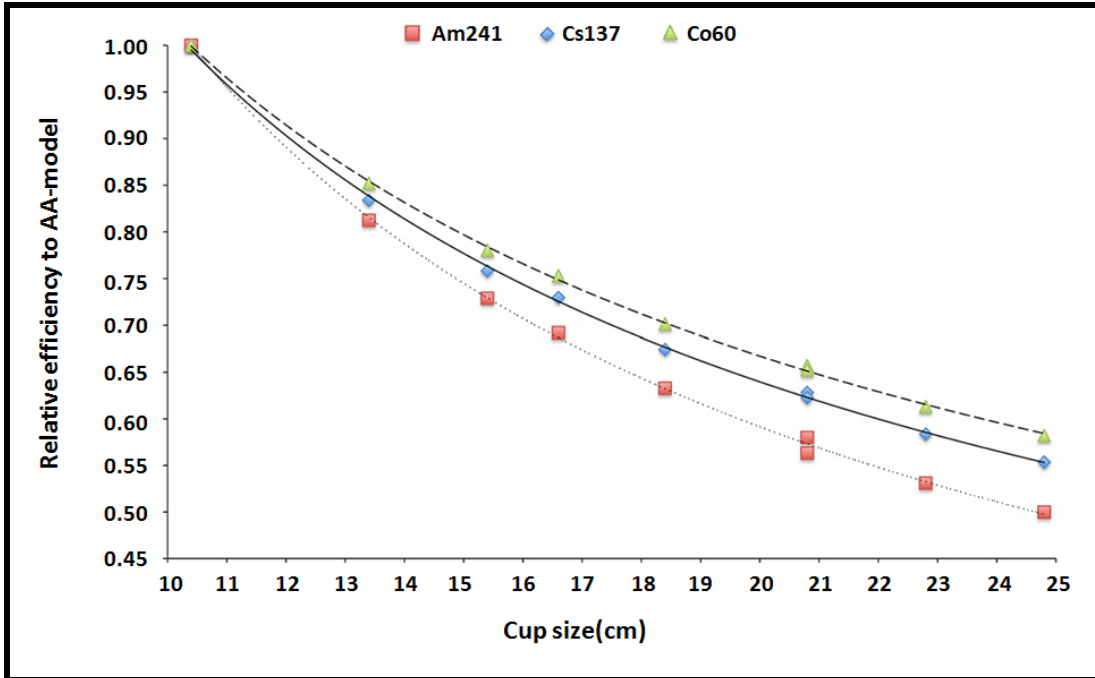


Figure 4.10: Relative counting efficiencies (counts per particle history) of the three nuclides, Am-241 (squares, dotted line), Cs-137 (diamonds, solid line), Co-60 (triangles, dashed line), normalized by the AA-model as a function of the total breast mass. The effects of chest attenuation on the counting efficiency and potential improvement to the use of one-size physical phantom are demonstrated in this “virtual calibration.” (Hegenbart et al. 2008).

Table 4.3: The E breast cup size phantom’s lung counting efficiency in comparison with 7% glandularity and with the ICRP recommended glandularity of 40% (Hegenbart et al. 2008).

Breast Glandularity	Counting Efficiency (counts per photon emitted)		
	Am-241 (20 ~ 80 keV)	Cs-137 (574 ~ 749 keV)	Co-60 (1056 ~ 1458 keV)
7%	0.0161	0.0167	0.0145
40%	0.0157	0.0166	0.0144

However, the result of shifting detectors of 45 mm towards the lungs just 1 mm above the skin of the AA-model, the detector efficiency increased by 33 %. This effect suggests that the breast glandularity is negligibly small compared to other sources of experimental error such as detector positioning.

4.4.4 RPI Walking Posture Phantoms

The organ dose calculations for walking posture phantoms on contaminated ground with planar sources of Cs-137 and Co-60 were implemented by MCNPX code in a joint effort with a fellow student (Han et al. 2009). The statistical uncertainty in most organ absorbed doses for the RPI-AM and RPI-AF walking phantoms are less than 1%, except the eye lens (less than 10%). The absorbed organ (e.g., liver, kidney, lungs, brain, gonads, and thyroid) doses for the complete cycle of walking posture phantoms are calculated and compared with those in their standing postures as shown in Table 4.4.

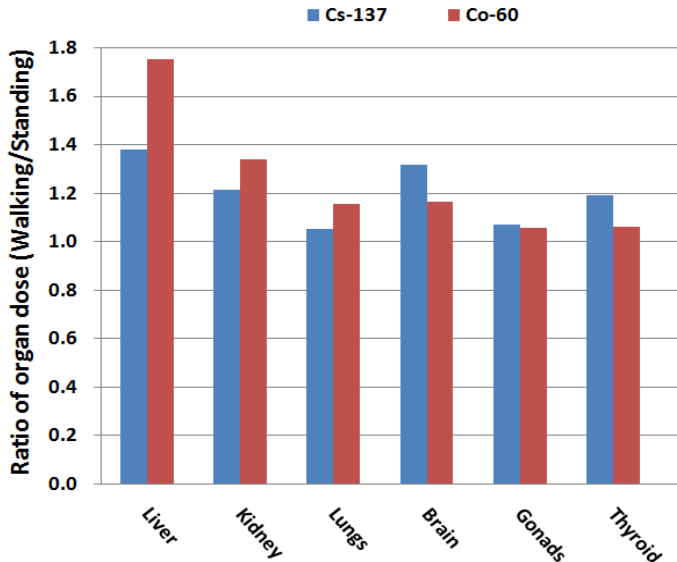
Table 4.4: Organ dose rates (nGy hour⁻¹) of the RPI standing and walking phantoms on radioactive contamination ground with concentration of 30kBq m⁻² (adopted from Han et al. 2009).

Organs	RPI-AM				RPI-AF			
	Cs-137		Co-60		Cs-137		Co-60	
	Standing	Walking	Standing	Walking	Standing	Walking	Standing	Walking
Liver	4.60	6.34	21.29	37.25	4.61	7.42	20.77	36.97
Kidneys	2.53	3.07	12.21	16.33	2.50	3.47	11.66	17.47
Lungs	1.80	1.89	8.94	10.31	2.23	2.50	9.98	12.43
Brain	0.21	0.27	1.83	2.13	0.31	0.37	2.57	2.97
Gonads	30.43	31.96	110.46	114.83	4.71	6.87	22.38	32.58
Thyroid	0.48	0.57	4.64	4.92	2.35	2.38	6.38	6.53

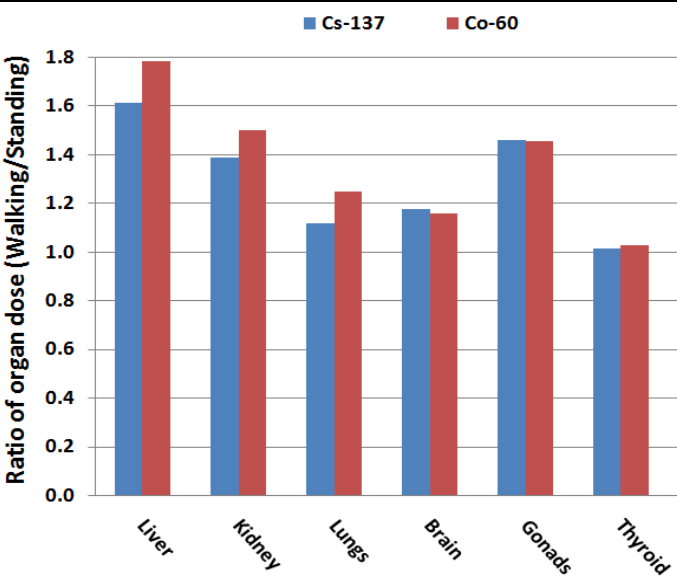
Figure 4.11 shows the organ absorbed doses ratios of the walking to standing phantoms on Cs-137 and Co-60 contaminated ground with concentration of 30 kBq/m². The walking posture phantoms receive higher organ doses than standing posture phantoms because the leg movements in the stages of walking can reduce shielding to

the organs, such as the liver, kidney, and gonads which are located in the lower portion of the body, from the photon irradiation emitted by the surface of ground.

In particular, the doses to the male gonads in the walking phantom are about 5.1% more than those in the standing phantom because the distance in-between two feet of the default RPI-AM standing phantom is already about 15cm. From this result, it can be discussed that the male walking posture may not be enough to diminish a lot of the shielding to male gonads. The absorbed doses for organs such as the brain and thyroid located in the upper portion of the body differ from 2% and 15% approximately. These can be reflected that the shielding from the legs is not considerably significant for the organs located in the upper portion than those in the lower portion of the body.



(a)



(b)

Figure 4.11: Organ absorbed doses ratios of the walking to standing phantoms on Cs-137 and Co-60 contaminated ground with concentration of 30 kBq/m²;(a) the RPI-AM; (b) the RPI-AF. (Han et al. 2009).

5. Conclusions

5.1 Summary

The methods to develop deformable phantom from a pair of basic 50th-percentile phantoms using software algorithms are successfully concluded through the results. The use of mesh-based geometrical data structure allows the deformation process to be computationally efficient. Furthermore, the mesh-based geometry allows the anatomical realism to be maintained. Finally, the methods avoid the difficult task of storing a large amount of anatomical data associated with organ volume and shapes and thus taking advantage of the software component of the dataset. The final step of converting meshes to voxels will be avoided in the future when direct Monte Carlo simulations in mesh geometry become possible, thus further improving the computational efficiency. This is the first time such a new approach has been successfully demonstrated.

To summarize the primary goal of this study was accomplished by the development of a pair of the mesh-based ICRP-compatible phantoms relying on a pair of 50th-percentile population phantoms the RPI-AM and RPI-AF. It has been demonstrated in this project that, through embedded software algorithms, this pair of phantoms can be deformed to various computational phantoms: (1) percentile-specific phantoms representing male and female workers from 5th to 95th percentiles of the population; (2) phantoms representing various female breast sizes; (3) phantoms with different body postures.

It needs to be pointed out that this study is possibly the first to systematically propose and demonstrate a new approach in developing future phantoms that are deformable. The method relies on an embedded deformation software component that interfaces with a pair of 50th-percentile adult male and female phantoms of detailed mesh geometries. A new phantom is only created when needed, thus avoiding the burden of storing an overwhelmingly large amount of anatomical phantom data required to cover various body and organ sizes. Furthermore, in this approach, the anatomical details can be accurately and consistently persevered. The detailed achievements and findings of this study are highlighted below:

5.1.1 RPI 50th-Percentile Adult Phantoms

This study first demonstrated the feasibility of mesh-based deformable whole-body computational phantom modeling with superior computationally efficiency and anatomical realism. The developed RPI-AM and RPI-AF are consisted of 70 internal organs, 4 muscle structures, and 45 bones which can be subdivided into cortical bones, spongiosa, and medullary cavities. Through the systematically developed mesh processing and deformation algorithms, all anatomical structures were adjusted to match the ICRP-89 recommend values for 50th-percentile reference adult males and females. The densities and elemental composition of internal organs are referred to the ICRP publications. These mesh-based phantoms were converted to voxel-based data for the Monte Carlo dose calculations in six-standard external photon irradiation geometries covering 23 energies from 10 keV to 10 MeV. At the photon energies higher than about 1 MeV, the organ doses in the RPI-AM and RPI-AF agree with those in REX and REGINA. Whereas photon energies less than 1 MeV, the significant disagreements were observed in individual organs because corresponding organs are located in different positions.

5.1.2 RPI Percentile-Specific Adult Phantoms

In this study, a detailed new approach to the development of next-generation deformable phantoms covering different body heights and weights has been demonstrated. Comprehensive anthropometric references from the NHANES report (1999-2002) and ICRP Publications 23 and 89 were adopted to compile a range of body height and weight values. With mesh-based organ deformation algorithms, a new phantom can now be created, on demand, to match any desired volumes and masses included in the dataset. To demonstrate the feasibility for dose calculations, phantoms representing a 5th-percentile phantom (165 cm in height and 56 kg in weight) and a 95th-percentile phantom (188 cm in height and 110 kg in weight) with those for a 50th-percentile phantom (176 cm in height and 73 kg in weight) were implemented in the MCNPX code to compare organ doses from 0.5 MeV to 1 MeV photon beam irradiations. The results suggest a general finding that the phantoms representing a skinner and shorter individual male received higher organ doses because of lesser

degree of photon attenuation due to smaller amount of body fat. In particular, doses to the prostate and adrenal in the 5th-percentile phantom is about 10% greater than those in the 50th-percentile phantom defined after the Reference Man. On the other hand, the doses to the prostate and adrenal in the 95th-percentile phantom are approximately 20% greater than those in the 50th-percentile phantom.

5.1.3 RPI Breast Deformable Adult Female Phantoms

In order to produce individual female phantoms with different brassiere cup size, the deformation methods have been demonstrated. The deformed breast sizes of the RPI-AF have been quantified by the brassiere cup size according to the standard industrial dimension for European clothing wares. The cup size was measured by the bust- and underbust girth of the female phantoms. The lung counting efficiencies in three different energy ranges have been simulated by the Monte Carlo methods with these individualized phantoms. The detector efficiencies for the low photon emitter Am-241 were considerably decreased with the increasing breast size.

5.1.4 RPI Walking Posture Adult Phantoms

For the environmental dose assessment, the whole-body frames of the RPI-AM and RPI-AF phantoms were deformed from their default upright standing posture to walking postures. The mesh deformation algorithms allowed adjusting their postures with movable arms and legs keeping the anatomical realism. The MCNPX code was used to simulate the entire walking cycle for assessment of organ absorbed doses from planar radioactive sources of Cs-137 and Co-60 involving the effects of contamination concentration of 30 kBq m⁻².

5.2 Future Research

In the future, research associated with this dissertation should focus on the following two general ideas:

Improvements the deformable adult phantoms. The anatomical references may have to be updated to include the most recent information (such as when the ICRP modifies the list of critical organs). With the advantages of flexible deformation software methods demonstrated here, it is easy to update anatomical parameters. This study also suggests

that, given person-specific anatomical information (even partial body information such as those from medical images), a new phantom can be created to represent that person (for that portion of the body, plus the rest of the body not imaged), thus offering an opportunity to perform person-specific dosimetry for certain situations involving high radiation exposures. This approach will require image registration between patient images with the existing phantom and similar deformation algorithms described here. Recently, this approach was attempted by Alziar et al. (2009) for assessing organ doses from radiation treatment. The different posture phantoms (e.g., sitting, working with glove box, and holding or pouring radioactive liquids, etc) are going to be demonstrated according to meet the continuing demands in the radiation protection dosimetry research communities for health physics and medical physics. Additional possible features of these deformable phantoms can include the ability to combine posture and motion data from multiple motion sensors in designing deformable phantoms in dose reconstruction for accidents. Additionally, physics based multi-organ deformations combined with virtual-reality approaches are also interesting (Ding et al. 2009).

Monte Carlo simulations with advanced geometries. As mentioned before, Monte Carlo codes are only able to carry out constructive solid geometries (CSG) limited by quadric equations or voxels, in spite of the fact that these contain excellent radiation physics algorithms. Ultimately, it needs to be pointed out that, since the deformation is performed with BREP modeling such as NURBS and/or polygonal meshes, it will be necessary to develop ways in the future to perform Monte Carlo calculations directly in such geometry instead of wasting time and anatomical detail to convert them to voxels.

5.3 List of Peer-reviewed Journal Articles and Conference Proceedings

The work described in this dissertation has been presented in the following peer-reviewed journals and conference proceedings:

Na YH, Zhang BQ, Zhang JY, Xu XG. Deformable Adult Human Phantoms for Radiation Protection Dosimetry: Anatomical Data for Covering 5th- 95th Percentiles of the Population and Software Algorithms. Physics in Medicine and Biology Submitted; 2009.

Han B, Zhang JY, Na YH, Caracappa PF, Xu XG Modeling and Monte Carlo Organ Dose Calculations for Workers Walking on Ground Contaminated with Cs-137 and Co-60 Gamma Sources. Physics in Medicine and Biology Submitted; 2009.

Zhang JY, Na YH, Caracappa PF, Xu XG. RPI-AM and RPI-AF,a pair of mesh-based, size-adjustable adult male and female computational phantoms using ICRP-89 parameters and their calculations for organ doses from monoenergetic photon beams. Physics in Medicine and Biology. 54: 5885-5908; 2009.

Na YH, Zhang JY, Ding AP, Xu XG. Chapter 14: Mesh-Based and Anatomically Adjustable Adult Phantoms and a Case Study in Virtual Calibration of Lung Counter for Female Workers in Handbook of Anatomical Models for Radiation Dosimetry, Ed. X. George Xu and Keith F. Eckerman. Boca Raton: Taylor & Francis. 347-375; 2009.

Hegenbart L, Na YH, Zhang JY, Urban M, Xu XG. A Monte Carlo study of lung counting efficiency for female workers of different breast sizes using deformable phantoms. Physics in Medicine and Biology. 53: 5527-5538; 2008.

Na YH, Zhang JY, Xu XG, Han B, Caracappa P. Next-Generation Deformable Patient Modeling for Monte Carlo Assessment of Organ Doses. American Association of Physicist in Medicine Annual Conference; 2009.

Mille M, Hegenbart L, Na YH, Zhang JY, Xu XG. Deformable computational breast phantoms for Monte Carlo based calibrations of detector systems used for assessing internal radioactivity burden in the lungs. American Association of Physicist in Medicine Annual Conference; 2009.

Han B, Zhang JY, Na YH, Caracappa P, Xu XG. Monte Carlo Modeling of Workers Walking on Contaminated Ground for Accurate Environmental Dosimetry. Health Physics Society Annual Conference; 2009.

Hegenbart L, Mille M, Na YH, Zhang J, Ding A, Urban M, Xu XG. Investigation Of The Effect Of Female Breast Size on Lung Counting Efficiency Using Virtual Deformable Phantoms. Health Physics Society Annual Conference; 2009.

Zhang J, Na YH, Han B, Caracappa P, Xu XG. Organ Doses from External Neutron Beams for A Pair of ICRP-89 50th-percentile Adult Phantoms. Health Physics Society Annual Conference; 2009.

Zhang JY, Na YH, Han B, Caracappa P, Xu XG. Organ Doses from External Proton Beams Calculated from A Pair of ICRP-89 50th-Percentile Adult Phantoms. Health Physics Society Annual Conference; 2009.

Zhang JY, Na YH, Ding AP, Xu XG. Deformable and Posture-changing Computational Phantoms and Dosimetry Data for Standard External-Beam Irradiations. International Conference on Mathematics, Computational Methods & Reactor Physics (M&C 2009); 2009.

Na YH, Xu XG. A Method to Create Size-Adjustable Whole-Body Patient Models for Radiological Studies of Organ Doses. The Medicine Meets Virtual Reality Conference; 2009.

Na YH, Zhang JY, Xu XG. A Mesh-Based Anatomical Deformation Method for Creating Size-adjustable Whole-body Patient Models. American Association of Physicist in Medicine Annual Conference; 2008

Zhang JY, Na YH, Xu XG. Development of Whole-Body Phantoms Representing An Average Adult Male and Female Using Surface-Geometry Methods. American Association of Physicist in Medicine Annual Conference; 2008.

Zhang JY, Na YH, Xu XG. Size Adjustable Worker Models For Improved Radiation Protection Dosimetry. Health Physics Society Annual Conference; 2008.

Xu XG, Zhang JY, Na YH. Preliminary Data for Mesh-Based Deformable Phantom Development: Is it Possible to Design Person-Specific Phantoms On-demand? ICRS-11 & RPSD-2008; 2008.

6. Bibliography

- Ackerman MJ. Accessing the Visible Human Project. D-Lib Magazine; 1995:1(Oct). [Available online at: www.dlib.org/dlib/october95/10ackerman.html; cited May 2007]
- Akkurt H and Eckerman KF: Development of PIMAL: Mathematical Phantom with Moving Arms and Legs. Report No. ORNL/TM-2007/14, Oak Ridge, TN: Oak Ridge National Laboratory; 2007.
- Allen SJ, Adair ER, Mylacraine KS, Hurt W, Ziriax J. Empirical and theoretical dosimetry in support of whole body resonant RF exposure (100 MHz) in human volunteers. Bioelectromagnetics 24: 502–9; 2003.
- Allen SJ, Adair ER, Mylacraine KS, Hurt W, Ziriax J. Empirical and theoretical dosimetry in support of whole body resonant radio frequency (RF) exposure seated human volunteers at 220 MHz. Bioelectromagnetics 26: 440–447; 2005.
- Alziar I, Bonniaud G, Couanet D, Ruaud JB, Vicente C, Giordana G, Ben-Harrath O, Diaz JC, Grandjean P, Kafrouni H, Chavaudra J, Lefkopoulos D, de Vathaire F, Diallo I. Individual radiation therapy patient whole-body phantoms for peripheral dose evaluations: method and specific software. Physics in Medicine and Biology 54: N375-N383; 2009.
- Amanatides J, Choi K. Ray Tracing Triangular Meshes, Proceedings of the Eighth Western Computer Graphics Symposium; 1997.
- Appel A. Some Techniques for Shading Machine Renderings of Solids. Proceeding. American Federation of Information Processing Societies, Spring Joint Computer Conferences 32:37-45; 1968.
- Armato S, Giger M, Moran C, Blackburn J, Doi K, MacMahon H. Computerized detection of pulmonary nodules on CT scans. RadioGraphics, 19:1303-1311; 1999.
- Beall MW, Shephard MS. A general topology-based mesh data structure, International Journal for Numerical Methods in Engineering, 40: 1573; 1997.
- Becker J, Zankl M, Fill U, Hoeschen C. Katja – the 24th week of virtual pregnancy for dosimetric calculations. Polish Journal of Medical Physics And Engineering 14:13-20; 2008.
- Becker J, Zankl M, Petoussi-Henss N, A software tool for modification of human voxel models used for application in radiation protection. Phys. Med. Biol. 52: N195-N205; 2007.

- Han B, Zhang JY, Na YH, Caracappa P, Xu XG. Monte Carlo Modeling of Workers Walking on Contaminated Ground for Accurate Environmental Dosimetry. *Health Phys.* 97(1): S79; 2009.
- Boyd E. Normal variability in weight of the adult human liver and spleen Archives of pathology. 16:350–372; 1933.
- Boyd E. Outline of Physical Growth and Development Burgess Publishing Co, Minneapolis, MN, USA; 1941.
- Boyd E. An Introduction to Human Biology and Anatomy for First Year Medical Students Child Research Council, Denver, CO, USA; 1952.
- Bozkurt A, Chao TC, Xu XG. Fluence-to-Dose Conversion Coefficients from Monoenergetic Neutron Beams Below 20 MeV Based on the VIP-Man Anatomical Model. *Physics in Medicine and Biology* 45:3059-3079; 2000.
- Briesmeister JF. MCNP-A General Monte Carlo N-particle transport code, Version 4B. Report No. LA 12625-M, Los Alamos, NM: Los Alamos National Laboratory ; 1997.
- Briesmeister JF. MCNP-A General Monte Carlo N-Particle Transport Code - Version 5. Report LA-UR05-8617, Los Alamos, NM: Los Alamos National Labortory; 2005.
- Caon M. Voxel-based computational models of real human anatomy: a review. *Radiation and Environmental Biophysics* 42: 229-235; 2004.
- Chen J. Mathematical models of the embryo and fetus for use in radiological protection. *Health Phys.* 86: 285–95; 2004.
- Cristy M. Representative breast size of reference female. *Health Physics* 43(6): 930–935; 1982.
- Cristy M, Eckerman K. Specific absorbed fractions of energy at various ages from internal photon sources. Report No. ORNL/TM-8381Nl (Oak Ridge, TN: Oak Ridge National Laboratory); 1987.
- Dawson TW, Caputa K, Stuchly MA. Numerical evaluation of 60 MHz magnetic induction in the human body in complex occupational environments. *Physics in Medicine and Biology* 44: 1025–40; 1999.
- Dawson TW, Caputa K, Stuchly MA. Magnetic field exposures for UK live-line workers *Physics in Medicine and Biology* 47: 995–1012; 2002.

Dekaban AS, Sadowsky D. Changes in brain weights during the span of human life: Relation of brain weights to body heights and body weights. *Annals of Neurology* 4: 345-356; 1978.

de la Grandmaison GL., Clairand I, Durigon M. Organ weight in 684 adult autopsies: new tables for a Caucasoid population *Forensic science international* 119:149–154; 2001.

Deuflhard P. Newton Methods for Nonlinear Problems. Affine Invariance and Adaptive Algorithms. Springer Series in Computational Mathematics, Berlin, Springer (35); 2004.

Dimbylow, P. Development of the female voxel phantom, NAOMI, and its application to calculations of induced current densities and electric fields from applied low frequency magnetic and electric fields, *Phys Med Biol*, 50, 1047, 2005a.

Dimbylow, P. Resonance behaviour of whole-body averaged specific energy absorption rate (SAR) in the female voxel model, NAOMI, *Phys Med Biol*, 50, 4053, 2005b.

Ding AP, Zhang D, Xu XG. Training Software Using Virtual-Reality Technology And Pre-Calculated Effective Dose Data. *Health Phys*. 96(5): 594-601; 2009.

Eckerman K, Poston J, Bolch W, Xu XG. Chapter 2. The Stylized Computational Phantoms Developed at ORNL and Elsewhere. *Handbook of Anatomical Models for Radiation Dosimetry*, TAYLOR & FRANCIS: 43-64; 2009.

EN 13402-1. Size designation of clothes - Part 1: Terms, definitions and body measurement procedure (ISO 3635:1981 modified), European Committee for Standardization, Brussels, Belgium; 2001.

EN 13402-2. Size designation of clothes - Part 2: Primary and secondary dimensions), European Committee for Standardization, Brussels, Belgium; 2002.

EN 13402-3. Size designation of clothes - Part 3: Measurements and intervals), European Committee for Standardization, Brussels, Belgium; 2004.

Fill U, Zankl M, Petoussi-Henss N, Sieben M, Regulla D. Adult female voxel models of different stature and photon conversion coefficients for radiation protection, *Health Phys* 86: 253; 2004.

Findlay RP and Dimbylow PJ. Effects of posture on FDTD calculations of specific absorption rate in a voxel model of the human model. *Physics in Medicine and Biology* 50: 3825–3835; 2005.

Findlay RP and Dimbylow PJ. FDTD calculations of specific energy absorption rate in a seated voxel model of the human body from 10 MHz to 3 GHz. Physics in Medicine and Biology 51: 2339–2352; 2006a.

Findlay RP and Dimbylow PJ. Variations in calculated SAR with distance to the perfectly matched layer boundary for a human voxel model. Physics in Medicine and Biology 51: N411–5; 2006b.

Fisher HL, Snyder WS. Distribution of dose in the body from a source of gamma rays distributed uniformly in an organ Report ORNL-4168 Oak Ridge National Laboratory, Oak Ridge, TN, USA; 1967.

Fisher HL, Snyder WS. Distribution of dose in the body from a source of gamma rays distributed uniformly in an organ Proc. 1st Int. Cong. Radiation Protection (Oxford: Pergamon), 1473–1486; 1968.

Gibbs SJ, Pujol A Jr. A Monte Carlo method for patient dosimetry from diagnostic x-ray, Dentomaxillofacial Radiology 11, 25; 1982.

Gibbs SJ, Pujol A Jr, Chen TS, Malcolm AW, James AE Jr. Patient Risk from Interproximal Radiography, Oral Surgery Oral Medicine Oral Pathology Oral Radiology and Endodontics 58: 347-354; 1984.

Gibbs SJ, Pujol A Jr, Chen TS, Carlton JC, Dosmann MA, Malcolm AW, James AE Jr. Radiation doses to sensitive organs from intraoral dental radiography. Dentomaxillofacial Radiology 16:67-77; 1987

Griffith RV, Dean PN, Anderson AL, Fisher JC. A Tissue Equivalent Torso Phantom for Intercalibration of in vivo Transuranic Nuclide Counting Facilities, Advances in Radiation Protection Monitoring, STI/PUB/494 Proc. IAEA Conf. IAEA-SM-229/56, Vienna: IAEA; 1978.

Hammersley JM and Handscomb DC. Monte Carlo methods. Monte Carlo Methods, Chapman and Hall, London & New York; 1964.

Han E, Bolch W, Eckerman K. Revisions to the ORNL series of adult and pediatric computational phantoms for use with the MIRD schema, Health physics 90(4):337-56; 2006.

Hegenbart L, Na YH, Zhang JY, Urban M, Xu XG. A Monte Carlo study of lung counting efficiency for female workers of different breast sizes using deformable phantoms. Phys. Med. Biol., 53: 5527-5538; 2008.

Hongning X, Kohkichi H, Atsushi MH, Kurioka., Kentaro T, Kohji M. Three-dimensional ultrasonic volume measurement of the ovary in women with polycystic ovary syndrome. Journal of Medical Ultrasonics 28: 7-10; 2001.

- IAEA. Compilation of Anatomical, Physiological and Metabolic Characteristics for a Reference Asian Man. IAEA-TECDOC-1005 1-2: International Atomic Energy Agency; 1998.
- ICRP. Report of the task group on Reference Man Publication 23. Pergamon Press. Oxford (UK): International Commission on Radiation Protection (ICRP); 1975.
- ICRP. Basic anatomical and physiological data for use in radiological protection: the skeleton. ICRP Publication 70: International Commission on Radiological Protection; 1995.
- ICRP. Annual report of the International Commission on Radiological Protection. ICRP Publication 89. Stockholm (Sweden): International Commission on Radiological Protection (ICRP); 2002.
- ICRP. Adult reference computational phantoms. ICRP Publication 108: International Commission on Radiological Protection (ICRP); 2009.
- ICRU. Phantoms and computational models in therapy, diagnosis and protection. ICRU Report 48. Bethesda, MD: International Commission on Radiation Units and Measurements; 1992.
- Inman VT, Ralston HJ, Todd F. Human Walking. Baltimore: Williams and Wilkins; 1981.
- Jain V, Zhang H. A spectral approach to shape-based retrieval of articulated 3D models, Computer-Aided Design, 39(5): 398-407; 2007.
- Kramer R, Drexler G. Representative breast size of reference female. Health Physics 40 913–914; 1981.
- Kramer R, Williams G, Drexler G. Reply to M. Cristy Health Physics:(43)932-935; 1982.
- Kramer R, Khoury H, Vieira J, Lima V. MAX06 and FAX06: update of two adult human phantoms for radiation protection dosimetry. Physics in Medicine and Biology 51: 3331-3346; 2006
- Kuczmarski R, Ogden C, Guo S, Grummer-Strawn L, Flegal K, Wei Z, Curtin L, Roche A, Johnson C. 2000 CDC Growth Charts for the United States: Methods and development. Vital and Health Statistics 11(246); 2002
- Lee C, Lodwick D, Hasenauer D, Williams JL, Lee C, Bolch WE. Hybrid computational phantoms of the male and female newborn patient: NURBS-based whole-body models. Physics in Medicine and Biology 52: 3309-3333; 2007.

- Lee C, Lodwick D, Williams JL, Bolch WE. Hybrid computational phantoms of the 15-year male and female adolescent: applications to CT organ dosimetry for patients of variable morphometry. *Medical Physics* 35(6): 2366-2382; 2008.
- Lee H, Hong K, Kim E. Measurement protocol of women's nude breasts using a 3D scanning technique. *Appl. Ergonom.* 35:353-359; 2004.
- Lee J, Appugliese D, Kaciroti N, Corwyn R, Bradley R, Lumeng J. Weight Status in Young Girls and the Onset of Puberty. *Pediatrics* 119: e624-e630; 2007.
- McDowell MA, Fryar CD, Hirsch R, Ogden CL. Anthropometric Reference Data for Children and Adults: U. S. Population, 1999-2002. Centers for Disease Control and Prevention, National Center for Health Statistics; 2005.
- Morris D, Mee J, Salt H. The calibration of female breast size by modeling, International Foundation of Fashion Technology Institutes Conference 2002, Hong Kong, China; 2002.
- Munn CS, Kiser LC, Wetzner SM and Baer JE. Ovary volume in young and premenopausal adults: US determination. *Work in progress Radiology* 159: 731-732; 1986.
- Na YH, Zhang JY, Ding AP, Xu XG. Chapter 14. Mesh-Based and Anatomically Adjustable Adult Phantoms and a Case Study in Virtual Calibration of Lung Counter for Female Workers. *Handbook of Anatomical Models for Radiation Dosimetry*, TAYLOR & FRANCIS: 347-375; 2009a.
- Na YH, Zhang BQ, Zhang JY, Xu XG. Deformable Adult Human Phantoms for Radiation Protection Dosimetry: Anatomical Data for Covering 5th- 95th Percentiles of the Population and Software Algorithms. *Physics in Medicine and Biology Submitted*; 2009b.
- Nagaoka T, Watanabe S, Sakurai K, Kunieda E, Watanabe S, Taki M and Yamanaka Y. Development of realistic high-resolution whole-body voxel models of Japanese adult males and females of average height and weight, and application of models to radio-frequency electromagnetic-field dosimetry. *Physics in Medicine and Biology* 49: 1-15; 2004.
- Nagaoka T, Watanabe S. Postured voxel-based human models for electromagnetic dosimetry. *Physics in Medicine and Biology* 53 7047-7061; 2008.
- NLM. Electronic imaging: report of the Board of Regents. U.S. Dept. of Health and Human Services, Public Health Service, National Institutes of Health, Long range plan. Bethesda (MD), National Library of Medicine; 1990.

Odgen C, Carroll M, Curtin L, McDowell M, Tabak C, Flegal K. Prevalence of overweight and obesity in the United States, 1999–2004 JAMA 295:1549–1555; 2006.

Ohanian OJ, Mass Properties in VTOL UAV Conceptual Design Software, Part I: Overview and General Algorithms, Proceedings, 64th Annual SAWE Conference, Annapolis, MD; 2005.

Ohbuchi R, Nakazawa M, Takei T. Retrieving 3D shapes based on their appearance, Proceedings of the 5th ACM SIGMM international workshop on Multimedia information retrieval(MIR): 39-45; 2003.

Pavlik EJ, DePriest PD, Gallion HH, Ueland FR, Reedy MB, Kryscio RJ, Jr v NJ. Ovarian volume related to age Gynecologic Oncology 77:410-412; 2000.

Pelowitz DB. Report LA-CP-05-0369MCNPX User's Manual version 2.5.0. LANL: Los Alamos National Laboratory (LANL); 2005.

Petoussi-Henss N, Zankl M, Fill U, Regulla D. The GSF family of voxel phantoms. Physics in Medicine and Biology 47: 89-106; 2002.

Platt JF, Bree RL, Davidson D. Ultrasound of the normal nongravid uterus: Correlation with gross and histopathology. Journal of Clinical Ultrasound 18: 15-19; 1990.

Prael RE and Madland DG. LAHET Code System Modifications for LAHET 2.8, Report LA-UR-95-3605: Los Alamos National Laboratory; 1995.

Richard AM, Matthew RP, Henry JB. Henry's clinical diagnosis and management by laboratory methods Henry's clinical diagnosis and management by laboratory methods;2007 .

Rogers D, Bielajew A. Monte Carlo techniques of electron and photon transport for radiation dosimetry in The Dosimetry of Ionizing Radiation, vol. III, K. Kase, B. Bjergaard and F. Attix, ed., Academic Press: 427-539; 1990.

Schlattl H, Zankl M, Petoussi-Henss N. Organ dose conversion coefficients for voxel models of the reference male and female from idealized photon exposures. Physics in Medicine and Biology 52: 2123–2145; 2007.

Sederberg TW and Parry SR. Free-form deformation of solid geometric models ACM Computer Graphics (SIGGRAPH 86 Conf. Proc.) 20: 15–160; 1986

Segars W, Lalush D, Tsui B. Modeling respiratory mechanics in the MCAT and spline-based MCAT phantom. IEEE Transactions on Nuclear Science 48: 89-97; 2001.

- Segars W, Tsui B. Study of the efficacy of respiratory gating in myocardial SPECT using the new 4D NCAT phantom. IEEE Transactions on Nuclear Science 49: 675-6795; 2002.
- Shi CY, Xu XG. Development of a 30-week-pregnant female tomographic model from computed tomography (CT) images for Monte Carlo organ dose calculations, Medical Physics 31(9): 2491-2497; 2004.
- Shutov VN, Travnikova IG, Bruk GY, Golikov VY, Balonov MI, Howard BJ, Brown J, Strand P, Kravtsova EM, Gavrilov AP, Kravtsova OS, Mubasarov AA: Current contamination by ^{137}Cs and ^{90}Sr of the inhabited part of the Techa river basin in the Urals. Journal of Environmental Radioactivity. 61(1): 91-109; 2002.
- Snyder WS, Ford MR, Warner GG, Fisher HL. Estimates of specific absorbed fractions for photon sources uniformly distributed in various organs of a heterogeneous phantoms. MIRD Pamphlet 5 Society of Nuclear Medicine, New York (NY); 1969.
- Snyder WS, Ford MR, Warner GG. Estimates of absorbed fractions for monoenergetic photon sources uniformly distributed in various organs of a heterogeneous phantoms. Medical Internal Radiation Dose Committee pamphlet no. 5. Revised edition. New York (NY): Society of Nuclear Medicine; 1978.
- Stabin M, Emmons M, Segars W, Fernald M, Brill A. ICRP-89 based adult and pediatric phantom series, Journal of Nuclear Medicine 49(Supplement 1): 14; 2008.
- Stovall M, Smith SA, Rosenstein M. Tissue doses from radiotherapy of cancer of the uterine cervix. Med Phys 16(5):726-733, 1989.
- Stroud I. Boundary Representation Modelling Techniques. Springer; 2006.
- Tanaka G, Kawamura H, Nakahara Y. Reference Japanese Man-I. Mass of Organs and Other Characteristics of Normal Japanese. Health Physics 36: 333-346; 1979.
- Tipton IH, Cook MJ. Weight of total gastrointestinal tract and its subfractions Health Physics Division Annual Progress Report for Period Ending July 31, 1969 Report ORNL-4446. Oak Ridge National Laboratory, Oak Ridge, TN 301-2;1969.
- Vauthey JN, Abdalla EK, Doherty DA, Gertsch P, Fenstermacher MJ, Loyer EM, Lerut J, Materne R, Wang X, Encarnacion A, Herron D, Mathey C, Ferrari G, Charnsangavej C, Do KA and Denys A. Body surface area and body weight predict total liver volume in Western adults Liver Transplant 8: 233-240; 2002.

Victor L. Katch, Barbara Campaigne, Patty Freedson, Stanley Sady, Frank I. Katch and Albert R. Behnke. Contribution of breast volume and weight to body fat distribution in females American Journal of Physical Anthropology 53:93-100; 1980.

Williams G, Zankl M, Abmayr W, Veit R, Drexler G. The calculation of dose from external photon exposures using reference and realistic human phantoms and Monte Carlo methods, Physics in Medicine and Biology 31(4): 449-452, 1986.

Xu XG, Chao TC, Bozkurt A. VIP-Man: an image-based whole-body adult male model constructed from color photographs of the Visible Human Project for multi-particle Monte Carlo calculations. Health Phys 78(5): 476-486; 2000.

Xu XG, Shi CY. Preliminary development of a 4D anatomical model for Monte Carlo simulations. In: Monte Carlo. Topical Meeting. The Monte Carlo method: versatility unbounded in a dynamic computing world [CD-ROM]. Chattanooga (TN): American Nuclear Society. Lagrange Park (IL); 2005.

Xu XG, Taranenko V, Zhang JY, Shi CY. A boundary-representation method for designing whole-body radiation dosimetry models: pregnant females at the ends of three gestational periods-RPI-P3, -P6 and -P9. Physics in Medicine and Biology 52: 7023-7044; 2007.

Xu XG, Zhang JY, Na YH. Preliminary data for mesh-based deformable phantom development: is it possible to design person-specific phantoms on-demand? ICRS-11 and RPSD 2008 (Callaway Gardens, Pine Mountain, GA, USA); 2008.

Xu XG. Chapter 1. Computational Phantoms for Radiation Dosimetry: A 40-Year History of Evolution. Handbook of Anatomical Models for Radiation Dosimetry, TAYLOR & FRANCIS: 3-41; 2009.

Xu XG, Chao TC, Bozkurt A, Shi CY, Zhang JY. Chapter 6. The 3D and 4D VIP-Man Computational Phantoms. Handbook of Anatomical Models for Radiation Dosimetry, TAYLOR & FRANCIS: 135-162; 2009a.

Xu XG, Shi CY, Stabin M, Taranenko V. Chapter 12. Pregnant Female/Fetus Computational Phantoms and the Latest RPI-P Series Representing 3, 6 and 9 Month Gestational Periods. Handbook of Anatomical Models for Radiation Dosimetry, TAYLOR & FRANCIS: 305-335; 2009b.

Xu XG, Stabin M, Bolch W, Segars W. Chapter 30: Summary and Future Needs Related to Computational Phantoms. Handbook of Anatomical Models for Radiation Dosimetry, TAYLOR & FRANCIS: 679-683; 2009c.

Zaidi H, Xu XG. Computational anthropomorphic models of the human anatomy: The path to realistic Monte Carlo modeling in radiological sciences. Annual Review of Biomedical Engineering 9: 471-500; 2007.

Zankl M, Becker J, Fill U, Petoussi-Henss N, Eckerman KF. GSF male and female adult voxel models representing ICRP Reference Man—the present status, Proceedings of The Monte Carlo Method: Versatility Unbounded in a Dynamic Computing World, Chattanooga, TN, American Nuclear Society, A Grange Park, USA; 2005.

Zankl M, Eckerman K, Bolch WE. Voxel-based models representing the male and female ICRP reference adult—the skeleton, Radiation Protection Dosimetry, 127(1-4):174-186; 2007.

Zankl M, Veit R, Williams G, Schneider K, Fendel H, Petoussi N, Drexler G. The construction of computer tomographic phantoms and their application in radiology and radiation protection, Radiation and Environmental Biophysics 27(2):153-164; 1988.

Zankl M, Fill U, Petoussi-Henss N, Rgulla D. Organ dose conversion coefficients for external photon irradiation of male and female voxel models, Physics in Medicine and Biology 47: 2367-2385; 2002.

Zelen M, Severo NC. Chapter 26, Probability Functions. Handbook of mathematical functions with Formulas, Graphs, and Mathematical Tables Edited by Milton Abramowitz and Irene A. Stegun: 925-995; 1972.

Zhang C, Chen T. Efficient feature extraction for 2D/3D objects in mesh representation. Image Processing, 2001. Proceedings. 2001 International Conference on 3: 935-938; 2001.

Zhang JY, Xu XG, Shi CY, Fuss M. Development of a Geometry-Based Respiratory-Motion-Simulating Patient Model for Radiation Dosimetry Using Monte Carlo Method. Journal of Applied Clinical Medical Physics 9(1): 16-28; 2008.

Zhang JY, Na YH, Caracappa P, Xu XG. RPI-AM and RPI-AF, a pair of mesh-based, size-adjustable adult male and female computational phantoms using ICRP-89 parameters and their calculations for organ doses from monoenergetic photon beams. Physics in Medicine and Biology 54: 5885-5908; 2009.

Appendix A. Organ/Tissue Data for 50th-Percentile Adult phantoms

Table A. 1: Organ/tissue masses, densities, and volumes for the 50th-percentile RPI-AM phantom.

ID	Masses(g)					
	RPI adult male		ICRP	Voxel versus	Reference	Volume for
	Mesh-based	Voxelized	Reference	Reference	Density (gcm ⁻³)	RPI voxel 3.0mm (cm ³)
Phantom	Phantom	Data	Error (%)			
1	7.00	7.02	7.00	0.32	1.02	6.89
2	7.00	7.00	7.00	-0.07	1.02	6.86
3	39.44	39.43	39.44	-0.01	1.03	38.29
5	30.73	30.70	31.00	-0.08	1.05	29.24
7	10.00	9.98	10.00	-0.16	1.03	9.69
8	30.00	30.01	30.00	0.02	1.03	29.13
9	68.30	0.86	0.85	0.78	1.06	0.81
10	145.69	271.89	271.93	0.00	1.06	256.50
11	36.76	15.74	15.72	0.11	1.06	14.85
12	88.00	83.03	83.04	0.00	1.06	78.33
13	135.24	136.29	135.26	0.77	1.92	70.98
14	184.84	184.68	184.86	-0.08	1.20	153.31
15	33.48	33.47	33.48	-0.01	0.98	34.16
16	128.02	128.04	128.03	0.02	1.92	66.69
17	59.73	59.70	59.73	-0.04	1.11	53.87
18	37.13	37.28	37.13	0.41	0.98	38.04
19	270.76	270.76	270.80	0.00	1.92	141.02
20	181.89	181.92	181.91	0.01	1.11	164.13
21	22.66	22.65	22.67	-0.06	0.98	23.11
22	179.71	179.68	179.74	-0.02	1.92	93.58
23	139.57	139.57	139.59	0.00	1.11	125.93
24	47.77	47.80	47.78	0.06	1.92	24.89
25	53.05	53.06	53.06	0.02	1.15	46.12
26	562.77	562.72	562.85	-0.01	1.92	293.09
27	451.00	450.99	451.06	0.00	1.16	389.64
28	261.64	261.64	261.68	0.00	1.92	136.27
29	471.97	472.00	472.05	0.01	1.12	419.99

30	25.78	25.77	25.78	-0.03	0.98	26.30
31	294.05	294.04	294.09	0.00	1.92	153.14
32	438.53	438.52	438.57	0.00	1.11	395.66
33	80.88	80.89	80.89	0.01	0.98	82.54
34	531.30	531.26	531.35	-0.01	1.92	276.70
35	729.31	729.31	729.38	0.00	1.11	658.02
36	78.66	78.00	78.67	-0.83	0.98	79.60
37	232.55	232.50	232.56	-0.01	1.92	121.10
38	507.73	506.69	507.78	-0.21	1.11	457.16
39	76.11	76.10	76.12	-0.01	1.92	39.64
40	73.89	73.87	73.90	-0.03	1.23	60.16
41	398.55	398.55	398.62	-0.01	1.92	207.58
42	681.09	681.07	681.18	0.00	1.12	606.74
43	365.13	365.11	365.16	0.00	1.92	190.16
44	519.99	519.98	520.06	0.00	1.17	446.15
45	221.11	221.10	221.13	0.00	1.92	115.16
46	192.19	190.37	192.21	-0.95	1.18	160.89
47	102.91	102.90	102.92	0.00	1.92	53.60
48	73.55	73.55	73.55	0.00	1.05	70.04
49	286.54	286.52	286.58	-0.01	1.92	149.23
50	335.29	335.27	335.34	-0.01	1.07	312.20
51	186.17	186.16	186.19	-0.01	1.92	96.96
52	302.03	301.08	302.07	-0.32	1.11	270.84
53	109.21	109.33	109.23	0.10	1.92	56.94
54	173.48	173.46	173.51	-0.01	1.03	168.18
55	9.89	9.90	9.89	0.11	1.92	5.16
56	56.30	56.28	56.31	-0.05	1.04	54.08
58	88.65	88.06	88.67	-0.67	1.10	80.06
61	1450.00	1451.53	1450.00	0.11	1.04	1395.70
62	0.36	7.49	7.50	-0.09	0.95	7.88
63	0.18	4.98	4.99	-0.18	1.02	4.89
64	0.27	7.49	7.50	-0.09	0.95	7.88
65	0.13	4.98	4.99	-0.18	1.02	4.89
66	0.20	0.21	0.20	3.96	1.10	0.19
67	7.30	7.29	7.30	-0.18	1.03	7.07

68	0.20	0.21	0.20	3.95	1.10	0.19
69	7.30	7.29	7.30	-0.18	1.03	7.07
70	10.00	10.01	10.00	0.12	1.03	9.72
71	58.00	57.65	58.00	-0.60	1.03	55.97
72	149.97	149.95	150.00	-0.01	1.04	144.18
73	249.97	250.98	250.00	0.40	1.04	241.33
75	999.90	999.87	1000.00	0.00	1.04	961.42
76	89.97	89.97	89.99	-0.01	1.04	86.51
77	55.02	55.01	55.02	-0.02	1.04	52.89
78	59.99	60.01	60.00	0.02	1.04	57.70
79	94.99	94.97	95.00	-0.02	1.04	91.31
80	59.99	60.01	60.00	0.02	1.04	57.70
81	40.01	39.99	40.01	-0.06	1.04	38.45
82	89.97	89.97	89.99	-0.01	1.04	86.51
83	34.99	34.99	35.00	-0.02	1.04	33.64
84	40.01	40.01	40.01	0.01	1.04	38.48
85	74.97	74.95	74.97	-0.03	1.04	72.06
86	29.98	30.10	29.98	0.41	1.04	28.94
87	329.94	330.14	330.00	0.06	1.05	314.42
88	510.43	509.55	510.00	-0.08	1.06	480.71
89	107.11	107.11	107.12	0.01	1.05	102.01
90	38.25	38.24	38.25	-0.01	1.05	36.42
91	7.63	7.63	7.63	-0.10	1.05	7.26
92	109.90	109.91	109.92	0.01	1.05	104.68
93	39.24	39.24	39.25	-0.02	1.05	37.37
94	7.86	7.85	7.87	-0.14	1.05	7.48
95	1799.75	1801.80	1800.00	0.11	1.05	1716.00
97	552.99	550.43	553.00	-0.47	0.25	2201.70
99	646.99	643.20	647.00	-0.59	0.25	2572.80
100	2.26	2.25	2.26	-0.23	1.03	2.19
101	6.40	6.40	6.40	-0.01	1.03	6.21
102	5.95	5.98	5.98	-0.07	1.03	5.81
103	87.98	104.37	104.40	-0.02	1.03	101.33
104	6.70	7.81	7.83	-0.16	1.03	7.59
105	9.45	11.10	11.10	-0.05	1.03	10.77

106	1217.68	1217.66	1217.81	0.00	1.05	1159.68
107	15004.57	15004.44	15006.82	0.00	1.05	14289.94
108	2750.14	2750.12	2750.53	0.00	1.05	2619.16
109	10023.56	10023.60	10024.97	0.00	1.05	9546.28
110	40.00	39.99	40.00	-0.02	1.03	38.83
113	140.00	140.05	140.00	0.04	1.05	133.38
114	0.58	0.58	0.60	0.71	1.03	0.57
115	17.00	17.01	17.00	0.08	1.05	16.28
119	N/A	21004.29	N/A	N/A	1.03	20399.63
120	42.09	42.70	42.50	-0.02	1.05	40.66
121	44.35	42.70	42.50	-0.02	1.05	40.66
125	N/A	3300.00	3300.00	N/A	0.42	7786.13
126	30.04	30.02	30.00	-0.06	1.04	28.86
127	150.00	149.57	150.00	-0.29	1.06	141.10
128	50.03	49.97	50.00	-0.13	2.75	18.17
129	17.48	17.47	17.50	-0.07	1.04	16.79
130	17.52	17.49	17.50	-0.12	1.04	16.82
131	25.12	25.11	25.00	-0.04	1.03	24.38
132	20.00	20.07	20.00	0.35	1.05	19.12
133	42.27	42.61	42.00	0.79	1.05	40.58
134	3.01	3.00	3.00	-0.23	1.03	2.92
135	8.50	8.51	8.50	0.06	1.03	8.26
136	7.49	7.51	7.50	0.27	1.03	7.29
137	50.00	50.01	50.00	0.02	1.04	48.09
138	200.00	199.09	200.00	-0.46	1.04	191.43
140	N/A		N/A		0	

Table A. 2: Organ/tissue masses, densities, and volumes for the 50th-Percentile RPI-AF phantom.

ID	Masses(g)					
	RPI adult female		ICRP Reference Data	Voxel versus Reference Error (%)	Reference Density (gcm ⁻³)	Volume for RPI voxel 2.5mm (cm ³)
	Mesh-based Phantom	Voxelized Phantom				
1	6.50	6.49	6.50	-0.21	1.02	6.36
2	6.50	6.49	6.50	-0.21	1.02	6.36
3	18.61	18.60	18.61	-0.04	1.03	18.06
5	9.02	9.01	9.00	-0.08	1.05	8.58
7	8.00	8.00	8.00	-0.02	1.03	7.77
8	25.00	24.99	25.00	-0.02	1.03	24.27
9	43.02	6.06	6.06	0.01	1.06	5.72
10	144.06	242.38	242.38	0.00	1.06	228.66
11	32.42	43.24	43.24	0.01	1.06	40.80
12	69.45	92.65	92.64	0.02	1.06	87.41
13	112.61	112.62	112.60	0.01	1.92	58.66
14	111.90	111.90	111.90	0.00	1.18	94.44
15	19.89	19.88	19.89	-0.07	0.98	20.28
16	102.20	102.21	102.21	0.00	1.92	53.23
17	52.78	52.77	52.78	-0.01	1.12	47.23
18	20.55	20.47	20.55	-0.36	0.98	20.89
19	155.15	155.16	155.14	0.01	1.92	80.81
20	91.24	91.23	91.24	0.00	1.12	81.66
21	33.59	33.60	33.59	0.00	0.98	34.28
22	104.08	104.04	104.08	-0.04	1.92	54.19
23	72.84	72.85	72.84	0.02	1.12	65.20
24	32.51	32.52	32.50	0.07	1.92	16.94
25	40.45	40.46	40.45	0.03	1.19	33.97
26	403.60	403.58	403.60	0.00	1.92	210.20
27	417.09	417.08	417.09	0.00	1.25	334.92
28	247.76	247.74	247.75	-0.01	1.92	129.03
29	225.05	225.01	225.05	-0.02	1.05	215.05
30	39.51	39.38	39.51	-0.32	0.98	40.19

31	232.47	232.49	232.47	0.01	1.92	121.09
32	174.67	173.96	174.67	-0.40	1.12	155.70
33	55.43	55.68	55.43	0.45	0.98	56.81
34	618.84	614.13	618.85	-0.76	1.92	319.86
35	586.53	586.53	586.52	0.00	1.12	524.95
36	87.65	87.65	87.65	0.00	0.98	89.44
37	171.74	171.75	171.75	0.00	1.92	89.45
38	270.35	270.35	270.35	0.00	1.12	241.97
39	44.95	44.97	44.94	0.06	1.92	23.42
40	34.67	34.65	34.67	-0.05	1.19	29.14
41	259.85	259.83	259.84	-0.01	1.92	135.33
42	445.07	445.00	445.07	-0.01	1.11	401.23
43	162.88	162.87	162.87	0.00	1.92	84.83
44	258.96	258.95	258.96	0.00	1.09	237.31
45	120.44	119.76	120.45	-0.57	1.92	62.38
46	96.86	96.86	96.87	-0.01	1.13	85.88
47	70.88	70.86	70.88	-0.03	1.92	36.91
48	72.81	72.81	72.81	0.01	1.14	64.14
49	203.77	203.96	203.78	0.09	1.92	106.23
50	252.56	252.56	252.56	0.00	1.08	233.05
51	154.62	154.62	154.62	0.00	1.92	80.53
52	261.28	261.27	261.28	0.00	1.17	223.17
54	140.44	140.81	140.44	0.26	1.05	133.84
55	1.86	1.68	1.67	0.67	1.92	0.88
56	47.42	47.41	47.41	-0.02	1.08	44.06
58	313.61	313.60	313.61	0.00	1.10	285.09
61	1299.99	1298.34	1300.00	-0.13	1.04	1248.40
62	150.05	150.00	150.00	0.00	0.95	157.89
63	47.16	99.66	100.00	-0.34	1.02	97.70
64	150.00	150.00	150.00	0.00	0.95	157.89
65	46.10	99.66	100.00	-0.34	1.02	97.70
66	0.20	0.21	0.20	3.13	1.10	0.19
67	7.30	7.29	7.30	-0.13	1.03	7.08
68	-0.20	0.21	0.20	3.13	1.10	0.19
69	7.30	7.29	7.30	-0.13	1.03	7.08

70	8.00	8.01	8.00	0.18	1.03	7.78
71	48.00	47.85	48.00	-0.32	1.03	46.45
72	140.01	139.99	140.00	0.00	1.04	134.61
73	229.99	229.86	230.00	-0.06	1.04	221.02
75	879.99	879.99	880.00	0.00	1.04	846.14
76	90.00	89.99	90.00	-0.01	1.04	86.53
77	100.01	100.00	100.00	0.00	1.04	96.16
78	55.00	55.01	55.00	0.01	1.04	52.89
79	60.00	59.98	59.99	-0.03	1.04	57.67
80	55.00	54.99	55.00	-0.02	1.04	52.88
81	30.00	30.00	30.01	-0.03	1.04	28.84
82	90.00	89.99	90.00	-0.01	1.04	86.53
83	50.00	50.00	50.00	0.00	1.04	48.08
84	45.01	45.01	45.01	0.01	1.04	43.28
85	80.00	79.98	79.99	-0.01	1.04	76.91
86	24.99	25.09	24.99	0.39	1.04	24.13
87	250.01	249.99	250.00	0.00	1.05	238.09
88	370.00	369.61	370.00	-0.11	1.06	348.69
89	104.64	105.00	104.63	0.35	1.05	100.00
90	37.37	37.36	37.37	-0.04	1.05	35.58
91	7.48	7.46	7.48	-0.17	1.05	7.11
92	87.87	87.87	87.87	0.00	1.05	83.69
93	31.38	31.37	31.38	-0.04	1.05	29.88
94	6.28	6.27	6.28	-0.15	1.05	5.97
95	1403.29	1400.07	1400.00	0.01	1.05	1333.40
97	421.25	422.28	422.00	0.07	0.25	1689.10
99	528.72	527.63	528.00	-0.07	0.25	2110.50
100	0.53	1.32	1.34	-1.15	1.03	1.28
101	1.54	3.86	3.86	-0.03	1.03	3.75
102	2.50	2.58	2.58	-0.03	1.03	2.50
103	7.05	57.65	57.66	-0.02	1.03	55.97
104	13.08	3.89	3.90	-0.01	1.03	3.78
105	11.59	9.79	9.80	-0.16	1.03	9.50
106	401.97	401.95	401.97	0.00	1.05	382.81
107	8518.19	8518.19	8518.23	0.00	1.05	8112.56

108	1524.92	1524.86	1524.87	0.00	1.05	1452.25
109	7054.94	7054.98	7054.94	0.00	1.05	6719.03
110	35.00	34.99	35.00	-0.03	1.03	33.97
111	5.50	5.49	5.50	-0.14	1.04	5.28
112	5.50	5.49	5.50	-0.14	1.04	5.28
113	120.00	119.68	120.00	-0.27	1.05	113.98
114	0.60	0.60	0.60	-0.23	1.03	0.58
119	N/A	24341.27	N/A	N/A	0.99	24647.00
120	24.72	34.99	35.00	-0.02	1.05	33.33
121	24.69	34.99	35.00	-0.02	1.05	33.33
125	N/A	2300.00	2300.00	N/A	0.39	5836.10
126	28.00	28.00	28.00	0.00	1.04	26.92
127	130.00	130.00	130.00	0.00	1.06	122.64
128	40.00	40.00	40.00	0.01	2.75	14.55
131	20.00	19.99	20.00	-0.06	1.03	19.41
132	17.00	17.08	17.00	0.47	1.05	16.27
133	50.98	51.15	50.00	0.34	1.05	48.72
134	3.00	3.01	3.00	0.32	1.03	2.92
135	7.50	7.64	7.50	1.93	1.03	7.42
136	7.50	7.52	7.50	0.21	1.03	7.30
137	40.00	39.99	40.00	-0.02	1.04	38.45
138	200.00	200.41	200.00	0.20	1.04	192.70
139	80.00	79.90	80.00	-0.13	1.05	76.09
140	N/A	0.00	N/A		0.00	

Appendix B. Organ/Tissue Data for Percentile-Specific Phantoms

To describe the organ-specific percentile data for major internal organs, the following methodologies are presented according to the organ ID numbers. The major organs of percentile volume and mass data for both the adult male and female in this study were derived using the normal CDF of 99.7% of the observations within almost three standard deviations of the mean. In each summary of key organs, the organ volume and mass values and the mesh-based anatomical structures are listed to easily compare with information in Tables B. 1-34 and Figure B. 1-24.

B.1 Adrenal glands (Organ ID# 001-002)

The size of each adrenal gland was approximately estimated one over thirtieth of an adult kidney size according to the ICRP Publication 89¹ in adults. In order to determine the percentile data of adults, the mean and standard deviation values of volume and mass were referred from the ICRP Publication 89, and the autopsy cases of normal Japanese adults², respectively.

ICRP Publication 89 (page 207)

Table (Reference values for the mass of two adrenal glands)

Adult Male: 14g, Adult Female: 13g

Reference Japanese man – I; Mass of organs and other characteristics of normal Japanese.

Table (Average weight of organs of the normal Japanese adult (20-50 yr) as compared with the data in the literature)

Adult male: 7.65±2.30g (left), 7.03±2.04g (right),

Adult female: 6.85±2.08g (left), 6.36±1.89g (right)

RPI-AM-50th: each: 7±2.0 g, RPI-AF-50th: each: 6.5±2.0 g

¹ICRP. Annual report of the International Commission on Radiological Protection. ICRP Publication 89. Stockholm (Sweden): International Commission on Radiological Protection (ICRP); 2002.

² Tanaka G, Kawamura H, Nakahara Y. Reference Japanese Man-I. Mass of Organs and Other Characteristics of Normal Japanese. Health Physics 36: 333-346; 1979.

Table B. 1: Percentile values for the mass and volume of left and right adrenal glands in adults.

Adult Male				Adult Female					
	Mass (g)		Volume (cm ³)			Mass (g)		Volume (cm ³)	
	Left	Right	Left	Right		Left	Right	Left	Right
Mean ± SD	7±2.0	7±2.0	6.86±1.96	6.86±1.96		6.5±2.0	6.5±2.0	6.37±1.96	6.37±1.96
Percentile									
5 th	3.71	3.71	3.64	3.64		3.21	3.21	3.15	3.15
10th	4.44	4.44	4.35	4.35		3.94	3.94	3.86	3.86
15th	4.93	4.93	4.83	4.83		4.43	4.43	4.34	4.34
20th	5.32	5.32	5.22	5.22		4.82	4.82	4.73	4.73
25th	5.65	5.65	5.54	5.54		5.15	5.15	5.05	5.05
30th	5.95	5.95	5.83	5.83		5.45	5.45	5.34	5.34
35th	6.23	6.23	6.11	6.11		5.73	5.73	5.62	5.62
40th	6.49	6.49	6.36	6.36		5.99	5.99	5.87	5.87
45th	6.75	6.75	6.62	6.62		6.25	6.25	6.13	6.13
50th	7.00	7.00	6.86	6.86		6.50	6.50	6.37	6.37
55th	7.25	7.25	7.11	7.11		6.75	6.75	6.62	6.62
60th	7.51	7.51	7.36	7.36		7.01	7.01	6.87	6.87
65th	7.77	7.77	7.62	7.62		7.27	7.27	7.13	7.13
70th	8.05	8.05	7.89	7.89		7.55	7.55	7.40	7.40
75th	8.35	8.35	8.19	8.19		7.85	7.85	7.70	7.70
80th	8.68	8.68	8.51	8.51		8.18	8.18	8.02	8.02
85th	9.07	9.07	8.89	8.89		8.57	8.57	8.40	8.40
90th	9.56	9.56	9.37	9.37		9.06	9.06	8.88	8.88
95th	10.29	10.29	10.09	10.09		9.79	9.79	9.60	9.60

B.2 Trachea (Organ ID# 007)

The ICRP Publication 23¹ described corresponding diameters of the tracheal lumen in the antero-posterior and the transverse directions to estimate reference tracheal masses for adult male and female. The bottom of trachea has outspreads to the point at which trachea divides into two main bronchi of the lungs². In this study, the total trachea was regarded as a one cylinder shape so as to calculate the cylinder radius. The total length of trachea was adapted to the average length of trachea in the ICRP Publication 23; (9-15 cm). Final percentile data of each male and female were adjusted by scaling based on the volume and mass values of the ICRP reference adults.

ICRP Publication 89 (page 90)

Table (Reference values for mass of the trachea)

Adult Male: 10(g), Adult Female: 8(g)

¹ ICRP. Report of the task group on Reference Man Publication 23. Pergamon Press. Oxford (UK): International Commission on Radiation Protection (ICRP); 1975.

² ICRP. Annual report of the International Commission on Radiological Protection. ICRP Publication 89. Stockholm (Sweden): International Commission on Radiological Protection (ICRP); 2002.

Table B. 2: Percentile values for mass and volume of the trachea in adults.

Percentile	Length (cm)	Total radius(cm)	Adult Male		Adult Female	
			Mass (g)	Volume (cm ³)	Mass (g)	Volume (cm ³)
5th	9.00	0.38	4.22	4.10	3.38	3.28
10th	9.30	0.39	4.66	4.52	3.72	3.62
15th	9.70	0.41	5.28	5.13	4.23	4.10
20th	10.00	0.42	5.79	5.62	4.63	4.50
25th	10.30	0.44	6.32	6.14	5.06	4.91
30th	10.70	0.45	7.09	6.88	5.67	5.51
35th	11.00	0.47	7.70	7.48	6.16	5.98
40th	11.30	0.48	8.35	8.11	6.68	6.49
45th	11.70	0.49	9.27	9.00	7.42	7.20
50th	12.00	0.51	10.00	9.71	8.00	7.77
55th	12.30	0.52	10.77	10.46	8.62	8.37
60th	12.70	0.54	11.86	11.51	9.48	9.21
65th	13.00	0.55	12.72	12.35	10.17	9.88
70th	13.30	0.56	13.62	13.22	10.89	10.58
75th	13.70	0.58	14.88	14.45	11.91	11.56
80th	14.00	0.59	15.88	15.42	12.71	12.34
85th	14.30	0.60	16.92	16.43	13.54	13.15
90th	14.70	0.62	18.39	17.85	14.71	14.28
95th	15.00	0.63	19.53	18.96	15.63	15.17

B.3 Bronchi (Organ ID# 008)

The structure of the bronchial or bronchial region (BB) region is subdivided into the trachea (Generation 0-8), main and intrapulmonary bronchi (Generation 9-15) and the alveolar interstitial (Generation 16-26) in the superior part of the respiratory system¹. The main bronchi branches into the last generation of the branches within the left and right lungs, called terminal bronchioles, at the end of air-conducting zone. This study covers the total volume and mass of bronchi structure up to the generation 15. According to the comparisons for the specifications of the tracheobronchial region in the ICRP Publication 23², the percentile data of male and female were estimated with the variance ranges of 20g to 40g and 15g to 35g for adult male and adult female, respectively. Each of percentile data was linearly scaled by the volume and mass values of the ICRP reference adults.

ICRP Publication 23 (page 165,166)

Table 69(Specifications of the tracheobronchial region)

Total T-B; estimated tissue wt. (g): 40

Table70 (Specifications of the tracheobronchial region)

Total T-B; estimated tissue wt. (g): 51

ICRP Publication 23 (page 173)

Weight of bronchial tree (g) male: 30, female: 25

ICRP Publication 89 (page 93)

Volume of non-respiratory bronchioles (Generations 9–15): ~ 5 x 10⁻⁵ m³.

Surface area of non-respiratory bronchioles: 2.4 x 10⁻¹ m².

¹ ICRP. Annual report of the International Commission on Radiological Protection. ICRP Publication 89. Stockholm (Sweden): International Commission on Radiological Protection (ICRP); 2002.

² ICRP. Report of the task group on Reference Man Publication 23. Pergamon Press. Oxford (UK): International Commission on Radiation Protection (ICRP); 1975.

Table B. 3: Percentile values for mass and volume of the bronchi in adults.

Percentile	Adult Male		Adult Female	
	Mass(g)	Volume(cm ³)	Mass(g)	Volume(cm ³)
5th	20.00	19.42	15.00	14.56
10th	22.00	21.36	17.00	16.50
15th	23.00	22.33	18.00	17.48
20th	24.00	23.30	19.00	18.45
25th	25.00	24.27	20.00	19.42
30th	26.00	25.24	21.00	20.39
35th	27.00	26.21	22.00	21.36
40th	28.00	27.18	23.00	22.33
45th	29.00	28.16	24.00	23.30
50th	30.00	29.13	25.00	24.27
55th	31.00	30.10	26.00	25.24
60th	32.00	31.07	27.00	26.21
65th	33.00	32.04	28.00	27.18
70th	34.00	33.01	29.00	28.16
75th	35.00	33.98	30.00	29.13
80th	36.00	34.95	31.00	30.10
85th	37.00	35.92	32.00	31.07
90th	38.00	36.89	33.00	32.04
95th	40.00	38.83	35.00	33.98

B.4 Skeletons (Organ ID# 013-058)

The skeleton components of the reference RPI-AM-50th and RPI-FM-50th phantoms substantially consist of outer and inner layer surfaces describing cortical bones, spongiosa and cavities. Since the total number of these surface meshes is 458 in mesh representation for each of adults, the percentile data of the skeletons was prioritized with the same scale factors of entire body size deformations in two ways: (1) scaled by the height percentile data; (2) adjusted by the weight percentile data. The whole skeleton components were able to be described with keeping the specific bone structures in both adults.

Table B. 4: Percentile values for mass of male skeletons.

Percentile	Adult Male																		
	05th	10th	15th	20th	25th	30th	35th	40th	45th	50th	55th	60th	65th	70th	75th	80th	85th	90th	95th
ID	Mass (g)																		
13	103.93	107.64	112.82	116.71	120.79	124.13	126.90	129.68	133.02	135.24	140.80	145.43	150.06	155.62	160.62	168.59	179.70	189.71	205.46
14	141.50	146.54	153.61	158.90	164.46	169.00	172.78	176.56	181.10	184.13	191.70	198.00	204.31	211.87	218.69	229.52	244.67	258.29	279.72
15	25.73	26.65	27.93	28.89	29.90	30.72	31.41	32.10	32.93	33.48	34.85	36.00	37.14	38.52	39.76	41.73	44.48	46.96	50.85
16	98.38	101.89	106.80	110.48	114.34	117.49	120.12	122.76	125.91	128.02	133.28	137.66	142.05	147.31	152.04	159.58	170.10	179.57	194.48
17	45.97	47.61	49.91	51.63	53.42	54.90	56.13	57.35	58.83	59.82	62.27	64.32	66.37	68.83	71.04	74.57	79.48	83.90	90.88
18	28.54	29.55	30.98	32.05	33.16	34.07	34.84	35.60	36.51	37.13	38.65	39.93	41.20	42.72	44.10	46.29	49.33	52.08	56.41
19	208.08	215.49	225.88	233.67	241.83	248.50	254.07	259.63	266.31	270.76	281.89	291.16	300.43	311.56	321.57	337.52	359.77	379.80	411.33
20	139.99	144.98	151.97	157.21	162.69	167.19	170.93	174.68	179.17	182.16	189.64	195.88	202.12	209.61	216.35	227.08	242.05	255.52	276.73
21	17.41	18.04	18.90	19.56	20.25	20.81	21.27	21.74	22.30	22.67	23.60	24.37	25.15	26.08	26.92	28.25	30.12	31.79	34.43
22	138.11	143.03	149.92	155.09	160.51	164.94	168.63	172.33	176.76	179.71	187.10	193.25	199.41	206.79	213.44	224.02	238.80	252.09	273.01
23	107.43	111.26	116.62	120.63	124.84	128.29	131.17	134.03	137.48	139.78	145.53	150.32	155.10	160.85	166.01	174.25	185.74	196.08	212.35
24	36.71	38.02	39.85	41.23	42.67	43.84	44.82	45.81	46.98	47.77	49.73	51.37	53.00	54.97	56.73	59.55	63.47	67.01	72.57
25	40.74	42.21	44.23	45.76	47.36	48.67	49.75	50.84	52.15	53.03	55.20	57.02	58.83	61.01	62.97	66.09	70.45	74.37	80.55
26	432.49	447.90	469.49	485.68	502.64	516.52	528.08	539.64	553.52	562.77	585.90	605.17	624.44	647.57	668.39	701.54	747.79	789.42	854.95
27	347.35	359.73	377.07	390.06	403.69	414.83	424.12	433.41	444.55	451.98	470.55	486.04	501.51	520.09	536.80	563.44	600.58	634.01	686.64
28	201.07	208.24	218.27	225.80	233.68	240.13	245.51	250.89	257.34	261.64	272.39	281.35	290.31	301.06	310.74	326.15	347.66	367.01	397.48
29	361.47	374.35	392.39	405.92	420.10	431.69	441.36	451.02	462.63	470.36	489.69	505.79	521.90	541.23	558.62	586.33	624.99	659.78	714.55
30	19.82	20.52	21.50	22.25	23.02	23.66	24.19	24.72	25.35	25.78	26.84	27.72	28.61	29.66	30.62	32.13	34.25	36.16	39.16
31	225.97	234.03	245.31	253.77	262.63	269.88	275.92	281.96	289.21	294.05	306.13	316.20	326.27	338.36	349.23	366.55	390.72	412.47	446.71
32	337.51	349.54	366.39	379.02	392.25	403.09	412.11	421.13	431.97	439.18	457.23	472.27	487.31	505.36	521.60	547.47	583.57	616.06	667.20

33	62.15	64.38	67.47	69.81	72.24	74.24	75.89	77.56	79.55	80.88	84.20	86.98	89.75	93.07	96.06	100.82	107.47	113.45	122.87
34	408.29	422.84	443.22	458.50	474.52	487.62	498.53	509.45	522.55	531.28	553.12	571.31	589.51	611.34	630.99	662.28	705.95	745.25	807.11
35	561.30	581.32	609.33	630.35	652.36	670.37	685.38	700.39	718.39	730.40	760.42	785.44	810.44	840.46	867.48	910.50	970.54	1024.56	1109.61
36	60.45	62.60	65.62	67.88	70.26	72.20	73.81	75.43	77.37	78.66	81.89	84.58	87.28	90.51	93.42	98.06	104.52	110.34	119.50
37	178.70	185.07	193.99	200.68	207.69	213.42	218.20	222.98	228.71	232.53	242.09	250.05	258.01	267.57	276.17	289.87	308.98	326.18	353.26
38	390.78	404.71	424.21	438.84	454.16	466.70	477.14	487.59	500.13	508.49	529.39	546.80	564.21	585.11	603.92	633.88	675.67	713.27	772.49
39	58.49	60.57	63.49	65.68	67.98	69.85	71.42	72.98	74.86	76.11	79.24	81.84	84.45	87.58	90.39	94.88	101.13	106.76	115.62
40	56.88	58.90	61.75	63.87	66.10	67.93	69.45	70.97	72.79	74.01	77.05	79.59	82.13	85.17	87.90	92.26	98.34	103.82	112.43
41	306.30	317.22	332.51	343.97	355.99	365.81	374.00	382.19	392.02	398.57	414.95	428.60	442.25	458.63	473.37	496.85	529.61	559.09	605.50
42	522.24	540.86	566.93	586.48	606.96	623.72	637.68	651.65	668.40	679.57	707.50	730.77	754.04	781.97	807.11	847.13	902.99	953.27	1032.39
43	280.67	290.68	304.69	315.20	326.20	335.21	342.71	350.22	359.22	365.23	380.24	392.74	405.25	420.26	433.77	455.28	485.30	512.32	554.85
44	401.16	415.46	435.47	450.50	466.22	479.09	489.82	500.55	513.42	522.00	543.45	561.33	579.21	600.65	619.96	650.71	693.61	732.23	793.01
45	169.92	175.98	184.46	190.82	197.48	202.93	207.48	212.02	217.47	221.11	230.19	237.77	245.34	254.42	262.60	275.63	293.80	310.16	335.90
46	147.30	152.55	159.90	165.41	171.18	175.91	179.86	183.79	188.52	191.67	199.55	206.11	212.67	220.55	227.63	238.93	254.68	268.86	291.18
47	79.08	81.90	85.85	88.81	91.91	94.45	96.56	98.68	101.21	102.90	107.13	110.66	114.18	118.41	122.22	128.28	136.74	144.35	156.33
48	56.51	58.53	61.35	63.46	65.68	67.49	69.01	70.52	72.32	73.54	76.56	79.08	81.60	84.62	87.34	91.68	97.71	103.15	111.72
49	218.63	226.43	237.34	245.52	254.10	261.11	266.96	272.80	279.82	284.49	296.18	305.93	315.67	327.36	337.88	354.64	378.03	399.07	432.20
50	257.68	266.87	279.73	289.37	299.48	307.74	314.63	321.52	329.80	335.31	349.09	360.57	372.05	385.83	398.23	417.98	445.55	470.35	509.39
51	143.35	148.46	155.62	160.99	166.61	171.21	175.04	178.87	183.47	186.54	194.20	200.59	206.98	214.65	221.55	232.53	247.87	261.67	283.39
52	231.77	240.03	251.59	260.27	269.36	276.80	282.99	289.19	296.63	301.59	313.99	324.31	334.64	347.03	358.19	375.95	400.74	423.04	458.16
53	83.92	86.92	91.12	94.25	97.56	100.24	102.49	104.74	107.42	109.21	113.70	117.45	121.19	125.68	129.72	136.15	145.13	153.20	165.93
54	133.14	137.89	144.53	149.51	154.74	159.01	162.56	166.13	170.40	173.25	180.36	186.30	192.23	199.36	205.76	215.96	230.21	243.02	263.20
55	7.60	7.87	8.25	8.54	8.83	9.08	9.28	9.48	9.73	9.89	10.30	10.64	10.97	11.38	11.75	12.33	13.14	13.87	15.03
56	43.24	44.78	46.95	48.57	50.26	51.65	52.80	53.96	55.35	56.27	58.58	60.51	62.44	64.75	66.83	70.15	74.78	78.94	85.49
58	68.13	70.55	73.96	76.51	79.18	81.37	83.19	85.01	87.20	88.65	92.30	95.34	98.37	102.01	105.29	110.52	117.80	124.36	134.68

Table B. 5: Percentile values for volume of male skeletons.

Percentile	Adult Male																		
	05th	10th	15th	20th	25th	30th	35th	40th	45th	50th	55th	60th	65th	70th	75th	80th	85th	90th	95th
ID	Volume (cm ³)																		
13	54.13	56.06	58.76	60.79	62.91	64.65	66.09	67.54	69.28	70.44	73.33	75.74	78.16	81.05	83.66	87.81	93.59	98.81	107.01
14	117.92	122.12	128.01	132.42	137.05	140.83	143.98	147.13	150.92	153.44	159.75	165.00	170.26	176.56	182.24	191.27	203.89	215.24	233.10
15	26.26	27.19	28.50	29.48	30.51	31.35	32.05	32.76	33.60	34.16	35.56	36.73	37.90	39.31	40.57	42.58	45.39	47.92	51.89
16	51.24	53.07	55.63	57.54	59.55	61.19	62.56	63.94	65.58	66.68	69.42	71.70	73.98	76.72	79.19	83.11	88.59	93.53	101.29
17	41.41	42.89	44.96	46.51	48.13	49.46	50.57	51.67	53.00	53.89	56.10	57.95	59.79	62.01	64.00	67.18	71.60	75.59	81.87
18	29.12	30.15	31.61	32.70	33.84	34.77	35.55	36.33	37.26	37.89	39.44	40.74	42.04	43.59	45.00	47.23	50.34	53.14	57.56
19	108.38	112.23	117.65	121.70	125.95	129.43	132.33	135.22	138.70	141.02	146.82	151.65	156.47	162.27	167.48	175.79	187.38	197.81	214.23
20	126.12	130.61	136.91	141.63	146.57	150.62	153.99	157.37	161.41	164.11	170.85	176.47	182.09	188.84	194.91	204.58	218.06	230.20	249.31
21	17.77	18.41	19.29	19.96	20.66	21.23	21.70	22.18	22.76	23.13	24.08	24.87	25.66	26.61	27.47	28.83	30.73	32.44	35.13
22	71.93	74.49	78.08	80.78	83.60	85.91	87.83	89.76	92.06	93.60	97.45	100.65	103.86	107.70	111.17	116.68	124.38	131.30	142.19
23	96.78	100.23	105.06	108.68	112.47	115.58	118.17	120.75	123.86	125.93	131.11	135.42	139.73	144.91	149.56	156.98	167.33	176.65	191.31
24	19.12	19.80	20.76	21.47	22.22	22.83	23.34	23.86	24.47	24.88	25.90	26.76	27.60	28.63	29.55	31.02	33.06	34.90	37.80
25	35.43	36.70	38.46	39.79	41.18	42.32	43.26	44.21	45.35	46.11	48.00	49.58	51.16	53.05	54.76	57.47	61.26	64.67	70.04
26	225.26	233.28	244.53	252.96	261.79	269.02	275.04	281.06	288.29	293.11	305.16	315.19	325.23	337.28	348.12	365.39	389.47	411.16	445.29
27	299.44	310.11	325.06	336.26	348.01	357.61	365.62	373.63	383.23	389.64	405.65	419.00	432.34	448.35	462.76	485.72	517.74	546.56	591.93
28	104.72	108.46	113.68	117.60	121.71	125.07	127.87	130.67	134.03	136.27	141.87	146.54	151.20	156.80	161.84	169.87	181.07	191.15	207.02
29	322.74	334.24	350.35	362.43	375.09	385.44	394.07	402.70	413.06	419.96	437.22	451.60	465.98	483.24	498.77	523.51	558.03	589.09	637.99
30	20.22	20.94	21.94	22.70	23.49	24.14	24.68	25.22	25.87	26.31	27.39	28.29	29.19	30.27	31.24	32.79	34.95	36.90	39.96
31	117.69	121.89	127.77	132.17	136.79	140.56	143.71	146.85	150.63	153.15	159.44	164.69	169.93	176.23	181.89	190.91	203.50	214.83	232.66
32	304.06	314.90	330.08	341.46	353.38	363.14	371.27	379.40	389.16	395.66	411.92	425.47	439.02	455.28	469.91	493.22	525.74	555.01	601.08

33	63.42	65.69	68.85	71.23	73.71	75.76	77.44	79.14	81.17	82.53	85.92	88.76	91.58	94.97	98.02	102.88	109.66	115.77	125.38
34	212.65	220.23	230.84	238.80	247.15	253.97	259.65	265.34	272.16	276.71	288.08	297.56	307.04	318.41	328.64	344.94	367.68	388.15	420.37
35	505.68	523.71	548.95	567.88	587.71	603.94	617.46	630.98	647.20	658.02	685.06	707.60	730.13	757.17	781.51	820.27	874.36	923.03	999.65
36	61.68	63.88	66.96	69.27	71.69	73.67	75.32	76.97	78.95	80.27	83.56	86.31	89.06	92.36	95.33	100.06	106.65	112.59	121.94
37	93.07	96.39	101.04	104.52	108.17	111.16	113.65	116.14	119.12	121.11	126.09	130.23	134.38	139.36	143.84	150.97	160.93	169.89	183.99
38	352.05	364.60	382.17	395.35	409.15	420.45	429.86	439.27	450.57	458.10	476.93	492.61	508.30	527.13	544.07	571.06	608.71	642.59	695.94
39	30.46	31.55	33.07	34.21	35.41	36.38	37.20	38.01	38.99	39.64	41.27	42.63	43.98	45.61	47.08	49.42	52.67	55.60	60.22
40	46.24	47.89	50.20	51.93	53.74	55.23	56.46	57.70	59.18	60.17	62.64	64.71	66.77	69.24	71.46	75.01	79.95	84.41	91.41
41	159.53	165.22	173.18	179.15	185.41	190.53	194.79	199.06	204.18	207.59	216.12	223.23	230.34	238.87	246.55	258.78	275.84	291.19	315.36
42	466.29	482.91	506.19	523.64	541.93	556.89	569.36	581.83	596.79	606.76	631.70	652.47	673.25	698.19	720.63	756.37	806.24	851.13	921.78
43	146.18	151.40	158.69	164.17	169.90	174.59	178.49	182.41	187.09	190.22	198.04	204.55	211.07	218.89	225.92	237.13	252.76	266.83	288.98
44	342.87	355.09	372.20	385.04	398.48	409.48	418.65	427.82	438.82	446.15	464.49	479.77	495.05	513.38	529.88	556.16	592.83	625.84	677.79
45	88.50	91.66	96.07	99.39	102.85	105.69	108.06	110.43	113.27	115.16	119.89	123.84	127.78	132.51	136.77	143.56	153.02	161.54	174.95
46	124.83	129.28	135.51	140.18	145.07	149.08	152.42	155.75	159.76	162.43	169.11	174.67	180.23	186.91	192.91	202.48	215.83	227.85	246.76
47	41.19	42.66	44.71	46.26	47.87	49.19	50.29	51.40	52.71	53.59	55.80	57.64	59.47	61.67	63.66	66.81	71.22	75.18	81.42
48	53.82	55.74	58.43	60.44	62.55	64.28	65.72	67.16	68.88	70.04	72.91	75.31	77.71	80.59	83.18	87.31	93.06	98.24	106.40
49	113.87	117.93	123.61	127.88	132.34	135.99	139.04	142.08	145.74	148.17	154.26	159.34	164.41	170.50	175.98	184.71	196.89	207.85	225.10
50	240.82	249.41	261.43	270.44	279.89	287.61	294.05	300.49	308.22	313.37	326.25	336.98	347.71	360.59	372.18	390.64	416.40	439.58	476.07
51	74.66	77.32	81.05	83.85	86.78	89.17	91.17	93.16	95.56	97.16	101.15	104.47	107.80	111.80	115.39	121.11	129.10	136.29	147.60
52	208.80	216.24	226.66	234.48	242.67	249.37	254.95	260.53	267.23	271.70	282.87	292.17	301.48	312.64	322.69	338.69	361.03	381.12	412.76
53	43.71	45.27	47.46	49.09	50.81	52.21	53.38	54.55	55.95	56.88	59.22	61.17	63.12	65.46	67.56	70.91	75.59	79.79	86.42
54	129.26	133.87	140.32	145.16	150.23	154.38	157.83	161.29	165.44	168.20	175.11	180.87	186.63	193.55	199.77	209.67	223.50	235.94	255.53
55	3.96	4.10	4.30	4.45	4.60	4.73	4.83	4.94	5.07	5.15	5.36	5.54	5.71	5.93	6.12	6.42	6.84	7.22	7.83
56	41.58	43.06	45.14	46.70	48.33	49.66	50.77	51.88	53.22	54.11	56.33	58.18	60.04	62.26	64.26	67.45	71.90	75.90	82.20
58	61.94	64.14	67.24	69.55	71.98	73.97	75.63	77.28	79.27	80.59	83.91	86.67	89.43	92.74	95.72	100.47	107.09	113.05	122.44

Table B. 6: Percentile values for mass of female skeletons.

Percentile	Adult Female																			
	ID	05th	10th	15th	20th	25th	30th	35th	40th	45th	50th	55th	60th	65th	70th	75th	80th	85th	90th	95th
		Mass (g)																		
13	76.89	82.51	88.52	93.77	97.14	100.14	101.27	105.96	108.77	112.52	117.02	120.96	126.58	131.27	136.90	144.40	155.65	165.03	170.66	
14	76.09	81.66	87.60	92.79	96.13	99.10	100.22	104.86	107.64	111.35	115.81	119.70	125.27	129.91	135.48	142.90	154.04	163.32	168.88	
15	13.58	14.58	15.64	16.57	17.16	17.69	17.89	18.72	19.22	19.88	20.67	21.37	22.36	23.19	24.19	25.51	27.50	29.16	30.15	
16	69.78	74.89	80.34	85.10	88.17	90.89	91.91	96.16	98.72	102.12	106.21	109.78	114.89	119.14	124.25	131.06	141.27	149.78	154.88	
17	36.13	38.77	41.59	44.06	45.64	47.05	47.58	49.78	51.11	52.87	54.98	56.83	59.48	61.68	64.32	67.85	73.13	77.54	80.18	
18	14.03	15.06	16.15	17.11	17.73	18.28	18.48	19.34	19.85	20.53	21.36	22.07	23.10	23.96	24.98	26.35	28.41	30.12	31.14	
19	105.94	113.69	121.96	129.19	133.85	137.98	139.53	145.99	149.87	155.03	161.24	166.66	174.41	180.87	188.62	198.96	214.46	227.38	235.13	
20	62.45	67.02	71.89	76.16	78.90	81.34	82.25	86.06	88.34	91.39	95.04	98.24	102.81	106.62	111.19	117.28	126.42	134.04	138.60	
21	22.94	24.62	26.41	27.97	28.98	29.88	30.21	31.61	32.45	33.57	34.91	36.09	37.76	39.16	40.84	43.08	46.44	49.23	50.91	
22	71.07	76.27	81.81	86.67	89.79	92.56	93.60	97.93	100.53	104.00	108.16	111.80	117.00	121.34	126.54	133.47	143.87	152.54	157.74	
23	49.85	53.50	57.39	60.80	62.99	64.93	65.66	68.70	70.52	72.96	75.87	78.43	82.08	85.11	88.76	93.63	100.92	107.00	110.65	
24	22.19	23.82	25.55	27.07	28.04	28.91	29.23	30.59	31.40	32.48	33.78	34.92	36.54	37.89	39.52	41.68	44.93	47.64	49.26	
25	27.59	29.61	31.77	33.65	34.86	35.94	36.34	38.03	39.03	40.38	42.00	43.41	45.43	47.11	49.13	51.82	55.86	59.23	61.24	
26	275.58	295.74	317.25	336.07	348.17	358.93	362.96	379.76	389.84	403.29	419.42	433.53	453.70	470.50	490.67	517.55	557.88	591.49	611.65	
27	284.79	305.63	327.85	347.30	359.80	370.92	375.09	392.45	402.87	416.76	433.43	448.02	468.86	486.22	507.06	534.84	576.52	611.25	632.09	
28	169.17	181.55	194.75	206.30	213.73	220.33	222.81	233.12	239.31	247.56	257.47	266.13	278.51	288.82	301.20	317.71	342.46	363.09	375.47	
29	154.21	165.49	177.53	188.06	194.83	200.84	203.10	212.50	218.15	225.67	234.69	242.59	253.88	263.28	274.56	289.61	312.17	330.98	342.26	
30	26.98	28.95	31.06	32.90	34.09	35.14	35.53	37.18	38.17	39.48	41.06	42.44	44.42	46.06	48.04	50.67	54.62	57.91	59.88	
31	158.73	170.35	182.74	193.58	200.55	206.74	209.06	218.74	224.55	232.29	241.58	249.71	261.33	271.01	282.62	298.11	321.34	340.69	352.31	
32	119.55	128.30	137.63	145.79	151.04	155.71	157.46	164.75	169.12	174.95	181.95	188.07	196.82	204.11	212.86	224.52	242.02	256.60	265.34	
33	37.85	40.62	43.57	46.15	47.82	49.29	49.85	52.15	53.54	55.39	57.60	59.54	62.31	64.62	67.39	71.08	76.62	81.23	84.00	

34	422.55	453.47	486.45	515.31	533.86	550.35	556.53	582.30	597.76	618.37	643.10	664.75	695.67	721.43	752.35	793.58	855.41	906.94	937.86
35	401.45	430.82	462.15	489.57	507.19	522.86	528.74	553.21	567.90	587.48	610.98	631.54	660.92	685.40	714.77	753.94	812.69	861.64	891.02
36	59.85	64.23	68.90	72.99	75.61	77.95	78.82	82.47	84.66	87.58	91.09	94.15	98.53	102.18	106.56	112.40	121.16	128.45	132.83
37	117.27	125.85	135.00	143.01	148.16	152.73	154.45	161.60	165.89	171.61	178.47	184.48	193.06	200.21	208.79	220.23	237.39	251.69	260.27
38	185.04	198.58	213.02	225.66	233.79	241.01	243.71	255.00	261.77	270.79	281.63	291.10	304.64	315.93	329.47	347.52	374.60	397.17	410.70
39	30.69	32.94	35.33	37.43	38.77	39.97	40.42	42.29	43.41	44.91	46.71	48.28	50.53	52.40	54.64	57.64	62.13	65.87	68.12
40	23.69	25.43	27.28	28.89	29.93	30.86	31.21	32.65	33.52	34.67	36.06	37.27	39.01	40.45	42.19	44.50	47.96	50.85	52.59
41	177.43	190.41	204.26	216.37	224.16	231.09	233.68	244.50	250.99	259.65	270.04	279.12	292.11	302.92	315.91	333.22	359.18	380.82	393.80
42	304.14	326.39	350.13	370.90	384.26	396.12	400.58	419.12	430.25	445.08	462.89	478.46	500.72	519.26	541.52	571.19	615.70	652.79	675.04
43	111.21	119.35	128.03	135.62	140.50	144.84	146.47	153.25	157.32	162.75	169.26	174.95	183.09	189.87	198.01	208.86	225.13	238.69	246.83
44	176.63	189.55	203.33	215.40	223.15	230.04	232.63	243.40	249.86	258.48	268.82	277.86	290.79	301.56	314.48	331.71	357.56	379.10	392.02
45	82.24	88.25	94.67	100.29	103.90	107.11	108.31	113.33	116.34	120.35	125.16	129.37	135.39	140.41	146.42	154.45	166.48	176.51	182.53
46	66.26	71.11	76.28	80.81	83.72	86.30	87.27	91.31	93.74	96.97	100.85	104.24	109.09	113.13	117.98	124.44	134.14	142.22	147.07
47	48.40	51.94	55.72	59.03	61.15	63.04	63.75	66.70	68.47	70.83	73.66	76.14	79.68	82.64	86.18	90.90	97.98	103.89	107.43
48	49.93	53.58	57.48	60.89	63.08	65.03	65.76	68.80	70.63	73.06	75.98	78.54	82.20	85.24	88.89	93.76	101.07	107.16	110.81
49	139.13	149.31	160.17	169.67	175.78	181.21	183.25	191.73	196.82	203.61	211.75	218.88	229.06	237.55	247.73	261.30	281.66	298.63	308.81
50	171.86	184.43	197.84	209.58	217.13	223.83	226.35	236.83	243.11	251.50	261.56	270.36	282.93	293.41	305.99	322.75	347.90	368.86	381.44
51	105.57	113.30	121.54	128.75	133.38	137.50	139.05	145.48	149.35	154.50	160.68	166.08	173.81	180.25	187.97	198.27	213.72	226.60	234.32
52	178.29	191.34	205.25	217.43	225.26	232.22	234.82	245.70	252.22	260.92	271.35	280.48	293.53	304.40	317.45	334.84	360.93	382.68	395.72
54	95.70	102.71	110.18	116.71	120.91	124.65	126.05	131.88	135.39	140.05	145.66	150.56	157.56	163.40	170.40	179.74	193.74	205.41	212.42
55	1.14	1.22	1.31	1.39	1.44	1.49	1.50	1.57	1.61	1.67	1.74	1.79	1.88	1.95	2.03	2.14	2.31	2.45	2.53
56	32.50	34.88	37.41	39.63	41.06	42.33	42.80	44.78	45.97	47.56	49.46	51.13	53.50	55.48	57.86	61.03	65.79	69.75	72.13
58	214.13	229.80	246.51	261.14	270.54	278.89	282.03	295.08	302.92	313.36	325.90	336.87	352.53	365.59	381.26	402.15	433.49	459.60	475.27

Table B. 7: Percentile values for volume of female skeletons.

Percentile	Adult Female																		
	05th	10th	15th	20th	25th	30th	35th	40th	45th	50th	55th	60th	65th	70th	75th	80th	85th	90th	95th
ID	Volume (cm ³)																		
13	76.89	42.97	46.10	48.84	50.59	52.16	52.74	55.19	56.65	58.60	60.95	63.00	65.93	68.37	71.30	75.21	81.07	85.95	88.89
14	76.09	69.20	74.24	78.64	81.47	83.98	84.93	88.86	91.22	94.36	98.14	101.44	106.16	110.09	114.81	121.10	130.54	138.41	143.12
15	13.58	14.88	15.96	16.91	17.51	18.05	18.26	19.10	19.61	20.29	21.09	21.81	22.82	23.66	24.68	26.03	28.06	29.76	30.77
16	69.78	39.01	41.84	44.32	45.92	47.34	47.87	50.08	51.42	53.19	55.32	57.18	59.84	62.05	64.71	68.26	73.58	78.01	80.67
17	36.13	34.62	37.13	39.34	40.75	42.01	42.48	44.45	45.63	47.21	49.09	50.74	53.11	55.07	57.43	60.58	65.29	69.23	71.59
18	14.03	15.37	16.48	17.46	18.09	18.65	18.86	19.73	20.26	20.95	21.80	22.52	23.57	24.45	25.49	26.89	28.99	30.73	31.78
19	105.94	59.21	63.52	67.29	69.71	71.86	72.67	76.04	78.06	80.74	83.98	86.80	90.84	94.20	98.24	103.63	111.70	118.43	122.46
20	62.45	59.84	64.19	68.00	70.45	72.63	73.44	76.84	78.88	81.60	84.86	87.71	91.79	95.20	99.28	104.71	112.88	119.68	123.75
21	22.94	25.12	26.95	28.54	29.57	30.49	30.83	32.26	33.11	34.26	35.62	36.83	38.53	39.96	41.67	43.96	47.39	50.23	51.95
22	71.07	39.72	42.61	45.14	46.77	48.21	48.75	51.01	52.36	54.17	56.33	58.23	60.94	63.20	65.91	69.52	74.93	79.45	82.16
23	49.85	47.77	51.24	54.29	56.24	57.97	58.63	61.34	62.96	65.14	67.74	70.03	73.29	75.99	79.25	83.60	90.11	95.54	98.79
24	22.19	12.41	13.31	14.10	14.60	15.06	15.22	15.93	16.35	16.92	17.59	18.19	19.03	19.73	20.58	21.71	23.40	24.81	25.66
25	27.59	24.88	26.70	28.28	29.29	30.20	30.54	31.96	32.80	33.93	35.29	36.48	38.18	39.59	41.29	43.55	46.94	49.77	51.46
26	275.58	154.03	165.23	175.04	181.34	186.94	189.04	197.79	203.04	210.05	218.45	225.80	236.30	245.05	255.56	269.56	290.56	308.07	318.57
27	284.79	245.43	263.27	278.89	288.93	297.86	301.20	315.14	323.51	334.67	348.05	359.77	376.50	390.44	407.18	429.49	462.96	490.85	507.58
28	169.17	94.56	101.43	107.45	111.32	114.76	116.05	121.42	124.64	128.94	134.10	138.61	145.06	150.43	156.88	165.47	178.36	189.11	195.56
29	154.21	157.61	169.08	179.10	185.55	191.28	193.43	202.38	207.76	214.92	223.51	231.04	241.79	250.74	261.49	275.82	297.30	315.22	325.96
30	26.98	29.54	31.69	33.57	34.79	35.86	36.26	37.94	38.95	40.29	41.90	43.31	45.33	47.00	49.02	51.70	55.73	59.09	61.10
31	158.73	88.72	95.18	100.82	104.45	107.68	108.89	113.93	116.95	120.98	125.82	130.06	136.11	141.15	147.20	155.27	167.36	177.44	183.49
32	119.55	114.55	122.88	130.17	134.86	139.03	140.59	147.10	151.00	156.21	162.46	167.92	175.73	182.24	190.05	200.46	216.09	229.11	236.91

33	37.85	41.45	44.46	47.09	48.80	50.30	50.87	53.21	54.63	56.52	58.78	60.76	63.58	65.94	68.77	72.53	78.18	82.89	85.71
34	422.55	236.18	253.36	268.39	278.05	286.64	289.86	303.28	311.33	322.07	334.95	346.22	362.33	375.74	391.85	413.32	445.53	472.36	488.47
35	401.45	384.66	412.63	437.12	452.85	466.84	472.09	493.94	507.05	524.54	545.52	563.88	590.11	611.96	638.19	673.16	725.62	769.32	795.55
36	59.85	65.54	70.31	74.48	77.15	79.54	80.43	84.15	86.39	89.37	92.95	96.07	100.54	104.27	108.73	114.69	123.63	131.07	135.54
37	117.27	65.55	70.31	74.48	77.17	79.55	80.44	84.17	86.40	89.38	92.95	96.08	100.55	104.28	108.74	114.70	123.64	131.09	135.56
38	185.04	177.30	190.20	201.48	208.74	215.19	217.60	227.68	233.72	241.78	251.46	259.91	272.00	282.08	294.17	310.29	334.46	354.62	366.70
39	30.69	17.16	18.40	19.49	20.19	20.82	21.05	22.03	22.61	23.39	24.33	25.15	26.32	27.29	28.46	30.02	32.36	34.31	35.48
40	23.69	21.37	22.92	24.28	25.15	25.93	26.23	27.44	28.17	29.13	30.30	31.32	32.78	33.99	35.45	37.39	40.30	42.73	44.19
41	177.43	99.17	106.39	112.69	116.75	120.36	121.71	127.34	130.72	135.23	140.65	145.38	152.14	157.77	164.54	173.55	187.07	198.34	205.10
42	304.14	294.05	315.43	334.14	346.18	356.86	360.88	377.59	387.61	400.97	417.02	431.05	451.10	467.80	487.86	514.59	554.68	588.10	608.14
43	111.21	62.16	66.68	70.64	73.18	75.44	76.29	79.82	81.94	84.77	88.16	91.12	95.36	98.89	103.13	108.78	117.26	124.32	128.56
44	176.63	173.90	186.54	197.61	204.72	211.05	213.42	223.30	229.23	237.14	246.62	254.92	266.78	276.66	288.51	304.32	328.04	347.80	359.65
45	82.24	45.96	49.31	52.23	54.11	55.79	56.41	59.03	60.59	62.68	65.19	67.38	70.52	73.13	76.26	80.44	86.71	91.93	95.07
46	66.26	62.93	67.50	71.51	74.09	76.37	77.23	80.81	82.96	85.81	89.25	92.25	96.54	100.12	104.41	110.12	118.71	125.86	130.15
47	48.40	27.05	29.02	30.74	31.85	32.83	33.20	34.74	35.66	36.89	38.36	39.66	41.50	43.04	44.89	47.34	51.03	54.11	55.95
48	49.93	47.00	50.42	53.41	55.33	57.04	57.68	60.35	61.96	64.09	66.65	68.89	72.11	74.77	77.97	82.25	88.66	94.00	97.20
49	139.13	77.77	83.42	88.37	91.55	94.38	95.44	99.86	102.51	106.05	110.29	114.00	119.30	123.72	129.03	136.09	146.70	155.54	160.84
50	171.86	170.77	183.19	194.06	201.05	207.25	209.58	219.29	225.10	232.87	242.19	250.33	261.97	271.68	283.32	298.84	322.13	341.54	353.19
51	105.57	59.01	63.30	67.06	69.47	71.61	72.42	75.77	77.79	80.47	83.69	86.50	90.53	93.88	97.90	103.27	111.31	118.02	122.04
52	178.29	163.54	175.43	185.84	192.53	198.48	200.70	210.00	215.57	223.01	231.92	239.73	250.88	260.17	271.32	286.19	308.49	327.08	338.22
54	95.70	97.82	104.93	111.15	115.15	118.71	120.05	125.60	128.94	133.38	138.72	143.39	150.06	155.62	162.29	171.18	184.51	195.63	202.30
55	1.14	0.64	0.68	0.72	0.75	0.78	0.78	0.82	0.84	0.87	0.91	0.93	0.98	1.02	1.06	1.11	1.20	1.28	1.32
56	32.50	32.30	34.64	36.69	38.02	39.19	39.63	41.46	42.56	44.04	45.80	47.34	49.54	51.37	53.57	56.51	60.92	64.58	66.79
58	214.13	208.91	224.10	237.40	245.95	253.54	256.39	268.25	275.38	284.87	296.27	306.25	320.48	332.35	346.60	365.59	394.08	417.82	432.06

B.5 Brain (Organ ID# 061)

The volume and mass measurements of human brain have been reported in various literatures. The ICRP Publication 89¹ was based on the results of Dekaban² and International Atomic Energy Agency (IAEA) Publication, IAEA-TECDOC-1005³. The percentile data of brain were subject to the autopsy cases of normal Japanese adults⁴ in conformity with the ICRP reference adults. The percentile data of brain were subject to the autopsy cases of normal Japanese adults by Tanaka in conformity with the ICRP reference adults.

ICRP Publication 89 (page 209)

Table (Reference values for mass of the brain)

Adult Male: 1450g, Adult Female: 1300g

Reference Japanese man – I; Mass of organs and other characteristics of normal Japanese.

Table (Average weight of organs of the normal Japanese adult (20-50 yr) as compared with the data in the literature)

Adult male: 1440±118 g, Adult female: 1308±103g

RPI-AM-50th:1450±115g, RPI-AF-50th:1300±125g

¹ ICRP. Annual report of the International Commission on Radiological Protection. ICRP Publication 89. Stockholm (Sweden): International Commission on Radiological Protection (ICRP); 2002.

² Dekaban AS, Sadowsky D. Changes in brain weights during the span of human life: Relation of brain weights to body heights and body weights. Annals of Neurology 4: 345-356; 1978.

³ IAEA. Compilation of Anatomical, Physiological and Metabolic Characteristics for a Reference Asian Man. IAEA-TECDOC-1005 1-2: International Atomic Energy Agency; 1998.

⁴ Tanaka G, Kawamura H, Nakahara Y. Reference Japanese Man-I. Mass of Organs and Other Characteristics of Normal Japanese. Health Physics 36: 333-346; 1979.

Table B. 8: Percentile values for mass and volume of the brain in adults.

	Adult Male		Adult Female	
	Mass(g)	Volume(cm ³)	Mass(g)	Volume(cm ³)
	Mean ± SD	1450.00 ± 115.00	1394.23 ± 110.58	1300.00 ± 125.00
Percentile				
5th	1260.84	1212.35	1094.39	1052.30
10th	1302.62	1252.52	1139.81	1095.97
15th	1330.81	1279.63	1170.45	1125.43
20th	1353.21	1301.16	1194.80	1148.85
25th	1372.43	1319.64	1215.69	1168.93
30th	1389.69	1336.24	1234.45	1186.97
35th	1405.69	1351.63	1251.83	1203.68
40th	1420.87	1366.22	1268.33	1219.55
45th	1435.55	1380.34	1284.29	1234.89
50th	1450.00	1394.23	1300.00	1250.00
55th	1464.45	1408.13	1315.71	1265.11
60th	1479.13	1422.24	1331.67	1280.45
65th	1494.31	1436.84	1348.17	1296.32
70th	1510.31	1452.22	1365.55	1313.03
75th	1527.57	1468.82	1384.31	1331.07
80th	1546.79	1487.30	1405.20	1351.15
85th	1569.19	1508.84	1429.55	1374.57
90th	1597.38	1535.94	1460.19	1404.03
95th	1639.16	1576.12	1505.61	1447.70

B.6 Breast (Organ ID# 062-065)

The total volume and mass values of female whole-breast fractions, such as adipose and glandular tissues, in the ICRP Publication 89¹ (ICRP 2002) were derived from the reviews of several literatures². Accordingly, in this study, the percentile data of volume and mass for both breasts of adult female were estimated in agreement with the ICRP Publication 89. Each of percentile data was linearly proportioned to the volume and mass values of the adipose and glandular tissues in reference adult female since the breasts assembled with adipose and glandular tissues.

ICRP Publication 23 (page 195)

Total weight of both breasts for reference adults

Adult Male: 25g, Adult Female: 500g

ICRP Publication 89 (page 211)

Table (Reference values for the mass of both breasts)

Adult Male: 25g, Adult Female: 500g

RPI-AF-50th: each of breasts 256±100 ml

¹ ICRP. Annual report of the International Commission on Radiological Protection. ICRP Publication 89. Stockholm (Sweden): International Commission on Radiological Protection (ICRP); 2002.

² Victor L. Katch, Barbara Campagne, Patty Freedson, Stanley Sady, Frank I. Katch and Albert R. Behnke. Contribution of breast volume and weight to body fat distribution in females American Journal of Physical Anthropology 53 93-100; 1980.

Kramer R, Drexler G. Representative breast size of reference female Health Physics: (40) 913–914; 1980.

Kramer R, Williams G, Drexler G. Reply to M. Cristy Health Physics:(43)932-935; 1982.

Cristy M. Representative breast size of reference female Health Physics (43)930-932; 1982.

Table B. 9: Percentile values for mass and volume of the left and right breasts in adult female.

Adult Female										
Percentile	Left				Right				Mean ± SD	
	Mass (g)		Volume (ml)		Mass (g)		Volume (ml)			
	Adipose	Glandular	Adipose	Glandular	Adipose	Glandular	Adipose	Glandular		
5th	53.63	35.76	56.46	35.05	53.63	35.76	56.46	35.05	256±100	
10th	74.93	49.95	78.87	48.97	74.93	49.95	78.87	48.97		
15th	89.30	59.53	94.00	58.36	89.30	59.53	94.00	58.36		
20th	100.71	67.14	106.01	65.83	100.71	67.14	106.01	65.83		
25th	110.51	73.67	116.32	72.23	110.51	73.67	116.32	72.23		
30th	119.3	79.54	125.58	77.98	119.3	79.54	125.58	77.98		
35th	127.46	84.97	134.16	83.31	127.46	84.97	134.16	83.31		
40th	135.19	90.13	142.31	88.36	135.19	90.13	142.31	88.36		
45th	142.67	95.11	150.18	93.25	142.67	95.11	150.18	93.25		
50th	150.00	100.00	157.89	98.04	150.00	100.00	157.89	98.04		
55th	157.41	104.94	165.69	102.88	157.41	104.94	165.69	102.88		
60th	164.88	109.92	173.56	107.77	164.88	109.92	173.56	107.77		
65th	172.62	115.08	181.71	112.82	172.62	115.08	181.71	112.82		
70th	180.77	120.52	190.29	118.15	180.77	120.52	190.29	118.15		
75th	189.57	126.38	199.55	123.9	189.57	126.38	199.55	123.90		
80th	199.36	132.91	209.86	130.30	199.36	132.91	209.86	130.30		
85th	210.78	140.52	221.87	137.77	210.78	140.52	221.87	137.77		
90th	225.15	150.10	237.00	147.16	225.15	150.10	237.00	147.16		
95th	246.44	164.30	259.42	161.07	246.44	164.30	259.42	161.07		

B.7 Gallbladder (Organ ID# 070-071)

The gallbladder consists of wall and content structures. The volume and mass values of empty gallbladder walls in adults were estimated by the computation of the gallbladder dimensions in the ICRP Publication 23¹. The volume and mass values of gallbladder contents in adults were assumed by the ratio, 0.8ml/kg of body weight, in the ICRP Publication 89². The percentile data of gallbladders in adults linearly scaled by the volume and mass values of the ICRP reference adults.

ICRP Publication 23 (page 148)

Weight of gallbladder for reference adults

Adult Male: 10g, Adult Female: 8g

ICRP Publication 89 (page 211)

Table (Reference values for mass of the gallbladder and contents)

Wall: Adult Male 10g, Adult Female 8g

Content: Adult Male 58g, Adult Female 48g

¹ ICRP. Report of the task group on Reference Man Publication 23. Pergamon Press. Oxford (UK): International Commission on Radiation Protection (ICRP); 1975.

² ICRP. Annual report of the International Commission on Radiological Protection. ICRP Publication 89. Stockholm (Sweden): International Commission on Radiological Protection (ICRP); 2002.

Table B. 10: Percentile values for mass and volume of the gallbladder in adults.

Percentile	Adult Male				Adult Female			
	Mass (g)		Volume(cm3)		Mass (g)		Volume(cm3)	
	Wall	Content	Wall	Content	Wall	Content	Wall	Content
5th	7.68	44.88	7.46	43.57	5.47	32.80	5.31	31.84
10th	7.96	46.48	7.73	45.13	5.87	35.20	5.70	34.17
15th	8.34	48.72	8.10	47.30	6.29	37.76	6.11	36.66
20th	8.63	50.40	8.38	48.93	6.67	40.00	6.47	38.83
25th	8.93	52.16	8.67	50.64	6.91	41.44	6.71	40.23
30th	9.18	53.60	8.91	52.04	7.12	42.72	6.91	41.48
35th	9.38	54.80	9.11	53.20	7.20	43.20	6.99	41.94
40th	9.59	56.00	9.31	54.37	7.53	45.20	7.31	43.88
45th	9.84	57.44	9.55	55.77	7.73	46.40	7.51	45.05
50th	10.00	58.40	9.71	56.70	8.00	48.00	7.77	46.60
55th	10.41	60.80	10.11	59.03	8.32	49.92	8.08	48.47
60th	10.75	62.80	10.44	60.97	8.60	51.60	8.35	50.10
65th	11.10	64.80	10.77	62.91	9.00	54.00	8.74	52.43
70th	11.51	67.20	11.17	65.24	9.33	56.00	9.06	54.37
75th	11.88	69.36	11.53	67.34	9.73	58.40	9.45	56.70
80th	12.47	72.80	12.10	70.68	10.27	61.60	9.97	59.81
85th	13.29	77.60	12.90	75.34	11.07	66.40	10.74	64.47
90th	14.03	81.92	13.62	79.53	11.73	70.40	11.39	68.35
95th	15.19	88.72	14.75	86.14	12.13	72.80	11.78	70.68

B.8 Stomach (Organ ID# 072-073)

The gastrointestinal (GI) tract study for 61 individuals (49 males and 12 females) has been reported by Tipton and Cook¹. On the basis of this report, the ICRP Publication 23² determined the volume and mass values of the stomach for the reference adults in terms of stomach wall and contents. The percentile data of volume and mass values of stomach contents in adults were assumed by the ratio, 1.67 and 1.64 of the mass of walls (g) for male and female, respectively.

ICRP Publication 23 (page 131), (Tipton and Cook, 1969)

(Weight of the stomach during postnatal life)

Male (n=49; mean age =43 y; mean W=73kg; mean L=169cm):

mean = 150g with an 80% range of 120-170g

Female (n=12; mean age =43 y; mean W=65kg; mean L=166cm):

mean = 140g with an 80% range of 120-160g

Adult Male: Male: 150±20g (80%: 120~170g), Adult Female: 140±18g (110~170g).

ICRP Publication 89 (page 211)

Table (Reference values for mass of the stomach wall (g))

Adult Male: 150g, Adult Female: 140g

RPI-AM-50th: 150±20 g (80% range ≈ 120-170g)

RPI-AF-50th: 140±18 g (80% range ≈ 110-170g)

¹ Tipton IH, Cook MJ. Weight of total gastrointestinal tract and its subfractions Health Physics Division Annual Progress Report for Period Ending July 31, 1969 Report ORNL-4446. Oak Ridge National Laboratory, Oak Ridge, TN 301-2;1969

² ICRP. Report of the task group on Reference Man Publication 23. Pergamon Press. Oxford (UK): International Commission on Radiation Protection (ICRP); 1975.

Table B. 11: Percentile values for mass and volume of the stomach in adults.

Adult Male				Adult Female				
	Mass (g)		Volume(cm3)		Mass (g)		Volume(cm3)	
	Wall	Content	Wall	Content	Wall	Content	Wall	Content
Mean ± SD	150.00 ± 20.00		144.23 ± 19.23		140.00 ± 18.00		134.62 ± 17.31	
Percentile								
5th	117.10	195.17	112.60	187.66	110.39	181.35	106.14	174.38
10th	124.37	207.28	119.59	199.31	116.93	192.10	112.43	184.71
15th	129.27	215.45	124.30	207.16	121.34	199.34	116.67	191.68
20th	133.17	221.95	128.05	213.41	124.85	205.11	120.05	197.22
25th	136.51	227.52	131.26	218.77	127.86	210.06	122.94	201.98
30th	139.51	232.52	134.14	223.57	130.56	214.49	125.54	206.24
35th	142.29	237.15	136.82	228.03	133.06	218.60	127.94	210.19
40th	144.93	241.55	139.36	232.26	135.44	222.51	130.23	213.95
45th	147.49	245.82	141.82	236.36	137.74	226.29	132.44	217.58
50th	150.00	250.00	144.23	240.38	140.00	230.00	134.62	221.15
55th	152.51	254.18	146.64	244.41	142.26	233.71	136.79	224.72
60th	155.07	258.45	149.11	248.51	144.56	237.49	139.00	228.36
65th	157.71	262.85	151.64	252.74	146.94	241.40	141.29	232.12
70th	160.49	267.48	154.32	257.20	149.44	245.51	143.69	236.07
75th	163.49	272.48	157.20	262.00	152.14	249.94	146.29	240.33
80th	166.83	278.05	160.41	267.36	155.15	254.89	149.18	245.09
85th	170.73	284.55	164.16	273.61	158.66	260.66	152.56	250.63
90th	175.63	292.72	168.88	281.46	163.07	267.90	156.80	257.60
95th	182.90	304.83	175.87	293.11	169.61	278.64	163.09	267.93

B.9 Small intestines (Organ ID# 075)

The total volume and mass values of small intestines for adult male and female in the ICRP Publication 89¹ were derived from the study of gastrointestinal (GI) tract for 61 individuals (49 males and 12 females) reported by Tipton and Cook². In order to estimate the percentile data of volume and mass values of the total small intestines for adults, the small intestines were subdivided into the wall and content. The percentile data of volume and mass values of the contents of small intestines in adults were assumed by the ratio, 0.54 and 0.47 of the masses of walls (g) for male and female, respectively.

ICRP Publication 89 (page 211)

Table (Reference values for mass of the small intestine wall (g))

Adult Male: 650g, Adult Female: 600g

RPI-AM-50th: *650±78 g (80% range ≈ 550-740g)*

RPI-AF-50th: *600±76 g (80% range ≈ 480-690g)*

¹ ICRP. Annual report of the International Commission on Radiological Protection. ICRP Publication 89. Stockholm (Sweden): International Commission on Radiological Protection (ICRP); 2002.

² Tipton IH, Cook MJ. Weight of total gastrointestinal tract and its subfractions Health Physics Division Annual Progress Report for Period Ending July 31, 1969 Report ORNL-4446. Oak Ridge National Laboratory, Oak Ridge, TN 301-2;1969

Table B. 12: Percentile values for mass and volume of the small intestines in adults.

Percentile	Adult Male				Adult Female			
	Mass (g)		Volume(cm3)		Mass (g)		Volume(cm3)	
	Wall	Content	Wall	Content	Wall	Content	Wall	Content
Mean ± SD	650.00 ± 78.00		625.00 ± 75.00		600.00 ± 76.00		576.00 ± 73.08	
5th	521.70	280.92	501.63	270.11	474.99	221.66	456.72	213.14
10th	550.04	296.18	528.88	284.78	502.60	234.55	483.27	225.53
15th	569.16	306.47	547.27	294.68	521.23	243.24	501.18	233.89
20th	584.35	314.65	561.88	302.55	536.04	250.15	515.42	240.53
25th	597.39	321.67	574.41	309.30	548.74	256.08	527.63	246.23
30th	609.10	327.98	585.67	315.36	560.15	261.40	538.61	251.35
35th	619.95	333.82	596.11	320.98	570.72	266.34	548.77	256.09
40th	630.24	339.36	606.00	326.31	580.75	271.02	558.41	260.59
45th	640.20	344.72	615.58	331.46	590.45	275.54	567.74	264.95
50th	650.00	350.00	625.00	336.54	600.00	280.00	576.92	269.23
55th	659.80	355.28	634.42	341.61	609.55	284.46	586.11	273.52
60th	669.76	360.64	644.00	346.77	619.25	288.98	595.43	277.87
65th	680.05	366.18	653.89	352.10	629.28	293.66	605.08	282.37
70th	690.90	372.02	664.33	357.71	639.85	298.60	615.24	287.11
75th	702.61	378.33	675.59	363.78	651.26	303.92	626.21	292.23
80th	715.65	385.35	688.13	370.53	663.96	309.85	638.42	297.93
85th	730.84	393.53	702.73	378.39	678.77	316.76	652.66	304.58
90th	749.96	403.82	721.12	388.29	697.40	325.45	670.58	312.94
95th	778.30	419.08	748.37	402.97	725.01	338.34	697.13	325.33

B.10 Large intestines (Organ ID# 076-086)

The large intestine is mainly consisted of the ascending, transverse, and descending segments, the sigmoid colon, and a terminal portion of the rectum. Each part of the volume and mass values of large intestines for adult male and female were summarized in the ICRP Publication 89¹ based on the study of gastrointestinal (GI) tract for 61 individuals (49 males and 12 females) by Tipton and Cook². The percentile data of volume and mass values of the each segment of both male and female were estimated by the wall and content subdivisions in this study.

ICRP Publication 89 (page 211)

Table (Summary of reference values for masses of walls in the gastrointestinal tract (g))

Adult Male: Right colon 150g, Left colon 150g, Rectosigmoid 70g.

Adult Female: Right colon 145g, Left colon 145g, Rectosigmoid 70g.

RPI-AM-50th:

Ascending colon: 90±14g (range ≈ 65~150 g), Transverse colon: 120±24g (range ≈ 40~190 g),

Descending colon: 90±23g (range ≈ 50~190 g), Sigmoid colon: 70±12g ((range ≈ 50~110)

RPI-AF-50th:

Ascending colon: 90±15g (range ≈ 75~120 g), Transverse colon: 110±14g (range ≈ 75~130 g),

Descending colon: 90±15g (range ≈ 65~110 g), Sigmoid colon: 70±12g ((range ≈ 55~95)

¹ ICRP. Annual report of the International Commission on Radiological Protection. ICRP Publication 89. Stockholm (Sweden): International Commission on Radiological Protection (ICRP); 2002.

² Tipton IH, Cook MJ. Weight of total gastrointestinal tract and its subfractions Health Physics Division Annual Progress Report for Period Ending July 31, 1969 Report ORNL-4446. Oak Ridge National Laboratory, Oak Ridge, TN 301-2;1969.

Table B. 13: Percentile values for mass and volume of the large intestines wall in adult male.

Adult Male (Wall)												
	Mass (g)						Volume(cm3)					
	Ascending	Left Transverse	Right Transverse	Descending	Sigmoid	Rectum	Ascending	Left Transverse	Right Transverse	Descending	Sigmoid	Rectum
Mean ± SD	90.00 ± 14.00	60.00 ± 12.00	60.00 ± 12.00	90.00 ± 23.00	70.00 ± 12.00	86.54 ± 13.46	57.69 ± 11.54	57.69 ± 11.54	86.54 ± 22.12	67.31 ± 11.54		
Percentile												
5th	66.97	40.26	40.26	52.17	28.73	21.53	64.39	38.71	38.71	50.16	27.63	20.70
10th	72.06	44.62	44.62	60.52	31.22	23.40	69.29	42.90	42.90	58.19	30.02	22.50
15th	75.49	47.57	47.57	66.16	32.90	24.66	72.59	45.74	45.74	63.62	31.63	23.71
20th	78.22	49.90	49.90	70.64	34.24	25.66	75.21	47.98	47.98	67.92	32.92	24.67
25th	80.56	51.91	51.91	74.49	35.39	26.52	77.46	49.91	49.91	71.63	34.03	25.50
30th	82.66	53.71	53.71	77.94	36.42	27.29	79.48	51.64	51.64	74.94	35.02	26.24
35th	84.61	55.38	55.38	81.14	37.37	28.01	81.36	53.25	53.25	78.02	35.93	26.93
40th	86.45	56.96	56.96	84.17	38.28	28.68	83.13	54.77	54.77	80.93	36.81	27.58
45th	88.24	58.49	58.49	87.11	39.15	29.34	84.85	56.24	56.24	83.76	37.64	28.21
50th	90.00	60.00	60.00	90.00	40.02	29.98	86.54	57.69	57.69	86.54	38.48	28.83
55th	91.76	61.51	61.51	92.89	40.88	30.63	88.23	59.14	59.14	89.32	39.31	29.45
60th	93.55	63.04	63.04	95.83	41.75	31.29	89.95	60.62	60.62	92.14	40.14	30.09
65th	95.39	64.63	64.63	98.86	42.66	31.96	91.72	62.14	62.14	95.06	41.02	30.73
70th	97.34	66.30	66.30	102.06	43.61	32.68	93.60	63.75	63.75	98.13	41.93	31.42
75th	99.44	68.10	68.10	105.51	44.64	33.45	95.62	65.48	65.48	101.45	42.92	32.16
80th	101.78	70.10	70.10	109.36	45.79	34.31	97.87	67.40	67.40	105.15	44.03	32.99
85th	104.51	72.44	72.44	113.84	47.13	35.31	100.49	69.65	69.65	109.46	45.32	33.95
90th	107.94	75.38	75.38	119.48	48.81	36.57	103.79	72.48	72.48	114.88	46.93	35.16
95th	113.03	79.74	79.74	127.83	51.30	38.44	108.68	76.67	76.67	122.91	49.33	36.96

Table B. 14: Percentile values for mass and volume of the large intestines content in adult male.

Adult Male (Content)										
Percentile	Mass (g)					Volume(cm3)				
	Ascending	Left Transverse	Right Transverse	Descending	Sigmoid	Ascending	Left Transverse	Right Transverse	Descending	Sigmoid
5th	40.94	26.85	63.75	20.29	53.83	39.37	25.82	61.30	19.51	51.76
10th	44.05	29.75	70.65	23.54	58.50	42.36	28.61	67.93	22.63	56.25
15th	46.15	31.72	75.31	25.73	61.65	44.38	30.50	72.41	24.74	59.28
20th	47.82	33.27	79.01	27.47	64.15	45.98	31.99	75.97	26.41	61.68
25th	49.25	34.61	82.18	28.97	66.31	47.36	33.28	79.02	27.86	63.76
30th	50.53	35.81	85.03	30.31	68.23	48.59	34.43	81.76	29.14	65.61
35th	51.72	36.93	87.68	31.55	70.02	49.73	35.51	84.31	30.34	67.33
40th	52.85	37.98	90.19	32.73	71.71	50.82	36.52	86.72	31.47	68.95
45th	53.94	39.00	92.61	33.88	73.35	51.87	37.50	89.05	32.58	70.53
50th	55.02	40.01	95.00	35.00	74.97	52.90	38.47	91.35	33.65	72.09
55th	56.10	41.02	97.39	36.12	76.59	53.94	39.44	93.64	34.73	73.64
60th	57.19	42.04	99.81	37.27	78.23	54.99	40.42	95.97	35.84	75.22
65th	58.32	43.09	102.32	38.45	79.92	56.08	41.43	98.38	36.97	76.85
70th	59.51	44.21	104.97	39.69	81.71	57.22	42.51	100.93	38.16	78.57
75th	60.79	45.41	107.82	41.03	83.63	58.45	43.66	103.67	39.45	80.41
80th	62.22	46.75	110.99	42.53	85.79	59.83	44.95	106.72	40.89	82.49
85th	63.89	48.30	114.69	44.27	88.29	61.43	46.44	110.28	42.57	84.89
90th	65.99	50.27	119.35	46.46	91.44	63.45	48.34	114.76	44.67	87.92
95th	69.10	53.17	126.26	49.71	96.11	66.44	51.13	121.40	47.80	92.41

Table B. 15: Percentile values for mass and volume of the large intestines wall in adult female.

Adult Female (Wall)												
	Mass (g)						Volume(cm3)					
	Ascending	Left Transverse	Right Transverse	Descending	Sigmoid	Rectum	Ascending	Left Transverse	Right Transverse	Descending	Sigmoid	Rectum
Mean ± SD	90.00 ± 15.00	55.00 ± 7.00	55.00 ± 7.00	90.00 ± 15.00	70.00 ± 12.00	86.54 ± 14.42	52.88 ± 6.73	52.88 ± 6.73	86.54 ± 14.42	67.31 ± 11.54		
Percentile												
5th	65.33	43.49	43.49	65.33	32.32	17.94	62.82	41.82	41.82	62.82	31.08	17.25
10th	70.78	46.03	46.03	70.78	35.12	19.50	68.06	44.26	44.26	68.06	33.77	18.75
15th	74.45	47.75	47.75	74.45	37.01	20.55	71.59	45.91	45.91	71.59	35.59	19.76
20th	77.38	49.11	49.11	77.38	38.52	21.38	74.40	47.22	47.22	74.40	37.04	20.56
25th	79.88	50.28	50.28	79.88	39.81	22.10	76.81	48.35	48.35	76.81	38.28	21.25
30th	82.13	51.33	51.33	82.13	40.97	22.74	78.97	49.36	49.36	78.97	39.39	21.87
35th	84.22	52.31	52.31	84.22	42.04	23.34	80.98	50.30	50.30	80.98	40.42	22.44
40th	86.20	53.23	53.23	86.20	43.06	23.90	82.88	51.18	51.18	82.88	41.40	22.98
45th	88.12	54.12	54.12	88.12	44.04	24.45	84.73	52.04	52.04	84.73	42.35	23.51
50th	90.00	55.00	55.00	90.00	45.01	24.99	86.54	52.88	52.88	86.54	43.28	24.03
55th	91.88	55.88	55.88	91.88	45.98	25.53	88.35	53.73	53.73	88.35	44.21	24.55
60th	93.80	56.78	56.78	93.80	46.96	26.08	90.19	54.60	54.60	90.19	45.15	25.08
65th	95.78	57.70	57.70	95.78	47.98	26.64	92.10	55.48	55.48	92.10	46.13	25.62
70th	97.87	58.67	58.67	97.87	49.05	27.24	94.11	56.41	56.41	94.11	47.16	26.19
75th	100.12	59.72	59.72	100.12	50.21	27.88	96.27	57.42	57.42	96.27	48.28	26.81
80th	102.62	60.89	60.89	102.62	51.50	28.60	98.67	58.55	58.55	98.67	49.52	27.50
85th	105.55	62.26	62.26	105.55	53.01	29.43	101.49	59.87	59.87	101.49	50.97	28.30
90th	109.22	63.97	63.97	109.22	54.90	30.48	105.02	61.51	61.51	105.02	52.79	29.31
95th	114.67	66.52	66.52	114.67	57.70	32.04	110.26	63.96	63.96	110.26	55.48	30.81

Table B. 16: Percentile values for mass and volume of the large intestines content in adult female.

Adult Female (Content)										
Percentile	Mass (g)					Volume(cm ³)				
	Ascending	Left Transverse	Right Transverse	Descending	Sigmoid	Ascending	Left Transverse	Right Transverse	Descending	Sigmoid
5th	72.59	23.72	47.44	36.29	57.43	69.80	22.81	45.62	34.89	55.22
10th	78.64	25.11	50.21	39.32	62.42	75.62	24.14	48.28	37.81	60.02
15th	82.72	26.04	52.09	41.36	65.77	79.54	25.04	50.09	39.77	63.24
20th	85.98	26.79	53.57	42.99	68.45	82.67	25.76	51.51	41.34	65.82
25th	88.76	27.43	54.85	44.38	70.75	85.35	26.38	52.74	42.67	68.03
30th	91.26	28.00	56.00	45.63	72.80	87.75	26.92	53.85	43.88	70.00
35th	93.58	28.53	57.06	46.79	74.71	89.98	27.43	54.87	44.99	71.84
40th	95.78	29.03	58.06	47.89	76.52	92.10	27.91	55.83	46.05	73.58
45th	97.91	29.52	59.04	48.96	78.26	94.14	28.38	56.77	47.08	75.25
50th	100.00	30.00	60.00	50.00	79.99	96.15	28.85	57.69	48.08	76.91
55th	102.09	30.48	60.96	51.04	81.72	98.16	29.31	58.62	49.08	78.58
60th	104.22	30.97	61.94	52.11	83.46	100.21	29.78	59.56	50.11	80.25
65th	106.42	31.47	62.94	53.21	85.27	102.33	30.26	60.52	51.16	81.99
70th	108.74	32.00	64.00	54.37	87.18	104.56	30.77	61.54	52.28	83.83
75th	111.24	32.57	65.15	55.62	89.23	106.96	31.32	62.64	53.48	85.80
80th	114.02	33.21	66.43	57.01	91.53	109.63	31.93	63.88	54.82	88.01
85th	117.28	33.96	67.91	58.64	94.21	112.77	32.65	65.30	56.38	90.59
90th	121.36	34.89	69.79	60.68	97.56	116.69	33.55	67.11	58.35	93.81
95th	127.41	36.28	72.56	63.71	102.55	122.51	34.88	69.77	61.26	98.61

B.11 Heart (Organ ID# 087-088)

The ICRP Publication 23¹ summarized the typical values of hearts on the basis of various autopsy result data. The ICRP Publication 89² described the masses of the atria, ventricles, septa, endocardium, and the visceral layer of the pericardium without and with the blood contents in the chambers to determine the total volume and mass values of the hearts for reference adults. Each of volume and mass percentile data of both male and female hearts were evaluated by three different steps: (1) determined the total mass and volume of hearts for each of adults; (2) approximated the total blood volume (TBV) using the whole-body weight³; (3) estimated the volume and mass of heart contents in conformity with the ICRP reference adults. The final percentile data of each male and female were adjusted by scaling on the basis of the volume and mass values of the ICRP reference adults.

ICRP Publication 89 (page 136)

Table (Reference values for mass of the heart (g))

Adult Male: Tissue only 350g, Tissue plus blood in chambers 840g

Adult Female: Tissue only 250g, Tissue plus blood in chambers 620g

¹ ICRP. Report of the task group on Reference Man Publication 23. Pergamon Press. Oxford (UK): International Commission on Radiation Protection (ICRP); 1975.

² ICRP. Annual report of the International Commission on Radiological Protection. ICRP Publication 89. Stockholm (Sweden): International Commission on Radiological Protection (ICRP); 2002.

³ Richard AM, Matthew RP, Henry JB. Henry's clinical diagnosis and management by laboratory methods Henry's clinical diagnosis and management by laboratory methods;2007 .

Table B. 17: Percentile values for mass and volume of the heart in adults.

Percentile	Adult Male				Adult Female			
	Mass (g)		Volume(cm ³)		Mass (g)		Volume(cm ³)	
	Wall	Content	Wall	Content	Wall	Content	Wall	Content
5th	253.60	391.93	241.53	369.75	170.83	252.83	162.70	238.52
10th	262.64	405.90	250.14	382.93	183.33	271.33	174.60	255.97
15th	275.30	425.47	262.19	401.38	196.67	291.07	187.30	274.59
20th	284.79	440.14	271.23	415.22	208.33	308.33	198.41	290.88
25th	294.74	455.51	280.70	429.72	215.83	319.43	205.56	301.35
30th	302.88	468.08	288.45	441.59	222.50	329.30	211.90	310.66
35th	309.66	478.56	294.91	451.47	225.00	333.00	214.29	314.15
40th	316.44	489.04	301.37	461.36	235.42	348.42	224.21	328.69
45th	324.58	501.62	309.12	473.22	241.67	357.67	230.16	337.42
50th	330.00	510.00	314.29	481.13	250.00	370.00	238.10	349.06
55th	343.56	530.96	327.20	500.90	260.00	384.80	247.62	363.02
60th	354.86	548.42	337.96	517.38	268.75	397.75	255.95	375.24
65th	366.16	565.89	348.73	533.86	281.25	416.25	267.86	392.69
70th	379.73	586.85	361.64	553.63	291.67	431.67	277.78	407.23
75th	391.93	605.71	373.27	571.43	304.17	450.17	289.68	424.69
80th	411.37	635.75	391.78	599.77	320.83	474.83	305.56	447.96
85th	438.49	677.67	417.61	639.31	345.83	511.83	329.37	482.86
90th	462.90	715.40	440.86	674.90	366.67	542.67	349.21	511.95
95th	501.33	774.78	477.46	730.93	379.17	561.17	361.11	529.40

B.12 Kidney (Organ ID# 089-094)

Each of left and right kidneys can be subdivided into the outer layer of cortex and the inner layer of medullar regions. The total volume and mass values of kidneys for adults in the ICRP Publication 89¹ were derived from the study of the organ weight in 684 adult autopsies by de la Grandmaison et al. (2001)². The percentile data of volume and mass values of each part of kidneys for adults were estimated by the cortex, medulla, and renal pelvis subdivisions. The percentile data of volume and mass values of the contents of kidneys in adults were scaled by the volume and mass values of the ICRP reference adults.

ICRP Publication 89 (page 148)

Table (Reference values for the mass of both kidneys)

Adult Male: 310g, Adult Female: 275g.

Organ weight in 684 adult autopsies: new tables for a Caucasoid population.

Table (Comparative data of organ weight (g) of males and females)

Males (n=355):

Right kidney 162±39g (Range 53-320), Left kidney 160±41g (Range 50-410).

Females (n=329):

Right kidney 135±39g (Range 45-360), Left kidney 136±37g (Range 40-300).

RPI-AM-50th: 310±68 g, **RPI-AF-50th:** 275±80 g.

¹ ICRP. Annual report of the International Commission on Radiological Protection. ICRP Publication 89. Stockholm (Sweden): International Commission on Radiological Protection (ICRP); 2002.

² de la Grandmaison GL., Clairand I, Durigon M. Organ weight in 684 adult autopsies: new tables for a Caucasoid population Forensic science international 119:149–154; 2001.

Table B. 18: Percentile values for mass and volume of the left and right kidneys in adult male.

Adult Male															
Mass (g)													Volume(cm3)		
Mean ± SD	310.00 ± 68.00						295.24 ± 64.76								
Percentile	Left			Right			Left			Right					
Percentile	Cortex	Medulla	Pelvis	Cortex	Medulla	Pelvis	Cortex	Medulla	Pelvis	Cortex	Medulla	Pelvis	Cortex	Medulla	Pelvis
5th	68.47	24.45	4.88	70.26	25.09	5.00	65.21	23.28	4.64	66.91	23.89	4.77			
10th	77.01	27.50	5.48	79.02	28.22	5.63	73.34	26.19	5.22	75.26	26.87	5.36			
15th	82.77	29.55	5.90	84.93	30.33	6.05	78.82	28.15	5.61	80.88	28.88	5.76			
20th	87.34	31.19	6.22	89.63	32.00	6.38	83.19	29.70	5.93	85.36	30.48	6.08			
25th	91.27	32.59	6.50	93.66	33.44	6.67	86.92	31.04	6.19	89.20	31.85	6.35			
30th	94.80	33.85	6.75	97.28	34.73	6.93	90.28	32.24	6.43	92.64	33.08	6.60			
35th	98.07	35.02	6.99	100.63	35.93	7.17	93.40	33.35	6.65	95.84	34.22	6.83			
40th	101.17	36.12	7.21	103.81	37.07	7.39	96.35	34.40	6.86	98.87	35.30	7.04			
45th	104.17	37.20	7.42	106.89	38.17	7.61	99.21	35.42	7.07	101.80	36.35	7.25			
50th	107.12	38.25	7.63	109.92	39.25	7.83	102.02	36.43	7.27	104.69	37.38	7.46			
55th	110.07	39.30	7.84	112.95	40.33	8.05	104.83	37.43	7.47	107.57	38.41	7.66			
60th	113.07	40.38	8.05	116.03	41.43	8.27	107.69	38.45	7.67	110.50	39.46	7.87			
65th	116.17	41.48	8.27	119.21	42.57	8.49	110.64	39.51	7.88	113.53	40.54	8.09			
70th	119.44	42.65	8.51	122.56	43.77	8.73	113.75	40.62	8.10	116.73	41.68	8.31			
75th	122.97	43.91	8.76	126.18	45.06	8.99	117.11	41.82	8.34	120.18	42.91	8.56			
80th	126.90	45.31	9.04	130.21	46.50	9.28	120.85	43.15	8.61	124.01	44.28	8.83			
85th	131.47	46.95	9.36	134.91	48.17	9.61	125.21	44.71	8.92	128.49	45.88	9.15			
90th	137.23	49.00	9.78	140.82	50.28	10.03	130.70	46.67	9.31	134.12	47.89	9.55			
95th	145.77	52.05	10.38	149.58	53.41	10.66	138.83	49.57	9.89	142.46	50.87	10.15			

Table B. 19: Percentile values for mass and volume of the left and right kidneys in adult female.

Adult Female												
Mass (g) Volume(cm3)												
Mean ± SD	275 ± 80						261.90 ± 76.19					
Percentile	Left			Right			Left			Right		
	Cortex	Medulla	Pelvis	Cortex	Medulla	Pelvis	Cortex	Medulla	Pelvis	Cortex	Medulla	Pelvis
5th	54.56	19.49	3.90	45.82	16.36	3.27	51.97	18.56	3.72	43.64	15.59	3.11
10th	65.62	23.44	4.69	55.11	19.68	3.93	62.50	22.32	4.47	52.49	18.74	3.75
15th	73.09	26.10	5.22	61.38	21.92	4.38	69.60	24.86	4.98	58.46	20.88	4.17
20th	79.01	28.22	5.65	66.36	23.70	4.73	75.25	26.88	5.38	63.20	22.57	4.51
25th	84.10	30.04	6.01	70.63	25.22	5.04	80.09	28.61	5.73	67.27	24.02	4.80
30th	88.67	31.67	6.34	74.47	26.59	5.31	84.45	30.16	6.04	70.92	25.33	5.06
35th	92.90	33.18	6.64	78.02	27.86	5.57	88.48	31.60	6.33	74.30	26.54	5.30
40th	96.92	34.62	6.93	81.39	29.07	5.81	92.30	32.97	6.60	77.52	27.68	5.53
45th	100.81	36.00	7.21	84.66	30.23	6.04	96.01	34.29	6.86	80.63	28.79	5.75
50th	104.63	37.37	7.48	87.87	31.38	6.27	99.65	35.59	7.12	83.69	29.89	5.97
55th	108.45	38.74	7.75	91.08	32.53	6.50	103.29	36.89	7.38	86.74	30.98	6.19
60th	112.34	40.12	8.03	94.35	33.69	6.73	106.99	38.21	7.65	89.85	32.09	6.41
65th	116.36	41.56	8.32	97.72	34.90	6.97	110.82	39.58	7.92	93.07	33.24	6.64
70th	120.59	43.07	8.62	101.27	36.17	7.23	114.85	41.02	8.21	96.45	34.44	6.88
75th	125.16	44.70	8.95	105.11	37.54	7.50	119.20	42.57	8.52	100.11	35.75	7.14
80th	130.25	46.52	9.31	109.38	39.06	7.81	124.04	44.30	8.87	104.18	37.20	7.43
85th	136.17	48.64	9.74	114.36	40.84	8.16	129.69	46.32	9.27	108.92	38.90	7.77
90th	143.64	51.30	10.27	120.63	43.08	8.61	136.80	48.86	9.78	114.88	41.03	8.20
95th	154.70	55.25	11.06	129.92	46.40	9.27	147.33	52.62	10.53	123.73	44.19	8.83

B.13 Liver (Organ ID# 095)

The volume and mass values of livers for adult male and female have been studied in numerous autopsy studies and established in different body size. The ICRP Publication 89¹ was based on the adult autopsies reported by Boyd² and the IAEA-TECDOC-1005 Publication³ to represent Western and Asian adults, respectively. The volume and mass values of livers for Western adults can also be approximated using total body weight and the body surface area⁴. The formulas are:

$$\text{Total liver volume (ml) based on body surface area} = -794.41 + 1267.28 \times \text{body surface area (m}^2\text{)}$$

$$\text{Total liver volume (ml) based on weight} = 191.80 + 18.51 \times \text{weight (kg)}$$

In this study, the percentile data of both male and female livers were approximated on the basis of the formula related to total body weight in conformity with the ICRP reference adults.

ICRP Publication 89 (page 148)

Table (Reference values for mass of the liver)

Adult Male: 1800g, Adult Female: 1400g.

¹ ICRP. Annual report of the International Commission on Radiological Protection. ICRP Publication 89. Stockholm (Sweden): International Commission on Radiological Protection (ICRP); 2002.

² Boyd E 1933 Normal variability in weight of the adult human liver and spleen Archives of pathology. 16:350–372; 1933.

Boyd E 1941 Outline of Physical Growth and Development Burgess Publishing Co, Minneapolis, MN, USA; 1941.

Boyd E 1952 An Introduction to Human Biology and Anatomy for First Year Medical Students Child Research Council, Denver, CO, USA; 1952.

³ IAEA. Compilation of Anatomical, Physiological and Metabolic Characteristics for a Reference Asian Man. IAEA-TECDOC-1005 1-2: International Atomic Energy Agency; 1998.

⁴ Vauthey JN, Abdalla EK, Doherty DA, Gertsch P, Fenstermacher MJ, Loyer EM, Lerut J, Materne R, Wang X, Encarnacion A, Herron D, Mathey C, Ferrari G, Charnsangavej C, Do KA and Denys A. Body surface area and body weight predict total liver volume in Western adults Liver Transplant 8: 233-240; 2002.

Table B. 20: Percentile values for mass and volume of the liver in adults.

Percentile	Adult Male		Adult Female	
	Mass(g)	Volume(cm3)	Mass(g)	Volume(cm3)
5th	1435.09	1366.75	1009.06	961.01
10th	1478.27	1407.88	1070.78	1019.79
15th	1538.73	1465.46	1136.63	1082.50
20th	1584.07	1508.64	1194.24	1137.37
25th	1631.58	1553.88	1231.28	1172.64
30th	1670.44	1590.90	1264.20	1204.00
35th	1702.83	1621.75	1276.54	1215.75
40th	1735.22	1652.59	1327.98	1264.74
45th	1774.09	1689.61	1358.84	1294.14
50th	1800.00	1714.29	1400.00	1333.33
55th	1864.78	1775.98	1449.38	1380.36
60th	1918.76	1827.39	1492.59	1421.51
65th	1972.74	1878.80	1554.31	1480.30
70th	2037.52	1940.49	1605.75	1529.29
75th	2095.82	1996.02	1667.48	1588.08
80th	2188.67	2084.44	1749.79	1666.46
85th	2318.22	2207.83	1873.24	1784.04
90th	2434.82	2318.88	1976.12	1882.02
95th	2618.36	2493.68	2037.85	1940.81

B.14 Lungs (Organ ID# 097-099)

The total volume and mass values of left and right lungs can be differently determined by the remaining blood inside of the lung tissues from the examinations of lung autopsy¹. According to the study of the organ weight in 684 adult autopsies by de la Grandmaison et al. (2001)² referred to the ICRP Publication 89, the percentile data of volume and mass values of both left and right lungs for adults were estimated with including pulmonary and bronchial blood.

ICRP Publication 89 (page 92)

Table (Reference values for the mass of both lungs)

Adult Male: 1200g, Adult Female: 950g.

Organ weight in 684 adult autopsies: new tables for a Caucasoid population (de la Grandmaison et al. 2001).

Table (Comparative data of organ weight (g) of males and females)

Males (n=355):

Right lung 663±239g (Range 200-1593), Left lung 583±216g (Range 206-1718).

Females (n=329):

Right lung 546±207g (Range 173-1700), Left lung 467±174g (Range 178-1350).

RPI-AM-50th: *Right lung 647±223g, Left lung 553±186g.*

RPI-AF-50th: *Right lung 528±189g, Left lung 422±129g.*

¹ ICRP. Annual report of the International Commission on Radiological Protection. ICRP Publication 89. Stockholm (Sweden): International Commission on Radiological Protection (ICRP); 2002.

² de la Grandmaison GL., Clairand I, Durigon M. Organ weight in 684 adult autopsies: new tables for a Caucasoid population Forensic science international 119:149–154;2001.

Table B. 21: Percentile values for mass and volume of the left and right lungs in adults.

Percentile	Adult Male				Adult Female			
	Mass (g)		Volume (cm ³)		Mass (g)		Volume (cm ³)	
	Left	Right	Left	Right	Left	Right	Left	Right
Mean ± SD	553 ± 186	647 ± 223	2228 ± 744	2588 ± 892	422 ± 129	528 ± 189	1688 ± 516	2112 ± 756
5th	247.06	280.20	988.24	1120.80	209.81	217.12	839.24	868.48
10th	314.63	361.21	1258.52	1444.84	256.68	285.79	1026.72	1143.16
15th	360.22	415.88	1440.88	1663.52	288.30	332.11	1153.20	1328.44
20th	396.46	459.32	1585.84	1837.28	313.43	368.93	1253.72	1475.72
25th	427.54	496.59	1710.16	1986.36	334.99	400.52	1339.96	1602.08
30th	455.46	530.06	1821.84	2120.24	354.35	428.89	1417.40	1715.56
35th	481.33	561.07	1925.32	2244.28	372.29	455.17	1489.16	1820.68
40th	505.88	590.50	2023.52	2362.00	389.32	480.12	1557.28	1920.48
45th	529.63	618.98	2118.52	2475.92	405.79	504.25	1623.16	2017.00
50th	553.00	647.00	2212.00	2588.00	422.00	528.00	1688.00	2112.00
55th	576.37	675.02	2305.48	2700.08	438.21	551.75	1752.84	2207.00
60th	600.12	703.50	2400.48	2814.00	454.68	575.88	1818.72	2303.52
65th	624.67	732.93	2498.68	2931.72	471.71	600.83	1886.84	2403.32
70th	650.54	763.94	2602.16	3055.76	489.65	627.11	1958.60	2508.44
75th	678.46	797.41	2713.84	3189.64	509.01	655.48	2036.04	2621.92
80th	709.54	834.68	2838.16	3338.72	530.57	687.07	2122.28	2748.28
85th	745.78	878.12	2983.12	3512.48	555.70	723.89	2222.80	2895.56
90th	791.37	932.79	3165.48	3731.16	587.32	770.21	2349.28	3080.84
95th	858.94	1013.80	3435.76	4055.20	634.19	838.88	2536.76	3355.52

B.15 Muscles (Organ ID# 106-109)

The skeletal muscle can be subdivided into four different body parts such as head, trunk, arms, and legs. The ICRP Publication 23¹ approximately proportioned the volume and mass values of the skeletal muscles in adults with the total body weight, 40% for adult males and 29% for adult females. The percentile data of gallbladders in adults linearly scaled by the volume and mass values of the ICRP reference adults.

ICRP Publication 89 (page 148)

Table (Reference values for mass of skeletal muscle)

Adult Male: 29000g, Adult Female: 17500g.

¹ ICRP. Report of the task group on Reference Man Publication 23. Pergamon Press. Oxford (UK): International Commission on Radiation Protection (ICRP); 1975.

Table B. 22: Percentile values for mass and volume of the skeleton muscles in adult male.

Adult Male								
Percentile	Mass (g)				Volume(cm3)			
	Head	Trunk	Arms	Legs	Head	Trunk	Arms	Legs
5th	935.99	11532.64	2113.76	7704.12	891.42	10983.47	2013.11	7337.26
10th	969.36	11943.79	2189.12	7978.78	923.20	11375.04	2084.88	7598.84
15th	1016.08	12519.39	2294.62	8363.30	967.69	11923.23	2185.35	7965.05
20th	1051.12	12951.09	2373.75	8651.69	1001.06	12334.37	2260.71	8239.70
25th	1087.82	13403.36	2456.64	8953.81	1036.02	12765.10	2339.66	8527.44
30th	1117.85	13773.38	2524.46	9201.00	1064.62	13117.50	2404.25	8762.85
35th	1142.88	14081.74	2580.98	9406.99	1088.46	13411.18	2458.07	8959.04
40th	1167.91	14390.11	2637.50	9612.99	1112.29	13704.87	2511.90	9155.23
45th	1197.94	14760.13	2705.32	9860.18	1140.89	14057.27	2576.49	9390.64
50th	1217.96	15006.82	2750.53	10024.97	1159.96	14292.21	2619.55	9547.59
55th	1268.01	15623.53	2863.56	10436.95	1207.63	14879.55	2727.2	9939.95
60th	1309.72	16137.47	2957.76	10780.28	1247.36	15369.02	2816.92	10266.93
65th	1351.43	16651.39	3051.96	11123.59	1287.08	15858.47	2906.63	10593.9
70th	1401.49	17268.13	3164.99	11535.59	1334.75	16445.84	3014.28	10986.27
75th	1446.54	17823.16	3266.72	11906.36	1377.65	16974.44	3111.17	11339.39
80th	1518.28	18707.13	3428.74	12496.88	1445.98	17816.31	3265.47	11901.79
85th	1618.39	19940.57	3654.81	13320.85	1541.32	18991.02	3480.77	12686.52
90th	1708.48	21050.65	3858.28	14062.42	1627.12	20048.24	3674.55	13392.78
95th	1850.3	22798.04	4178.55	15229.72	1762.19	21712.42	3979.57	14504.50

Table B. 23: Percentile values for mass and volume of the skeleton muscles in adult female.

Adult Female								
Percentile	Mass (g)				Volume(cm3)			
	Head	Trunk	Arms	Legs	Head	Trunk	Arms	Legs
5th	274.68	5820.79	1042.00	4820.88	261.60	5543.61	992.38	4591.31
10th	294.78	6246.70	1118.24	5173.62	280.74	5949.24	1064.99	4927.26
15th	316.22	6701.01	1199.56	5549.88	301.16	6381.91	1142.44	5285.60
20th	334.97	7098.52	1270.72	5879.12	319.02	6760.5	1210.21	5599.16
25th	347.03	7354.07	1316.47	6090.77	330.51	7003.88	1253.78	5800.73
30th	357.75	7581.23	1357.14	6278.90	340.72	7220.22	1292.51	5979.91
35th	361.77	7666.41	1372.38	6349.45	344.55	7301.34	1307.03	6047.09
40th	378.52	8021.33	1435.92	6643.40	360.50	7639.36	1367.54	6327.05
45th	388.57	8234.29	1474.04	6819.77	370.07	7842.18	1403.85	6495.02
50th	401.97	8518.23	1524.87	7054.94	382.83	8112.60	1452.26	6718.99
55th	418.05	8858.96	1585.87	7337.14	398.14	8437.11	1510.35	6987.75
60th	432.12	9157.09	1639.23	7584.06	411.54	8721.04	1561.18	7222.91
65th	452.22	9583.00	1715.48	7936.80	430.68	9126.67	1633.79	7558.86
70th	468.97	9937.94	1779.02	8230.77	446.63	9464.70	1694.30	7838.82
75th	489.06	10363.85	1855.26	8583.51	465.77	9870.33	1766.91	8174.77
80th	515.86	10931.74	1956.92	9053.85	491.30	10411.18	1863.73	8622.71
85th	556.06	11783.55	2109.40	9759.34	529.58	11222.43	2008.96	9294.61
90th	589.56	12493.41	2236.48	10347.25	561.48	11898.48	2129.98	9854.52
95th	609.65	12919.32	2312.72	10699.99	580.62	12304.11	2202.59	10190.47

B.16 Oesophagus (Organ ID# 110)

The volume and mass values of oesophaguses for reference adults in the ICRP Publication 89¹ were rounded in the basis of the study of gastrointestinal (GI) tract for 61 individuals (49 males and 12 females) reported by Tipton and Cook (1969)².

ICRP Publication 89 (page 110, 111)

Table 6.1(Measured mass of the oesophagus in 49 adult males), (Tipton and Cook, 1969)

Oesophagus mass 37±6 (g), Median 26(g), Range 23-50(g)

Table 6.2 (Measured mass of the oesophagus in 12 adult females), (Tipton and Cook, 1969)

Oesophagus mass 34±7 (g), Median 34(g), Range 25-50(g)

Table (Reference values for mass of the oesophagus (g))

Adult Male: 40g, Adult Female: 35g

RPI-AM-50th: 40±9 g (Range ≈ 26~53g)

RPI-AF-50th: 35±8g (Range ≈ 26~51 g)

¹ ICRP. Annual report of the International Commission on Radiological Protection. ICRP Publication 89. Stockholm (Sweden): International Commission on Radiological Protection (ICRP); 2002.

² Tipton IH, Cook MJ. Weight of total gastrointestinal tract and its subfractions Health Physics Division Annual Progress Report for Period Ending July 31, 1969 Report ORNL-4446. Oak Ridge National Laboratory, Oak Ridge, TN 301-2;1969.

Table B. 24: Percentile values for mass and volume of the oesophagus in adults.

	Adult Male		Adult Female	
	Mass(g)	Volume(cm ³)	Mass(g)	Volume(cm ³)
Mean ± SD	40.00 ± 9.00	38.83 ± 8.74	35.00 ± 8.00	33.98 ± 7.77
Percentile				
5th	25.20	24.47	21.84	21.20
10th	28.47	27.64	24.75	24.03
15th	30.67	29.78	26.71	25.93
20th	32.43	31.49	28.27	27.45
25th	33.93	32.94	29.60	28.74
30th	35.28	34.25	30.80	29.90
35th	36.53	35.47	31.92	30.99
40th	37.72	36.62	32.97	32.01
45th	38.87	37.74	33.99	33.00
50th	40.00	38.83	35.00	33.98
55th	41.13	39.93	36.01	34.96
60th	42.28	41.05	37.03	35.95
65th	43.47	42.20	38.08	36.97
70th	44.72	43.42	39.20	38.06
75th	46.07	44.73	40.40	39.22
80th	47.57	46.18	41.73	40.51
85th	49.33	47.89	43.29	42.03
90th	51.53	50.03	45.25	43.93
95th	54.80	53.20	48.16	46.76

B.17 Ovary (Organ ID# 111-112)

The ovaries volume and mass values for the reference adult female summarized in the ICRP Publication 23¹ from the various literatures. More recently, the volume and mass data of ovaries have been examined by ultrasonography². According to these references, the percentile data of volume and mass values of both left and right ovaries for adult female were estimated.

ICRP Publication 23 (page 187)

Total weight of both ovaries for reference adult female: 11g

RPI-AF-50th: each: 5.5 ± 1.78 g

¹ ICRP. Report of the task group on Reference Man Publication 23. Pergamon Press. Oxford (UK): International Commission on Radiation Protection (ICRP); 1975.

² Munn CS, Kiser LC, Wetzner SM and Baer JE. Ovary volume in young and premenopausal adults: US determination. Work in progress Radiology 159: 731-732; 1986.

Pavlik EJ, DePriest PD, Gallion HH, Ueland FR, Reedy MB, Kryscio RJ, Jr v NJ. Ovarian volume related to age Gynecologic Oncology 77:410-412; 2000.

Hongning X, Kohkichi H, Atsushi MH, Kurioka., Kentaro T, Kohji M. Three-dimensional ultrasonic volume measurement of the ovary in women with polycystic ovary syndrome. . Journal of Medical Ultrasonics 28: 7-10; 2001.

Table B. 25: Percentile values for mass and volume of the left and right ovaries in adult female.

Adult Female				
	Left		Right	
	Mass(g)	Volume(cm ³)	Mass(g)	Volume(cm ³)
Mean ± SD	5.5 ± 1.78	5.29 ± 1.71	5.5 ± 1.78	5.29 ± 2.06
Percentile				
5th	2.58	2.48	2.58	2.48
10th	3.22	3.10	3.22	3.10
15th	3.66	3.52	3.66	3.52
20th	4.00	3.85	4.00	3.85
25th	4.31	4.14	4.31	4.14
30th	4.57	4.39	4.57	4.39
35th	4.82	4.63	4.82	4.63
40th	5.05	4.86	5.05	4.86
45th	5.28	5.08	5.28	5.08
50th	5.50	5.29	5.50	5.29
55th	5.72	5.50	5.72	5.50
60th	5.95	5.72	5.95	5.72
65th	6.19	5.95	6.19	5.95
70th	6.44	6.19	6.44	6.19
75th	6.70	6.44	6.70	6.44
80th	7.00	6.73	7.00	6.73
85th	7.34	7.06	7.34	7.06
90th	7.78	7.48	7.78	7.48
95th	8.42	8.10	8.42	8.10

B.18 Pancreas (Organ ID# 113)

The ICRP Publication 89¹ referred the reports of the organ weight in 684 adult autopsies by de la Grandmaison et al. (2001)² and the IAEA-TECDOC-1005 Publication³ to compare the volume and mass values of pancreas for adults in Western and Asian adults, respectively.

ICRP Publication 89 (page 125)

Table (Reference values for mass of the pancreas)

Adult Male: 140g, Adult Female: 120g.

RPI-AM-50th: 140 ± 35 g, **RPI-AF-50th:** 120 ± 33 g.

¹ ICRP. Annual report of the International Commission on Radiological Protection. ICRP Publication 89. Stockholm (Sweden): International Commission on Radiological Protection (ICRP); 2002.

² de la Grandmaison GL., Clairand I, Durigon M. Organ weight in 684 adult autopsies: new tables for a Caucasoid population Forensic science international 119:149–154;2001.

³ IAEA. Compilation of Anatomical, Physiological and Metabolic Characteristics for a Reference Asian Man. IAEA-TECDOC-1005 1-2: International Atomic Energy Agency; 1998.

Table B. 26: Percentile values for mass and volume of the brain in adults.

Percentile	Adult Male		Adult Female	
	Mass(g)	Volume(cm ³)	Mass(g)	Volume(cm ³)
	Mean ± SD	140.00 ± 35.00	133.33 ± 33.33	120.00 ± 33.00
5th	82.43	78.50	65.72	62.59
10th	95.15	90.62	77.71	74.01
15th	103.72	98.78	85.80	81.71
20th	110.54	105.28	92.23	87.84
25th	116.39	110.85	97.74	93.09
30th	121.65	115.86	102.69	97.80
35th	126.51	120.49	107.28	102.17
40th	131.13	124.89	111.64	106.32
45th	135.60	129.14	115.85	110.33
50th	140.00	133.33	120.00	114.29
55th	144.40	137.52	124.15	118.24
60th	148.87	141.78	128.36	122.25
65th	153.49	146.18	132.72	126.40
70th	158.35	150.81	137.31	130.77
75th	163.61	155.82	142.26	135.49
80th	169.46	161.39	147.77	140.73
85th	176.28	167.89	154.20	146.86
90th	184.85	176.05	162.29	154.56
95th	197.57	188.16	174.28	165.98

B.19 Prostate gland (Organ ID# 115)

The volume and mass values of prostate gland for the reference adult male summarized in the ICRP Publication 23¹ from the various literatures. In order to determine the percentile data of adult male, the mean and standard deviation values of volume and mass were referred from the ICRP Publication 89², and the IAEA-TECDOC-1005 Publication³, respectively.

ICRP Publication 89 (page 92)

Table (Reference values for mass of the prostate gland)

Adult Male: 17g.

Compilation of anatomical, physiological and metabolic characteristics for a Reference Asian Man: IAEA-TECDOC-1005 Vienna; IAEA; 1998

v. 1: Data summary and conclusions. (Page 43),

Table XV Male Adult Organ Mass (7 Countries)

Prostate: IND 19.1± 10.9(g)

RPI-AM-50th: 17±8.8 g

¹ ICRP. Report of the task group on Reference Man Publication 23. Pergamon Press. Oxford (UK): International Commission on Radiation Protection (ICRP); 1975.

² ICRP. Annual report of the International Commission on Radiological Protection. ICRP Publication 89. Stockholm (Sweden): International Commission on Radiological Protection (ICRP); 2002.

³ IAEA. Compilation of Anatomical, Physiological and Metabolic Characteristics for a Reference Asian Man. IAEA-TECDOC-1005 1-2: International Atomic Energy Agency; 1998.

Table B. 27: Percentile values for mass and volume of the prostate in adult male.

Adult Male		
	Mass(g)	Volume(cm ³)
Mean ± SD	17.00 ± 8.80	16.19 ± 8.38
Percentile		
5th	2.53	2.41
10th	5.72	5.45
15th	7.88	7.50
20th	9.59	9.13
25th	11.06	10.53
30th	12.39	11.80
35th	13.61	12.96
40th	14.77	14.07
45th	15.89	15.13
50th	17.00	16.19
55th	18.11	17.25
60th	19.23	18.31
65th	20.39	19.42
70th	21.61	20.58
75th	22.94	21.85
80th	24.41	23.25
85th	26.12	24.88
90th	28.28	26.93
95th	31.47	29.97

B.20 Salivary glands (Organ ID# 120-121)

The salivary glands can be subdivided by the pair of the parotid gland, the submaxillary gland, and the sublingual gland. The ICRP Publication 23¹ described the total volume and mass values of salivary glands in these three pairs for reference adults. The final mass values of salivary glands were assumed to be reached up to 85 g in the adult male and 70 g in the adult female. The parotid, submaxillary, and sublingual glands were proportioned by the ratio of 10:5:2, respectively². The percentile data of salivary glands in adults linearly scaled by the volume and mass values in conformity with the ICRP reference adults.

ICRP Publication 89 (page 105)

Table (Reference values for mass of pairs of major salivary glands)

Adult Male: 85g, Adult Female: 70g.

¹ ICRP. Report of the task group on Reference Man Publication 23. Pergamon Press. Oxford (UK): International Commission on Radiation Protection (ICRP); 1975.

² ICRP. Annual report of the International Commission on Radiological Protection. ICRP Publication 89. Stockholm (Sweden): International Commission on Radiological Protection (ICRP); 2002.

Table B. 28: Percentile values for mass and volume of the salivary glands in adults.

Percentile	Adult Male				Adult Female			
	Mass (g)		Volume (cm ³)		Mass (g)		Volume (cm ³)	
	Left	Right	Left	Right	Left	Right	Left	Right
5th	35.00	35.00	33.34	33.34	28.75	28.75	27.38	27.38
10th	35.85	35.85	34.15	34.15	29.45	29.45	28.05	28.05
15th	36.65	36.65	34.91	34.91	30.10	30.10	28.67	28.67
20th	37.50	37.50	35.72	35.72	30.80	30.80	29.33	29.33
25th	38.35	38.35	36.53	36.53	31.50	31.50	30.00	30.00
30th	39.15	39.15	37.29	37.29	32.20	32.20	30.67	30.67
35th	40.00	40.00	38.10	38.10	32.90	32.90	31.33	31.33
40th	40.85	40.85	38.91	38.91	33.60	33.60	32.00	32.00
45th	41.65	41.65	39.67	39.67	34.25	34.25	32.62	32.62
50th	42.50	42.50	40.48	40.48	34.95	34.95	33.29	33.29
55th	43.35	43.35	41.29	41.29	35.65	35.65	33.95	33.95
60th	44.15	44.15	42.05	42.05	36.30	36.30	34.57	34.57
65th	45.00	45.00	42.86	42.86	37.00	37.00	35.24	35.24
70th	45.85	45.85	43.67	43.67	37.70	37.70	35.90	35.90
75th	46.65	46.65	44.43	44.43	38.35	38.35	36.52	36.52
80th	47.50	47.50	45.24	45.24	39.05	39.05	37.19	37.19
85th	48.35	48.35	46.05	46.05	39.75	39.75	37.86	37.86
90th	49.15	49.15	46.81	46.81	40.40	40.40	38.48	38.48
95th	50.00	50.00	47.62	47.62	41.10	41.10	39.14	39.14

B.21 Spleen (Organ ID# 127)

The ICRP Publication 89¹ were compared the age and gender dependant data from the autopsies reported by Boyd² and the IAEA-TECDOC-1005 Publication³ to present the volume and mass values of spleens for adults in Western and Asian adults, respectively. The percentile data of volume and mass values of spleens for adults were estimated as follows the IAEA-TECDOC-1005 Publication.

ICRP Publication 89 (page 105)

Table (Reference values for mass of the spleen)

Adult Male: 150g, Adult Female: 130g.

Compilation of anatomical, physiological and metabolic characteristics for a Reference Asian Man: IAEA-TECDOC-100, 5 Vienna; IAEA; 1998

v. 1: Data summary and conclusions. (Page 43)

Table XV Male Adult Organ Mass (7 Countries)

Spleen: male (n=6 countries): 142 ± 21 (g), female (n=6 countries): 125± 15 (g)

RPI-AM-50th: 150±29 g, **RPI-AF-50th:** 130±20 g.

¹ ICRP. Annual report of the International Commission on Radiological Protection. ICRP Publication 89. Stockholm (Sweden): International Commission on Radiological Protection (ICRP); 2002.

² Boyd E 1933 Normal variability in weight of the adult human liver and spleen Archives of pathology. 16:350–372; 1933.

Boyd E 1941 Outline of Physical Growth and Development Burgess Publishing Co, Minneapolis, MN, USA; 1941.

Boyd E 1952 An Introduction to Human Biology and Anatomy for First Year Medical Students Child Research Council, Denver, CO, USA; 1952.

³ IAEA. Compilation of Anatomical, Physiological and Metabolic Characteristics for a Reference Asian Man. IAEA-TECDOC-1005 1-2: International Atomic Energy Agency; 1998.

Table B. 29: Percentile values for mass and volume of the spleen in adults.

Percentile	Adult Male		Adult Female	
	Mass(g)	Volume(cm ³)	Mass(g)	Volume(cm ³)
	Mean ± SD	150.00 ± 29.00	141.51 ± 27.36	130.00 ± 20.00
5th	102.30	96.51	97.10	91.60
10th	112.84	106.45	104.37	98.46
15th	119.94	113.15	109.27	103.08
20th	125.59	118.48	113.17	106.76
25th	130.44	123.06	116.51	109.92
30th	134.79	127.16	119.51	112.75
35th	138.83	130.97	122.29	115.37
40th	142.65	134.58	124.93	117.86
45th	146.36	138.08	127.49	120.27
50th	150.00	141.51	130.00	122.64
55th	153.64	144.94	132.51	125.01
60th	157.35	148.44	135.07	127.42
65th	161.17	152.05	137.71	129.92
70th	165.21	155.86	140.49	132.54
75th	169.56	159.96	143.49	135.37
80th	174.41	164.54	146.83	138.52
85th	180.06	169.87	150.73	142.20
90th	187.16	176.57	155.63	146.82
95th	197.70	186.51	162.90	153.68

B.22 Thymus (Organ ID# 131)

The ICRP Publication 23¹ summarized the volume and mass values of thymus for the Western males and females from various literatures. The ICRP Publication 89² compared this data with the autopsy cases of normal Japanese adults³. In order to determine the percentile data of adults in this study, the mean and standard deviation values of volume and mass were referred from the normal Japanese subjects in conformity with the ICRP reference adults.

ICRP Publication 89 (page 225)

Table (Reference values for mass of the thymus)

Adult Male: 25g, Adult Female: 20g

Reference Japanese man – I; Mass of organs and other characteristics of normal Japanese.

Table (Weight of the thymus and relative weight as a function of postnatal age)

Age 19-20, male (n=14) 29.2 ± 13.1 (g), female (n=12) 24.1 ± 13.5 (g),

RPI-AM-50th: 25±8.9 g, RPI-AF-50th: 20±9.4 g

¹ ICRP. Report of the task group on Reference Man Publication 23. Pergamon Press. Oxford (UK): International Commission on Radiation Protection (ICRP); 1975.

² ICRP. Annual report of the International Commission on Radiological Protection. ICRP Publication 89. Stockholm (Sweden): International Commission on Radiological Protection (ICRP); 2002.

³ Tanaka G, Kawamura H, Nakahara Y. Reference Japanese Man-I. Mass of Organs and Other Characteristics of Normal Japanese. Health Physics 36: 333-346; 1979.

Table B. 30: Percentile values for mass and volume of the thymus in adults.

Percentile	Adult Male		Adult Female	
	Mass(g)	Volume(cm ³)	Mass(g)	Volume(cm ³)
	Mean ± SD	25.00 ± 8.90	24.27 ± 8.64	20.00 ± 9.40
5th	10.36	10.06	4.54	4.41
10th	13.59	13.19	7.95	7.72
15th	15.78	15.32	10.26	9.96
20th	17.51	17.00	12.09	11.74
25th	19.00	18.45	13.66	13.26
30th	20.33	19.74	15.07	14.63
35th	21.57	20.94	16.38	15.90
40th	22.75	22.09	17.62	17.11
45th	23.88	23.18	18.82	18.27
50th	25.00	24.27	20.00	19.42
55th	26.12	25.36	21.18	20.56
60th	27.25	26.46	22.38	21.73
65th	28.43	27.60	23.62	22.93
70th	29.67	28.81	24.93	24.20
75th	31.00	30.10	26.34	25.57
80th	32.49	31.54	27.91	27.10
85th	34.22	33.22	29.74	28.87
90th	36.41	35.35	32.05	31.12
95th	39.64	38.49	35.46	34.43

B.23 Thyroid gland (Organ ID# 132)

The volume and mass values of the thyroid gland can be sensitively particularized by the factors, such as age, sex, diet, geography, climate, and external and internal stimuli, than other glands in the body¹ (ICRP, 1975). The ICRP Publication 89²(ICRP, 2002) estimated the mass data of thyroid glands from various literatures included autopsy studies, as well as sonographic measurements. This study derived the percentile data of volume and mass values of thyroid gland in adults from the study of the organ weight in 684 adult autopsies reported by de la Grandmaison et al. (2001)³.

ICRP Publication 89 (page 227)

Table (Reference values for mass of the thyroid gland)

Adult Male: 20g, Adult Female: 17g.

Organ weight in 684 adult autopsies: new tables for a Caucasoid population.

Table (Comparative data of organ weight (g) of males and females)

Males (n=355): Thyroid 25±11g (Range 12-87),

Females (n=329): Thyroid 20±9g (Range 5-88).

RPI-AM-50th: 20±6 g, **RPI-AF-50th:** 17±6 g.

¹ ICRP. Report of the task group on Reference Man Publication 23. Pergamon Press. Oxford (UK): International Commission on Radiation Protection (ICRP); 1975.

² ICRP. Annual report of the International Commission on Radiological Protection. ICRP Publication 89. Stockholm (Sweden): International Commission on Radiological Protection (ICRP); 2002.

³ de la Grandmaison GL., Clairand I, Durigon M. Organ weight in 684 adult autopsies: new tables for a Caucasoid population Forensic science international 119:149–154;2001.

Table B. 31: Percentile values for mass and volume of the thyroid gland in adults.

Percentile	Adult Male		Adult Female	
	Mass(g)	Volume(cm ³)	Mass(g)	Volume(cm ³)
	Mean ± SD	20.00 ± 6.00	19.05 ± 5.71	17.00 ± 6.00
5th	10.13	9.65	7.13	6.79
10th	12.31	11.72	9.31	8.87
15th	13.78	13.12	10.78	10.27
20th	14.95	14.24	11.95	11.38
25th	15.95	15.19	12.95	12.33
30th	16.85	16.05	13.85	13.19
35th	17.69	16.85	14.69	13.99
40th	18.48	17.60	15.48	14.74
45th	19.25	18.33	16.25	15.48
50th	20.00	19.05	17.00	16.19
55th	20.75	19.76	17.75	16.90
60th	21.52	20.50	18.52	17.64
65th	22.31	21.25	19.31	18.39
70th	23.15	22.05	20.15	19.19
75th	24.05	22.90	21.05	20.05
80th	25.05	23.86	22.05	21.00
85th	26.22	24.97	23.22	22.11
90th	27.69	26.37	24.69	23.51
95th	29.87	28.45	26.87	25.59

B.24 Tongue (Organ ID# 133)

The volume and mass values of tongue for reference adults were assumed by the ratio, 0.1% of total body mass in the ICRP Publication 89¹. The percentile data of tongue in adults linearly scaled by the values of the ICRP reference adults.

ICRP Publication 89 (page 106)

Table (Reference values for mass of the tongue)

Adult Male: 73g, Adult Female: 60g

¹ ICRP. Annual report of the International Commission on Radiological Protection. ICRP Publication 89. Stockholm (Sweden): International Commission on Radiological Protection (ICRP); 2002.

Table B. 32: Percentile values for mass and volume of the tongue in adults.

Percentile	Adult Male		Adult Female	
	Mass(g)	Volume(cm ³)	Mass(g)	Volume(cm ³)
5th	56.10	53.43	41.00	39.05
10th	58.10	55.33	44.00	41.90
15th	60.90	58.00	47.20	44.95
20th	63.00	60.00	50.00	47.62
25th	65.20	62.10	51.80	49.33
30th	67.00	63.81	53.40	50.86
35th	68.50	65.24	54.00	51.43
40th	70.00	66.67	56.50	53.81
45th	71.80	68.38	58.00	55.24
50th	73.00	69.52	60.00	57.14
55th	76.00	72.38	62.40	59.43
60th	78.50	74.76	64.50	61.43
65th	81.00	77.14	67.50	64.29
70th	84.00	80.00	70.00	66.67
75th	86.70	82.57	73.00	69.52
80th	91.00	86.67	77.00	73.33
85th	97.00	92.38	83.00	79.05
90th	102.40	97.52	88.00	83.81
95th	110.90	105.62	91.00	86.67

B.25 Urinary bladder (Organ ID# 137-138)

The urinary bladder consists of wall and content structures. The ICRP Publication 23¹ estimated the volume and mass values of urinary bladder tissue in adults within the range 30 – 60g. The percentile data of the urinary bladder walls in adults were linearly interpolated as follows the ICRP reference adults. The contents data of the urinary bladders estimated the volume and mass of heart contents in conformity with the ICRP reference adults.

ICRP Publication 89 (page 153)

Table (Reference values for mass of the urinary bladder)

Adult Male: 50g, Adult Female: 40g

¹ ICRP. Report of the task group on Reference Man Publication 23. Pergamon Press. Oxford (UK): International Commission on Radiation Protection (ICRP); 1975.

Table B. 33: Percentile values for mass and volume of the urinary bladder in adults.

Percentile	Adult Male				Adult Female			
	Mass (g)		Volume(cm ³)		Mass (g)		Volume(cm ³)	
	Wall	Content	Wall	Content	Wall	Content	Wall	Content
5th	30.00	120.00	28.85	115.38	30.00	150.00	28.85	144.23
10th	32.22	128.89	30.98	123.93	31.11	155.56	29.91	149.57
15th	34.44	137.78	33.12	132.48	32.22	161.11	30.98	154.91
20th	36.67	146.67	35.26	141.03	33.33	166.67	32.05	160.26
25th	38.89	155.56	37.39	149.57	34.44	172.22	33.12	165.60
30th	41.11	164.44	39.53	158.12	35.56	177.78	34.19	170.94
35th	43.33	173.33	41.67	166.67	36.67	183.33	35.26	176.28
40th	45.56	182.22	43.80	175.21	37.78	188.89	36.32	181.62
45th	47.78	191.11	45.94	183.76	38.89	194.44	37.39	186.97
50th	50.00	200.00	48.08	192.31	40.00	200.00	38.46	192.31
55th	51.11	204.44	49.15	196.58	42.22	211.11	40.60	202.99
60th	52.22	208.89	50.21	200.85	44.44	222.22	42.74	213.68
65th	53.33	213.33	51.28	205.13	46.67	233.33	44.87	224.36
70th	54.44	217.78	52.35	209.40	48.89	244.44	47.01	235.04
75th	55.56	222.22	53.42	213.68	51.11	255.56	49.15	245.73
80th	56.67	226.67	54.49	217.95	53.33	266.67	51.28	256.41
85th	57.78	231.11	55.56	222.22	55.56	277.78	53.42	267.09
90th	58.89	235.56	56.62	226.50	57.78	288.89	55.56	277.78
95th	60.00	240.00	57.69	230.77	60.00	300.00	57.69	288.46

B.26 Uterus (Organ ID# 139)

The volume and mass values of the uterus for the reference adult female described in the ICRP Publication 23¹ based on several studies. The percentile data of volume and mass values of uterus for adult female in this study were derived from the ultrasound volume assessment of the normal nongravid uterus by Joel F. Platt et al. (1990)².

ICRP Publication 89 (page 158)

Table (Reference values for mass of the uterus)

Adult Male: 80g.

Ultrasound of the Normal Nongravid Uterus: Correlation with Gross and Histopathology

Table (Mean Values and Suggested Upper Limits of Normal for Premenopausal Uterine Weight as a Function of Parity)

Total uterine Weight (n=61) 109±37g

RPI-AF-50th: 80±8g

¹ ICRP. Report of the task group on Reference Man Publication 23. Pergamon Press. Oxford (UK): International Commission on Radiation Protection (ICRP); 1975.

² Joel F, Robert L, Darrell D. Ultrasound of the normal nongravid uterus: Correlation with gross and histopathology Journal of Clinical Ultrasound 18:15-19; 1990.

Table B. 34: Percentile values for mass and volume of the uterus in adult female.

Adult Female		
	Mass(g)	Volume(cm ³)
Mean ± SD	80.00 ± 8.00	76.19 ± 7.62
Percentile		
5th	66.84	63.66
10th	69.75	66.43
15th	71.71	68.30
20th	73.27	69.78
25th	74.60	71.05
30th	75.80	72.19
35th	76.92	73.26
40th	77.97	74.26
45th	78.99	75.23
50th	80.00	76.19
55th	81.01	77.15
60th	82.03	78.12
65th	83.08	79.12
70th	84.20	80.19
75th	85.40	81.33
80th	86.73	82.60
85th	88.29	84.09
90th	90.25	85.95
95th	93.16	88.72

B.27 Other miscellaneous organs

There are spatial limitations to allow some of organs to be deformed in various shapes and sizes because the organs are located inside of certain bone structures such as eyes, spinal cord, and inner-tongue. The shapes of these organs are depended upon the shape of the adjacent skeleton surfaces. The percentile data for these types of organs were determined by the result volumes of initial whole-body size adjustment.

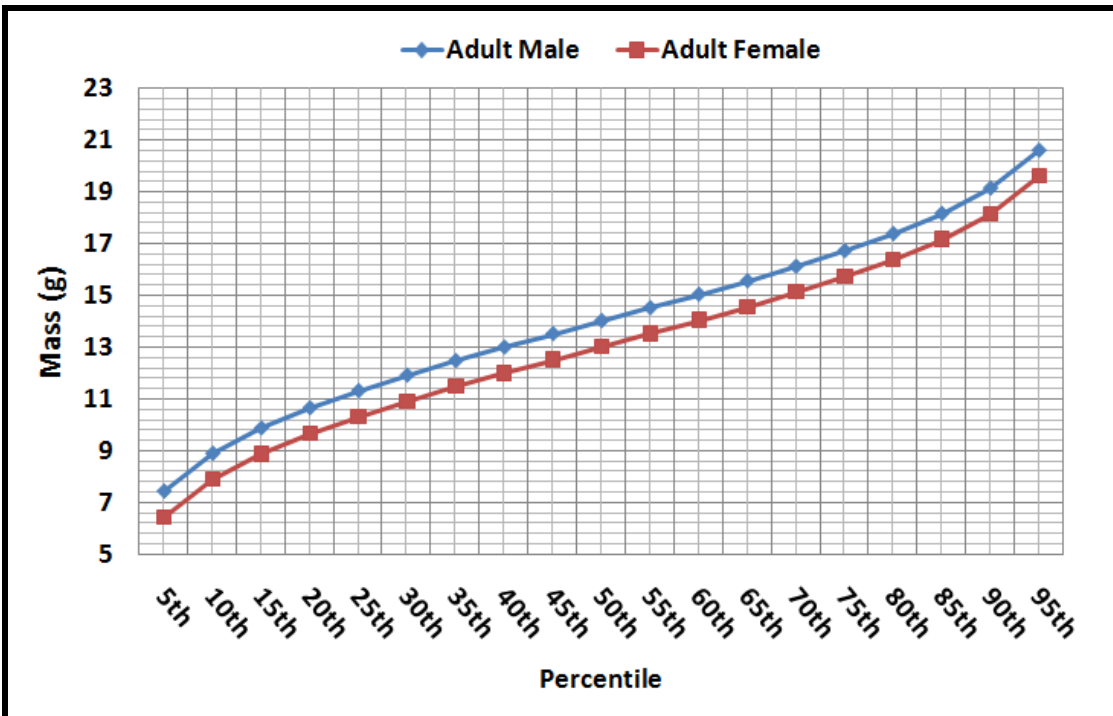


Figure B. 1: RPI deformable phantoms: adrenal glands percentiles.

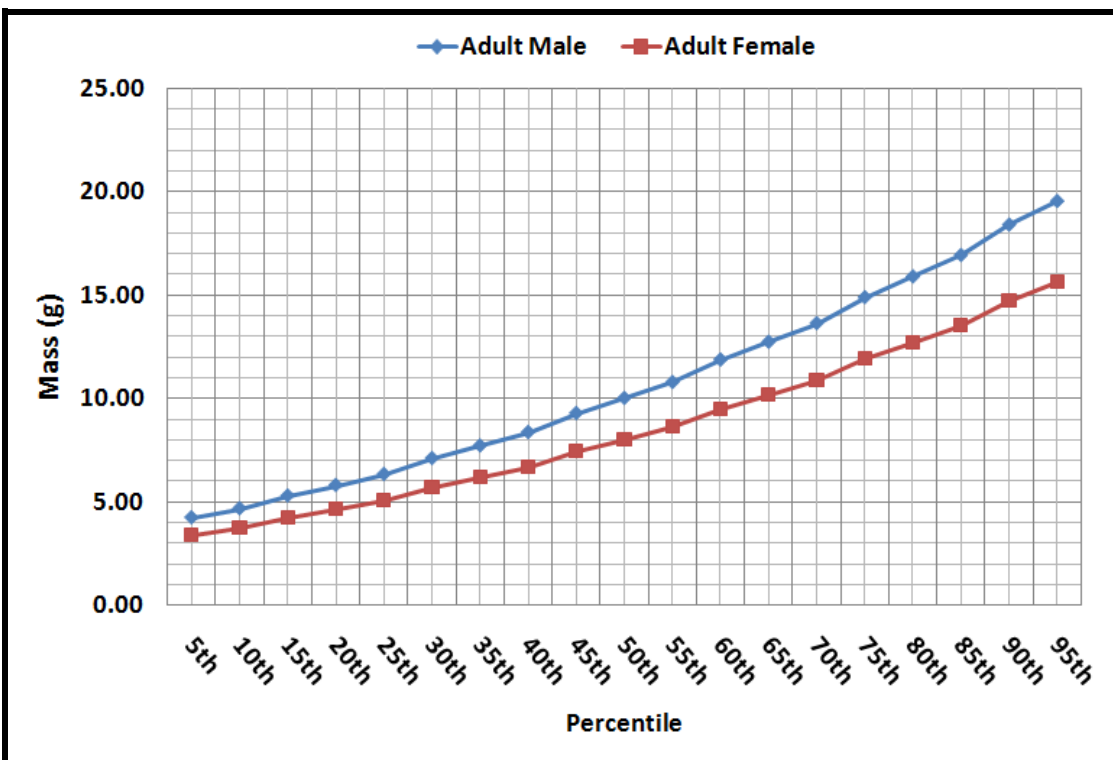


Figure B. 2: RPI deformable phantoms: trachea percentiles.

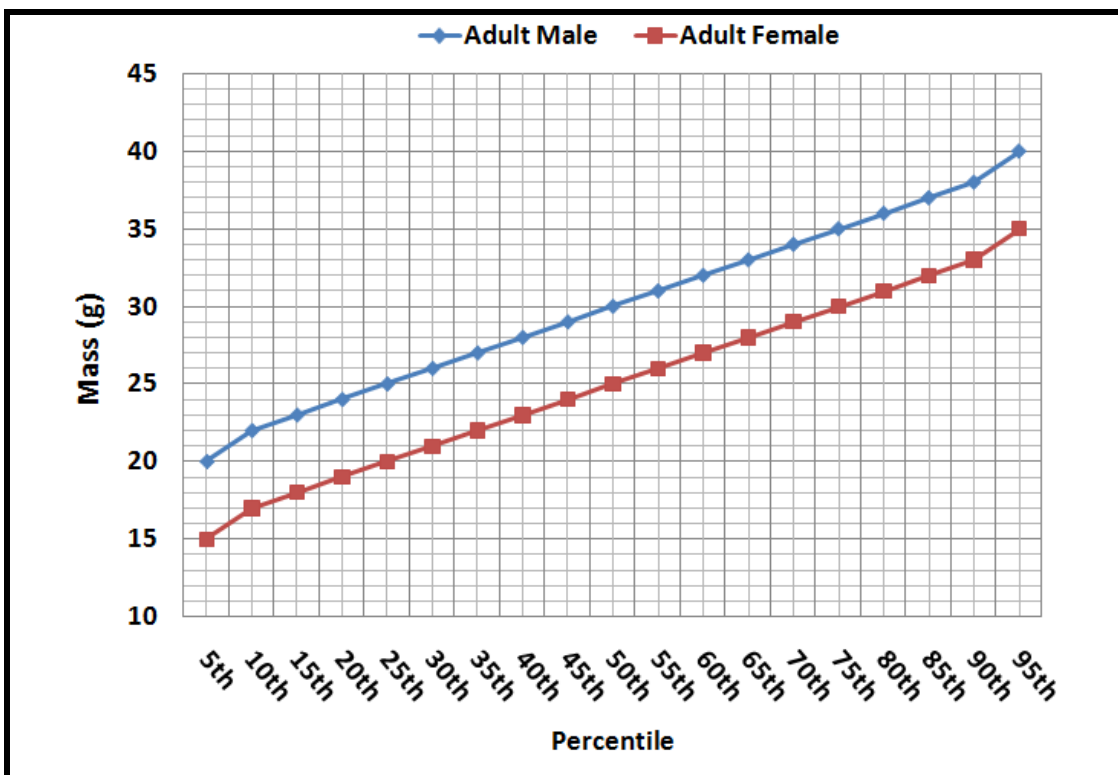


Figure B. 3: RPI deformable phantoms: bronchia percentiles.

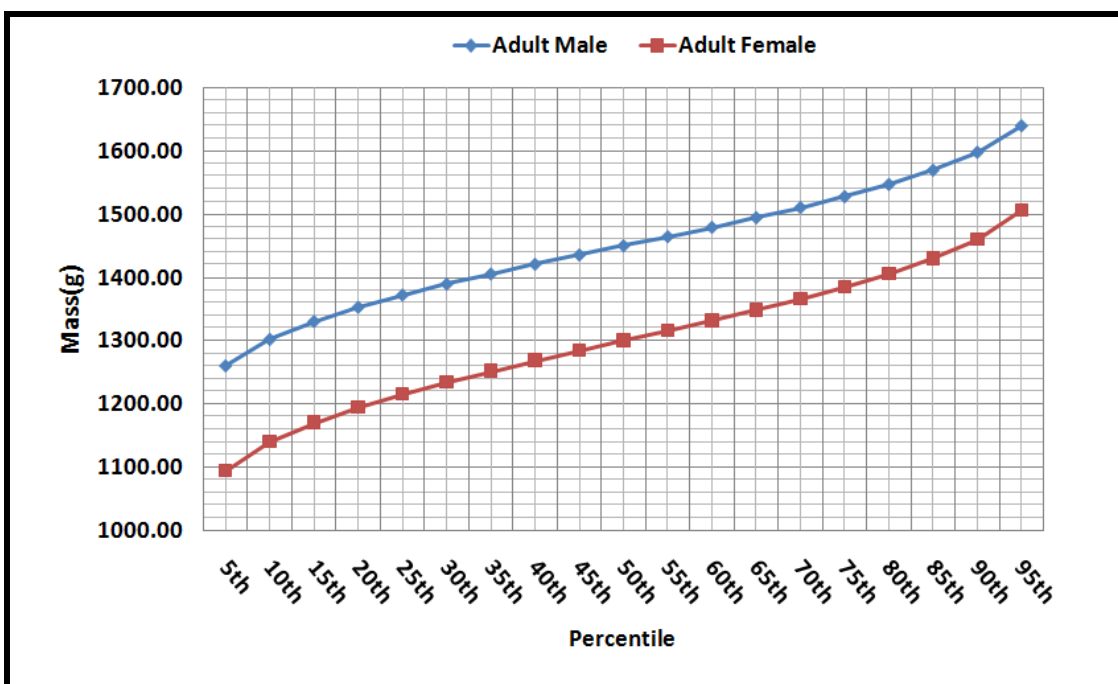


Figure B. 4: RPI deformable phantoms: brain percentiles.

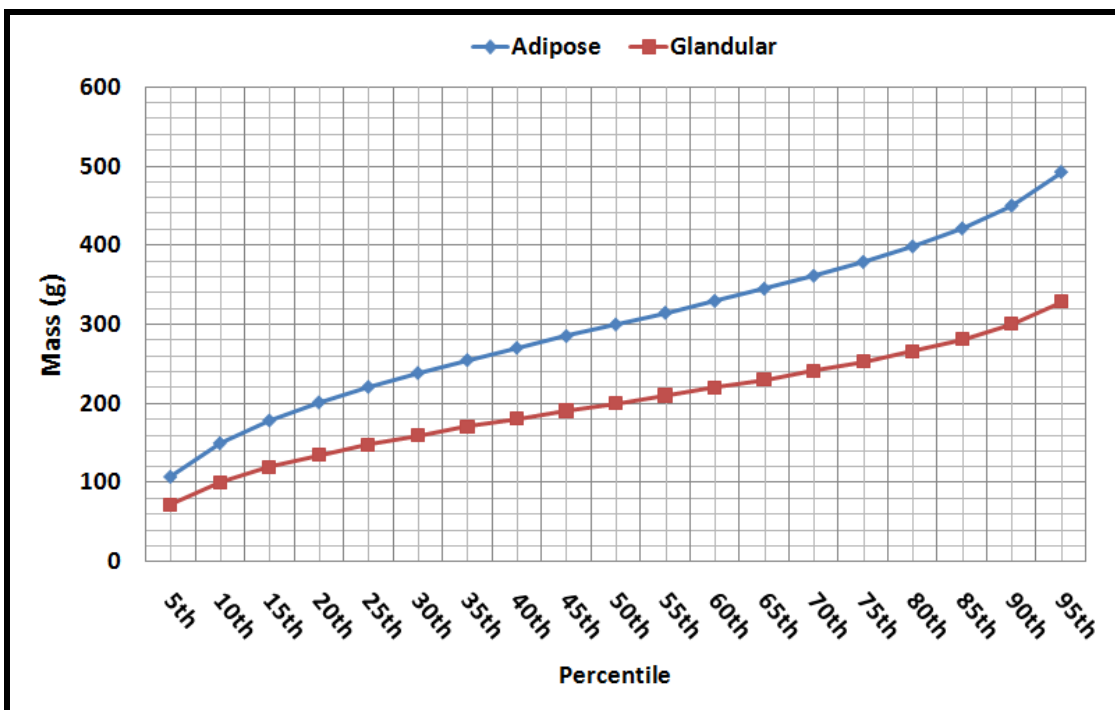


Figure B. 5: RPI deformable female phantom: breast tissue percentiles.

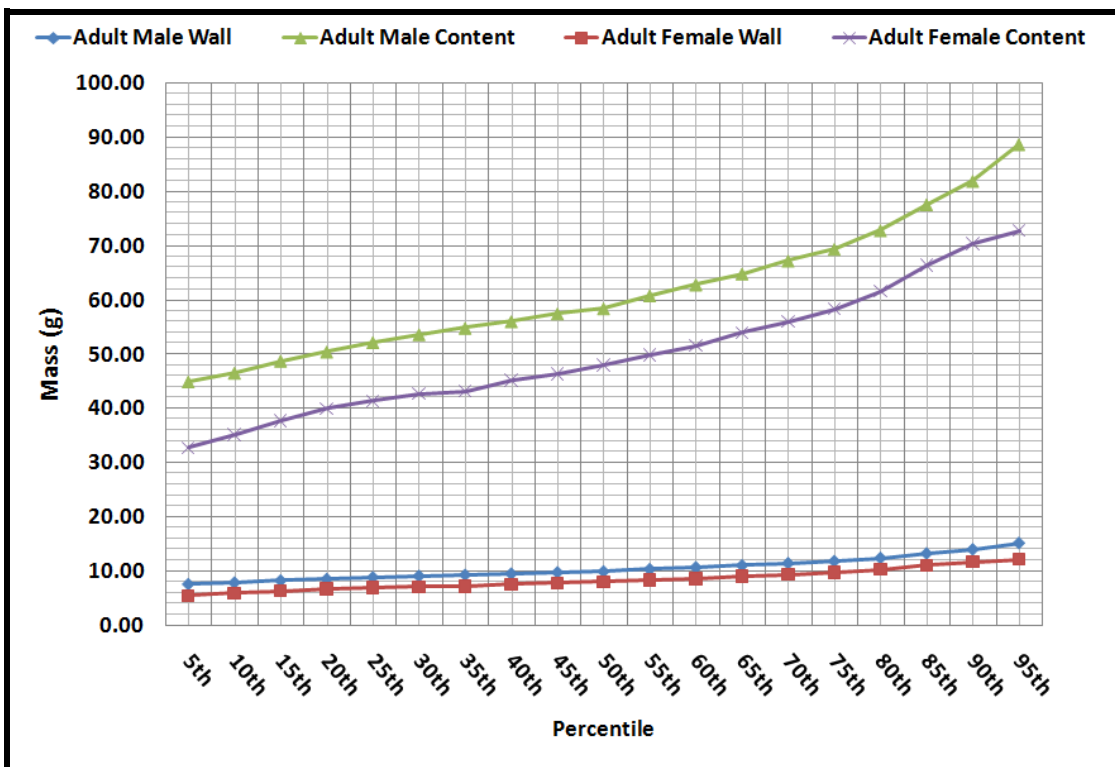


Figure B. 6: RPI deformable phantoms: gall bladder percentiles.

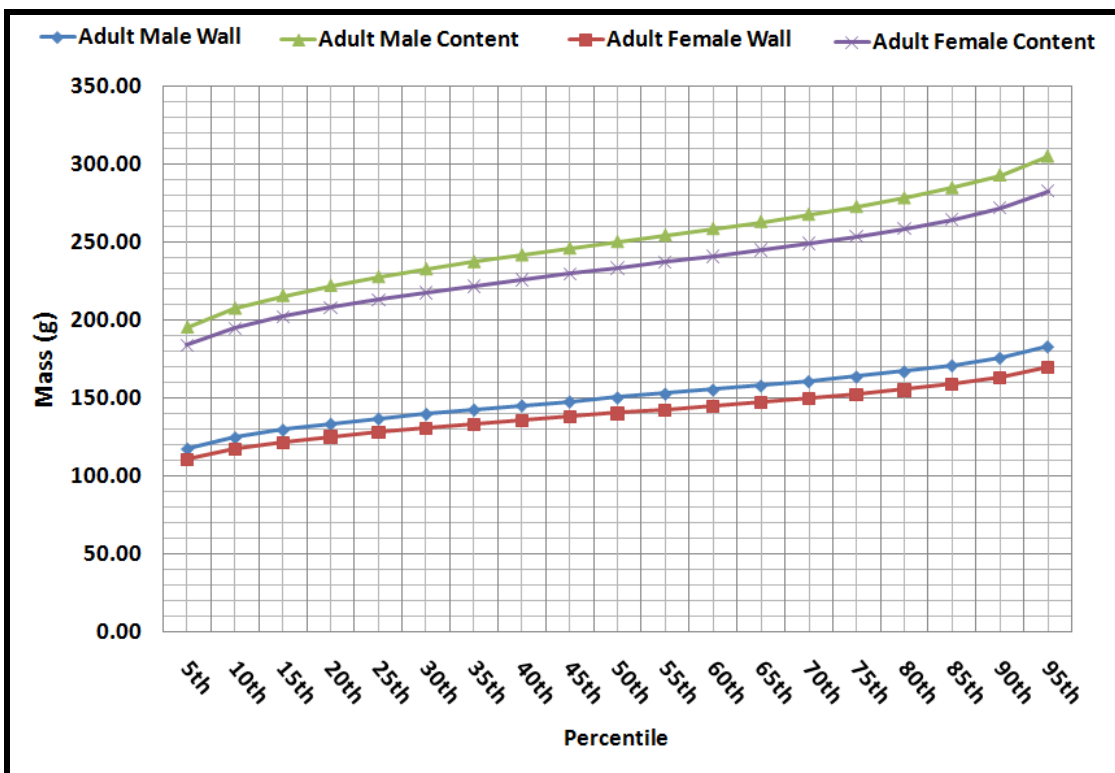


Figure B. 7: RPI deformable phantoms: stomach percentiles.

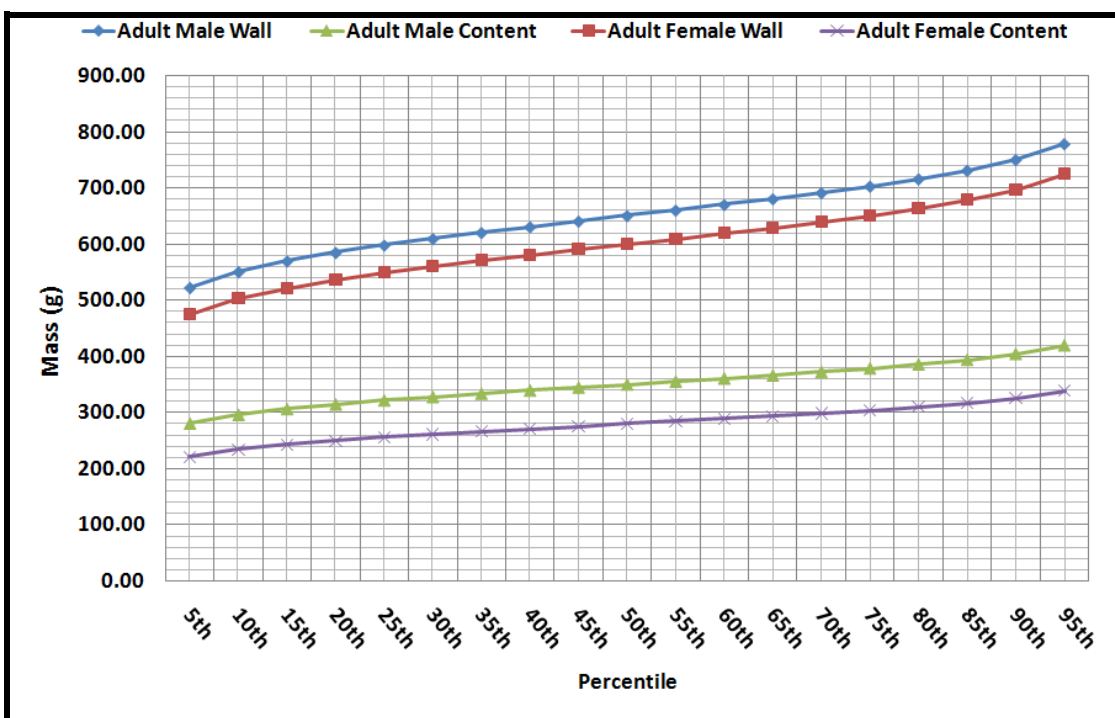


Figure B. 8: RPI deformable phantoms: small intestine percentiles.

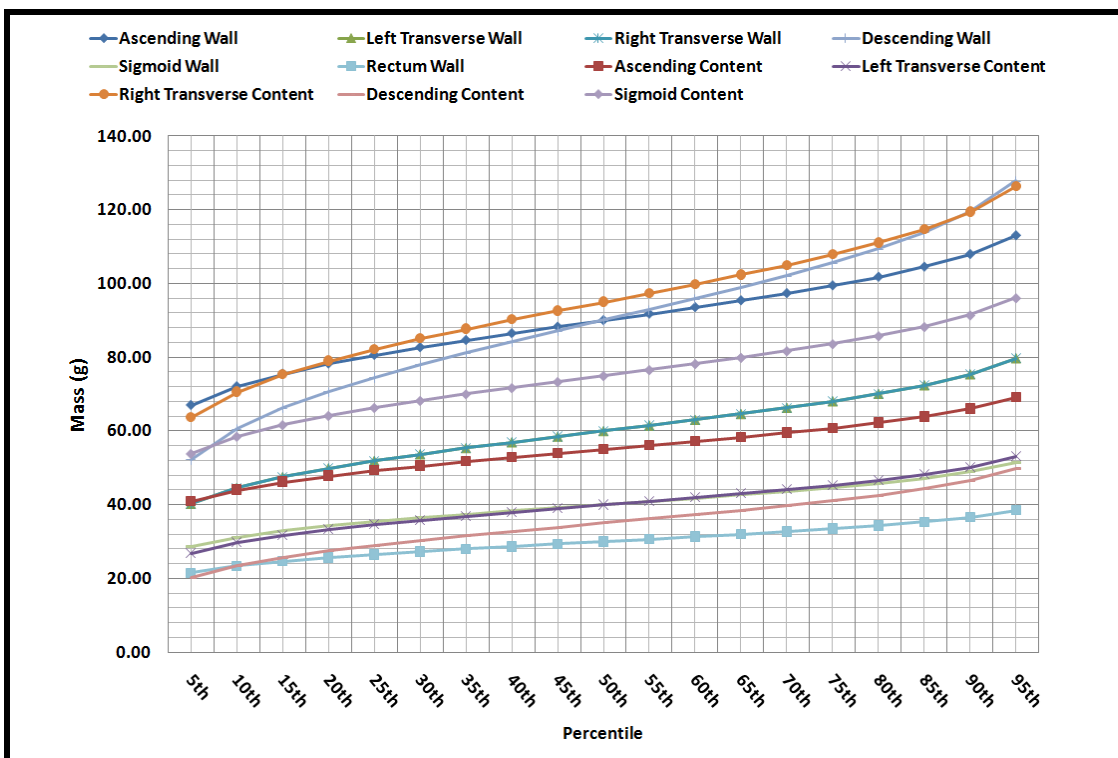


Figure B. 9: RPI deformable male phantom: large intestine percentiles.

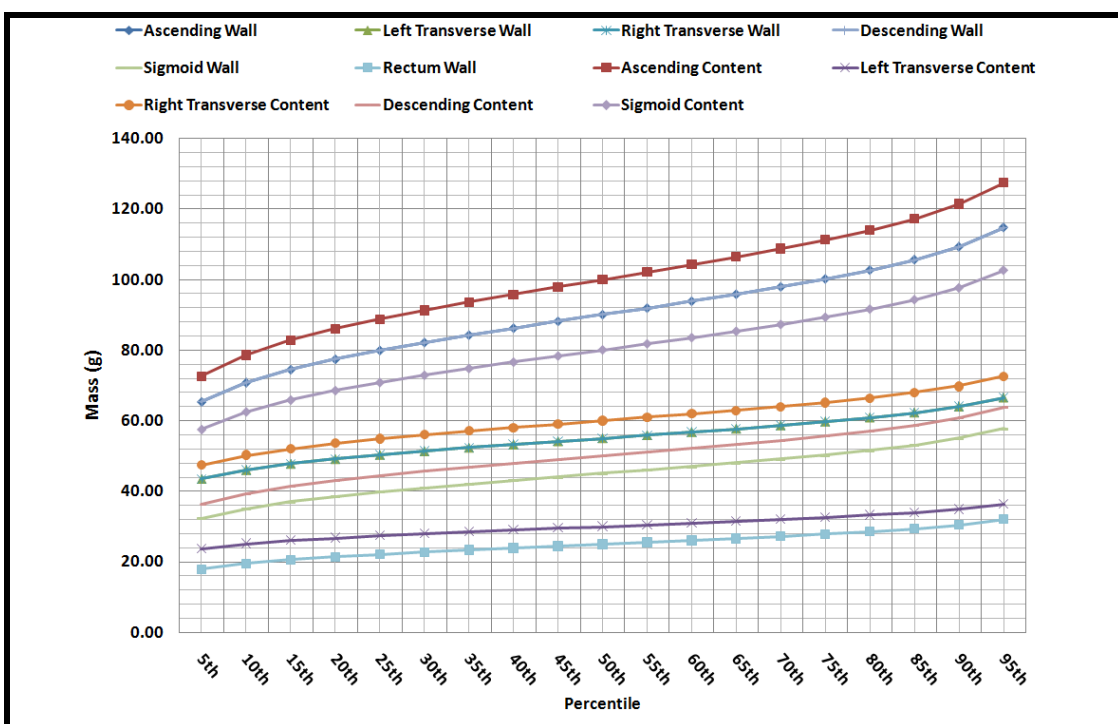


Figure B. 10: RPI deformable female phantom: large intestine percentiles.

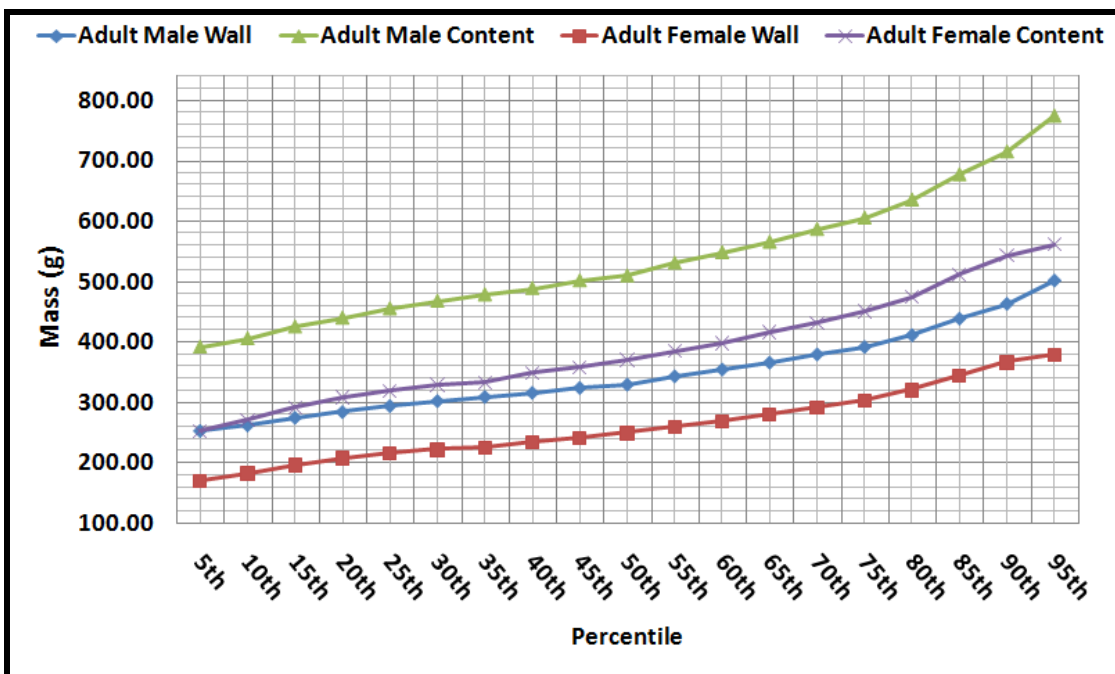


Figure B. 11: RPI deformable phantoms: heart percentiles.

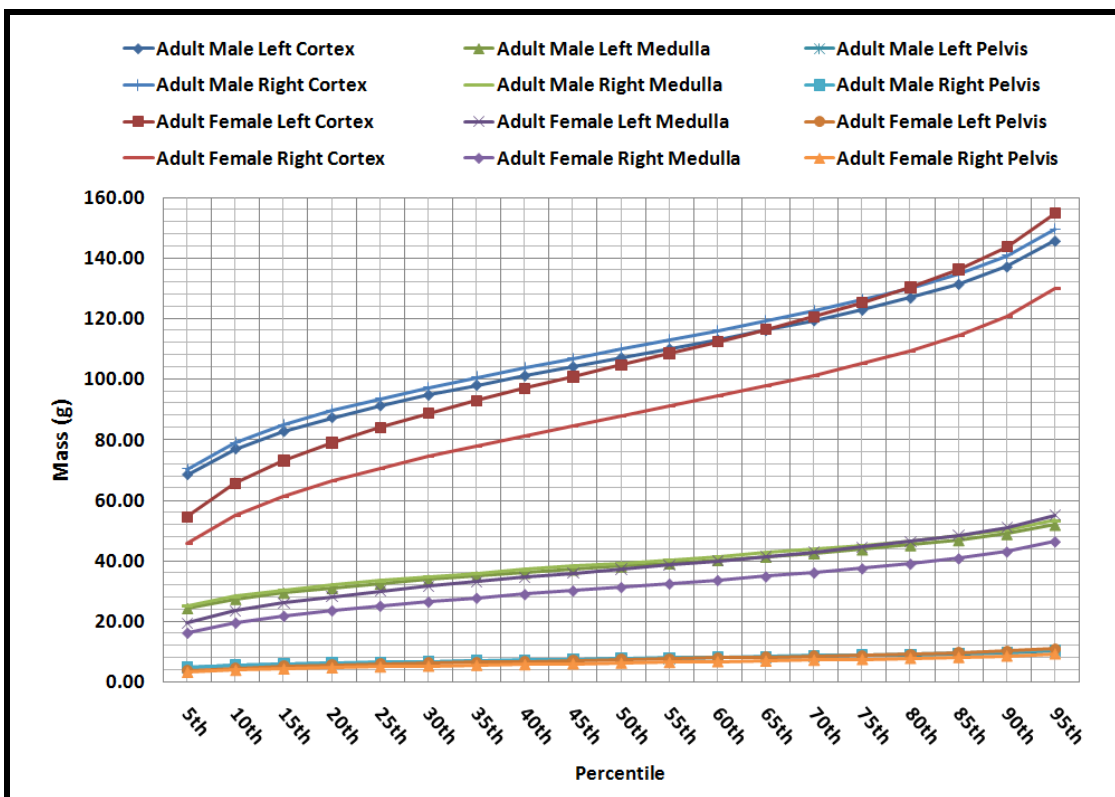


Figure B. 12: RPI deformable phantoms: kidney percentiles.

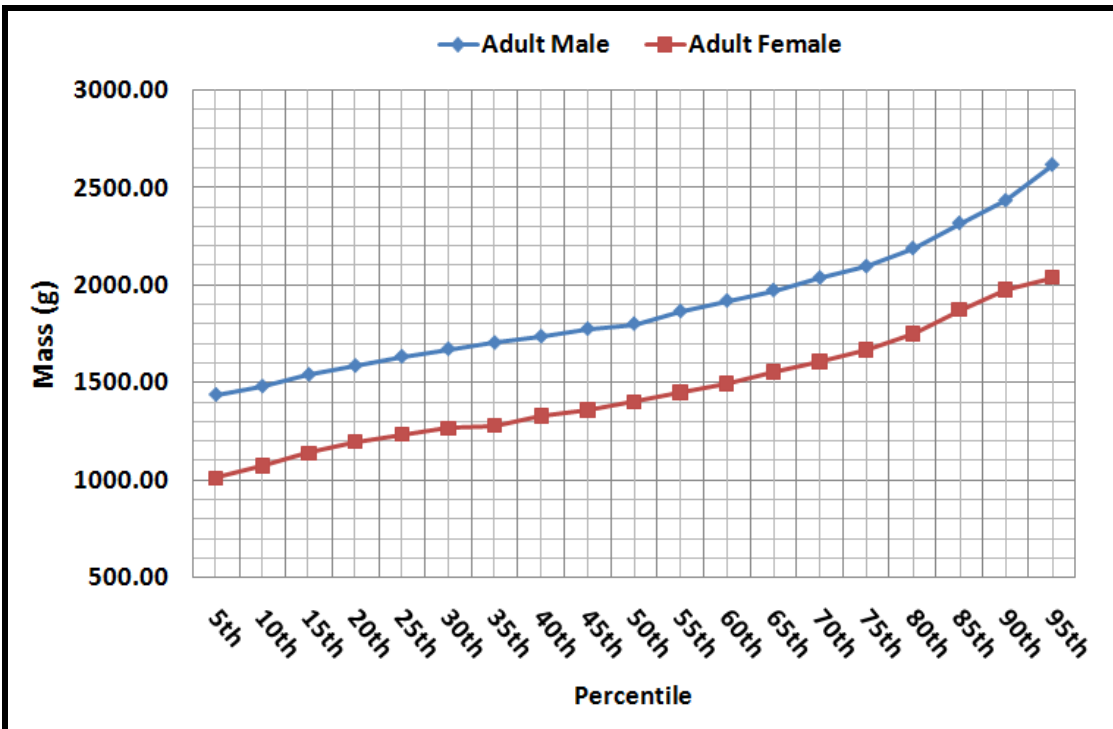


Figure B. 13: RPI deformable phantoms: liver percentiles.

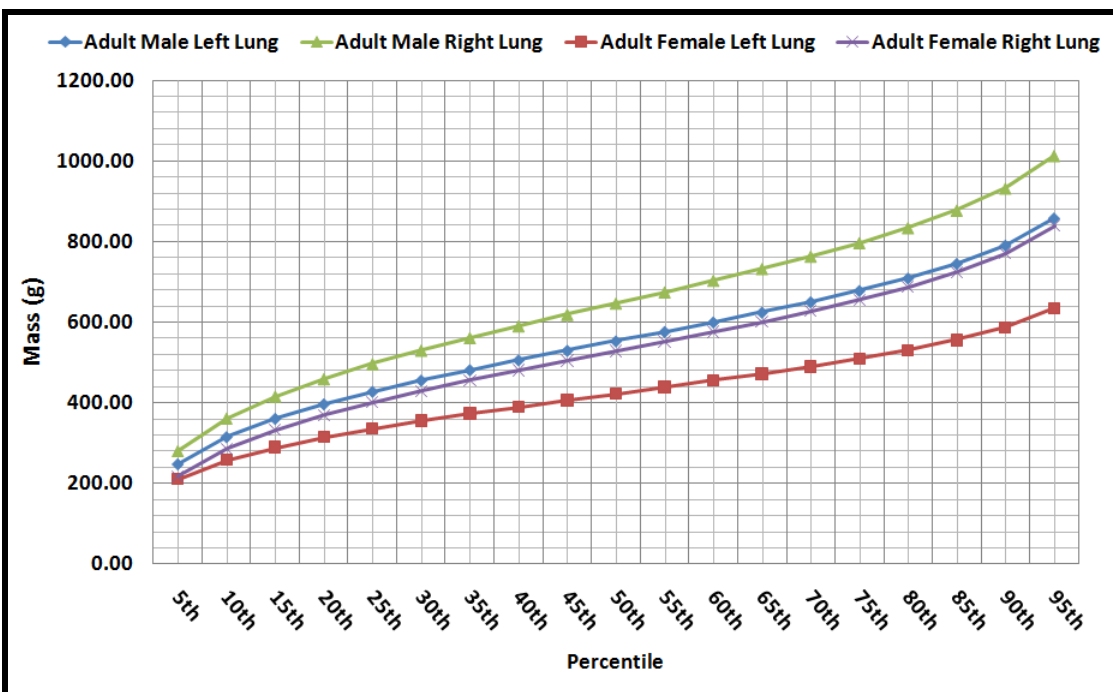


Figure B. 14: RPI deformable phantoms: lung percentiles.

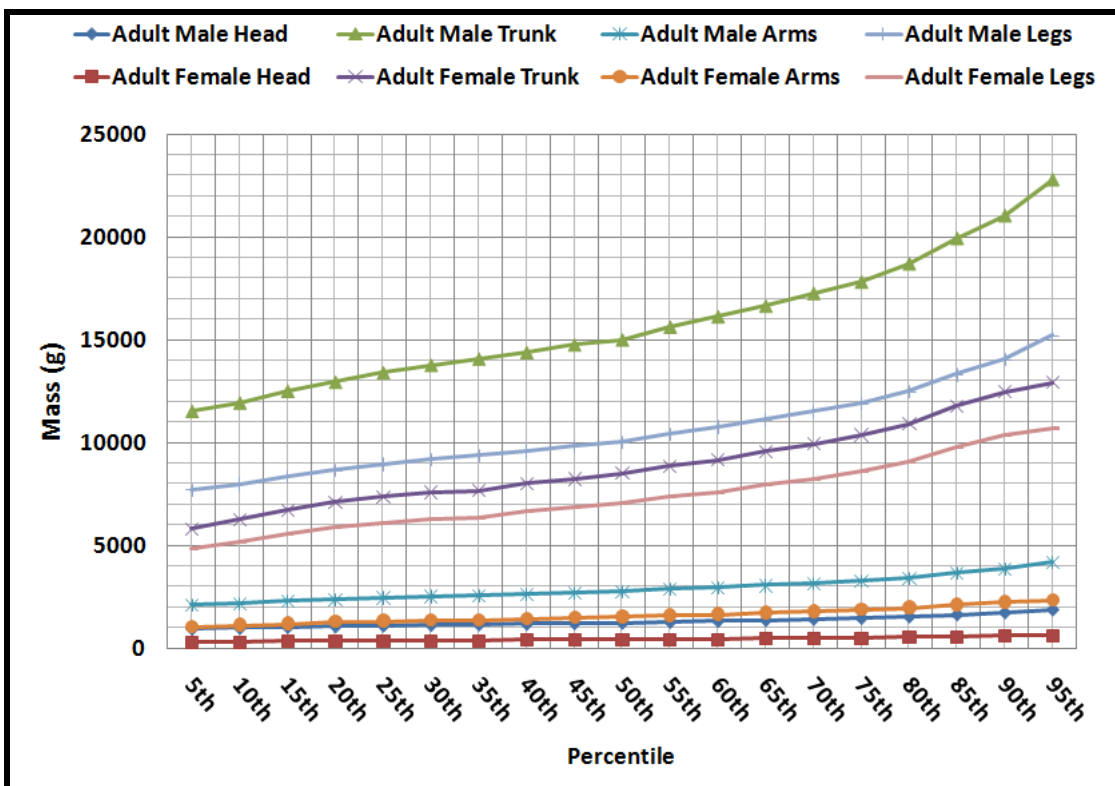


Figure B. 15: RPI deformable phantoms: muscle percentiles.

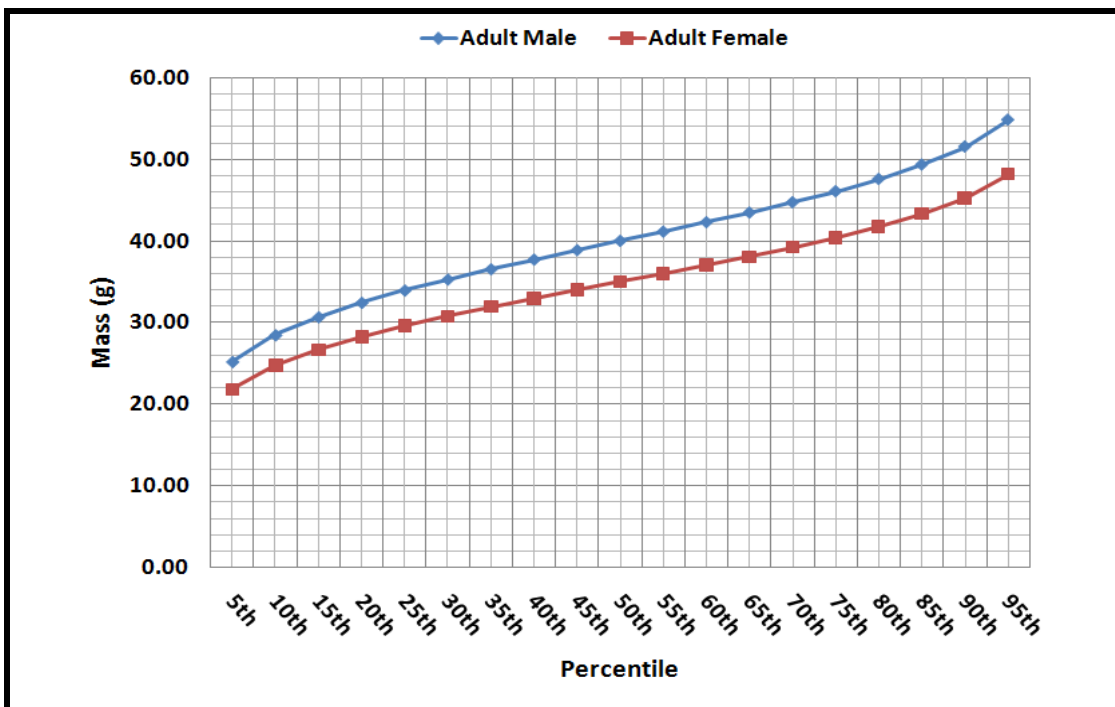


Figure B. 16: RPI deformable phantoms: oesophagus percentiles.

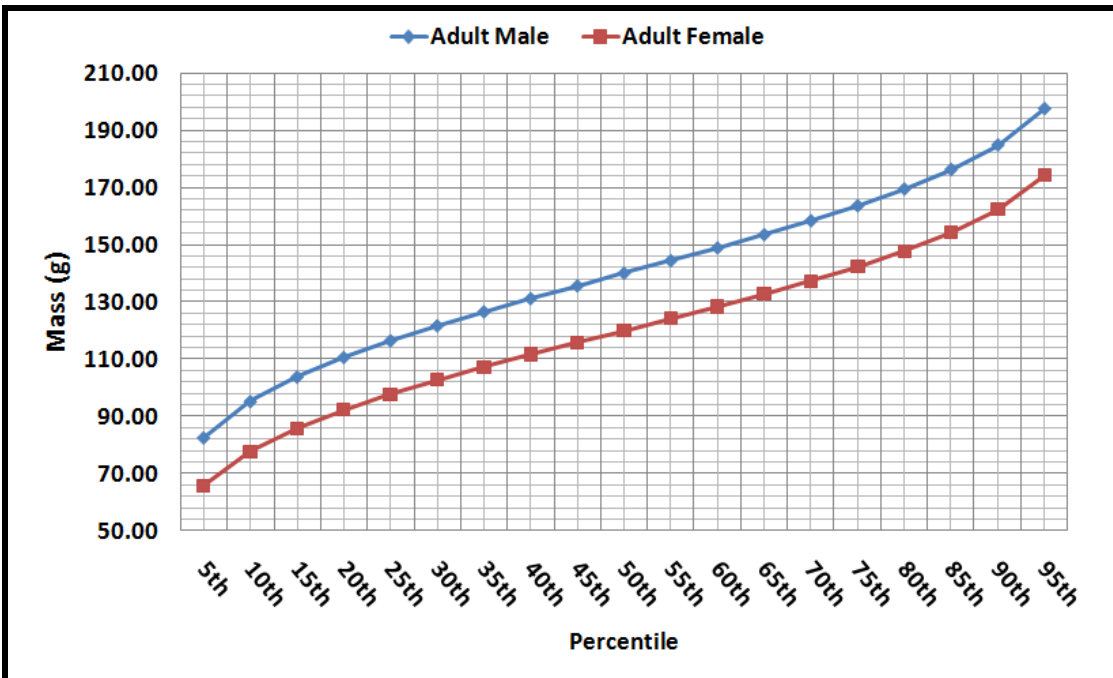


Figure B. 17: RPI deformable phantoms: pancreas percentiles.

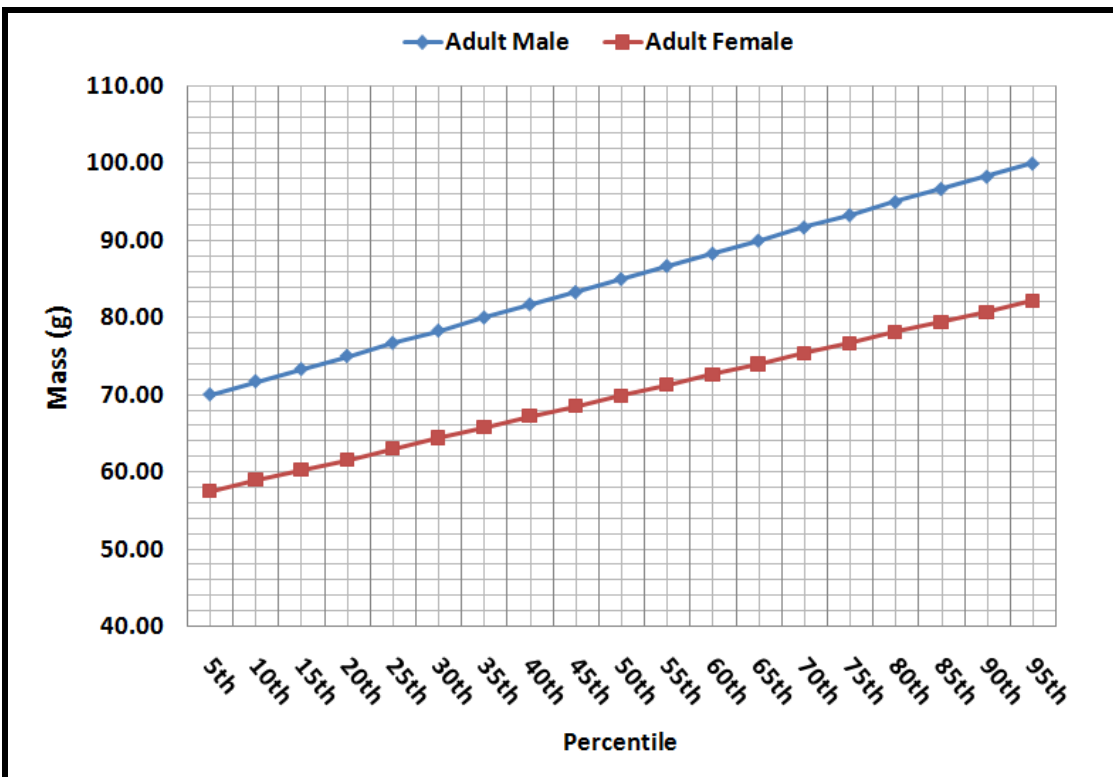


Figure B. 18: RPI deformable phantoms: salivary gland percentiles.

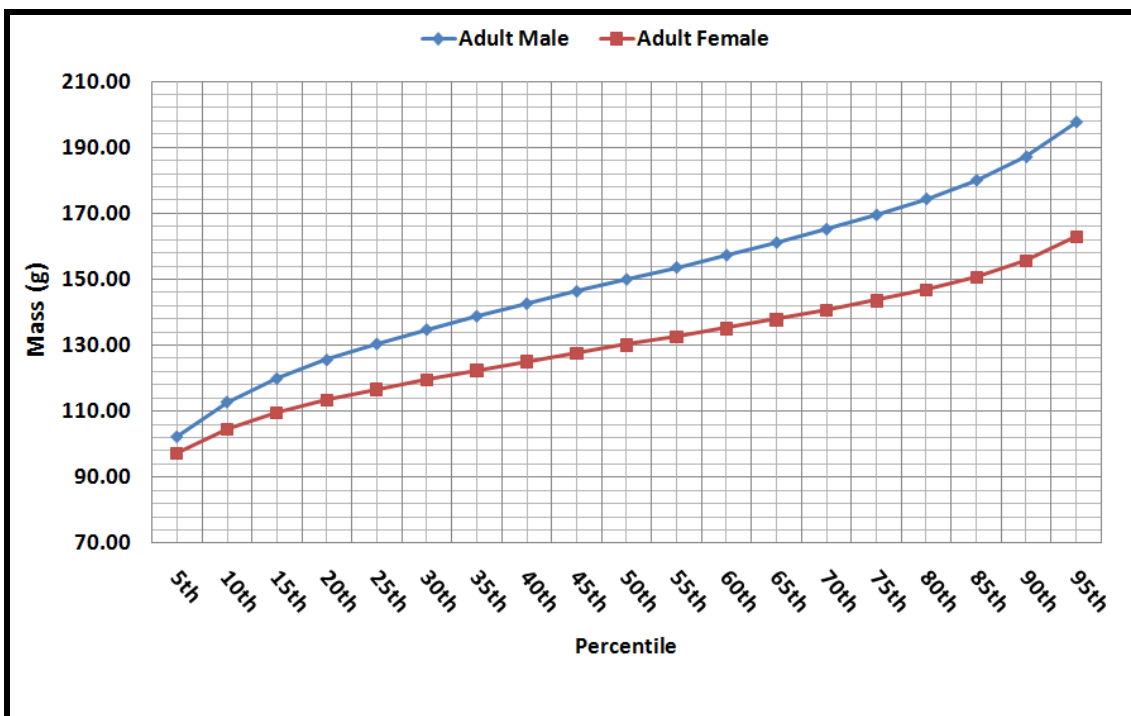


Figure B. 19: RPI deformable phantoms: spleen percentiles.

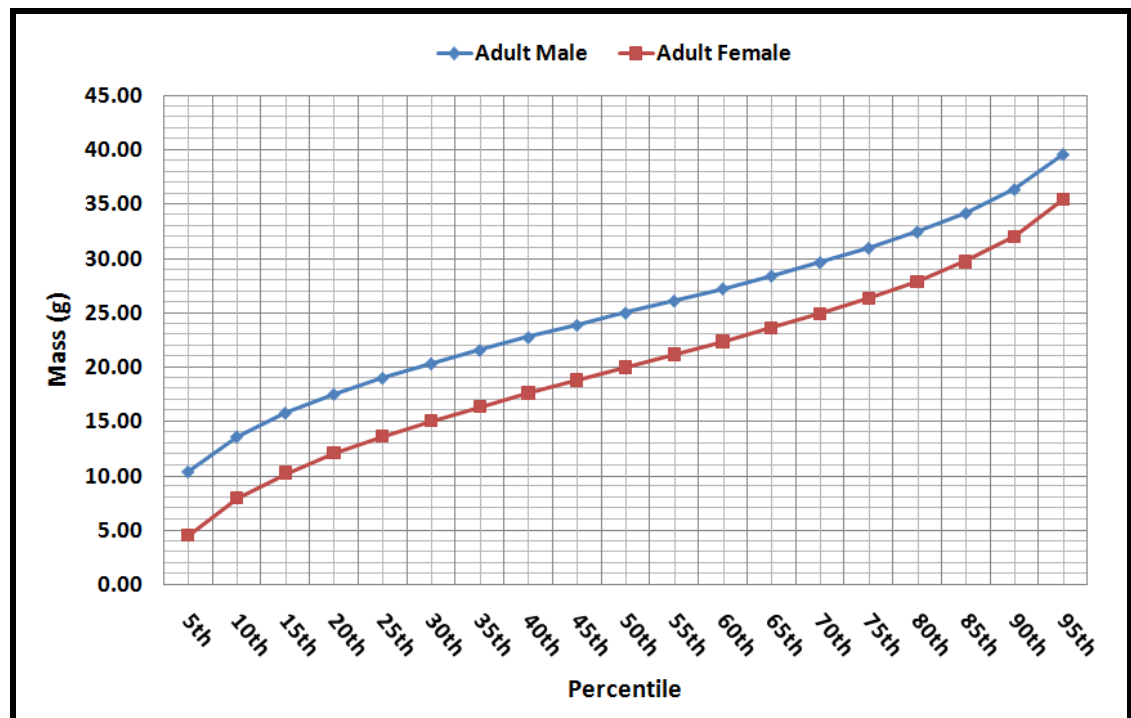


Figure B. 20: RPI deformable phantoms: thymus percentiles.

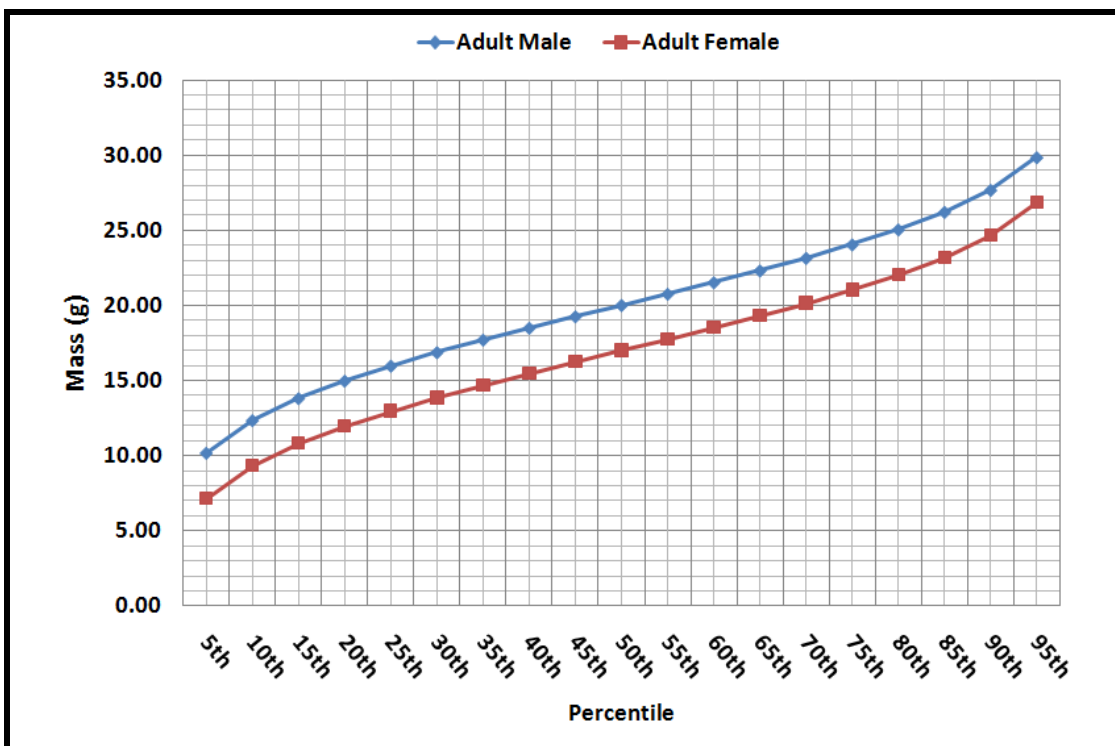


Figure B. 21: RPI deformable phantoms: thyroid percentiles.

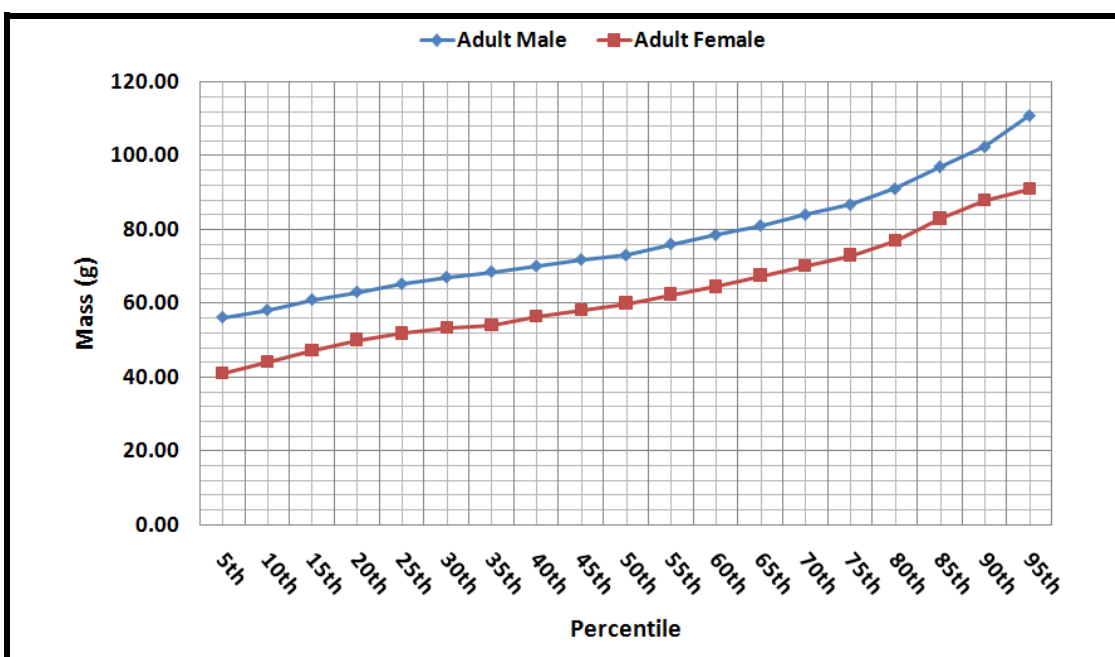


Figure B. 22: RPI deformable phantoms: tongue percentiles.

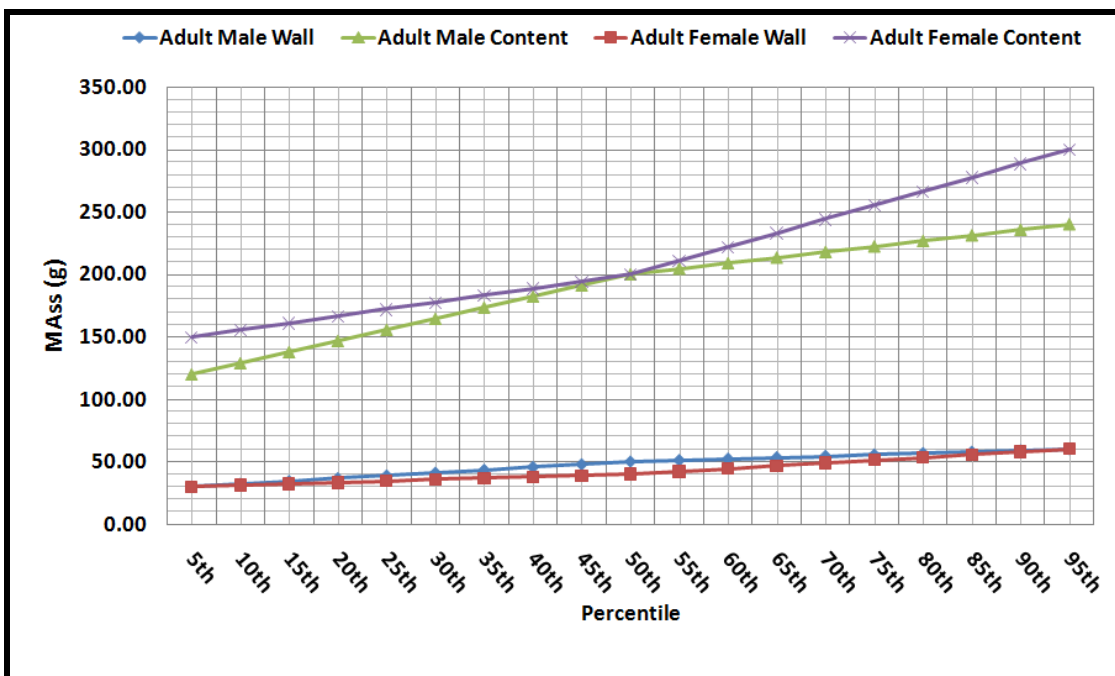


Figure B. 23: RPI deformable phantoms: urinary bladder percentiles.

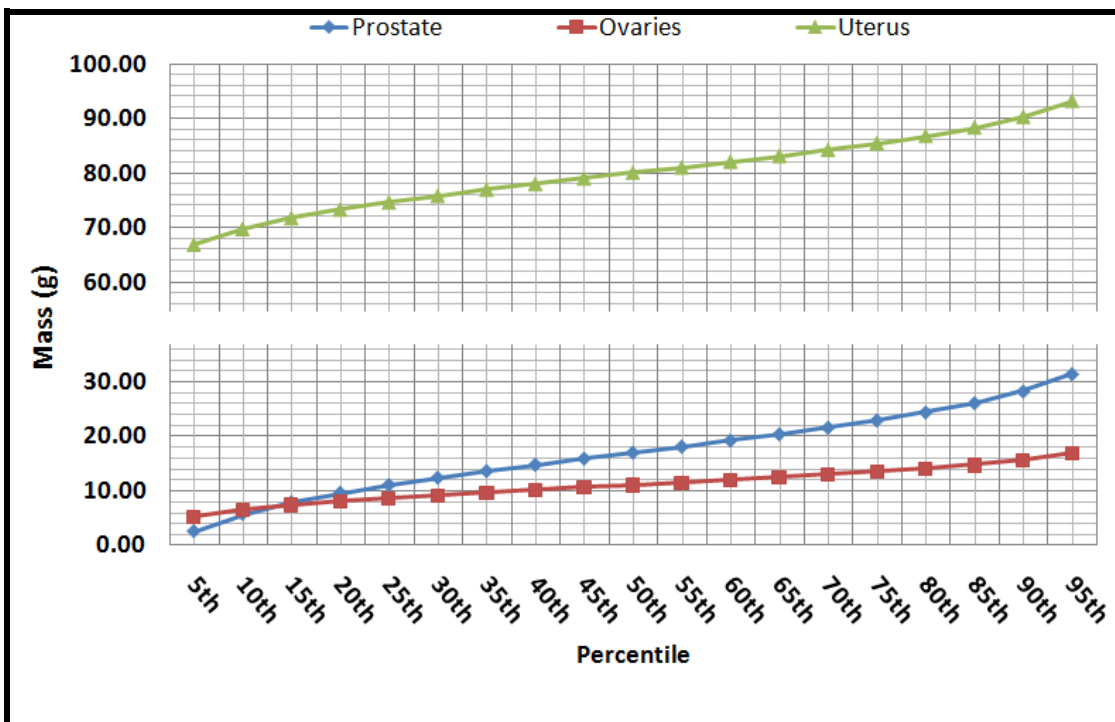


Figure B. 24: RPI deformable male phantom: prostate & RPI deformable female phantom: ovary and uterus percentiles.